UNIVERSIDADE FEDERAL DE RIO GRANDE – FURG

CURSO DE PÓS GRADUAÇÃO EM OCEANOGRAFIA FÍSICA, QUÍMICA E GEOLÓGICA

Modelagem Numérica do Comportamento das Ondas no Sul do Brasil e suas Interações com os Depósitos Lamíticos na Praia do Cassino

DEBORA COPSTEIN CUCHIARA

.   Tese apresentada ao Programa de Pós-graduação em Oceanografia Física, Química e Geológica da Universidade Federal de Rio Grande como requisito parcial à obtenção do título de DOUTOR

Orientador: Elisa Helena Fernandes

Co-Orientador: Lauro Júlio Calliari

RIO GRANDE

Agosto de 2008

Livros Grátis

Dedico este trabalho aos meus pais
Jaime Copstein (*in memoriam*) e
Stella Copstein (*in memoriam*)
ao Paulo Renato, a Cristina e ao Gustavo

Nada do que foi será

De novo do jeito que já foi um dia

Tudo passa, tudo sempre passará

A vida vem em ondas, como um mar

Num indo e vindo infinito

Tudo que se vê não é

Igual ao que a gente viu a um segundo

Tudo muda o tempo todo no mundo

Não adianta fugir

Nem mentir pra si mesmo agora

Há tanta vida lá fora

Aqui dentro sempre

Como uma onda no mar

(*Como uma onda – Lulu Santos*)

Modelagem Numérica do Comportamento das Ondas no Sul do Brasil e suas Interações com os Depósitos Lamíticos na Praia do Cassino

Débora Copstein Cuchiara

Resumo

A costa do Estado do Rio Grande do Sul se caracteriza por praias arenosas abertas predominantemente dominadas por ondas, que devido a sua topografia complexa, influencia os processos físicos que determinam as características das ondas e o transporte de sedimentos na costa. Os sedimentos finos presentes na ante-praia do Cassino, que são esporadicamente remobilizados e lançados sobre a praia e zona de arrebentação, ocasionam importantes efeitos de curta e longa duração sobre as características praiais e sobre as atividades turísticas na região. O objetivo geral deste estudo foi de caracterizar o clima de ondas ao longo da costa do Rio Grande do Sul, com especial enfoque na investigação da atenuação da energia das ondas sobre os depósitos lamíticos existentes na região costeira adjacente à Praia do Cassino. Estes objetivos foram atingidos através da caracterização do clima de ondas na costa do Rio Grande do Sul com base em dados pretéritos e dados de campo combinados com experimentos de modelagem numérica realizados com o modelo de ondas SWAN na versão padrão e na versão com lama fluída na sua formulação. Um estudo de caso foi realizado na região costeira adjacente a Praia do Cassino, investigando o amortecimento da energia das ondas nesta região, avaliando também a influência dos parâmetros característicos da lama fluida na atenuação das ondas. De forma complementar, foi avaliada a contribuição do aninhamento de modelos numéricos de ondas para as escalas global, regional e local, no estudo do comportamento das ondas nesta região. A utilização de um modelo numérico de ondas que considere a presença de fundos lamosos em sua formulação possibilitou obter resultados realísticos e fundamentais para a região onde este fenômeno é observado. De forma complementar, esta ferramenta contribuirá sobremaneira para a determinação do potencial energético das ondas na costa do Rio Grande do Sul, pois conforme este estudo comprovou, a presença dos depósitos lamíticos afeta de forma significativa a energia das ondas na região.

Wave numerical modeling in the South of Brazil and its Interactions with Mud Deposits at Cassino Beach

Débora Copstein Cuchiara

Abstract

The Rio Grande do Sul State coastal area is characterized by open sandy beaches exposed to wave action. The coastal topography is complex and influences the physical processes determining the waves and the sediment transport at the coast. The shoreface of Cassino Beach is characterized by extensive offshore mud deposits. During storms these deposits occasionally migrate and attach to the coast, exerting important effects on the surf zone and on tourism. The main objective of this study is the characterization of the wave climate in the Southern Brazilian Shelf based on a thorough revision of existing field data and on numerical modeling experiments, with special attention to the wave damping induced by the mud deposits observed in the area. These goals were achieved through the characterization of the climate of waves throughout the coast of Rio Grande do Sul based on field data and numerical modeling experiments carried out with the SWAN wave model without and with the mud effects in its formulation. A case study was accomplished in the adjacent coastal area the Beach of the Casino, investigating the reduction of the wave energy in this area due to the presence of the mud deposits, also evaluating the influence of the mud characteristic parameters in the attenuation of the wave energy. It was also evaluated the contribution of nesting wave models, covering spatial scales ranging from global to local, in the study of the attenuation of the wave energy. The use of a wave model that considers the mud effects in its formulation produced realistic and essential results for an area where this phenomenon is observed. This tool will also contribute to the determination of the waves energy potential throughout the coast of Rio Grande do Sul State, which can be affected by the presence of mud deposits.

SUMÁRIO

Lista de Figuras

Lista de Tabelas

Agradecimentos

♥ Gostaria de agradecer a todos aqueles que de alguma forma participaram desta jornada tanto nas horas de trabalho como nos momentos de lazer e que com certeza foram muitos sendo impossível citar todos. Entretanto gostaria de citar algumas pessoas que atuaram de forma mais direta:

♥ À professora Dra. Elisa Helena Fernandes, orientadora, pelos conhecimentos transmitidos, dedicação e compreensão, com certeza é mais uma grande amiga, do que simples orientadora, sendo sua ajuda de importância fundamental para a realização deste trabalho.

♥ Ao professor Dr. Lauro Júlio Calliari, co-orientador, por sua confiança, críticas e sugestões na realização deste estudo.

♥ Aos professores do Curso de Pós- Graduação em Oceanografia, Física, Química e Geológica, pelos conhecimentos transmitidos.

♥ Aos colegas Igor, Wilian, André, Rafael, e Bizu pelos auxílios no desenvolvimento deste trabalho.

♥ A professora Dra. Susana Vinzon coordenadora do projeto *Wave attenuation on muddy bottoms offshore Cassino beach*, por ter me concedido uma bolsa de doutorado pelo período de fevereiro de 2006 a fevereiro de 2007.

♥ Aos *US Office of Naval Research* e *Naval Research Laboratory* que através do projeto ONR N0004051484, financiou o meu estágio de 3 meses na Delft Hydraulics Institute, na Holanda, entre fevereiro e maio de 2006.

♥ *I am grateful to WL/Delft Hydraulics Institute, Holland, for making available the SWAN model considering mud, and to Han Winterwerp for the valuable training and special attention received during my stay in the WL/Delft Hydraulics Institute.*

♥ De uma forma muito especial gostaria de agradecer ao meu marido Paulo Renato e aos meus filhos Cristina e Gustavo, pela paciência, compreensão e apoio indispensáveis para a conclusão deste trabalho.

Capítulo 1

Introdução

Capítulo 1

Introdução

1.1. Introdução

A importância das zonas costeiras é a muito tempo reconhecida, não apenas pela comunidade científica, mas também por populações litorâneas. Esses ecossistemas apresentam privilegiados recursos naturais, econômicos e humanos, e atuam como áreas de interface crítica entre o oceano e os continentes, desempenhando um papel fundamental no desenvolvimento destas populações. Em especial, as atividades turísticas, de recreação, e de comércio fornecem suporte econômico para um número crescente de comunidades. Desta forma, conhecer e entender os efeitos das variações nas condições energéticas (oceanográficas e meteorológicas) da zona costeira no presente e no passado, bem como fazer projeções para o futuro, é essencial para a maioria dos projetos de engenharia, sendo um requisito básico para o gerenciamento costeiro.

Os estuários são ambientes costeiros de transição entre o continente e o oceano adjacente, onde a água do mar é diluída pela água doce da drenagem continental. A concentração de material em suspensão e sua precipitação no estuário são condicionadas, principalmente, pelo aporte de água doce e pela extensão da intrusão da água salgada que, dependendo da intensidade, pode ressuspender o material depositado. Os sedimentos fornecidos a um estuário entram em um meio extremamente complexo, podendo sofrer repetidos ciclos de ressuspensão e deposição antes de sua permanente acumulação ou transporte para o mar (Nichols, 1986). Uma das importantes funções sedimentológicas dos estuários é a mistura e diluição de sedimentos fluviais, funcionando como uma bacia receptora natural para a acumulação e armazenagem destes, particularmente silte e argila em suspensão. Nos estuários, a concentração de sedimentos finos em suspensão é geralmente alta e seu transporte é afetado por processos específicos, tais como floculação, erosão, deposição e consolidação. Os sedimentos finos (menores de 62 µm), também chamados lamosos ou coesivos, têm larga área superficial em relação à sua massa e apresentam abundantes minerais argilosos (Nichols e Biggs, 1985). A superfície destas partículas tem cargas iônicas que promovem interação eletrostática e, desta forma, não permanecem como partículas individuais e sim como flocos de partículas (Dyer, 1986). Esse processo de floculação aumenta a velocidade de decantação dentro do fluido em várias ordens de magnitude, promovendo a deposição de partículas em períodos de baixa dinâmica, e gerando uma zona de máxima turbidez que identifica o limite da intrusão salgada. Uma vez depositadas, a coesão destas partículas pode permitir maior resistência à erosão (Nichols e Biggs, 1985), gerando o assoreamento de portos e canais. Entretanto, sob determinadas condições hidrodinâmicas, como períodos de grande vazão, os sedimentos fluviais são exportados diretamente para a região costeira. Este processo transforma a função geológica de sumidouro dos estuários em fonte de sedimentos fluviais

para a região costeira, podendo acarretar um aumento na ocorrência de depósitos de lama na plataforma interna.

A explicação usual sobre depósitos de lama em plataformas (McCave, 1970; 1972), enfatiza o fato de que a localização e taxa de acumulação de lama são controlados pelo balanço entre o suprimento de sedimentos e a habilidade de transporte marinho. Dessa forma, sedimentos, como silte e argila em suspensão, podem ser depositados a uma determinada profundidade na plataforma, onde as correntes geradas por ondas apresentam baixas velocidades. Essa profundidade depende da exposição da costa, ou seja, onde a ressuspensão de sedimento pelo efeito das ondas é baixa, e a concentração de material em suspensão é alta o bastante para suprir e manter depósitos de lama permanentes, que resistam aos efeitos de bioturbação e às correntes erosivas de tempestade (Smith & Hoplins, 1972). A resistência à ressuspensão é função do grau de compactação, o qual depende do conteúdo de água. Logo após a deposição, a lama pode ser facilmente ressuspendida devido à grande quantidade de água ainda presente. Porém, em períodos nos quais os processos de floculação são favorecidos, a deposição dos flocos é rápida, formando camadas com altas concentrações. (Migniot, 1968, Owen, 1970 e Drake, 1976).

Depósitos de lama fluída têm sido encontrados em rios, estuários e costas ao redor do mundo (Jian et al, 1989). Extensos trechos da costa Atlântica da América do Sul são caracterizados por grandes depósitos lamosos regionais, especialmente onde um ou mais rios aportam significativas quantidades de sedimento fino em suspensão no mar (Kjerfve et al, 2003). Além da disponibilidade de sedimentos finos de origem continental, os processos dinâmicos de transporte e deposição de lama na plataforma interna resultam da interação entre as correntes costeiras geradas por ventos, ondas associadas à passagem de sistemas frontais, e a baixa amplitude das marés (Drake,1976).

Resultantes da ação do vento sobre a superfície dos oceanos, as ondas de gravidade encontram-se intimamente associadas às variações dos regimes atmosféricos, possuindo grande variabilidade espacial e temporal, e exercendo um papel fundamental na formação das feições costeiras. Uma vez geradas, as ondas são capazes de se propagar, transportando através do oceano a energia transferida pelo vento (Melo Filho et al., 1993). Esta energia que chega à costa exerce trabalho sobre o fundo e pode causar erosão, definindo padrões de transporte de sedimento.

As ondas chamadas vagas (*wind-sea* ou *sea*) compõe os campos de ondas que se encontram na zona de geração, ainda sobre influência do vento. Estas ondas são altamente complexas, pois apresentam formas irregulares e variabilidade na direção de propagação resultando em uma composição de ondas com alturas e períodos variados (Komar, 1998). Quando estas ondas deixam a área de geração, elas se tornam mais regulares e desenvolvem as denominadas ondulações (*swell*), com alturas e distâncias entre cristas mais uniformes. As ondulações, especialmente as de longo período, são capazes de se propagar por grandes distâncias, sofrendo pouca atenuação e transferindo energia pelo oceano até alcançar a costa (Komar, 1998).

Dean e Darlymple (1991) comentam que vários são os fatores que contribuem para a evolução e a transformação do campo de ondas gerado por ventos ao largo (em águas profundas) e para sua propagação sobre a plataforma continental, em direção à costa. A evolução do campo de ondas em águas profundas resulta da transferência de energia do campo de ventos para a superfície do mar, da perda de energia por arrebentação e da troca de energia entre ondas de diversos comprimentos através de um mecanismo de ressonância não-linear. A transformação do campo de ondas em águas rasas ocorre devido aos processos de refração, por interações com o relevo submarino e/ou correntes costeiras, de difração, de empolamento (*shoaling)*, de reflexão, de arrebentação e de dissipação de energia por atrito

com o fundo. Assim, quaisquer modificações no regime de ondas incidentes ou nas características da costa, implicarão em um desequilíbrio dinâmico e um conseqüente ajuste da morfologia do sistema ao novo regime, feito através do transporte de sedimentos de forma paralela ou perpendicular à costa.

A dissipação de energia com o fundo ocorre através da fricção, percolação e atenuação por viscosidade (WMO,1998). Estes mecanismos tornam-se importantes quando a plataforma costeira sobre o qual o campo de ondas se propaga tem características como extensão, alta porosidade, sedimentos de grande diâmetro granulométrico, ou ainda fundos lamosos.

Quando as ondas entram em águas intermediárias e rasas, os depósitos lamosos existentes afetam as ondas que estão se propagando e estas interagem com o fundo. As interações dos fundos lamosos com as ondas produzem uma dissipação gradual da energia, resultando na atenuação da altura da onda (Jian et al, 1989). Por outro lado, as pressões exercidas no fundo pelas ondas causam a ressuspensão e o transporte da lama. Ambos os efeitos são de grande importância.

Conceitualmente o amortecimento das ondas sobre fundos lamosos é caracterizado por uma seqüência de eventos (Winterwerp et al., 2007). Inicialmente pequenas deformações elásticas são geradas dentro do solo oceânico pelas tensões cíclicas induzidas pelas ondas. Quando estas tensões excederem a resistência do fundo, ocorrem falhas internas, resultando na liquefação do solo oceânico ou em parte dele. (Winterwerp et al., 2007). O fundo resultante pode, então, ser caracterizado como lama fluida. As ondas que agem sobre este fundo geram ondas internas na interface lama-água, que são dissipadas através da fricção interna dentro da camada de lama fluida. Conseqüentemente, a espessura da camada liquefeita é determinada pelas propriedades da lama e do clima de ondas de cada sistema costeiro.

Várias formulações teóricas de dissipação da energia das ondas induzida por fundos lamosos foram propostas com base em diferentes modelos de reologia: fluidos visco-

Newtonianos (Dalrymple e Liu, 1978; Ng, 2000), visco-eláticos (Jiang e Mehta, 1995), visco-plásticos (Mei e Liu, 1987), poro-elásticos (Yamamoto e Takahashi, 1985), de percolação (Liu, 1973), entre outros.

Um dos primeiros modelos analíticos para prever o amortecimento da altura da onda sobre lama fluida foi desenvolvido por Gade (1958). O autor tratou o sistema água-fundo com um sistema de duas camadas fluidas, no qual a camada superior consiste de água não viscosa e a camada inferior de uma lama fluida altamente viscosa. O modelo de duas camadas de Gade ignorou o efeito da viscosidade na camada superior, e os efeitos de elasticidade, porosidade e plasticidade na camada inferior.

Dalrymple e Liu (1978) estenderam a teoria de Gade, desenvolvendo um modelo de duas camadas para estudar a atenuação das ondas sobre fundos lamosos, que foi caracterizado como um fluido Newtoniano laminar viscoso. Eles propuseram um modelo completo, que era resolvido numericamente para todas as profundidades de lama, e uma aproximação analítica para a camada limite para o caso de uma camada de lama espessa. Jiang e Zhao (1989) incluíram o efeito da viscosidade na camada superior. Ng (2000) desenvolveu um modelo considerando lama no fundo caracterizando um fluido viscoso. Alguns autores também estenderam o problema para lama não Newtoniana (Chou et al., 1993; Foda et al., 1993).

Outros autores propuseram modelos viscosos, elásticos e plásticos para descrever o comportamento da lama fluida e o subseqüente amortecimento da onda. Os componentes viscosos e elásticos de alguns modelos podem ser acoplados em série pelo modelo de Kelvin–Voigt (MacPherson, 1980; Hsiao and Shemdin, 1980; Chou et al., 1993) ou em paralelo usando o modelo Maxwell (Maa, 1986; Maa and Mehta, 1990; Jiang and Mehta, 1995; 1996; Rodriguez, 2000; Rodriguez e Mehta, 2001). Mehta (1996) propôs a combinação do acoplamento em série e paralelo através da aproximação de três elementos.

Outras séries de modelos foram propostas por Mei e Liu (1987) e Liu e Mei (1989), nos quais os efeitos das deformações plásticas de fundos lamosos foram considerados nas aproximações chamadas de viscoso-plásticas. O conhecido modelo Bingham (Bingham, 1922) é um dos modelos viscoso plásticos mais utilizados, entretanto vários outros modelos também foram elaborados, tal como o modelo Herschel–Bulkley (Hemphill et al., 1993).

Liu (1973), Yamamoto et al. (1978), Yamamoto e Takahashi (1985) e Spierenburg (1987) incluíram os efeitos de porosidade do fundo do mar através da inclusão da descrição poro-elástica. Verbeek e Cornelisse (1997) aplicaram o modelo poro-visco-elástico. Entretanto com exceção dos processos de fluidização, esses modelos focam em uma única fase da lama. Entretanto, apesar dos modelos preverem diferentes efeitos de amortecimento (Lee, 1995), e cada um deles poder ser aplicado em diferentes situações (Mei e Liu, 1987), nenhum deles cobre a gama inteira de condições de lama encontradas na natureza.

É evidente que o problema da interação entre as ondas e os fundos lamosos tem despertado o interesse da comunidade científica (Holland et al. 2003). Vários estudos baseados em medições de campo e experimentos realizados em laboratório têm mostrado que as ondas que se propagam sobre solos com fundos lamosos sofrem atenuação. Tubman e Suhayda (1976) concluíram que a energia da onda foi dissipada em aproximadamente 50% ao longo de 3.5 km de trajetória sobre a lama fluida através de medições realizadas em East Bay nas proximidades da boca do Rio Mississippi. Wells e Coleman (1981) registraram dissipação de energia em mais de 90% das ondas incidentes sobre 20 km de planícies lamosas ao largo da costa do Suriname. Wells e Kemp (1986) mediram a altura de ondas em três estações na área costeira do Suriname, caracterizada por camadas de lama oriundas do rio Amazonas. Eles observaram que a onda que viajou a partir da estação monitorada mais distante da costa teve sua energia dissipada entre 88% e 96% Quando chegou à costa. Além disso, eles observaram o amortecimento da onda ao longo de todo espectro de energia, inclusive nas ondas mais

curtas. Matthew et al. (1995) encontraram uma diminuição de 85% na altura das ondas e uma redução de 95% na energia incidente causada pela propagação das ondas sobre bancos de lama fluida analisando dados de onda da costa da Kerala, na Índia. Sheremet e Stone (2003) analisaram medições de ondas realizadas em Atchafalaya Bay, onde uma das estações estava localizada em fundo de areia e a outra em fundo lamoso. Eles observaram uma redução maior que 70% na altura da onda no local lamoso em comparação com o local arenoso.

Mais recentemente, Winterwerp et al. (2007) avaliaram o amortecimento das ondas no sistema costeiro da Guiana, através da comparação com dados experimentais e modelados. O modelo utilizado foi baseado na aproximação de um sistema de duas camadas proposto por Gade (1958), e implementado no modelo SWAN. Os valores modelados concordaram com os dados experimentais. Os autores concluíram que o modelo quantificou a atenuação da altura significativa da onda, e que as mudanças computadas no espectro de energia de onda concordaram qualitativamente com os valores medidos.

Logo, a quantificação da energia das ondas em regiões costeiras, e da sua atenuação em função da existência de depósitos lamíticos de fundo, é um estudo dinâmico e particular para cada região. O entendimento desta interação é fundamental para qualquer obra costeira de engenharia, podendo afetar também atividades esportivas náuticas, navais e portuárias (segurança para a praticabilidade do porto, transbordo de navios, entre outras) realizadas nas proximidades da costa. Além disso, o entendimento da interação das ondas com os depósitos lamíticos encontrados em regiões costeiras é essencial para a exploração da energia das ondas. A energia das ondas é uma fonte limpa e inesgotável de energia renovável, ainda pouco explorada na atualidade, que pode contribuir para a melhoria da qualidade da matriz energética brasileira.

As atividades e perspectivas acima apresentadas, e suas respectivas conseqüências e necessidades, destacam a importância do conhecimento do clima de ondas de uma região.

Dentro deste contexto, o desenvolvimento e aprimoramento de ferramentas através das quais seja possível a previsão e o entendimento do comportamento das ondas em regiões costeiras e oceânicas é fundamental.

Até a década de 40, o único modo de descrever o estado do mar era a escala de Beaufort, criada em 1805. Com ela, era possível relacionar a intensidade do vento com a força do mar (WMO, 1998). Em 1943, Sverdrup e Munk desenvolveram o Método da Onda Significativa realizando as primeiras previsões de ondas. Desde então, por várias décadas, foram utilizados modelos empíricos para a previsão de ondas a partir de modificações realizadas no trabalho de Sverdrup e Munk (1947).

Bretschneider (1970, 1973) deu origem a ábacos que relacionavam a pista, a duração e a intensidade do vento com a altura da onda significativa e o período de pico resultante. Esses ábacos, no entanto, consideravam a intensidade e duração do vento constantes e/ou pista ilimitados. Wilson (1955, 1963) contornou parte desta dificuldade criando um método capaz de estimar o comportamento das ondas em um domínio com velocidade de vento variável através da integração de diversas pequenas áreas sobre as quais o vento poderia ser considerado constante.

Pierson et al. (1955) e Khandekar (1989) desenvolveram um método capaz de prever o espectro das ondas através de uma função matemática relacionando o quadrado das alturas das ondas com a freqüência. Este método pode ser considerado como um passo em direção aos modelos espectrais, entretanto, ainda não havia sido desenvolvido uma formulação capaz de descrever a dinâmica da evolução dos espectros (Komen et al., 1994).

A primeira tentativa de desenvolvimento de um modelo numérico de previsão de ondas surgiu na década de 50 (Cavaleri et al, 2007). Desde então, estes modelos vem sendo desenvolvidos com o intuito de prever a propagação das ondas desde a sua zona de geração até as regiões costeiras, possibilitando estudar eventos passados com dados atmosféricos

pretéritos (*hindcasting*), e prever situações futuras, forçando os modelos com condições previstas por análises e previsões (*forecasting*).

Os modelos de ondas podem diferir em vários aspectos, tais como a forma de representar o espectro e as fontes e sumidouros de energia. Gelci et al. (1957) realizou a primeira tentativa de desenvolver um modelo de previsão de ondas baseado na equação diferencial de transporte de escalares, utilizando expressões empíricas para a determinação da evolução espectral. A partir dos trabalhos de Phillips (1957) e Miles (1957) sobre a transferência de energia entre a atmosfera e o oceano, e o estudo de Hasselmann (1962) sobre a função de transferência não linear de energia, foi possível estabelecer a formulação utilizada até os dias de hoje (Komen et al., 1994).

Vários autores (SWAMP, 1985; WMO, 1998) classificam os modelos espectrais baseando-se na determinação do termo de interação não linear. Nos modelos denominados de primeira geração ou desacoplados, cada componente do espectro de energia se propaga com sua própria velocidade de grupo, desenvolvendo-se independentemente dos demais, até atingir um nível individual de saturação. Este nível pode se representado pela energia do espectro de um mar plenamente desenvolvido, através do espectro de Pierson-Moscowitz (1964). Nestes modelos, a interação não linear é desprezada ou, se parametrizada, é considerada pouco significativa, sendo representada de uma forma simples (WMO, 1998). Modelos dessa classe foram utilizados com sucesso por diversos anos. No entanto, sues resultados subestimam o crescimento das ondas (Khandekar, 1989), pelo fato de superestimar a entrada de energia pelo vento e subestimar a interação não linear entre as ondas na região de alta freqüência.

Nos modelos denominados de segunda geração, as interações não lineares são representadas através de parametrizações, impedindo o crescimento independente dos diversos componentes do espectro. Os modelos dessa classe, chamados acoplados, são subdivididos em híbridos e discretos. Os modelos híbridos consideram a forma do espectro

constante na freqüência das vagas para uma grande variedade de situações de geração, com diferenças apenas nas escalas de freqüência e energia (WMO,1998). Com isso, a evolução das vagas é representada através de um ou mais parâmetros adimensionalizados em função da aceleração da gravidade e da intensidade de vento. No entanto, as ondulações não podem ser descritas dessa maneira, uma vez que seu espectro não possui tais características. Neste caso, devem ser utilizados os modelos de primeira geração. Um modelo híbrido poderia ser descrito, portanto, como a combinação entre um modelo paramétrico para as vagas e um modelo desacoplado para as ondulações (WMO, 1998), tendo como vantagem o baixo custo computacional para operação (Janssen et al., 1984).

Nos modelos discretos, todo o espectro é representado em freqüências discretas, eliminando dessa forma os problemas de interface entre vagas e ondulações (SWAMP, 1985). Embora essa representação discreta do espectro seja a principal diferença em relação aos modelos híbridos (Khandekar, 1989), ela pode não ser tão evidente ou vantajosa (SWAMP, 1985; WMO,1998) devido ao menor número de variáveis utilizadas na parametrização da interação não linear em relação ao espectro de ondas, podendo induzir a forma irreal do espectro (SWAMP, 1985). Alguns modelos discretos utilizam como parametrização da interação não linear uma redistribuição de energia baseada em um espectro de forma pré-determinada, como, por exemplo, o JONSWAP (*Joint North Sea Wave Project*) (Golding, 1983). Outra forma de parametrização é uma combinação entre um espectro de desenvolvimento em pista limitada e um espectro exponencial tipo Miles (WMO, 1998). As principais deficiências dos modelos de segunda geração residem na dificuldade de representação de mares complexos gerados por rápidas alterações na direção do vento (WAMDI, 1988).

Nos modelos conhecidos como de terceira geração o espectro é computado pela integração do balanço da energia espectral, sem restrições quanto à forma do espectro

(WAMDI, 1988). O modelo WAM (WAve Model), criado pelo grupo WAMDI (*Wave Model Development and Implementation Group*), foi a primeira tentativa de implementação de um modelo de ondas operacional de terceira geração. Este modelo utiliza duas condições: a parametrização exata da fonte de transferência não linear de energia com o mesmo número de graus de liberdade do espectro, e a especificação de uma função representativa da dissipação que feche o balanço de energia (WAMDI, 1988). Esta interação não linear é parametrizada, de forma a reduzir o esforço computacional, permitindo sua operacionalização (Banner e Young, 1994). A versão para águas rasas inclui, entre outros, um termo de fricção no fundo, a alteração da expressão da velocidade de grupo, a alteração da parametrização do fornecimento de energia pelo vento e os efeitos de refração pela variação da profundidade (WAMDI, 1988). A primeira tentativa de incluir nos modelos de terceira geração a forma exata das interações não lineares de quarta ordem foi feita por Hasselmann e Hasselmann (1981).

Um dos primeiros modelos de terceira geração utilizado para estudar o clima de ondas em águas profundas foi o WAVEWATCH-III (WW3) (Tolman, 2002a), similar ao modelo WAM (WAMDI, 1988 e Komen et al. 1994), que utiliza a equação da conservação de energia espectral. O Modelo WWATCH III é uma evolução de WWATCH I, desenvolvido pela *Delft University of Technology* (Tolman 1990), e do WWATCH II, desenvolvido na NASA (*Goddard Space Flight Center*) (Tolman 1992). Nestes modelos, a energia é discretizada em componentes espectrais, onde as variáveis como altura significativa, período médio, direção, são obtidas. A física do modelo inclui geração de energia, dissipação devido à quebra de ondas e a interação com o fundo, refração, e advecção, e interações não lineares quádruplas. Entretanto a física do modelo não é apropriada para águas rasas (menos de 40 metros de profundidade).

O Modelo SWAN (Simulating WAves Nearshore), desenvolvido pela *Delft University of Technology*, é um modelo de ondas de terceira geração que calcula a propagação espectral da

agitação marítima, sendo projetado para obter uma estimativa realista dos parâmetros de agitação marítima em regiões costeiras e estuários. O modelo é baseado na equação do balanço de energia, e segue a mesma filosofia de modelos de ondas de terceira geração, mas considera o comportamento físico das ondas em águas rasas. Os seguintes processos estão representados para geração e dissipação de energia: geração de ondas pelo vento, dissipação tipo (*whitecapping)*, quebra de ondas induzida pelo fundo, dissipação devido ao fundo e interações não lineares (triplas e quádruplas) (Ris et al., 1994; Booij et al., 1999; Holthuijsen e Booij, 2003; Holthuijsen et al., 2004). A dissipação com o fundo não é só um processo de dissipação de energia na interface água fundo. Shemdin et. al (1978) fez um resumo dos diferentes efeitos de interação com o fundo, onde dois mecanismos foram salientados: amortecimento devido a percolação em camadas com fundo permeável e absorção de energia em camada de fundos lamosos. O SWAN é o único modelo de onda que possui em sua formulação modulo com termo fonte de dissipação de energia para fundos lamosos implementado por Winterwerp et al. (2007).

1.2. Objetivos:

O objetivo geral deste estudo é caracterizar o clima de ondas ao longo da costa do Rio Grande do Sul, com especial enfoque na investigação da atenuação da energia das ondas sobre os depósitos lamíticos existentes na região costeira adjacente à Praia do Cassino, de forma a fornecer subsídios para o entendimento dos processos que controlam a dinâmica e o transporte sedimentar desta região.

Para atingir este objetivo geral, foram desenvolvidos os seguintes objetivos específicos:

- Caracterização do clima de ondas na costa do Rio Grande do Sul com base em dados pretéritos e dados de campo combinados com experimentos de modelagem numérica.

- Investigação do amortecimento da energia das ondas na região costeira adjacente à Praia do Cassino.

- Avaliação da influência dos parâmetros característicos das propriedades de lama fluida na atenuação das ondas na Praia do Cassino.

1.3. Justificativas

A costa do Estado do Rio Grande do Sul (610 km de extensão) está localizada entre 28°S e 34°S (Figura 1.1A), e apresenta orientação Nordeste-Sudoeste, sendo caracterizada por praias arenosas abertas predominantemente dominadas por ondas (Villwock e Martins, 1972). Esta linha de costa possui apenas uma interrupção significativa na entrada da Lagoa dos Patos (32°S) (Figura 1.1B), na cidade de Rio Grande, onde está localizado o único porto marítimo do Estado. A topografia costeira é complexa, o que influencia os processos físicos que determinam as características das ondas e o transporte de sedimentos na costa (Villwock e Martins, 1972).

A lama depositada na antepraia da Praia do Cassino (Figura 1.1C) se origina no estuário Lagoa dos Patos, que recebe aportes continentais de uma bacia de drenagem de aproximadamente 200.000 km^2. O sistema lagunar da Lagoa dos Patos contribui anualmente com 4.5 milhões de toneladas de material particulado em suspensão (Herz,1977 apud Hartmann et al., 1990). Quando a água doce (rica em material em suspensão) se mistura com a água do mar ocorre o processo de floculação. A floculação consiste na coagulação dos sedimentos argilosos ou sílticos que se agregam pela presença de sal (presença de íons de carga elétrica oposta) formando flocos, ficando mais pesados e depositando-se no fundo (Villwock e Martins, 1972). Desta maneira, formam-se os depósitos de lama fluída ao longo da costa do Cassino (Villwock e Martins, 1972).
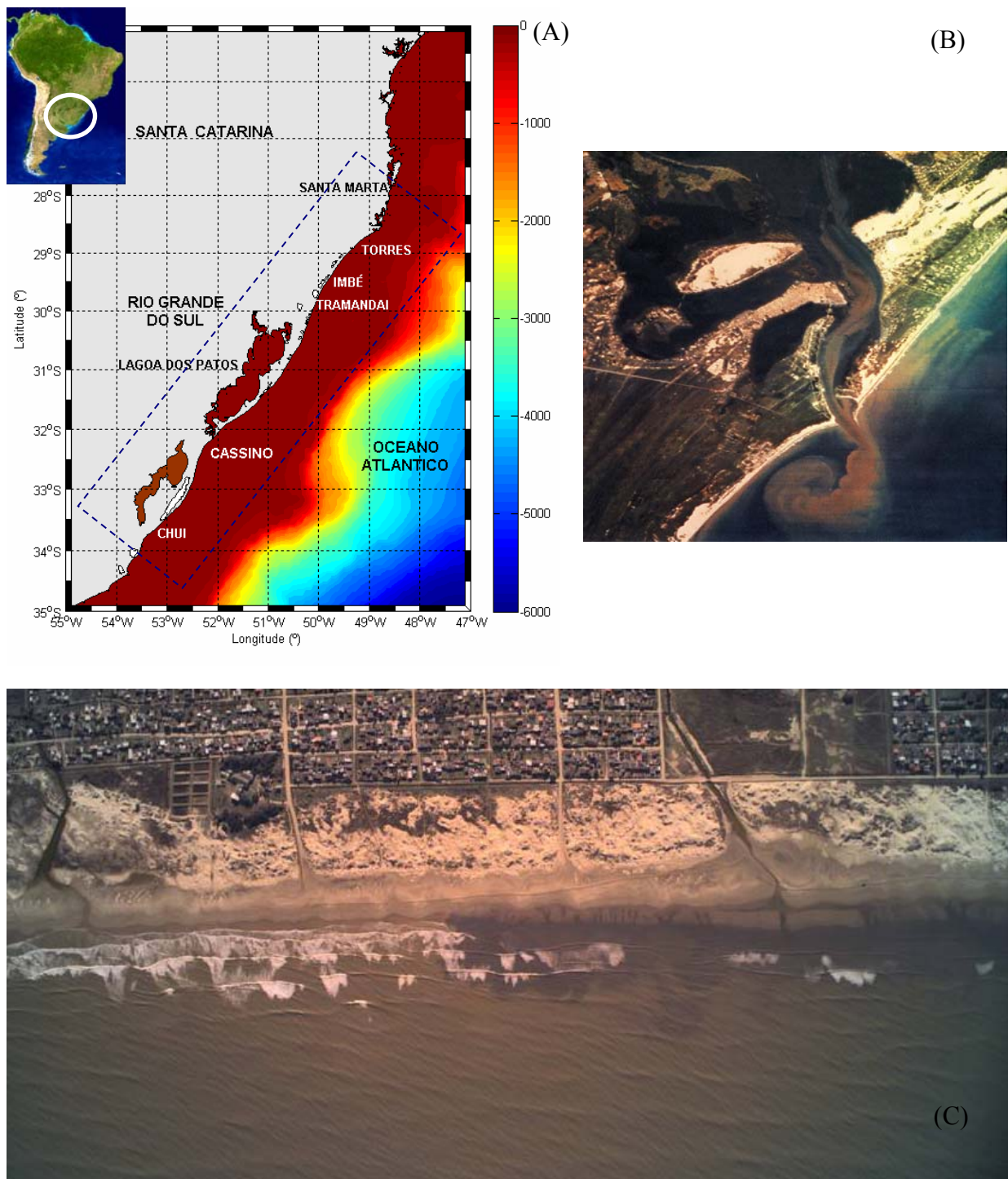
Figura 1.1 – A) Localização da área de estudo. Em destaque a plataforma sul do Brasil. B) Imagem aérea da desembocadura da lagoa dos Patos. C) Foto aérea da praia do Cassino mostrando regiões onde as ondas quebram normalmente, e onde a sua energia é amortecida pela presença de depósitos de lama.

Estes depósitos predominam ao sul dos molhes da barra devido às correntes e ventos predominantes da região (Calliari e Fachin,1993). Além da contribuição natural da Lagoa dos

Patos, contribuições antrópicas locais (dragagens, obras portuárias, ressuspensão de material por hélices de navios), ainda não quantificadas, também devem contribuir para a formação dos depósitos lamíticos da antepraia da Praia do Cassino.

Os sedimentos finos localizados nesta antepraia são esporadicamente remobilizados e lançados sobre a praia e zona de arrebentação (Villwock e Martins, 1972; Calliari et al. 2000), trazendo importantes efeitos de curta e longa duração sobre as características praiais, e conseqüências negativas para o ecossistema e a economia da região.

Calliari, et al (2000), comentam sobre os impactos ecológicos da deposição de lama sobre o mecanismo respiratório da fauna bentônica. O bloqueio deste mecanismo é a principal causa da mortalidade de moluscos, crustáceos e outros invertebrados. Embora não existam registros de acidentes fatais associados ao aprisionamento de banhistas nos bolsões de lama, a ocorrência de vários incidentes envolvendo surfistas ressalta o risco eminente de sinistros. (Figura 1.2). Além disso, as atividades turísticas na região são fortemente afetadas pela ocorrência de depósitos de lama na Praia do Cassino, que recebe mais de 100 mil turistas no verão.

A primeira ocorrência de depósitos estacionários de lama na orla do Balneário Cassino data de 1901, e foi registrada no jornal Correio Mercantil, de Pelotas (Calliari et al.,1999). Desde então, cerca de 30 eventos foram observados. A segunda referência ao fenômeno foi noticiada no jornal Rio Grande, em 29 de dezembro de 1954, onde foi relatado que a praia do Cassino havia sido invadida por uma extensa camada de lama, na qual banhistas ficavam aprisionados (Calliari et al.,1993).

Figura 1.2– Ilustração dos efeitos da deposição da lama na praia do Cassino. A) Impacto sobre a fauna local (Calliari, et at. 2000), B) Resgate do aprisionamento de surfistas C) Carros atolados (Fotos B e C são uma cortesia da Secretaria Especial do Cassino, maio 1998).

Apenas em 1972, os pesquisadores Villwock e Martins (1972) fizeram a primeira descrição científica deste fenômeno, detalhando os mecanismos de deposição e discutindo sobre a origem da lama. De acordo com estes autores e com Martins et al. (1979;1983), a lama que se deposita na parte subaérea da praia teria origem na plataforma continental interna,

em profundidades menores que 10 m, sendo facilmente erodida e colocada em suspensão pela ação de tempestades.

Figura 1.3– Representação esquemática dos eventos de deposição de lama ocorridos na Praia do Cassino. Jornal Agora, novembro de 1998.

Nos eventos de deposição ocorridos em 1987/1988, Borzone e Griep (1991) detectaram e estudaram as características texturais dos depósitos de lama superficial, relacionando sua existência com a formação e a deposição deste material na parte subaérea da praia. Estes autores constataram que os sedimentos lamosos se localizam em regiões mais rasas nos meses de junho, deslocando-se para maiores profundidades nos meses subseqüentes, embora ao sul dos molhes eles reapareçam, a partir de novembro, mais próximos da linha de praia.

Calliari e Fachin (1993) também descreveram a presença de lama superficial entre os 14 e 20 m de profundidade, com as maiores espessuras em direção à praia e na frente do Balneário Querência (3 km ao sul da Praia do Cassino). Neste estudo, foram mapeados depósitos de lama com cerca de 1 m de espessura na antepraia da zona costeira adjacente à desembocadura da Lagoa dos Patos. Os autores concluíram que este material era formado principalmente por silte e argila (Borzone e Griep, 1991). Calliari e Fachin, (1993), confirmaram a presença de fácies lamosa e de lama arenosa em profundidades rasas ao sul da desembocadura, enquanto que ao norte a ocorrência de lama em maiores profundidades.

O mapeamento destes depósitos após as tempestades ocorridas em janeiro e março de 1998 indicaram sua localização próxima à costa, entre as profundidades de 6 a 15 metros,

tendo sua porção mais próxima à praia apresentado um estado mais fluidizado (Calliari et al., 1999). Estas deposições ocorreram na forma de lama fluida, ou seja, concentrações de silte e argila que variam entre 20g 1^{-1} e várias centenas de gramas por litro, com alto teor de água. Logo, estes depósitos podem ser facilmente colocados em suspensão e levados para a praia pelas ondas de tempestade (Willwock e Martins, 1972).

A última e mais extensa deposição de lama na Praia do Cassino ocorreu em 1998, e foi associada a diversos fatores, tais como: remobilização do material depositado na antepraia por fortes tempestades, influência de dragagens no canal portuário, ocorrência de maiores concentrações de material em suspensão e alta precipitação resultante do fenômeno EI Niño. Acredita-se que este fenômeno tenha exercido grande influência neste período, pois promoveu grande precipitação durante todo ano de 1997.

Os estudos anteriores sobre a dinâmica praial mencionados acima estão baseados em observações e mapeamentos superficiais dos depósitos lamíticos.(Calliari et al., 2000) Entretanto, nunca foram feitos estudos sobre a evolução temporal do depósito lamítico e sua influência sobre a morfodinâmica da praia. Entretanto, pelas características da última grande deposição observada, a qual abrangeu uma área de 13 Km de comprimento por 8 Km de largura, e pelas conseqüências ambientais e econômicas observadas na região, é fundamental o entendimento dos fatores que controlam a dinâmica dos depósitos lamíticos observados na Praia do Cassino.

Willwock e Martins (1972) mencionam que a dinâmica destes depósitos lamíticos está diretamente relacionada ao clima de ondas da região. Conseqüentemente, o entendimento da interação entre a dinâmica das ondas na região e os depósitos lamíticos é essencial, com especial enfoque na quantificação da energia das ondas nesta região, e no estudo da sua atenuação em função da existência destes depósitos de fundo. Além disso, a existência e dinâmica destes depósitos na região Sul do Brasil afeta diretamente diversas outras atividades

econômicas desenvolvidas (ou com potencial de desenvolvimento) na região, onde se destacam atividades portuárias e de exploração de energia.

Dos três portos organizados do Estado do Rio Grande do Sul, o Porto do Rio Grande, além de ser o único porto marítimo do Estado, apresenta uma localização geográfica privilegiada na região de maior profundidade do Atlântico Sul, possuindo conexão com o Estado, o País, e com diversos outros países do Mercosul. Nos últimos anos, a combinação entre fatores como a demanda ambiental e comercial e a necessidade de manutenção e expansão da atual capacidade do Porto de Rio Grande, gerou a necessidade de realização de obras portuárias e dragagens visando à melhoria das condições de navegabilidade do seu canal de acesso. As informações necessárias sobre a morfodinâmica, assoreamento, dragagem e despejo de material dragado estão diretamente relacionadas a dinâmica das ondas na região portuária (canal de acesso e área de descarte de material dragado).

Recentemente, através de uma iniciativa da Petrobrás, a viabilidade de instalação de uma usina de geração de energia elétrica a partir da energia das ondas no litoral do Rio Grande do Sul vem sendo analisada. Este estudo de viabilidade do empreendimento originou a necessidade de determinar o potencial energético das ondas na região. Para este estudo, existe a necessidade de determinar a variabilidade espacial e temporal da dinâmica das ondas e das correntes na plataforma continental do Rio Grande do Sul.

Dentro do contexto regional acima apresentado, a combinação entre dados de campo e utilização de técnicas de modelagem numérica figura como a melhor opção para fornecer os subsídios necessários para caracterizar o clima de ondas na costa do Rio Grande do Sul. Especial atenção deve ser dada à atenuação da energia das ondas nos fundos lamosos existentes na região, e ao entendimento dos mecanismos que controlam a remobilização periódica destes bancos de lama presentes na costa. Logo, o desenvolvimento e aplicação de técnicas de modelagem numérica das ondas apresentado neste trabalho é uma importante

contribuição para o entendimento destes processos, permitindo a simulação de eventos passados (*hindcasting*), e futuros (*forecasting*).

1.4. Organização da tese

O Capítulo 1 apresenta a Introdução do trabalho, destacando a importância da zona costeira, a origem dos depósitos de lama observados em regiões costeiras ao redor do mundo, e os processos responsáveis pela sua dinâmica. O efeito das ondas é mencionado como um destes fatores, sendo destacada a importância do entendimento da evolução do campo de ondas de águas profundas para águas rasas e da conseqüente dissipação de energia. O mecanismo conceitual de atenuação de energia em fundos lamosos é apresentado, comentando sobre os principais modelos teóricos desenvolvidos, e sobre estudos realizados no mundo sobre este assunto. Além disso, é apresentada a evolução temporal do desenvolvimento de ferramentas para o estudo do comportamento das ondas, com especial destaque para os modelos numéricos. Na seqüência, são apresentados os objetivos do trabalho, e a sua justificativa, destacando o histórico dos eventos ocorridos na Praia do Cassino e os impactos associados ao fenômeno de deposição de lama na Praia.

O capítulo 2 caracteriza a área de estudo através de sua localização, aspectos físicos e geomorfológicos, clima, maré, ventos, ondas, correntes e ainda faz uma breve descrição de alguns resultados obtidos durante o Experimento Cassino

O capítulo 3 descreve a metodologia utilizada no desenvolvimento do trabalho descrevendo os modelos numéricos utilizados, domínio computacional e condições iniciais e de contorno utilizadas na inicialização dos modelos.

Os capítulos 4 e 5 apresentam os resultados do trabalho, na forma de artigos aceitos ou submetidos para publicação em revistas científicas de renome internacional. É válido ressaltar que os trabalhos são apresentados na íntegra, sendo inevitável a repetição de algumas partes

do texto principal da tese, principalmente no que se refere à descrição da área e à metodologia. As únicas modificações feitas nos artigos referem-se à numeração das figuras e tabelas, que se distinguem pela introdução do número do capítulo ao qual pertencem.

O artigo apresentado no Capítulo 4, intitulado "*Determination of the wave climate for the Southern Brazilian Shelf*", foi aceito em 2008 para ser publicado na revista *Continental Shelf Research*. Este capítulo caracteriza o clima de ondas na plataforma sul do Brasil com base em dados pretéritos e dados de campo combinados com experimentos de modelagem numérica.

O Capítulo 5 apresenta o artigo "*Modeling wave dumping over fluid mud at Cassino Beach coastal area, Brazil,*" submetido em 2008 no *Journal of Coastal Research*. Este capítulo investiga o amortecimento da energia das ondas em regiões de fundo lamoso, onde um estudo de caso foi realizado para a região costeira adjacente a Praia do Cassino, onde foi avaliada a influência dos parâmetros característicos das propriedades de lama fluida na atenuação das ondas. Este estudo foi realizado com base em dados de campo combinados com experimentos de modelagem numérica considerando as propriedades (espessura, extensão, densidade e viscosidade) e localização real do depósito de lama fluida.

O capítulo 6 apresenta uma discussão geral sobre o assunto principal da tese.

O capítulo 7 apresenta as conclusões finais da tese através da integração dos principais resultados obtidos nos artigos. Finalmente, no capítulo 8 são listadas as referências citadas nos capítulos anteriores.

Capítulo 2

Caracterização da Área de Estudo

Capítulo 2

Caracterização da Área de Estudo

2.1 Localização

A plataforma sul do Brasil está localizada entre o Cabo de Santa Marta e o Chuí, entre os paralelos de 28° a 34°S (Castro e Miranda, 1998) (Figura 1.1). A região costeira adjacente à plataforma sul do Brasil é caracterizada pela presença de uma extensa barreira arenosa quase ininterrupta.

A Praia do Cassino (Figura 1.1), área de interesse deste estudo, está inserida na chamada Planície Costeira do Rio Grande do Sul, que apresenta cerca de 700 km de comprimento e até 120 km de largura onde um sistema múltiplo e complexo de barreiras aprisiona o gigantesco sistema lagunar formado pela Lagoa dos Patos e pela Lagoa Mirim (Figura 1.1) (Villwock, 1994).

2.2 Caracterização física e geomorfológica da região

A plataforma continental do Rio Grande do Sul se estende desde a margem continental até aproximadamente a isóbata de 200 metros. A sua declividade é suave, com gradiente médio de 1:1000 na porção sul, aumentando gradativamente em direção ao norte. Apresenta largura variando entre 110 km e 170 km e o seu estreitamento na porção norte exercem influência na hidrografia local e distribuição das propriedades físicas (Zembruscki, 1971). No Estado do Rio Grande do Sul, a largura média da plataforma é de 125 km, com largura máxima e mínima entre 180 e 100 km, com uma sedimentação marcadamente de origem deltaica e litorânea (Martins et al, 1975). Segundo estes mesmos autores, a superfície desta plataforma apresenta feições marcantes como antigas barras, dunas submarinas e restingas paralelas à atual linha de costa. Corrêa e Ponzi (1978) e Fachin (1998), comentam que esta plataforma se caracteriza por inúmeros vales pertencentes à paleodrenagens fluviais e pela presença de inúmeros bancos arenosos com depósitos biodetríticos associados.

Na área adjacente à desembocadura da Laguna dos Patos, a plataforma continental do Rio Grande do Sul apresenta duas regiões com características distintas quanto à morfologia de fundo. A região ao sul da desembocadura apresenta um fundo extremamente homogêneo e liso. Ao norte, a plataforma apresenta irregularidades topográficas representadas por bancos arenosos lineares, cujas diferenças entre cava e crista podem atingir 5 m.

Estes bancos arenosos foram estudados por Figueiredo (1975), Corrêa (1983) e Calliari e Abreu (1984), e encontram-se distribuídos entre as profundidades de 8 a 30 metros, podendo atingir aproximadamente 220 km de extensão, estando por vezes ligados à praia ou separados desta. Os principais bancos arenosos estão concentrados na região central do Rio Grande do Sul, e são denominados Banco Minuano (situado entre 15 e 20 m de profundidade), e Banco Capela (situado em uma região de aproximadamente 10 m de profundidade). Outro banco arenoso de destaque é o chamado Parcel do Carpinteiro, localizado a 30 km ao norte da

desembocadura da Lagoa dos Patos, que foi mapeado por Calliari & Abreu (1984), Calliari et al. (1994) e Fachin (1998).
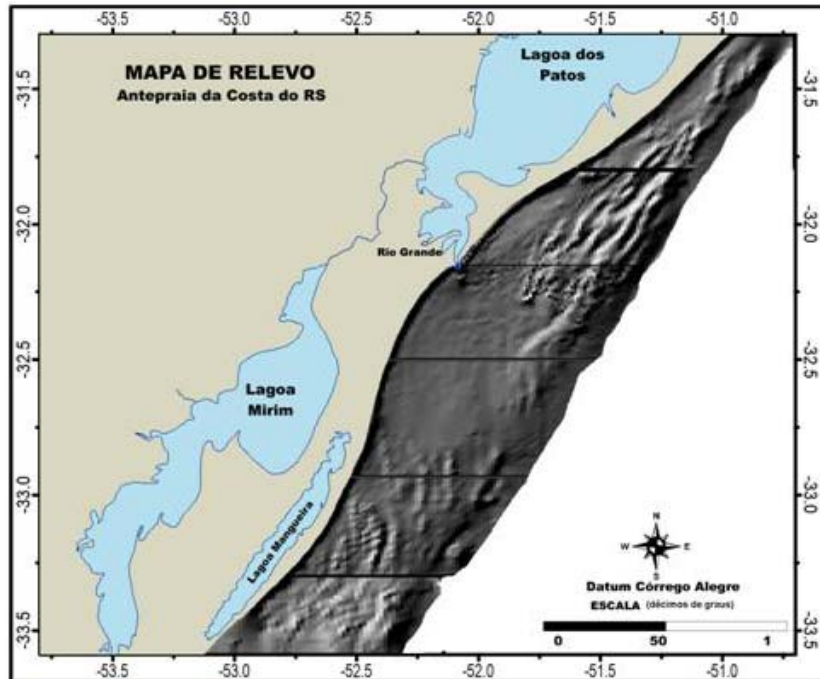
Figura 2.1– Morfologia da plataforma e região adjacente à desembocadura da Laguna dos Patos (Calliari et al. 2007)

O estudo realizado por Calliari e Fachin (1994), mostrou que a região adjacente à desembocadura ao sul da Laguna dos Patos apresenta geomorfologia totalmente diferenciada em relação às regiões norte e do extremo sul (Figura 2.1). Nesta região, a plataforma apresenta-se mais larga, com pequena declividade e totalmente homogênea, com ausência de feições morfológicas e predominância de sedimentos finos. Esta região sofre significativa influência da contribuição de sedimentos finos em suspensão da pluma costeira da Lagoa dos Patos (Marques et al., submetido). A região ao norte e do extremo sul desta área apresentam dois padrões diferenciados quanto à presença e orientação dos bancos arenosos, sendo que ambas as regiões caracterizam-se por apresentarem elevados teores de sedimentos grossos. No extremo sul, os bancos arenosos estão dispostos obliquamente em relação à linha de costa, com direção predominante de sudeste (SE) nordeste (NE). Ao norte, estes bancos apresentam

orientação paralela à linha de costa, são mais extensos e situam-se mais afastados da costa, podendo ser observados em profundidades de 18 a 22 m.

Fachin (1998) também comenta que a ausência de feições morfológicas ao sul da desembocadura da lagoa é causada pelo elevado aporte continental de sedimentos finos da Lagoa dos Patos, e conseqüentemente pela ausência de teores significativos de areia, uma vez que a formação de tais feições morfológicas está associada à hidrodinâmica e presença de sedimentos de granulometria grosseira. A complexidade morfológica da ante-praia e da plataforma interna desta área é o resultado de vários episódios transgressivos e regressivos gerados por mudanças glaciais e pós-glaciais do nível do mar (Calliari e Klein, 1994).

Segundo a divisão da margem continental Sul Riograndense realizada por Martins et al. (1967), as principais províncias faciológicas da plataforma são:

• Seqüência arenosa, entre os 20 e 40 m de profundidade, composta predominantemente por areias quartzosas depositadas em ambiente praial e eólico, retrabalhadas durante o Pleistoceno, que representam o recobrimento mais interno da plataforma em praticamente toda sua extensão. Segundo Martins (1972) esta seqüência arenosa é apenas interrompida nas adjacências da Lagoa dos Patos, pelo fundo lamoso conhecido como Fácie Patos.

• Seqüência transicional mista, consistindo de misturas de lama e areia;

• Seqüência lamítica, constituída por sedimentos finos depositados durante o período Wisconsiniano, que ocorre na plataforma externa e na quebra da plataforma. Este depósito externo, teria uma origem fluvial prévia à formação da ilha-barreira que hoje separa a Laguna dos Patos do Oceano Atlântico.

2.3 Clima
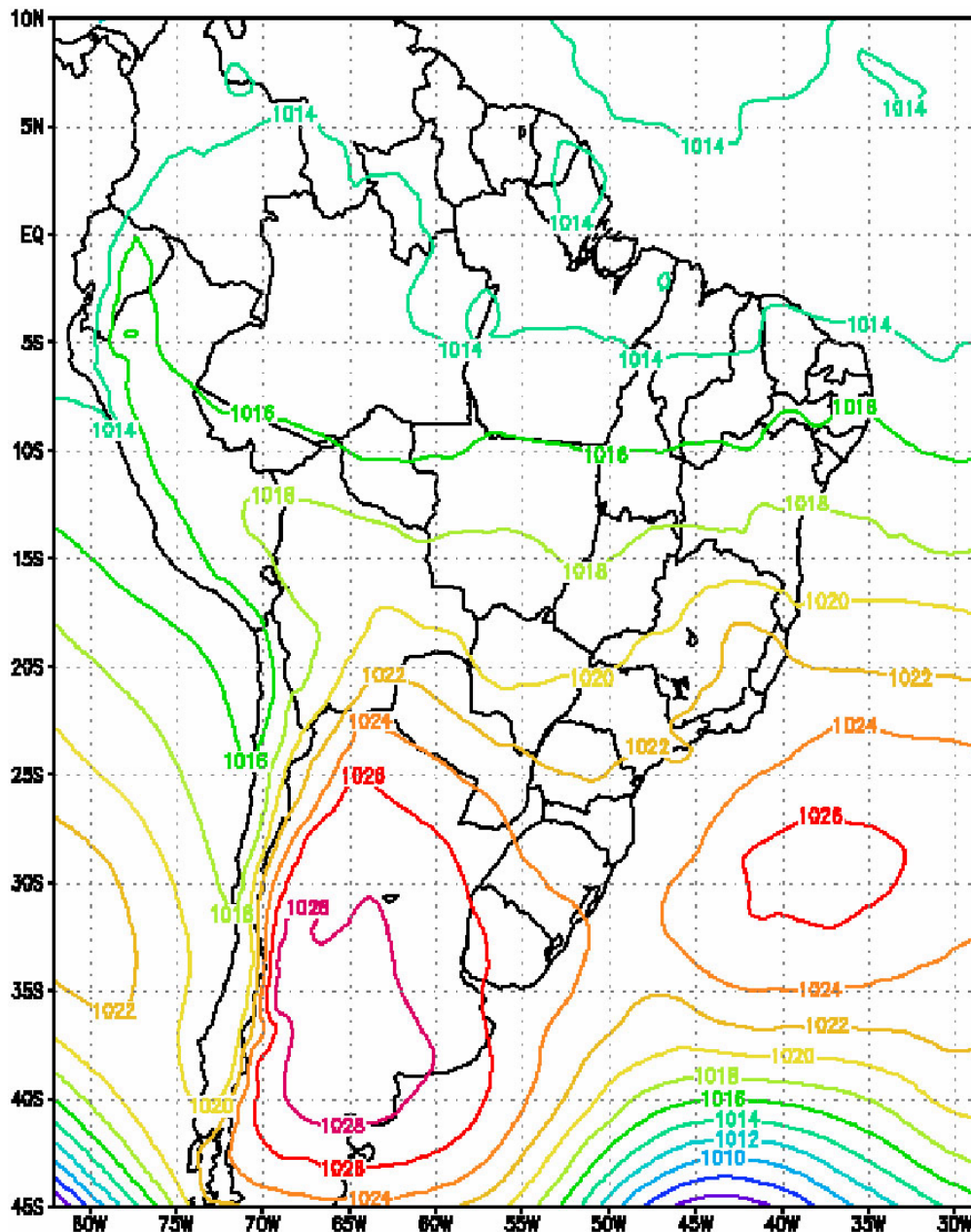
Figura 2. 2 – Previsão de modelo regional (CPTEC/INPE) para 8/7/99 mostrando os dois anticiclones de Fetter (1999).

O clima da região é do tipo subtropical, com temperatura média anual de 17,5°C e média pluviométrica anual de 1300 mm no litoral (Delaney, 1965). As temperaturas médias mensais variam entre 13°C e 24°C em junho e janeiro, respectivamente. (IBGE, 1986). A região está sobre a influência de dois centros de alta pressão, o Anticiclone do Atlântico Sul, mais ativo

durante os meses de verão, e o Anticiclone Polar, mais influente durante o inverno, o qual durante a sua passagem provoca a diminuição da temperatura (Figura 2.2). A precipitação pluviométrica anual (1200-1500 mm) varia marcadamente a cada ano e está relacionada, principalmente, ao padrão e freqüência da passagem de frentes frias (Paz, 1985; Hartmann et al., 1986; Nobre et al., 1986; Gan, 1992; K1ein ,1998).

2.4 Forçantes físicas - maré e ventos

De acordo com Tomazelli e Villwock (1992), na costa do Rio Grande do Sul, as marés astronômicas são de pequena amplitude e secundárias em relação às variações de nível associadas à ação dos agentes meteorológicos (ventos e pressão atmosférica). Segundo a Tábua de Marés da Diretoria de Hidrografia e Navegação do Ministério da Marinha do Brasil, a amplitude média de maré no Rio Grande do Sul é de 50 cm. Portanto, de acordo com a classificação proposta por Davies (1980), esta é uma costa de micromarés.

As principais oscilações do nível do mar que afetam a região são condicionadas por períodos de tempestade, devido aos fortes ventos associados à migração dos centros de alta pressão (Tomazelli e Villwock, 1992). Esta influência meteorológica, que pode promover a subida e descida do nível do mar é conhecida como maré meteorológica. Na costa do Rio Grande do Sul, as marés meteorológicas causadas pelos ventos do quadrante Sul chegam a promover uma elevação do nível do mar de até 2 m. Tozzi (1995), Calliari et al. (1998) e Calliari e Pereira da Silva (1998), consideram as marés meteorológicas como agentes efetivos na erosão das praias e na retração das dunas frontais na costa gaúcha. Quando este fenômeno ocorre em combinação com marés astronômicas de sizígia, as conseqüências podem ser intensificadas, causando as maiores variações morfológicas do perfil praial na costa do Rio Grande do Sul.

Delaney (1965) apresenta as médias anuais e sazonais de vento em diferentes posições geográficas no Rio Grande do Sul, verificando o predomínio de ventos com direção nordeste (NE), principalmente para a região norte do Rio Grande do Sul. De acordo com os estudos de Bicalho (1883, apud Calliari, 1980), os ventos da região podem ser classificados em quatro grupos. O primeiro grupo é formado pelos ventos de nordeste (NE), norte nordeste (NNE) e leste nordeste (ENE) constituindo o grupo dos ventos predominantes, sendo o de nordeste (NE) o principal. Os ventos de leste (E), sul (S) e sudeste (SE) formam o segundo grupo, sendo o de sudeste (SE) o vento predominante deste grupo. O terceiro grupo é formado pelos ventos de sul sudoeste (SSW), de sudoeste (SW) e de oeste sudoeste (WSW). Estes ventos são causadores de tempestades, e junto com os ventos de sudeste (SE) e de sul (S), provocam o empilhamento de água junto à costa, elevando o nível do mar. O último grupo é formado pelos ventos de norte (N) a oeste (W), especialmente o de noroeste (NW), que tem menor importância devido à sua fraca intensidade.

Analisando dados de intensidade e direção de ventos na região entre Rio Grande e Torres, Tomazelli (1993) também verificou que a direção predominante dos ventos é de nordeste (NE), existindo algumas diferenças significativas entre as estações do ano. Apesar da direção mais freqüente ser de nordeste (NE), os ventos com maior intensidade são os ventos de sul (S), de sudoeste (SW) e de oeste (W). A maior variabilidade direcional dos ventos foi registrada em Rio Grande, causada por sua posição mais meridional em relação às outras estações (Imbé e Torres no litoral norte) e sua localização em território plano, aberto, e distante de qualquer efeito relacionado à topografia.

De forma semelhante, na região sul entre Rio Grande e Chuí, existe uma predominância de ventos provindos do quadrante nordeste (NE) nos meses de setembro a fevereiro, e os de sudoeste (SW) de abril a agosto (Godolphim, 1976). Para esta região, ventos de sudoeste (SW), sul (S) e sudeste (SE) estão associados a eventos de tempestade, principalmente nos

meses de inverno, e são importantes por sua intensidade (Delaney, 1965; Herz, 1977; Calliari, 1980).

Mais recentemente, o Atlas Eólico do Rio Grande do Sul (Camargo et. al., 2002) foi criado a partir de medições realizadas através de anemômetros e dados de reanálise (NCAR), para um período representativo de quinze anos (Figura 2.3).
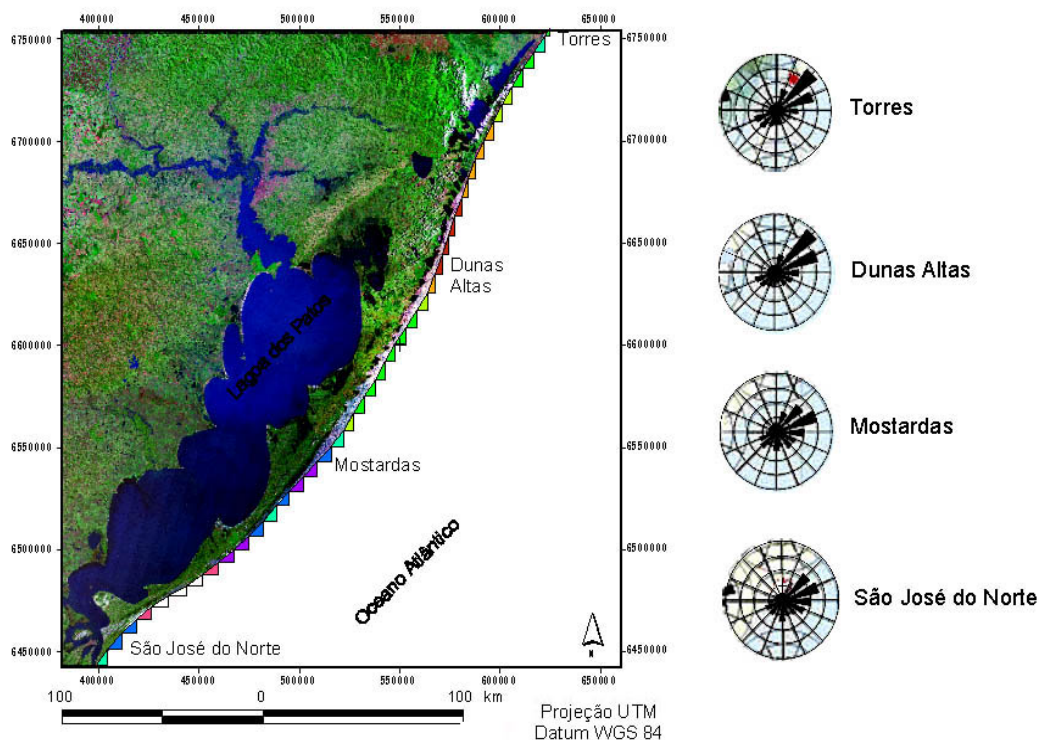
Figura 2. 3 – Freqüência e intensidade dos ventos no litoral do Estado do Rio Grande do Sul, de acordo com Camargo et. al. (2002).

De acordo com o diagrama da rosa dos ventos deste atlas, as estações mais ao norte apresentam ventos de nordeste (NE) e de leste (L) com maior freqüência e intensidade. De Mostardas para o Sul, a freqüência e intensidade dos ventos de nordeste (NE) são reduzidas notando-se um aumento regional das componentes de sudeste (SE) e de sul (S). Krusche et. al. (2003) calculando as normais climatológicas provisórias para Rio Grande entre 1991 e 2000 encontraram também o vento de nordeste (NE) como predominante, tendo, porém determinado o de sudeste (SE) como vento secundário.

Cuchiara et al. (2007) realizaram análises preliminares dos dados de vento obtidos durante o Experimento Cassino, no período entre 13 de maio e 25 de junho de 2005, através de medições realizadas na Praia do Cassino (Figura 1.1). Os dados foram coletados a 10 m de altura do solo e registrados de 10 em 10 min. Os resultados mostraram que no período analisado os ventos predominantes foram de nordeste (NE) e de sul (S) (Figuras 2.4 e 2.5).
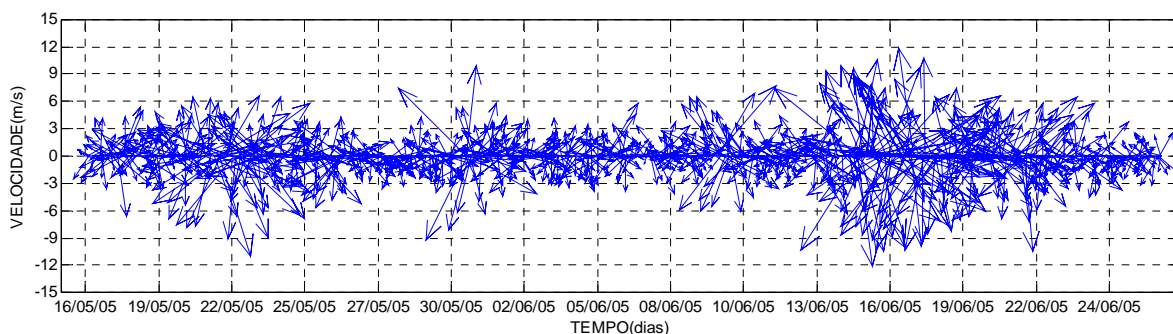
Figura 2. 4 - Série temporal de velocidade média e direção vento medido na Praia do Cassino entre 15/05 e 25/06 de 2005. Valores positivos (negativos) indicam ventos de norte (sul).
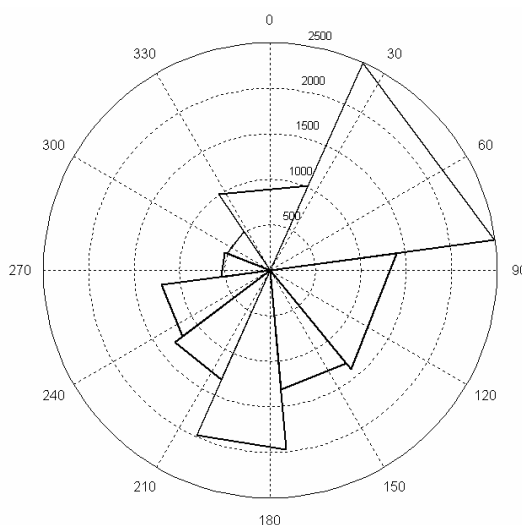
Figura 2. 5 – Freqüência de ocorrência da velocidade e direção do vento medidas na Praia do Cassino entre 15/05 e 25/06 de 2005.

2.5 Ondas

Embora não exista um estudo sistemático do clima de ondas na costa do Rio Grande do Sul como um todo, alguns trabalhos foram realizados buscando caracterizar certas regiões da costa. Estes trabalhos estão baseados em diferentes fontes de dados, que abrangem a

utilização de ondógrafos, observações de campo, dados históricos em navios de oportunidade e sensores remotos.

No início dos anos 60, dados de ondas registrados por Wainer (1963) e posteriormente por Motta (1967) para a região da desembocadura da Laguna de Tramandaí, e por Motta (1969) para a desembocadura da Lagoa dos Patos, foram extrapolados para diferentes regiões da costa do Rio Grande do Sul. Nesta época, segundo as *Sea and Swell Charts* do *U.S. Hidrographic Office* (1943, apud Motta, 1969), o clima de ondas para águas profundas foi considerado semelhante para toda a costa do Rio Grande do Sul.

Motta (1969) determinou a altura máxima de onda em Tramandaí em função de dados obtidos entre outubro de 1962 e setembro de 1963 (12 meses de dados), utilizando um ondógrafo não direcional, fundeado a 17,5 m de profundidade. A altura máxima observada foi de 7,0 m em abril de 1963, e a altura significativa máxima foi de 4,8 m, ambas para um período de retorno de 30 anos. Para um período de retorno de 100 anos, a altura máxima foi de 7,6 m e a altura significativa máxima de 5,5 m. A direção de incidência das ondas foi adquirida visualmente indicando que, no local de observação, predominavam cristas praticamente paralelas à costa.

Estudos realizados por Coli (1994) combinaram a análise de dados de altura e direção de ondas obtidos através de navios de oportunidade (entre 1946 e 1979), com dados do satélite Topex/Poseidon (1993), e determinaram a variação espacial e temporal na altura e na direção das ondas para as áreas costeiras e oceânicas do estado do Rio Grande do Sul. Seus resultados mostram que as ondas de inverno são maiores que as de verão. As ondas com direção de nordeste, leste e sudeste possuem maior ocorrência na primavera e verão, enquanto que as de norte, oeste e sudoeste se amplificam no outono e inverno. Os valores mais expressivos de altura média correspondem à direção sudoeste e, secundariamente as direções sul, oeste e norte. Quanto à média anual para cada um dos quadrantes de direção de propagação das

ondas, os dados demonstraram uma grande diversidade nas direções, possuindo como ocorrência principal ondas provenientes de nordeste, seguidas pelas ondulações de sul. Através da análise dos dados do satélite Topex/Poseidon, foi possível averiguar que na porção oceânica sul da área de estudo predomina as maiores ondas em relação à porção norte da mesma. Abaixo da latitude de 33ºS, os mapas históricos demonstram a permanência de núcleos de maiores alturas de ondas, os quais aumentam espacialmente e se intensificam no outono, atingindo um máximo no inverno.

No final dos anos 90, Strauch (1998) realizou medições com um ondógrafo direcional do tipo Waverider localizado na boca do estuário da Lagoa dos Patos. O instrumento foi fixado a 15 m de profundidade com o objetivo fornecer informações preliminares sobre as características da agitação local e a determinação da onda de projeto para a área.
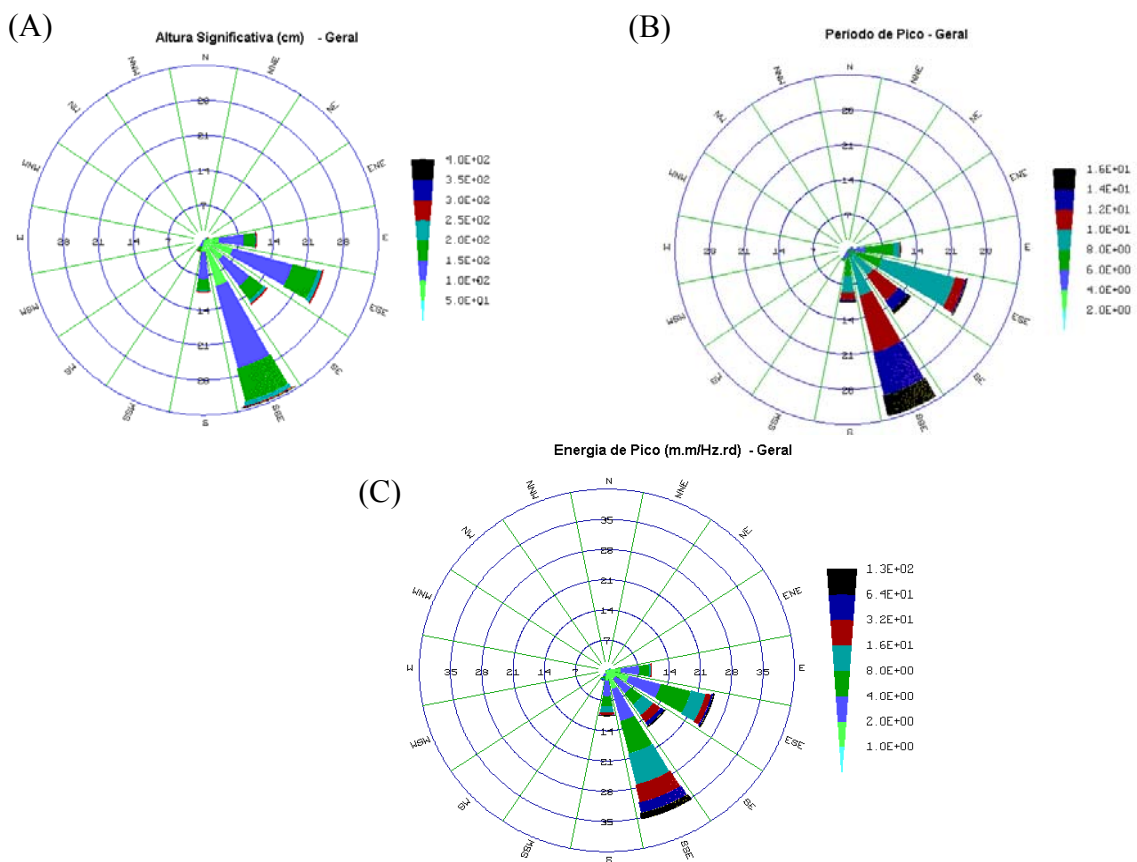
Figura 2. 6 – Histograma polar dos parâmetros das ondas para o período de outubro/96 a agosto/97 e de janeiro/98 a abril/98. A) Altura significativa, B) período de pico e C) energia de pico. (Strauch,1998).

Os dados obtidos mostraram altura significativa média de 1,0 m na direção 100º SE, com período variando entre 10 e 12 s correspondendo a ondulações (*swell*), e vagas (*sea*) com altura significativa média de 1,5 m na direção 160º SE, com período variando entre 6 e 8 s.(Figura 2.6). Nesta direção foram observados os maiores picos de energia de ondas. Os valores máximos de altura significativa foram observados em abril de 1998, alcançando 4,2 m, com direção de propagação de 140º.

Mais recentemente, Coli (2000) descreveu o clima de ondas de superfície para a região próxima aos Molhes da Barra de Rio Grande, com base em um arquivo histórico (1949 e 1979) composto por ondas estimadas visualmente a partir de navios de oportunidade, e dados de onda adquiridos por um ondógrafo direcional entre outubro de 1996 e agosto de 1997. A partir destes dados, foi realizada uma estatística de curto e longo prazo. O autor concluiu que a onda característica de curto prazo para a região tem altura significativa entre 1,0 e 1,5 m, período médio entre 5 e 6 s e direção predominante de sudeste. Não foram encontradas alturas significativas de ondas maiores que 4 m, e não houve período médio maior do que 12 s nos registros do arquivo instrumental. Embora os parâmetros de altura e período não tenham apresentado variações significativas entre as estações do ano, foram encontradas diferenças na forma do espectro da onda. Nos meses de verão a posição do pico espectral foi mais freqüente na porção das vagas (8 a 10 s), enquanto que no inverno esteve nos períodos característicos de ondulação (10 a 14 s).

Cuchiara et al. (2007) realizaram análises preliminares nos dados de ondas obtidos durante o Experimento Cassino, no período entre 13 de maio e 25 de junho de 2005, através de um ondógrafo direcional com aquisição digital fixado a 25 m na Praia do Cassino (32°26'37" S e 51° 55' 53"). Na figura 2.7 está representada a série temporal das alturas significativas fornecidas diariamente pelo ondógrafo para o período analisado.
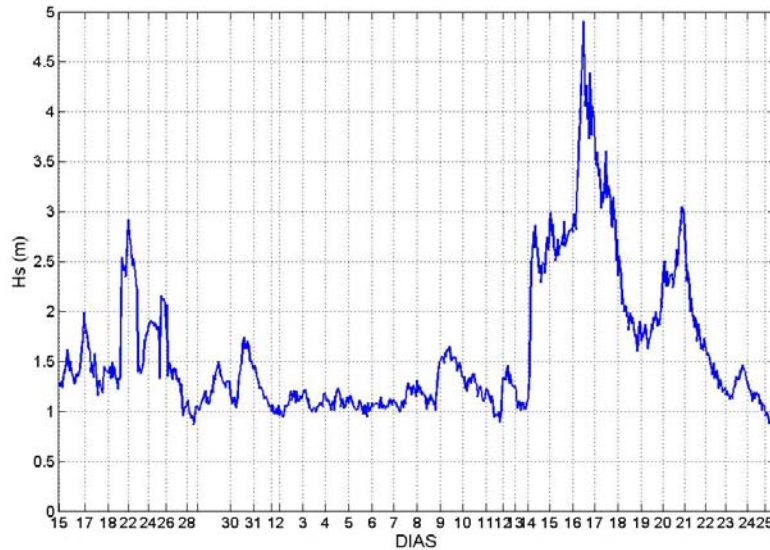
 Figura 2. 7 – Altura significativa medida por ondógrafo direcional localizado a 32º10'002"S e 51º58'913" W no período entre13 de maio e 25 de junho de 2005, durante o experimento Cassino. (Cuchiara et al., 2007).

A distribuição de freqüência conjunta dos principais parâmetros de onda, altura significativa, período de pico e direção média, obtidos a partir da análise realizada nos dados espectrais registrados pela própria bóia estão representados no histograma polar da figura 2.8.
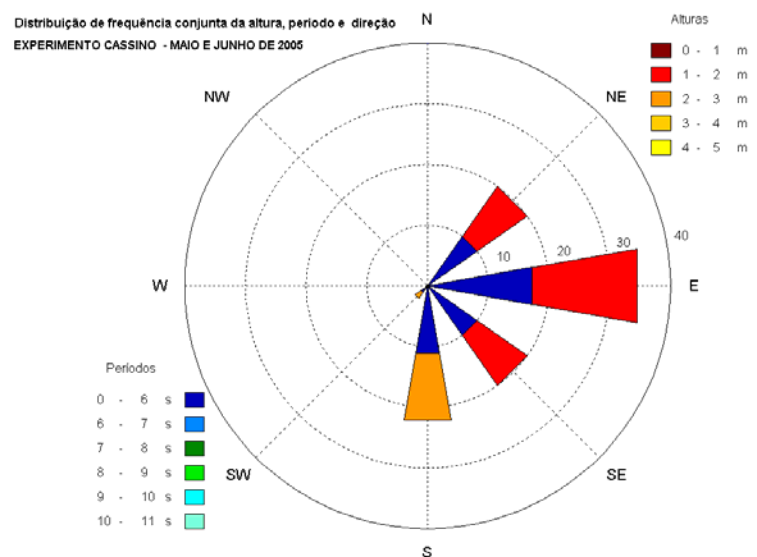
 Figura 2. 8 – Histograma polar da distribuição de freqüência conjunta da altura significativa, período médio e direção das ondas medidas no período entre 13 de maio e 25 de junho de 2005, durante o Experimento Cassino. (Cuchiara et al., 2007).

Neste histograma polar, a altura dos triângulos isósceles radiais representa a freqüência de ocorrência para cada setor de 45°, a parte mais externa dos mesmos corresponde ao intervalo de classe de altura, e a mais interna representa o intervalo do período. Os resultados indicam altura significativa de onda entre 1.0 e 3.0 m, período médio menor que 6 s e direção predominante de nordeste (NE) e de sul (S). (Figuras 2.7 e 2.8).

A compilação dos dados existentes sobre o clima de ondas ao longo da costa do Rio Grande do Sul caracterizou um comportamento típico de agitação local baseado nas análises estatísticas de distribuição de freqüências, que relacionou os valores predominantes de altura, direção e período das ondas. Os resultados indicaram que na plataforma sul do Brasil a direção predominante das ondas é entre 100º e 160º(E-SE), com altura das ondas variando entre 1 e 1,50 m. O período das ondas variou entre 6 e 14 s, com predominância de período médio da onda de 8 s (vagas) e 12 s (ondulações).

O estudo do clima de ondas através de experimentos de modelagem numérica, por outro lado, figuram como uma importante ferramenta para avaliação e entendimento de processos influenciados pelas ondas. Alguns destes fenômenos necessitam de séries temporais de ondas de longo período. A falta destes dados pode ser suprida através da utilização da modelagem numérica na reconstituição de eventos passados ou previsão de eventos futuros. A precisão dos resultados desejados depende diretamente da escolha do modelo e das condições de contorno utilizadas nas simulações. Dentro deste contexto, estudos relacionados com a implementação de condições de contorno são cada vez mais importantes para o estudo do comportamento físico das ondas.

2.6 Correntes

A deriva litorânea promovida basicamente pela incidência oblíqua de ondas na costa, resultante do deslocamento lateral de sedimentos arenosos ao longo da linha da costa do Rio Grande do Sul, se processa em ambos os sentidos da linha de costa, mas com predominância no sentido NE. Motta (1967), e Tomazelli e Villwock (1992) demonstraram que a ação morfogênica na costa do Estado Rio Grande do Sul, relacionada à ação de correntes, é controlada basicamente pelas correntes litorâneas induzidas por ventos e ondas. Concluíram através da análise do regime de ondas, pela configuração retilínea da costa e por indicadores geomorfológicos, que a deriva litorânea de sedimentos arenosos na costa do Rio Grande do Sul tem uma direção dominante no sentido nordeste (NE). Toldo Jr. et al. (1993) realizaram medições de correntes longitudinais na Praia de Imbé, onde encontraram valores de velocidades da ordem de 0,9 m s^{-1} e observaram que existe um nítido domínio das correntes com sentido nordeste (NE) ,em relação às correntes com sentido sudoeste (SW).

2.7 Experimento Cassino

Calliari et al. (2005) descreveram a fase experimental do Projeto Cassino, realizada entre 26 de abril e 29 de maio de 2005 na Praia do Cassino (Figura 1.1), 9 Km ao sul dos molhes de Rio Grande. O Projeto Cassino é um projeto internacional realizado em colaboração com cientistas do Brasil, Estados Unidos, Alemanha e Holanda, e financiado pela *US Office of Naval Research* e o *Naval Research Laboratory*. O principal objetivo do projeto é o entendimento dos mecanismos que controlam a remobilização periódica dos bancos de lama presentes na costa do Rio Grande do Sul, bem como a avaliação da atenuação da energia das ondas sob estes fundos lamosos. Para atingir estes objetivos foram realizadas campanhas de campo, análises de caracterização do sedimento, e experimentos de modelagem numérica. O

Projeto Cassino ocorreu em duas fases: 1) mapeamento e caracterização dos depósitos sedimentares, e 2) realização de um experimento de campo para coletar dados sinópticos e multidisciplinares dos campos de ondas e características dos depósitos de sedimentos da ante-praia .

O mapeamento superficial e sub-superficial dos depósitos de lama foram realizados através de levantamentos ecobatimétricos, sísmicos e de amostragem geológica, efetuados entre 18 e 19 de outubro de 2004 e entre 26 e 28 de março de 2005. A área mapeada foi escolhida com base em trabalhos anteriores associados a observações visuais da variação de energia das ondas na zona de arrebentação. Foram usados dois ecobatímetros de 200 kHz (*Raytheon* e *Odom-hydrographics*) e um perfilador sísmico de 2-16 kHz (*GEOSTAR/Edgetech*), sendo a perfilagem contínua posicionada através do sistema DGPS da Omnistar. Esta perfilagem conjunta efetuada desde o início dos levantamentos permitiu verificar que a lama fluída era caracterizada por registros que mostravam um padrão de eco duplo nos ecobatímetros. No primeiro levantamento, efetuado em outubro de 2004, lama fluída foi mapeada entre 5 e 14 m de profundidade. Os levantamentos de março de 2005 identificaram lama fluída em profundidades maiores, a partir de 8 m, indicando que o depósito migrou para *offshore* ou foi coberto por depósitos arenosos. Em maio de 2005 novos levantamentos foram efetuados através de um *jet ski* com ecobatímetro de 200 kHz. Através destes dados, foi possível associar diferentes padrões de ecos a fácies de areia, lama fluída e lama mais densa. Neste levantamento foi identificada lama fluída com densidade média de 1.14 g cm^{-3} a partir de 8 m de profundidade. Os resultados obtidos nestes levantamentos foram registrados no mapa de isópacas da lama fluida (Figura 2.9), mostrando espessura máxima de 0.6 m no centro do depósito, e diminuição tanto em direção à praia quanto para maiores profundidades. Trabalhos anteriores identificaram esse mesmo padrão para o depocentro do depósito nesta região, porém numa faixa batimétrica mais profunda (Calliari et

al.,2000). Da mesma forma, a maior largura do depósito de lama fluida coincide com o vórtice associado à pluma de material em suspensão quando as águas da lagoa em forma de jato deixam a extremidade dos molhes (Figura 1.1C). Os autores associaram ainda o estreitamento do depósito para o norte com a área de proteção que se prolonga por 3 Km a partir do molhe oeste.
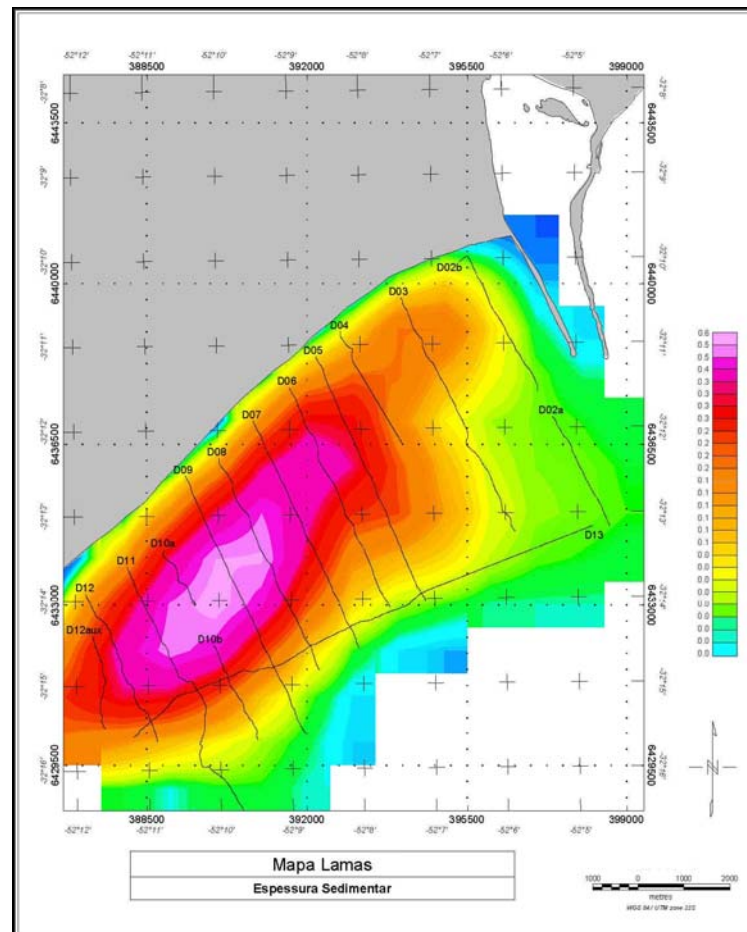
Figura 2. 9 - Mapa da espessura de lama fluída obtido pelo eco duplo do ecobatímetro de 200 KHz. (Calliari et al.,2005).

Durante o trabalho de campo realizado em maio de 2005, foi fundeado na zona de arrebentação (2 m de profundidade) uma torre instrumental com um conjunto vertical de 5 correntometros eletromagnéticos (Ems), 4 turbidímetros de reflectância óptica (Obs) e dois sensores de pressão (Figura 2.10).
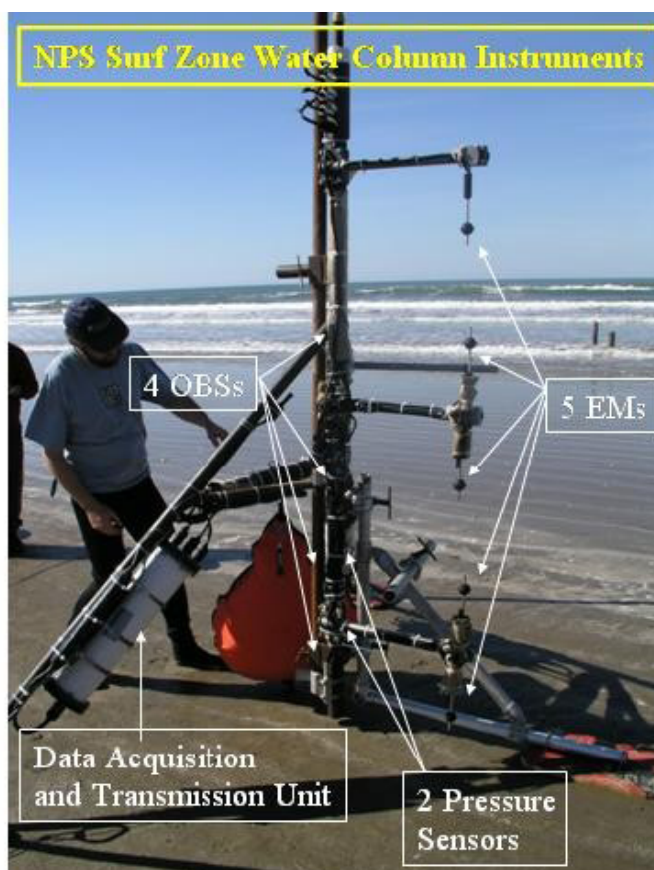
Figura 2. 10 - Torre de instrumentos com Correntômetros eletromagnéticos (EM), Sensores ópticos de refletância (OBSs), sensores de pressão e sistema geral de aquisição dos dados (Calliari et al.,2005).

Adicionalmente, 4 aparelhos (PUVs), cada um contendo um sensor de pressão, um correntômetro eletromagnético e dois sensores ópticos também foram instalados num perfil transversal a praia, tendo a torre como centro. A profundidade destes PUV's variou entre 0.5 m e 2.8 m. A disposição dos equipamentos pode ser vista na Figura 2.11.
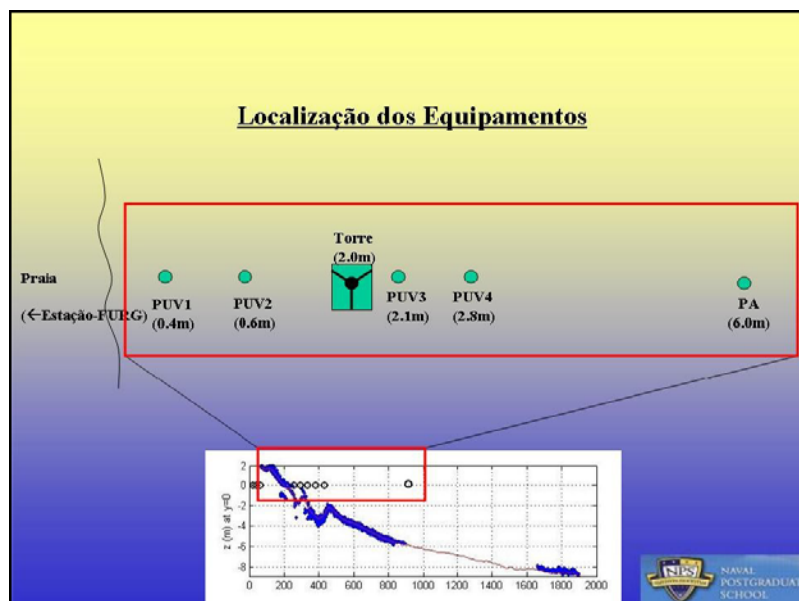
Figura 2. 11 - Perfil esquemático da posição dos equipamentos ao longo da zona de surfe (Calliari et al.,2005).

A Figura 2.12 apresenta algumas das séries temporais obtidas com esta estrutura, entre 21 e 26 de maio. Os dois primeiros gráficos indicam que a altura significativa das ondas variou entre 1 e 2 m, com seu período de pico oscilando entre 6 e 15 s. Entretanto, valores superiores a 10 s foram observados na maior parte do tempo. O gráfico do meio mostra a velocidade das correntes transversal e longitudinalmente à costa (cm s^{-1}). A velocidade transversal registrada pelo correntômetro EM3 (Figura 2.11) mostra que a velocidade transversal permaneceu sempre com valores inferiores a 50 cm s^{-1} e em direção ao mar. A linha em vermelho indica que a velocidade da corrente longitudinal atingiu valores superiores a 50 cm s^{-1}, predominantemente para norte. Os autores salientam duas inversões no sentido da corrente. A primeira para sul antes do dia Juliano 144, tendo permanecido nesse sentido durante aproximadamente 12 horas e atingindo valores máximos de 50 cm s^{-1}. Após estas 12 horas, ocorreu outra reversão para norte, com valores baixos durante o mesmo período de tempo e atingindo novamente valores máximos de 50 cm s^{-1}. Os resultados indicam que durante este período a corrente longitudinal para norte esteve associada a maior altura significativa das ondas. A inversão da corrente para sul esteve associada à diminuição progressiva de

aproximadamente 0.6 m na altura significativa das ondas. Nenhuma relação entre a direção da

corrente e o período de pico das ondas foi observada.
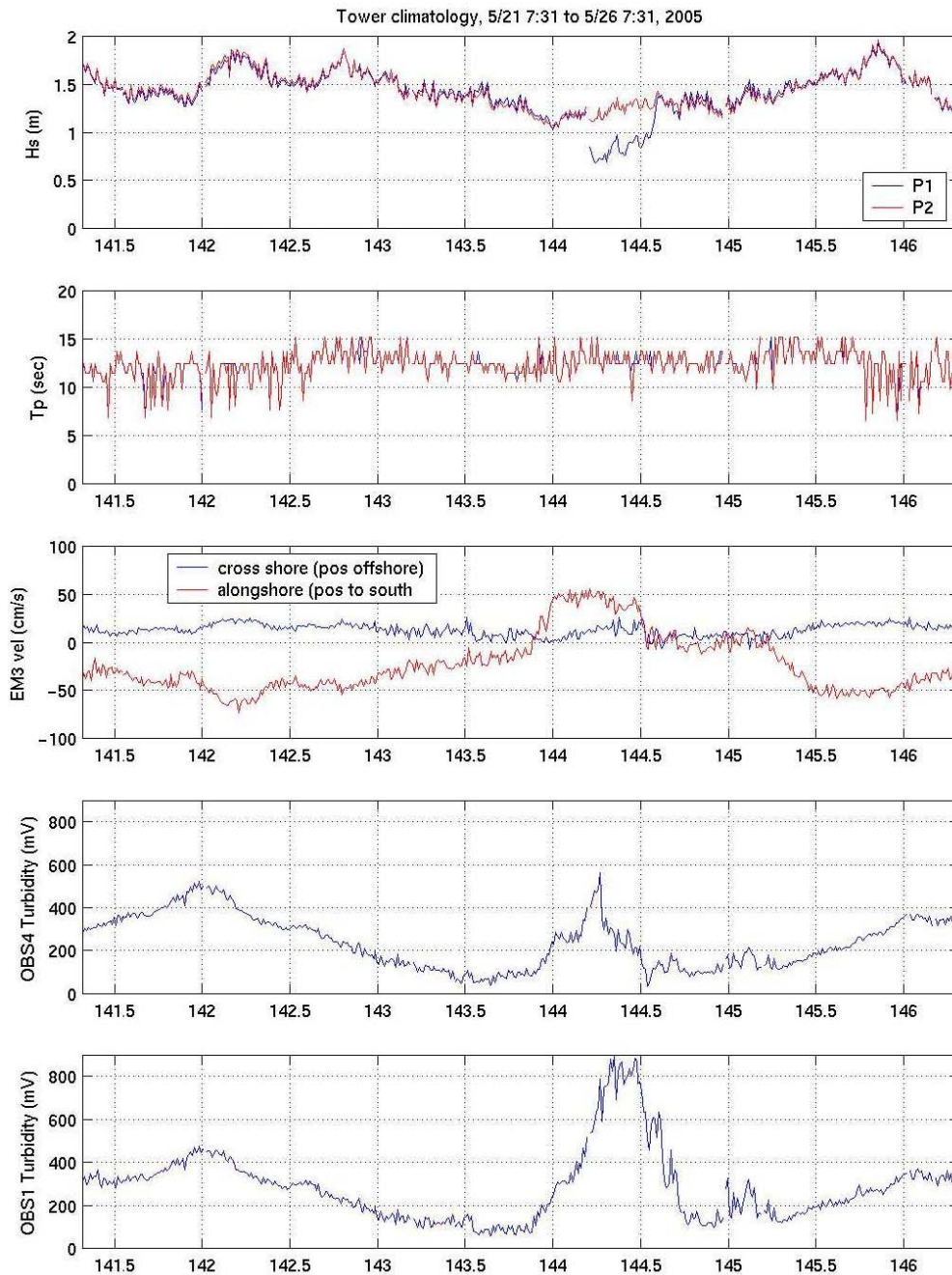
Figura 2. 12 - Gráficos de altura significativa das ondas (Hs), período de pico Tp, velocidade de

corrente no correntômetro eletromagnético EM3 e dados não calibrados dos sensores de turbidez

OBS4 e OBS1. (Calliari et al.,2005).

Os dois gráficos inferiores mostram valores de turbidez ainda não calibrados medidos

pelos dois turbidímetros (OBS4) e (OBS1) (Figura 2.11), posicionados ,respectivamente, a

maior e menor altura na torre. Os dados mostram um aumento brusco da turbidez, coincidente com a inversão da corrente para sul. Os autores comentam que a interpretação completa destes resultados será finalizada quando associada com os dados do ondógrafo fundeado *offshore* e com as medições meteorológicas da estação da FURG localizada no local do experimento.

Calliari et al. (2005) concluíram que a metodologia empregada para mapeamento dos depósitos de lama, tanto fluida como mais compactada, mostrou-se eficiente podendo a mudança de fundos de areia para lama fluída e daí para compactada possível de ser delineada com ecobatimetros de 200 Khz. A batimetria da zona de surf obtida com o *jet ski* mostrou-se um método rápido e preciso para mapeamento da zona de surf e da ante-praia em locais com fundos de areia, e de lama com densidade variável. As modificações morfológicas dos bancos ocorridas em função da mudança nas condições hidrodinâmicas mostraram-se significativas, e corresponderam a alterações de dois bancos rítmicos para lineares sem ritmicidade.
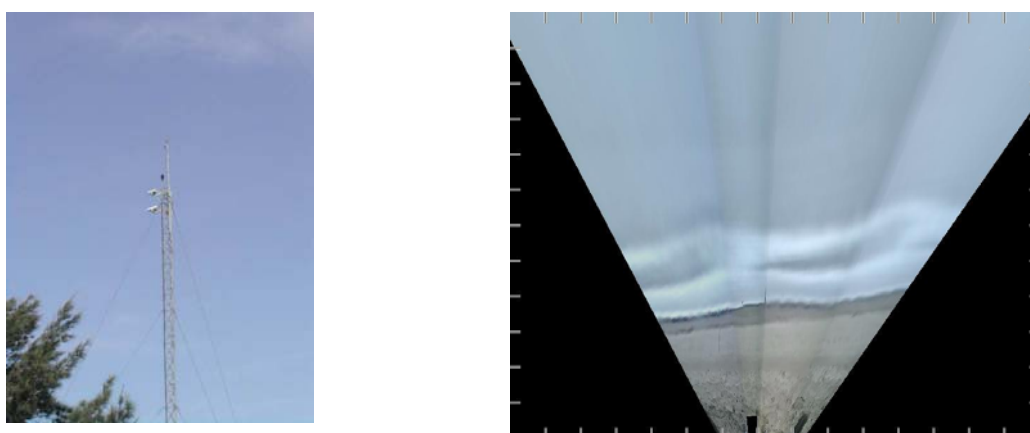
Figura 2. 13 – A) Torre onde foram istaladas as cameras de vídeo. B) Imagem merged (composta) da praia e bancos arenosos no Cassino no dia 13 de junho de 2005. (Calliari et al.,2005).

Além disso, com o objetivo de monitorar possíveis alterações na hidrodinâmica e morfologia da zona arrebentação em função do transporte de lama para a praia, foram instaladas 4 câmeras de vídeo que filmam diferentes setores da zona costeira adjacente (nordeste/leste, leste leste/sudeste e sudeste/sul) (Figura 2.13). Este método está baseado no

principio da "*time lapse photography*", onde câmaras colocadas em posições fixas registram automaticamente uma seqüência de fotos tomadas a intervalos fixos de tempo. Estas imagens são analisadas individualmente ou combinadas mostrando as modificações morfológicas em tempo real. Os dados são coletados em intervalos de 1 hora durante o período de luz natural e consistem em imagens oblíquas instantâneas (*snap shots*) e séries temporais (*time exposure images/Timex*), as quais fazem a média das intensidades registradas nas câmeras durante 10 min com imagens obtidas a intervalos de 1 s, representando assim uma média de 600 imagens individuais. O resultado obtido com este monitoramento iniciado em maio de 2005 confirmou a existência de pelo menos três bancos arenosos na área de abrangência, sendo dois deles bem definidos na maioria das imagens.

Capítulo 3

Metodologia

Capítulo 3

Metodologia

3.1 Introdução

O estudo da caracterização do clima de ondas ao longo da costa do Rio Grande do Sul, com especial enfoque na investigação da atenuação da energia das ondas sobre os depósitos lamíticos existentes na região costeira adjacente à Praia do Cassino, foi realizado combinando dados pretéritos e dados de campo com experimentos de modelagem numérica. Os dados de campo utilizados foram obtidos no contexto do experimento de campo do Projeto Cassino (Figura 3.1 e Secção 2.8). O modelo numérico utilizado foi o modelo SWAN na versão padrão e o modelo SWAN que considera fundos lamosos em sua formulação. Especial atenção foi dada a modelagem de ondas em função da ocorrência de depósitos lamíticos nas proximidades da costa do Rio Grande do Sul.

Apesar da limitada disponibilidade de dados de onda, a verificação da versão básica do modelo SWAN foi realizada mediante a comparação dos parâmetros de onda obtidos com o modelo e dados de onda medidos com um ondógrafo direcional fundeado próximo a entrada do estuário da lagoa dos Patos, em 1998 (Figura 3.1). Os dados de vento utilizados foram medidos na Praticagem da Barra de Rio Grande (Figura 3.1) durante o mesmo período. O detalhamento dos exercícios de verificação é apresentado no Anexo II.

A validação do modelo SWAN foi efetuada através da comparação com dados de campo de onda e vento obtidos durante o Experimento Cassino, realizado em 2005. Durante esta campanha de campo, dados de onda foram obtidos por um ondógrafo direcional fundeado na Praia do Cassino (Figura 3.1), onde a velocidade e direção do vento foram medidas durante o mesmo período. Esta validação é apresentada no capítulo 4.

A verificação do modelo SWAN com lama fluída, por outro lado, foi realizada através de uma análise de sensitividade da resposta do modelo quanto ao efeito da lama em termos de atenuação da altura e amortecinento na energia das ondas. Os parâmetros modelados com esta foram analisados mediante comparação com os resultados do modelo na versão padrão. A validação do modelo SWAN com lama foi efetuada através da comparação com dados de campo de onda, vento e parâmetros da lama obtidos no Experimento Cassino (Figura 3.1). Esta validação está descrita no Capítulo 4.

As versões do modelo SWAN padrão e com lama fluída foram, então, aplicadas em um estudo de caso na Praia do Cassino (Figura 3.1). Os resultados que compõe o trabalho apresentado no Capítulo 4 caracterizam o clima de ondas da Praia do Cassino no período de realização do Experimento Cassino, considerando a presença dos depósitos lamíticos observados nesta área. A diferença no comportamento das ondas sob o efeito da lama, registrada e observada visualmente na área estudada, levou a uma avaliação mais detalhada da

influência dos parâmetros característicos da lama fluida na atenuação da energia das ondas na Praia do Cassino. Esta análise está descrita no Capítulo 5.

Abaixo são apresentadas as formulações dos modelos numéricos utilizados, bem como a metodologia para a geração da grade e inicialização dos modelos.
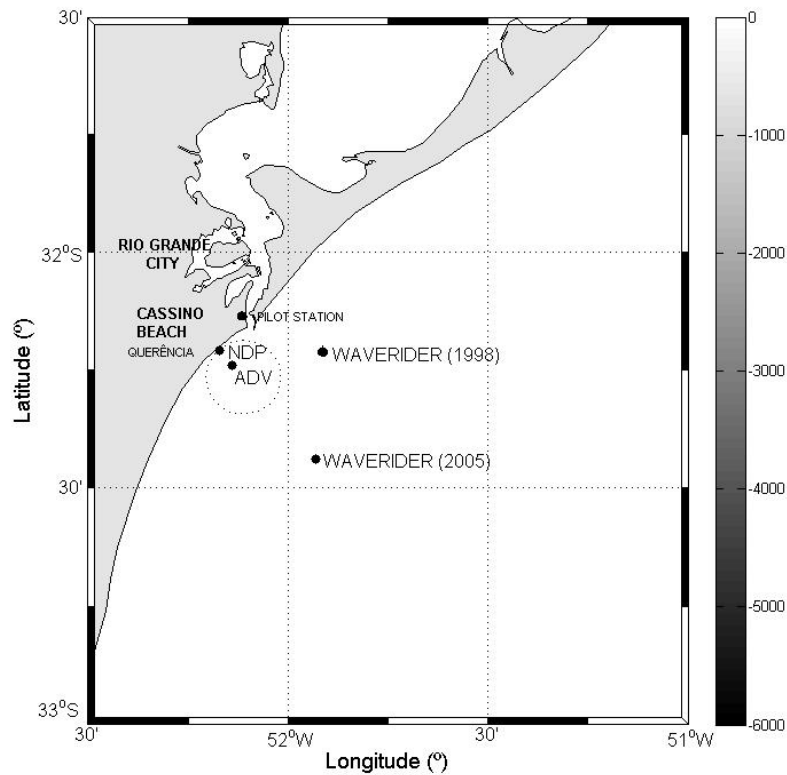
Figura 3. 1 – Localização das estações onde os dados de campo de ventos e ondas foram medidos.

3.2 O Modelo SWAN

O modelo SWAN (*Simulating WAves Nearshore*) (Booij et al., 1999; Zijlema and Van der Westhuijsen, 2005), desenvolvido pela Universidade de Delft, é um modelo de ondas de terceira geração que calcula a propagação espectral da agitação marítima, projetado para obter uma estimativa realista dos parâmetros de agitação marítima em regiões costeiras e estuários. Partindo do conhecimento das condições de vento, batimetria e correntes na área de estudo, o

modelo resolve a equação de conservação do movimento na forma espectral e permite calcular a evolução do espectro direcional e respectivos momentos estatísticos. Os seguintes processos estão representados para geração e dissipação de energia: refração e empinamento (*shoaling*) associados à variação da profundidade, geração de ondas pelo vento, dissipação tipo carneirinho (*whitecapping*), dissipação de quebra de ondas induzida pelo fundo, dissipação devido ao fundo e interações não lineares. As ondas são computadas através da evolução do espectro de densidade de ação, representada pela equação do balanço da ação espectral (ou balanço de energia na ausência de correntes), incluindo fontes e sumidouros.

A equação governante do modelo no plano bidimensional, em coordenadas cartesianas, descrita pela equação do balanço espectral é dada:

$$\frac{\partial}{\partial t}N + \frac{\partial}{\partial x}c_x N + \frac{\partial}{\partial y}c_y N + \frac{\partial}{\partial \sigma}c_\sigma N + \frac{\partial}{\partial \theta}c_\theta N = \frac{S}{\sigma} \tag{3.1}$$

Onde σ é a freqüência relativa (freqüência da onda medida em uma referência que se move com a velocidade de propagação), θ é a direção da onda (direção normal da crista da onda de cada componente espectral), N é a ação de densidade igual a densidade de energia dividida pela freqüência relativa ($N = E / \sigma$), c é a velocidade da ação de propagação da onda no espaço em (x, y, σ, θ).

O primeiro termo do lado esquerdo da Equação (3.1) representa a taxa de variação da densidade de ação no tempo. O segundo e o terceiro termo indicam a propagação da densidade de ação no espaço geográfico (com velocidades de propagação *cx* e *cy* no plano *x* e *y*, respectivamente). O quarto termo trata da variação das freqüências relativas devido às mudanças de profundidade e devido à presença de correntes (com velocidade de propagação c_σ). O quinto termo, por sua vez, representa a refração induzida pelas variações de profundidade e de corrente (com velocidade de propagação c_θ). O termo fonte S (= S(σ, θ)) representa os efeitos de geração, dissipação e interações não-lineares onda-onda.

O termo fonte S geralmente é escrito como a soma de termos fonte, cada um representando os diferentes tipos de processos.

$$S = S_{in} + S_{ds} + S_{nl} \qquad (3.2)$$

Onde S_{in} representa a geração da onda pelo vento, S_{ds} a dissipação de energia por carneirinhos *whitecapping*, fricção com o fundo e quebra induzida pelo fundo, e S_{nl} transferência de energia devido a interações onda-onda não lineares (ambas as interações triplas S_{nl3} e quádruplas S_{nl4}). A evolução espectral em águas rasas é o resultado de interações tríades, enquanto nas interações de quarta ordem os termos quádruplos são importantes em profundidades intermediárias e fundas. (Ris, 1997).

A energia total obtida pela integração da Equação (3.1) é implementada no modelo SWAN com um esquema de diferenças finitas em cinco dimensões: tempo, espaço geográfico (direções x e y) e espaço espectral (freqüência e direção).

O termo fonte que alimenta o modelo correspondente ao mecanismo de transferência de energia do vento é descrito como a soma do crescimento linear e exponencial:

$$S_{in}(\sigma,\theta) = A + BE(\sigma,\theta) \qquad (3.3)$$

Onde A e B dependem da freqüência e direção da onda, e da velocidade e direção do vento.

Os efeitos das correntes são informados ao modelo através da velocidade e direção do vento local. A expressão para o termo A é devido a Cavaleri e Malanotte-Rizzoli (1981), com um filtro para evitar o crescimento para freqüências mais baixas do que a freqüência de *Pierson-Moskowitz* (Tolman, 1992a). Para o coeficiente B, duas expressões opcionais são usadas no modelo. A primeira é obtida em Snyder et al. (1981), e foi reformulada em termos

de velocidade de fricção U* por Komen et al. (1984). O coeficiente de arraste para relacionar U* com a velocidade do vento à 10 m de altura (U_{10}) é dado por Wu (1982). A segunda expressão para B está baseada em Janssen (1991a), e considera explicitamente a interação entre o vento e as ondas, considerando o efeito da camada limite da atmosfera e o comprimento da irregularidade da superfície do mar. O conjunto de equações é resolvido pelo método iterativo de Mastenbroek et al. (1993).

O termo de dissipação da energia da onda é representado pela adição de três diferentes contribuições: whitecapping $S_{ds,w}$, fricção com o fundo $S_{ds,bf}$ e quebra induzida pelo fundo $S_{ds,br}$ O *whitecapping* é inicialmente controlado pela declividade das ondas, e essa formulação é baseada no modelo em pulsos (Hasselmann, 1974), adaptado por WAMDI (1988):

$$S_{ds,w}(\sigma,\theta) = -\Gamma \tilde{\sigma} \frac{k}{\tilde{k}} E(\sigma,\theta) \tag{3.4}$$

Onde Γ é um coeficiente que depende da declividade, k é o numero de onda, $\tilde{\sigma}$ e $\tilde{k}$ representam a freqüência média e o número de onda médio respectivamente (WAMDI, 1988). Komen et al. (1984) estimaram o valor de Γ pelo equilíbrio da energia das ondas em condições completamente desenvolvidas.

A dissipação induzida pelo fundo pode ser causada por fricção com fundo, movimento do fundo, percolação ou espalhamento nas irregularidades de fundo (Shemdin et al., 1978). Para plataformas continentais com fundo de areia, o mecanismo predominante é a fricção com o fundo (Bertotti and Cavaleri, 1994), que geralmente pode ser representado pela equação:

$$S_{ds,b}(\sigma,\theta) = -C_{bottom} \frac{\sigma^2}{g^2 \sinh^2(kd)} E(\sigma,\theta) \tag{3.5}$$

3.2.1 O Modelo SWAN com lama fluída

O modelo SWAN com lama fluida consiste da formulação do amortecimento da onda obtida através do modelo de duas camadas proposto por Gade (1958), e implementado por Winterwerp et al. (2007). A abordagem é aplicada por direção da onda, e as soluções individuais podem ser adicionadas linearmente. Na nova formulação, o termo sumidouro por dissipação viscosa em camadas de lama foi acrescentado na Equação (3.14), resultando em:

$$S = S_{in} + S_{ds} + S_{ds,m} + S_{nl}$$

(3.6)

A formulação proposta por Gade (1958) considera a camada superior não viscosa e a camada inferior viscosa, mas é limitada para águas rasas, considerando que as ondas são sinusoidais e pequenas comparadas com a profundidade, sendo negligenciadas as acelerações verticais.
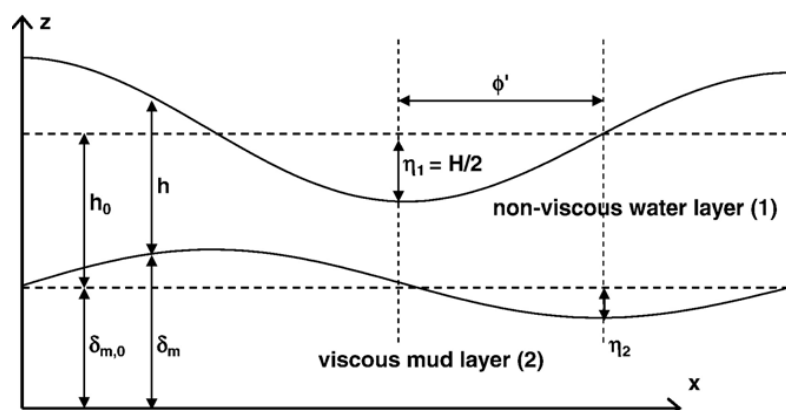
Figura 3. 2 - Esquema de um sistema de duas camadas com lama fluida e definições baseadas na teoria de Gade (1958) (Winterwerp et al., 2007).

A Figura 3.2 apresenta o esquema do sistema de duas camadas e as definições dos principais parâmetros, onde a camada de lama fluida descreve uma onda na camada interna. O h_o representa a espessura da camada não viscosa de água e δ_m a camada de lama viscosa em condições de equilíbrio. Os termos h_o e δ_m representam a distância da interface até a superfície livre e a distância do fundo rígido até a interface, respectivamente. h_1 e h_2 são as amplitudes da superfície e da onda interna, respectivamente, e H a profundidade total da camada líquida.

Na situação apresentada, ondas internas livres na camada de lama fluida não são consideradas pelo fato de que a distância percorrida pelas ondas deve ser muito longa em relação à extensão do depósito de lama fluida.

O sistema de duas camadas proposto é descrito através do seguinte conjunto de equações para a continuidade (Equações. 3.7 e 3.9) e conservação do momento (Equações. 3.8 e 3.10), aplicadas para as camadas superior e inferior, respectivamente:

$$\frac{\partial u_1}{\partial x} + \frac{\partial w_1}{\partial z} = 0 \tag{3.7}$$

$$\frac{\partial u_1}{\partial t} + \frac{1}{\rho_1}\frac{\partial p_1}{\partial x} = 0$$

$$\tag{3.8}$$

$$\frac{\partial w_1}{\partial t} + \frac{1}{\rho_1}\frac{\partial p_1}{\partial x} = -g$$

$$\frac{\partial u_2}{\partial x} + \frac{\partial w_2}{\partial z} = 0 \tag{3.9}$$

$$\frac{\partial u_2}{\partial t} + \frac{1}{\rho_m}\frac{\partial p_2}{\partial x} = v_m \frac{\partial^2 u_2}{\partial z^2}$$

$$\tag{3.10}$$

$$\frac{\partial w_2}{\partial t} + \frac{1}{\rho_2}\frac{\partial p_2}{\partial x} = -g$$

Onde p representa a pressão, u a velocidade horizontal do fluxo, w a velocidade vertical do fluxo, o número 1 indica a camada superior e o número 2 a inferior. Os termos h e δ_m são as espessuras das camadas superior e inferior, respectivamente, e v_m a viscosidade constante da camada de lama fluida. As coordenadas horizontal e vertical são dadas por x e z (x na direção das ondas), e t é o tempo.

As equações acima são resolvidas com são as seguintes condições de contorno, onde k é o numero de onda complexo:

- na superfície livre (z=h+δm): p=0, η1=η^1exp{i(kx−σt)} e w1=∂η1 /∂t

- na interface (z=δm): ∂p/∂z=0, ∂u2 /∂z=0 e w1=w2= ∂η2 /∂t

- no fundo rígido (z=0): u2=w2=0.

Gade (1958) resolveu estas equações através do método harmônico, considerando o número de onda complexo, a espessura da camada e a velocidade (De Wit, 1995), apresentando resultados para um campo de ondas unidirecional monocromático. Entretanto a formulação do SWAN requer o termo de dissipação de energia $S_{ds,m}$ (σ, θ), obtido pela integração do trabalho realizado pela superfície das ondas sobre o período. A altura da onda foi obtida a partir da solução harmônica das equações (3.7) a (3.10).

Estendendo a análise de Gade, e assumindo a superposição de soluções, a dissipação da energia por freqüência σ e direção θ da onda resulta:

$$S_{ds,m} = \alpha g h_0 \sigma R \frac{\hat{\eta}_2}{\hat{\eta}_1} \sin\left(\phi' - \phi\right) E \tag{3.11}$$

$$k = k_r + i k_i, \quad \text{é o número de onda complexo (De Wit, 1995)} \tag{3.12}$$

$$\left[\frac{\rho_m - \rho_0}{\rho_m} \frac{gk}{\sigma^2}\left(k\delta_{m,0} - \frac{k}{\lambda_g}\tanh\{\lambda_g\delta_{m,0}\}\right) - 1\right]\left[\frac{gk}{\sigma^2}\tanh\{kh_0\} - 1\right]$$
$$-\frac{\rho_0}{\rho_m}\left[k\delta_{m,0} - \frac{k}{\lambda_g}\tanh\{\lambda_g\delta_{m,0}\}\right]\left[\frac{gk}{\sigma^2} - \tanh\{kh_0\}\right] = 0 \tag{3.13}$$

Onde

$$\lambda_g = (1-i)\sqrt{\sigma/2\nu_m} \tag{3.14}$$

Da Equação (3.3) pode ser obtido:

$$k_r, k_i, R = \left[\left(k_r{}^2 + k_i{}^2\right)/v^2\right] \tag{3.15}$$

O ângulo de fase entre a elevação da água e a velocidade de fluxo é:

$$\phi = \left[2a\tan\left(k_i/kr\right)\right] \tag{3.16}$$

E o ângulo de fase entre a superfície e as ondas internas é:

$$\tan\phi' = \frac{h_0 gR\sin\phi}{h_0 gR\cos\phi - 1} \tag{3.17}$$

A razão entre as amplitudes da superfície e das ondas internas é:

$$\frac{\hat{\eta}_2}{\hat{\eta}_1} = \sqrt{\left[1 - gh_0 R\cos(\phi)\right]^2 + \left[1 - gh_0 R\sin(\phi)\right]^2} \tag{3.18}$$

Winterwerp et al. (2007) adicionaram um coeficiente de calibração extra α prevendo possíveis efeitos não lineares, e visando uma utilização mais adequada do modelo SWAN em locais onde existem depósitos de lama.

3.3 Domínio Computacional - Grade numérica
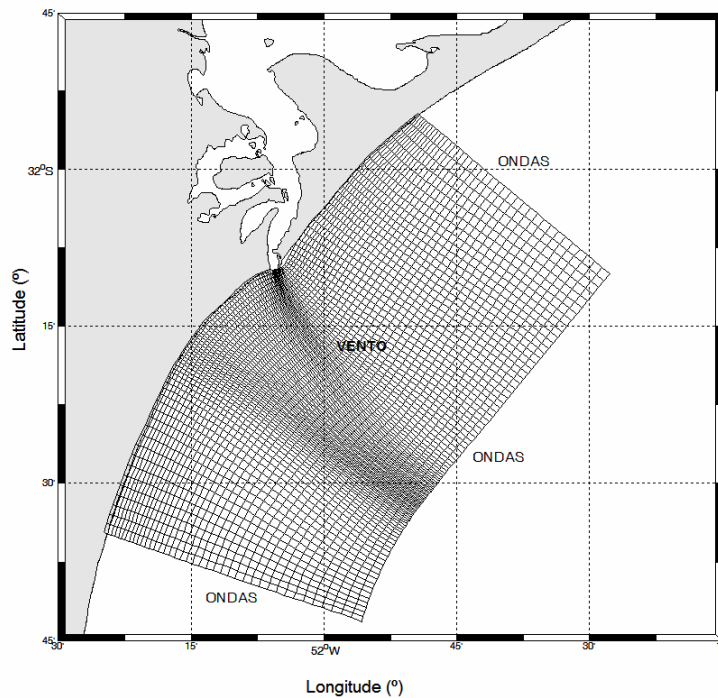
Figura 3. 3 - Grade curvilinear de diferenças finitas utilizada pelo modelo SWAN, com destaque para as fronteiras abertas e os parâmetros prescritos como condição de contorno.

Os dados batimétricos necessários para a geração da malha do domínio estudado estão baseados nas cartas náuticas fornecidas pela Diretoria de Hidrografia e Navegação (DHN), e foram complementados com levantamentos batimétricos mais recentes e detalhados da região,

realizados durante o Projeto LEPLAC, da Marinha do Brasil. Estes dados batimétricos foram complementados por dados de linha de costa e topografia de fundo disponíveis na internet na NOAA/National Geophysical Data Center. http://www.ngdc.noaa.gov/mgg/global/seltopo.html).

A grade curvilinear utilizada pelo modelo SWAN abrange uma área de 100 km^2, localizada entre as longitudes 51º 75' W e 52º 25'W e as latitudes 31º 50' S e 32º45' S, se estendendo 50 km em direção ao oceano até a profundidade de 29 m (Figura 3.3). A grade resultante possui 4264 células com tamanho variável entre 1.5 km próximo aos contornos abertos e 1.0 km próximo aos Molhes de Rio Grande.

3.4 Dados de campo

Para os experimentos numéricos realizados com o modelo SWAN para o ano de 1998, foram utilizados como condição inicial os dados de velocidade e direção do vento medidos na Estação da Praticagem da Barra (Figura 3.1) relativo ao mês de fevereiro.

Apesar da limitada disponibilidade de dados de onda, a verificação da versão básica do modelo SWAN foi realizada mediante a comparação dos parâmetros de onda obtidos com o modelo e dados pretéritos de onda, disponíveis na literatura. O modelo foi forçado com campos de vento medidos na estação da Praticagem da Barra, no Porto de Rio Grande (Figura 3.1). Para a avaliação dos resultados modelados, foram utilizados os dados de onda medidos pelo ondógrafo direcional, fundeado próximo a boca do estuário da Lagoa dos Patos, na profundidade de 15 m (Figura 3.1). As comparações foram realizadas em termos de altura significativa, período de pico, direção média e densidade de energia. A seleção de casos significativos para os experimentos com o modelo SWAN foi baseado na caracterização do estado do mar disponível na literatura para a área estudada. Dois tipos de ondas oceânicas geradas pelo vento foram selecionados: ondulações (*swell*) e vagas (*sea*).

A análise realizada por Strauch (1998) em dados de onda medidos mostrou que na área de estudo predominam ondulações de sul, com período de pico de 12 s e vagas com período de pico de 8 s. O trabalho apresentado por Tomazelli (1990) mostrou que na área de estudo predominam os ventos de nordeste (NE) e de sudoeste (SW). Para as simulações foram escolhidos períodos correspondentes a duas direções de vento predominantes, onde os dados de onda medidos pelo ondógrafo representassem os dois estados característicos do mar na área de estudo.

A Tabela 1 apresenta os parâmetros das ondulações registrados pelo ondógrafo no seu ponto de fundeio e a velocidade e direção do vento medido em três diferentes horários do dia 11 de fevereiro de 1998. Já a Tabela 2 apresenta os parâmetros das vagas registrados pelo ondógrafo no seu ponto de fundeio e a velocidade e direção do vento medido em três diferentes horários do dia 4 de fevereiro de 1998.

Tabela 3.1 – Parâmetros de onda observados no ponto de fundeio do ondógrafo e velocidade e direção do vento medidos em três horários no dia 11 de fevereiro de 1998.

	Parâmetros da onda observados					Ventos medidos	
	Hs (m)	Tm (s)	Tp (s)	DIR(graus)	DSPR(graus)	V (m/s)	DIR(graus)
09:15	2.1	4.8	12.5	167	18.2	8.08	225.0 (SW)
17:00	2.0	5.2	12.5	159	17.9	7.15	202.5 (SSW)
22:00	2.0	5.9	12.5	159	12.9	4.48	180.0 (S)

Tabela 3.2– Parâmetros de onda observados no ponto de fundeio do ondógrafo e velocidade e direção do vento medidos em três horários no dia 4 de fevereiro de 1998.

	Parâmetros da onda observados					Ventos medidos	
	Hs (m)	Tm (s)	Tp (s)	DIR(graus)	DSPR(graus)	V (m/s)	DIR(graus)
01:10	2.0	4.7	6.3	113	27.6	11.20	67.5 (ENE)
04:00	2.7	5.0	6.7	105	22.0	14.80	90.0 (E)
07:00	1.8	5.0	7.1	125	21.5	7.20	45.0 (NE)

Com base nestas informações várias simulações foram realizadas variando as condições iniciais e de contorno. A descrição das simulações realizadas estão detalhadas no Anexo II, que apresenta o procedimento de verificação da versão padrão do modelo SWAN .

A verificação do modelo SWAN com lama foi realizada através de uma análise de sensitividade do modelo mediante a comparação da atenuação da altura significativa e amortecimento da densidade de energia da onda perante variações nos coeficientes físicos. Para esta verificação, dois casos previamente utilizados na verificação da versão padrão do SWAN foram selecionados (em destaque nas Tabelas 3.1 e 3.2): um caso representativo de ondulações, 11 de fevereiro de 1998, às 09:15 h, e o outro de representativo de vagas, 4 de fevereiro de 1998, às 01:10 h.

Os parâmetros relativos à lama utilizados como condições iniciais e de contorno são a localização geográfica do depósito, a espessura, a densidade e a viscosidade. A localização geográfica foi definida em função do levantamento feito durante o Experimento Cassino, em 2005, e os parâmetros físicos foram definidos de acordo com Torronteguy (2000). Nestas simulações, a espessura da camada e a sua densidade foram consideradas constantes em todo o domínio do modelo. A viscosidade da lama funcionou como um fator de calibração. A descrição dos parâmetros utilizados é apresentada na Tabela 3.3.

Tabela 3. 3 – Descrição e variação dos parâmetros da lama fluida prescritos no modelo SWAN com lama

Parâmeteros	**valores**	**descrição**
espessura	σ_m = 1.00m	Variação especial no domínio [m] Máximo de 1.24 m
densidade	ρ_m = 1300 kg/m^3	Entre 98 and 1450 kg/m^3
viscosidade	ν_m = 0.001 m^2/s	Parâmetro de calibração variando entre 0.01, 0.001 e 0.0001 m^2/s
parâmetro de calibração	α = 1	1.0

As simulações de validação do modelo SWAN (com e sem lama fluída) utilizaram como condições iniciais e de contorno dados obtidos na fase experimental do Projeto Cassino:

- Os dados de vento prescritos como condição de contorno superficial foram medidos na Estação Marinha de Aquacultura (EMA) da FURG, situada na Praia do Cassino, 9 km ao sul dos Molhes de Rio Grande, no período compreendido entre 15 de maio e 24 de junho de 2005.

- Os parâmetros de onda utilizados foram medidos para o mesmo período por um ondógrafo direcional fundeado na Praia do Cassino, na profundidade de 25 m (32°26'37" S e 51° 55' 53") (Figura 3.1).

- Os parâmetros relativos aos depósitos lamíticos existentes na região, respectivamente, a localização geográfica, a espessura, e a densidade, foram obtidos durante a coleta de dados do Projeto Cassino, no período compreendido nos meses de entre 18 e 19 de outubro de 2004 e 26 e 28 de março de 2005. A viscosidade foi estabelecida com base nos valores encontrados na literatura.

Capítulo 4

Determination of the Wave Climate for the Southern Brazilian Shelf

Cuchiara, D.C., Fernandes E. H. , Strauch, J. C. , Winterwerp, J.C., Calliari, L. J.
Continental Shelf Research. Aceito para publicação.

Determination of the Wave Climate for the Southern Brazilian Shelf

Cuchiara, D.C.[1], Fernandes E. H. [1], Strauch, J. C. [1], Winterwerp, J.C.[2], Calliari, L. J. [3]

[1,3]Fundação Universidade Federal do Rio Grande, CP 474, CEP: 96201-900, Rio Grande - RS – Brazil
[1]Departamento de Física, dmtdc@furg.br, dfsehf@furg.br, dfsjcss@furg.br
[2]Delft Hydraulics, PO Box 177, 2600 MH Delft, The Netherlands, han.winterwerp@wldelft.nl;
also Delft University of Technology, Faculty of Civil Engineering, The Netherlands
[3]Departamento de Geociências, tsclauro@furg.br

Abstract

The main objective of this study is the characterization of the wave climate in the Southern Brazilian Shelf based on a through review of existing field data and on numerical modeling experiments. A quantitative knowledge about the wave climate of this area is important to understand the mechanisms driving episodic mud bank attachments to the sandy shore, and the interaction of these banks with the flow and waves. The statistical analysis of existent data on the wave climate throughout the SBS indicates that the predominant wave directions are 100° and 160° (E-SE), with wave heights varying between 1 and 1.50 m. The wave period varies between 6 and 14 s, with predominance of mean wave period of 8 s (sea conditions) and 12 s (swell conditions). The spectral wave model SWAN version 40.41 (Booij et al. 2004) is used to simulate the wave climate for the region. Special attention is given to Cassino Beach, describing the wave climate observed during the Cassino Experiment, carried out in 2005. The verification of the standard SWAN model was carried out based on the comparison between numerical modeling results and available data of significant wave height, peak period, mean wave direction and energy density for the period relative to February of 1998. Results showed satisfactory model predictions of significant wave height and reasonably accurate predictions of peak spectral wave period and direction. The model performance is also considered satisfactory in the representation of the wave climate of the region when the

wave spectrum has only one spectral peak, but presents limitations for bimodal wave spectrum. When two spectral peaks are observed, the SWAN model agrees with the spectral level observed in the low frequency, but underestimates the spectral level in the high frequency band. When considering the presence of mud deposits in the area, model results predict that although the presence of mud attenuates most of the wave energy on the low frequency peak, it has a smaller effect in attenuating the wave energy on the high frequency peak.

The comparison between significant wave heights calculated by the SWAN model (with and without mud) and measured with a NDP (Acoustic Doppler Profiler) for the NDP localization point, and with data from a waverider relative to the 2005 survey for the studied period showed that all the time series have a similar pattern. Observed and calculated results without mud are in agreement, following the expected behavior. By considering the presence of mud in the whole domain, the model with mud shows a clear decrease of the significant wave height in relation to the NDP localization point. Furthermore, the significant wave height is underestimated due to the consideration of a constant mud thickness, extend, density and viscosity in the whole domain.

Keywords: waves, numerical modeling, wave climate, SWAN

4.1. Introduction

The wind blowing over the water surface induces shear stresses and pressure variations which result in waves that grow in the direction of the wind until a balance arises between the energy input and the dissipation in the wave field (Kinsman, 1965). The properties of the wind field (i.e., speed, direction, and duration) and the geometry of the water body where the

waves are being generated (i.e., fetch, bottom type and water depth) determine the wave height, period, and direction. Waves generated on the open sea will ultimately reach shallow water, where depth-limited wave breaking occurs and the wave energy is mainly dissipated, resulting in gradual wave height decay. Thus, the energy transferred from the wind to the waves is dissipated in a narrow strip close to shore (nearshore zone) creating a dynamic and highly variable environment. This process has important implications for the water and material transport in the nearshore zone, as well as for the water and material exchange between the coastal and offshore areas (Blomgren et al., 2001). Furthermore, the waves play a fundamental role in the formation of coastal features, and affect several recreational and economical activities (e.g. sailing, harbor operations and oil extraction).

Several physical processes are observed when the waves propagate from deep to shallow waters, which involve mechanisms conserving, adding or removing energy from the domain. To resolve the dynamics of these processes, detailed knowledge of the wave field in time and space is needed, including the complete energy distribution over frequency and direction (directional-frequency spectrum). The understanding of the wave field allows the determination of additional quantities such as orbital velocities, shear stresses, and energy dissipation (Populus et al., 1991; Goldstein et al., 1994).

A description of the wave field based on field data alone is a difficult task, which involves operational and economical problems. The main problems are related to the spatial and temporal limitations of the measurements, the hinderance of the measurements by fishing activities, and the high budget needed to establish a spatial coverage of information for one region. Thus, numerical models figure as an alternative method for this task.

Models to predict the evolution of surface waves under the influence of a wind field have improved significantly during the last years (Komen et al., 1994). Two types of numerical wave models have been developed to simulate the wave evolution in coastal areas: phase

resolving and phase averaged wave models. The phase resolving models are usually based on a Hamiltonian approach (e.g., Miles, 1981; Radder, 1992), on a Boussinesq approach (e.g., Peregrine, 1966; Nwogu, 1994; Madsen and Sorensen, 1992) or on the mild-slope equation (Berkhoff, 1972; and its parabolic version, Radder, 1979). These phase resolving models are often used for rapidly varying wave conditions, where the local phase averaged properties vary rapidly within distances of the order of a wave length or less. Such phase resolving models reconstruct the sea surface elevation in space and time with fairly high accuracy, usually in the absence of generation and dissipation. These models have the great advantage that they account for diffraction and refraction effects. Moreover, the Hamiltonian and Boussinesq type of models also implicitly account for nonlinear effects such as quadruplet-wave interactions and triad-wave interactions. Non-linear dissipative processes can be incorporated in these models but the incorporation of wind effects is rather difficult. The space and time resolution that is required to calculate the wave evolutions are of the order of a small fraction of the wave length and period, respectively. The absence of wind effects and the required high spatial resolution make these models impractical for wind-wave problems with spatial dimensions of the order of a dozen wave lengths or more (Holthuijsen et al., 1994; Ris, 1997).

Phase averaged wave models, on the other hand, assume that the wave properties vary slowly on the scale of a wave length. In these models the irregular sea surface is described by a spectral energy density function (or action density in the presence of currents). The wave kinematics can be described in a Lagrangian approach (wave rays), an Eulerian approach (a grid model), or with the combination of these two. The traditional phase averaged models are based on the Lagrangian approach, where the wave energy propagates from deep water to the shore along wave rays. The change in wave ray direction in response to changes in the bathymetry and current is governed by the Snell's law (Holthuisen et al., 1994; Ris, 1997).

One major disadvantage of the Lagrangian approach is that the models are numerically inefficient when non-linear effects are to be accounted for (Ris, 1997). The reason is that the propagation of each spectral wave component is ca1culated independently of all the other components, so that the wave information is only available along the wave rays, which are scattered over the area of interest. It is then more efficient to use an Eulerian approach, in which the wave evolution is formulated in terms of spectral energy on a grid. The wave model is then formulated on a grid and offers the opportunity to explicitly and efficiently include the propagation, generation, dissipation and nonlinear wave-wave interactions of random short crested waves using a spectral formulation.

The development of the phase averaged models based on the concept of the wave spectrum started with the pioneering work of Gelci (1956) for deep water applications. Since then, many spectral wave models (usually of the Eulerian type) have been developed with numerous and continuing extensions and improvements (e.g., Ewing, 1971; Uji, 1975; Golding, 1983; the WAMDI group, 1988; Tolman, 1991; Li and Mao, 1992; Benoit et. al., 1996). The processes of generation, dissipation and wave-wave interactions have been represented in deep water models by first, second and third generation formu1ations depending on the level of parameterizations of these processes (see e.g., the WAMDI group, 1988).

In first-generation models, which were developed in the 1970's, the quadruplet-wave interactions are not expressed explicitly. The wave spectrum is allowed to grow to an assumed upper limit which is usually the wind dependent Pierson-Moskowitz (1964) spectrum, with a standard directional distribution. Second-generation wave models tried to remedy this by parameterizing these interactions and by using the JONSWAP spectrum as an upper limit (e.g. Golding, 1983; Holthuijsen and De Boer, 1988; Young, 1988). It appeared from a large intercomparison study of first and second generation wave models (the SWAMP group, 1985)

that there were some basic shortcomings in these models and that they lose their reliability in extreme conditions (particularly in rapidly changing wind fields). This has led to the development of third-generation wave models in which the quadruplet-wave interactions are incorporated explicitly. In third-generation models the spectrum is computed by integrating the spectral energy balance equation without any a priori restrictions on the spectrum. A first attempt to include the exact form of the non-linear quadruplet-wave interactions was made by Hasselmann and Hasselmann (1981).

The SWAN wave model is the main third generation spectral model used for shallow waters, and it has been applied at the coast, and in lakes, estuaries and nearshore areas where the water depth is shallow and fine-resolution computational domains are needed, normally nested within coarser–resolution basin-scale domains, in order to resolve complex topography, coastline features, and shallow water wave physics (Ris et al., 1994; Booij et al., 1996; Booij et al., 1999; Holthuijsen and Booij, 2003; Rogers et al., 2006).

Similar to several places in the world, the Brazilian coast lacks observational data to describe the wave climate in detail. Especially regarding the Southern Brazilian Shelf (SBS) (Figure1), a systematic study of the wave climate does not exist, although some local efforts have been done in order to characterize certain areas. These studies were based on several sources of data, which include field measurements (Motta,1963, Strauch,1998) and observations (Motta, 1963; Melo and Alves, 1993), historical data from opportunity ships (NCC, 1980), and remote sensing (Coli, 1994; 2000). The compilation of the existent data on the wave climate throughout the Southern Brazilian Shelf (SBS) highlights the limitations on the information available in the literature for the area (Cuchiara et al., 2005), indicating the necessity of applying alternative methods for a more detailed study of the wave climate of the region.

Thus, the main objective of this study is the characterization of the wave climate in the SBS based on a thorough revision of previous field data and on numerical modeling

experiments. The specific case study will be Cassino Beach, located in the Rio Grande do Sul (RS) coast, in the south of Brazil. Special attention will be given to describe the wave climate observed at Cassino Beach during the Cassino Experiment, carried out in 2005, addressing the wave damping induced by the mud deposits observed in the area.
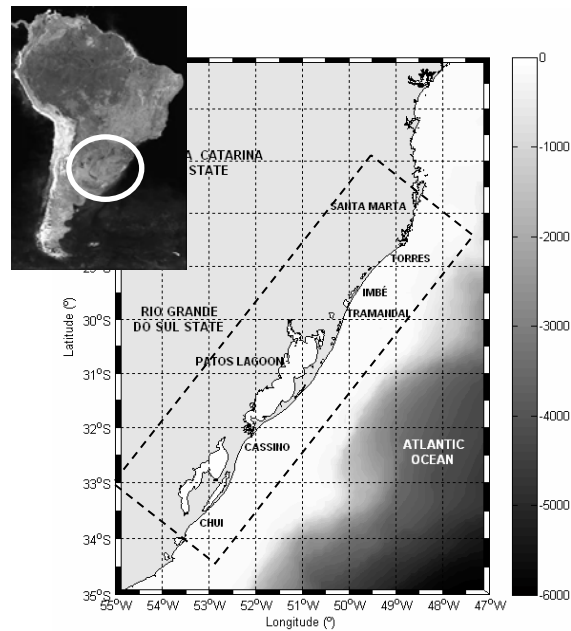
Figure 4.1 – The Southern Brazilian Shelf (dotted rectangle).
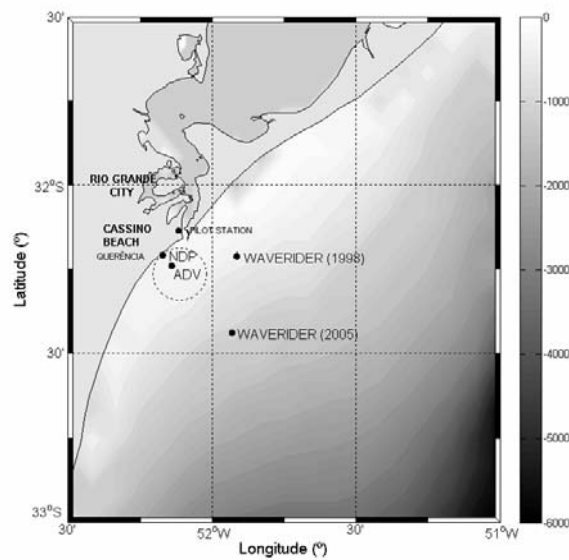
Figure 4. 2 - Location of the stations where wind and wave data for the SWAN model verification and application were obtained. The dotted circle indicates the mud deposit. The location where a NDP and an ADV were moored at 9 m and 12 m depth, respectively, during the Cassino Experiment (2005).

4.2. The wave climate of the study area

The Southern Brazilian Shelf (SBS) is located between Cabo de Santa Marta and Chui (28.5 ^{o}S to 34 ^{o}S) (Castro and Miranda, 1998), throughout the RS State coastal area (Figure 4.1). The coast of RS State presents a Northeast-Southwest orientation, and is characterized by open sandy beaches exposed to wave action. The coastal topography is complex and influences the physical processes determining the waves and the sediment transport at the coast. Over the whole 640 Km that separates Torres headland in the north (29.5^{o}S) and the Chuí estuary in the south (33.8^{o}S), the only significant interruption occurs at the entrance of the Patos Lagoon (32°S).

The regional winds that affect the coast of RS State are mainly related to two high pressure systems observed in this area: the South Atlantic Anticyclone and the Polar Migratory Anticyclone (Nimer, 1977). From January to December of 1982, Tomazelli (1990), analyzed data registered in three meteorological stations located in the cities of Torres, Imbé (Figure 1) and Rio Grande (Figure 4.2), and established the wind regime for the area. Based on the classification proposed by Fryberger (1979), the area was characterized as being of high energy, presenting variability in two predominant directions. The most frequent winds come from northeast (NE) and, although it blows throughout the year, it is stronger in the spring and summer months. Winds from the west (W) and southwest (SW) are also important, although more effective during the winter. Tomazelli et al., (1992) also observed that the northeast wind (NE) is predominant, and inferred a higher occurrence of wind velocities between 5 and 7 m s^{-1}. Camargo et al., (2002) corroborated this in the Eolic Atlas of Rio Grande do Sul, and concluded that the stations towards the north of the RS State present winds from the northeast (NE) and east (E) with higher frequency and intensity, while from

the middle to the south, the frequency and intensity of the northeast winds (NE) is reduced, and an increase of the southeast (SE) and south (S) wind components is observed.

The main wave field measurements in shallow/intermediary waters at the coastal area of RS State resulted from two studies accomplished in the surroundings of Tramandaí beach (Figure 4.1) (Motta, 1963), and Rio Grande city (Figure 4.2) (Strauch, 1998). Motta (1963) determined the maximum wave height in Tramandaí based on historical data obtained between October 1962 and September 1963 (12 months of data), using a non-directional wave meter, fixed at 17.5 m depth. The observed maximum height was 7.0 m in April 1963, and the maximum value of the significant height was 4.8 m, both for a 30 years return period. For a 100 years return period, the maximum height reached 7.6 m and the maximum significant height 5.5 m. The direction of wave incidence was acquired visually, indicating that crests were almost parallel to the coast.

Strauch (1998) carried out field measurements with a directional Waverider with digital acquisition located close to the mouth of the Patos Lagoon estuary ($32^o10'00''$ S and $51^o58'91''$ W) during the period between 10/1996 to 08/1997 and 01/1998 to 04/1998 (Figure 4.2). The instrument was fixed at 15 m with the objective of supplying preliminary information about the characteristics of the local agitation and the determination of the project wave for the area. The typical behavior of the local agitation was characterized based on a statistical analysis of the frequency distribution carried out on the recorded data, which provided the predominant values of significant wave height, peak period, and peak energy density. In these polar histograms (Figures 4.3, 4.4 and 4.5) the size of the circular sections indicates the frequency of occurrence in that specific direction and the colors of each section the frequency of the observations in the class intervals.
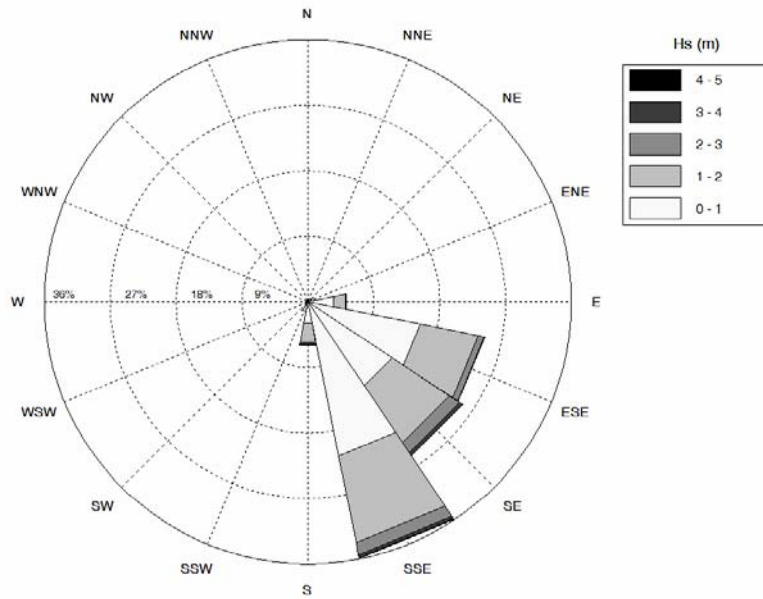
Figure 4.3 - Polar histogram of frequency distribution of significant wave height between 10/1996 to 08/1997 and 01/1998 to 04/1998, represented as a function of the direction of propagation (Strauch, 1998).
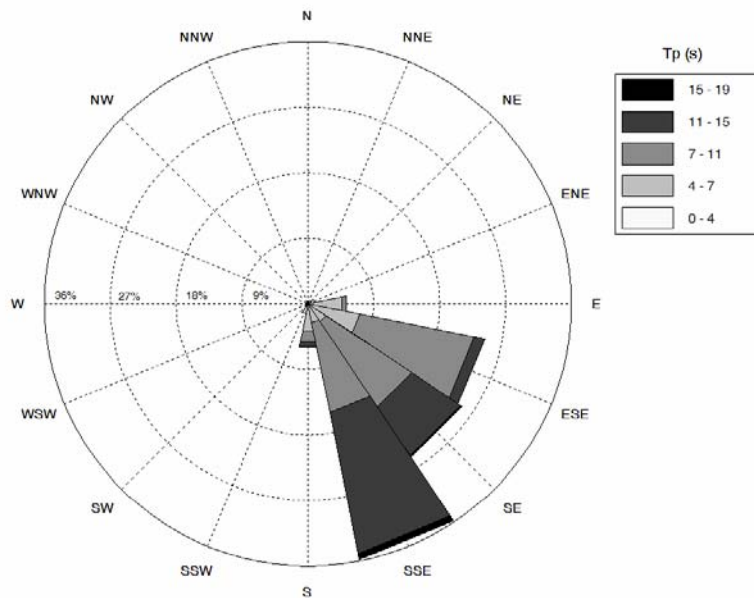
Figure 4.4 - Polar histogram of frequency distribution of peak period between 10/1996 to 08/1997 and 01/1998 to 04/1998, represented as a function of the direction of propagation (Strauch, 1998).
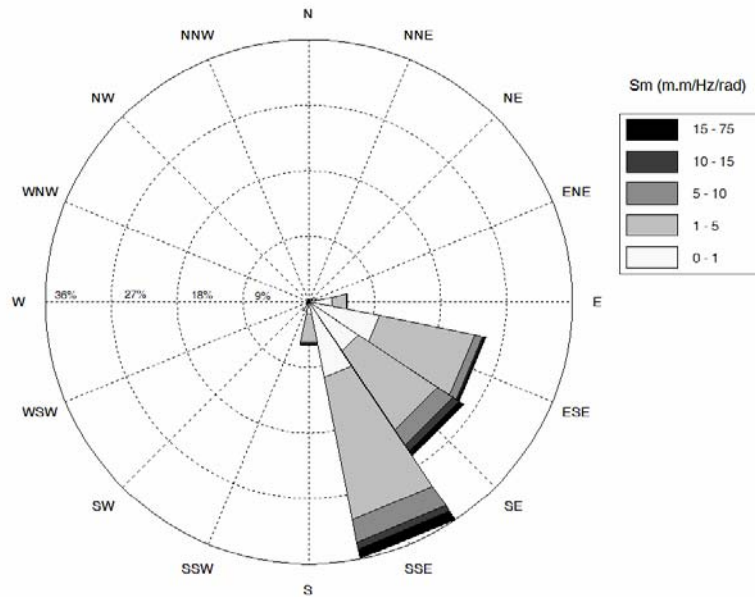
Figure 4.5 - Polar histogram of frequency distribution of peak energy density between 10/1996 to 08/1997 and 01/1998 to 04/1998, represented as a function of the direction of propagation (Strauch, 1998).

The Figure 4.3 indicates significant heights smaller than 5.0 m, with predominant directions between the east-southeast (ESE) and south-southeast (SSE). Figure 4.4 shows the peak period smaller than 19.0 s, with predominant directions between the east-southeast (ESE) and south-southeast (SSE). While in the Figure 4.5 the results indicates the peak energy density smaller than 75 m.m.hz^{-1}.rd^{-1}, and were consistent with the previous directions.

Strauch (1998) concluded that in the studied period the predominant wave directions were from 100° and 160°, with wave heights varying between 1 and 1.50 m. The predominant wave period was between 6 and 14 s, although in extreme situations the predominant mean wave period is either 8 s (sea conditions) or 12 s (swell conditions).

Complementary studies were carried out by Colli (1994), who combined the analysis of wave height and direction data obtained through opportunity ships (between 1946 and 1979), with data from the satellite Topex/Poseidon (1993), and determined the spatial and temporal variation in wave height and direction at the coastal and oceanic areas off RS State. His results showed that winter waves are larger than summer waves. The northeast, east and

southeast waves are more frequent in spring time, while the north, west and southwest waves are amplified during autumn and winter time. Waves of medium height are from the Southwest direction and, secondarily, to the south, west and north directions. The data demonstrated significant variability regarding the annual mean for each of the quadrants of wave propagation, with waves coming mainly from the northeast and from the south. Based on the analysis of the Topex/Poseidon data, it was possible to determine that in the southern oceanic limit of the study area the largest waves prevail in relation to the northern limit. Under the latitude of 33ºS, historical maps demonstrated the occurrence of centers of larger wave heights, which are intensified during autumn, and reach its maximum during winter time.

Later, Coli (2000) described the climate of surface waves for the area to the east of Rio Grande city (Figure 4.2), based on a historical file (1949 and 1979) composed by information about the wave height acquired visually by opportunity ships, and wave data acquired by a directional Waverider between October 1996 and August 1997 (Strauch, 1998). These data provided the base for a short and long period statistical analysis of the wave parameters. The author concluded that the short period characteristic wave had significant height between 1,0 and 1,5 m, mean period between 5 and 6 s and southeast predominant direction. Wave data with significant heights larger than 4 m and mean period larger than 12 s were not observed. Although the height and period parameters did not present significant seasonal variations, there were differences in the form of the wave spectrum.

More recently, Araújo et al. (2003) provided a statistical description of wave conditions in the Southern Brazilian coast based on wave measurements collected in Santa Catarina (SC) State, just north of RS State (Figure 4.1). The identification of distinct sea states and the seasonal variability of the wave climate were assessed using a one-year time series obtained with a Datawell directional waverider deployed 35 km off SC State at a depth of

approximately 80 m. The innovative aspect of this work is the use of clustering techniques to group primary waves with similar characteristics. Multimodal normalized T_p (peak period) and θ_p (peak direction) information was used in the analysis, which shows five distinct groups with similar structures among the seasons. Results show a frequent bimodal sea-swell configuration. In order to capture the concomitant occurrence of this sea-swell condition, an automatic procedure for multimodal sea wave spectra identification was implemented, revealing 31% of 2 peaked spectra for the whole year. These multimodal sea conditions occur more in summer (43%) and less in winter (24%), showing a significant seasonal variation. An analysis of bivariational histograms showed a well defined 12 s swell from the South and a 8 s sea from the East. Their results indicate that during autumn and winter, swell conditions prevail over local sea conditions. In the summer there is a balance between these two states, and in spring, sea conditions prevail.

The compilation of the existent data on the wave climate throughout the SBS characterized the typical behavior of the local agitation based on statistical analysis of frequency distribution, which provided the predominant values of wave height and direction, as well as wave period. Results indicate that in the SBS the predominant wave directions are 100° and 160° (E-SE), with wave heights varying between 1 and 1,50 m. The wave period varies between 6 and 14 s, with predominance of mean wave period of 8 s (sea conditions) and 12 s (swell conditions).

The wave climate of the SBS determines the behavior of the fine sediments observed in the foreshore of Cassino beach (Figure 4.2), which are periodically suspended, transported and deposited onshore and on the surf zone (Villwock and Martins, 1972; Calliari et al. 2000), exerting important effects on the short and long features observed on the beach. Historical records show that since 1972, more than 30 episodes of mud deposition along Cassino beach were recorded (Delaney, 1965; Willwock and Martins, 1972; Martins et al., 1979), bringing

negative consequences for the ecosystem and the economy of the area. Particularly in 1998, three storms happened at Cassino beach. During that year, Torronteguy (2000) and others, carried out measurements on the Cassino beach shoreface. In this study the mud deposits located between 12 to 4 m (an area approximately of 48 km^2) were sampled, generating maps with the characteristics of the deposits. The author concluded that the data obtained in the sediment analysis were in agreement with the general pattern of muddy sediments and presented a high percentile of fine, organic matter and water content. The volume of fluid mud found close the shore was relatively low, covering approximately 12 km of extension and around 3 to 4 km of width, from shoreline towards the sea. The fluid mud map revealed that the thickness of the fluid mud increased gradually from the south to the north, and towards the coast, achieving 1.24 m. The density varied between 0.98 and 1.45 g cm^{-3}.

4.3. Model Description

4.3.1. Standard SWAN model (without mud)

The SWAN model (Simulating WAves Nearshore) version 40.41 (Booij et al. 2004) was used in this study. SWAN is a 3rd generation numerical model of high resolution, developed for obtaining realistic estimates of wave parameters in coastal areas, lakes and estuaries based on given wind field, bottom topography, water level and current field conditions in waters of deep, intermediate and shallow depth. Conceptually, the SWAN model is an extension of the deep water third-generation wave models and incorporates the state-of-the-art formulations for the deep water processes of wave generation, dissipation and the quadruplet-wave interactions from the WAM model (both WAM cycle 3; the WAMDI group, and WAM Cycle 4. The model uses formulations for wave growth by wind, wave dissipation by whitecapping and four waves nonlinear interactions (quadruplets or quads) adapted for the finite water

depth. It also includes physical processes associated with intermediate-depth and shallow water: bottom friction, depth-induced shoaling, refraction and breaking.

The SWAN model used in this study is a two-dimensional fully spectral state-of-the-art wave propagation model. The evolution of waves in the SWAN model is based on an Eulerian formulation of the spectral discrete wave action balance equation (or energy balance in the absence of currents), including sources and sinks. The model is discrete and spectral in frequencies and directions, and the kinematics behavior of the waves (including the effect of currents) is described with the linear theory of surface gravity waves. The governing equation of the model in Cartesian coordinates is described by the spectral action balance as:

$$\frac{\partial}{\partial t}N + \frac{\partial}{\partial x}c_{g,x}N + \frac{\partial}{\partial y}c_{g,y}N + \frac{\partial}{\partial \sigma}c_{g,\sigma}N + \frac{\partial}{\partial \theta}c_{g,\theta}N = \frac{S}{\sigma} \tag{4.1}$$

Where σ is the relative frequency (the wave frequency measured from a frame of reference moving with the action propagation velocity), θ the wave direction (the direction normal to the wave crest of each spectral component), N is the wave action density, equal to the energy density divided by the relative frequency ($N = E \, / \, \sigma$), C_g is the wave action propagation speed in ($x, \, y, \, \sigma, \, \theta$) space and S is the total of source/sink, which is generally written as the sum of a number of separate source terms, each representing a different type of process.

$$S = S_{in} + S_{ds} + S_{nl} \tag{2}$$

where S_{in} represents the wave generation by winds, S_{ds} the dissipation of the wave energy due to whitecapping, wave-bottom interactions and in very shallow water depth-induced wave

breaking, and S_{nl} is the wave energy transfer due to conservative nonlinear wave-wave interactions (both quadruplet interactions S_{nl4} and triad interactions S_{nl3}).

The initial conditions for the model were wind speed and direction at user-specified time intervals together with the bathymetry of the area. The boundary conditions were specified in terms of integral wave parameters: significant wave height, the characteristic wave period of the energy spectrum, which may be the value of the peak period or the value of the mean period, and the mean wave direction. From input parameters the model calculates wave energy spectra, represented at discrete frequency-direction bands, in every grid cell. From these spectra, characteristic wave heights, periods, and directions of propagation are determined.

4.3.2. The SWAN model considering mud

The SWAN model considering mud consists of a fluid mud induced wave-damping formulation obtained from the modified two-layer model proposed by Gade (1958), which was implemented in the standard version of the SWAN model by Winterwerp et al. (2007). In (2) a sink term accounting for viscous dissipation in the mud layer $S_{ds,m}$ has been implemented (not elaborated here) resulting in

$$S = S_{in} + S_{ds} + S_{ds,m} + S_{nl} \qquad (3)$$

The new SWAN model is a standalone program, and the fluid mud parameters have to be provided to the model, including the thickness and extension of the mud layer (σ_m (x, y, t)), and its viscosity (v_m') and density (r_m). The elasticity, plasticity and porosity effects were ignored.

In the work carried out by Winterwerp et al. (2007), the new SWAN model was applied to simulate laboratory experiments and field observations on wave damping at the Guyana coastal system. The model results compared favorably with observations, though detailed field data were not available for an in depth verification.

4.4. Model Verification for February 1998

Before the application of the SWAN model in the standard format (without mud) and considering mud, the model was verified for each situation. The SWAN model without mud was verified based on the comparison between modeling results and data available from wave measurements for the period relative to February of 1998. The verification of the SWAN model considering mud was carried out in the form of a sensitivity analysis, using the deep water wave climate for the area.

4.4.1. Standard SWAN model (without mud)

The results of the standard SWAN model with default parameter settings were compared with data available from wave measurements at 15 m water depth. Modeling results were compared against data from a directional waverider relative to February of 1998 with digital acquisition located close to the mouth of the Patos Lagoon estuary (at 15 m of depth, Figure 4.2). Comparisons were carried out in terms of significant wave height, peak period, mean wave direction and energy density. The SWAN model was applied to the studied area presented in Figure 4.9, which covers a 100 km wide coastal area and extends about 50 km offshore throughout the RS State, and includes the Cassino Beach area. The depth at the cross-shore boundaries of the domain varies between 1 to 29 m. The bottom topography of the

area was established based on data from the Brazilian Navy Nautical Charts. The wave model uses a curvilinear grid that comprises 41 by 104 points, with approximately 4264 active points (Figure 4.6). The dimensions of the grid cells vary from 1.5 km near the boundaries to approximately 1.0 km near the jetties and around Cassino Beach.
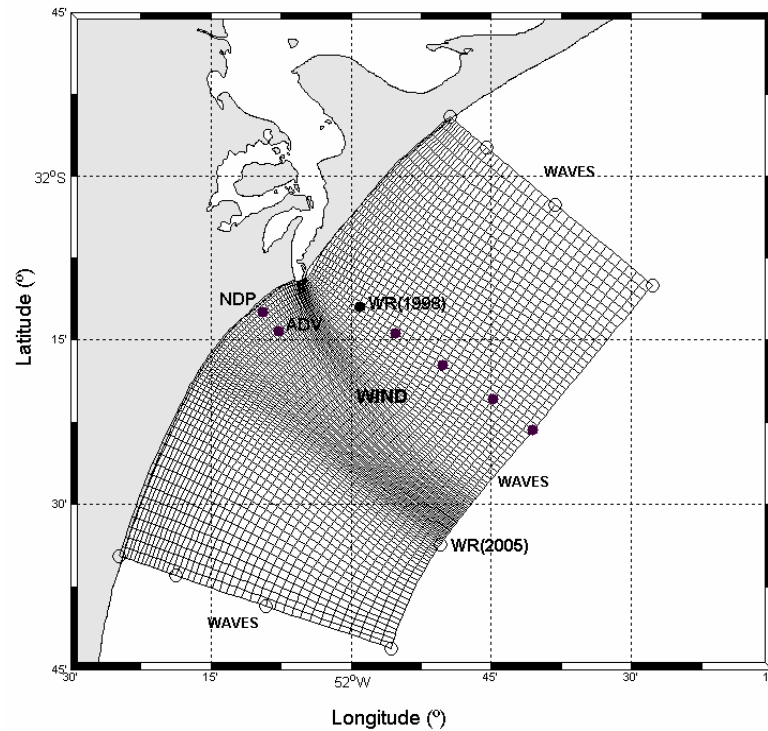
Figure 4. 6 – Model domain and curvilinear grid for the numerical experiments showing the selected points in the open boundaries where wave data is prescribed. Location of the output parameters for SWAN model verification and application.

A time series of hourly wind speed and direction measured at the Pilots Station (Figure 4.2) during February 1998 was used to establish selected periods for the simulations (Figure 4.7). The wind was considered constant in time and in space and was prescribed as the surface boundary condition over the entire domain of the model.
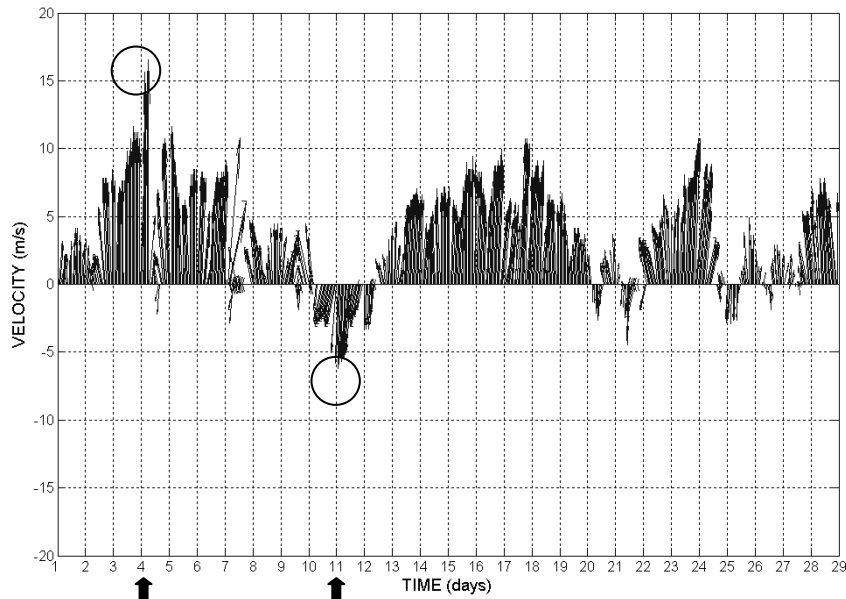
Figure 4. 7 - Time series of hourly wind velocity and direction measured at the Pilots Station in February 1998. (Positive values indicate winds from the north, while negative values indicate winds from the south). The highlighted periods were selected for the numerical simulations.
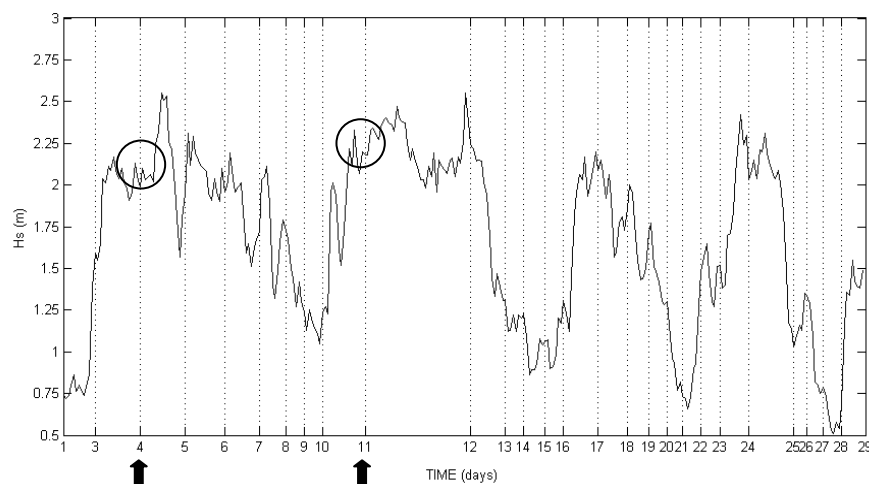
Figure 4. 8 - Time series of significant height measured from the directional waverider located at 32º10'002"S and 51º58'913" W (close to the mouth of the Patos Lagoon estuary) relative to February, 1998. The highlighted periods were selected for the numerical simulations.

Information about the significant wave height (Hs) for the same periods were selected from Strauch (1998) (Figure 4.8) and applied at the ocean boundaries of the domain. The wave data is relative to February of 1998 and was obtained from a directional waverider with digital acquisition, located at 32º10'002"S and 51º58'913" W (close to the mouth of the Patos Lagoon estuary) and fixed at 15 m of depth (Figure 4.2). The numerical experiments focused

on the predominant state of the sea conditions indicated by literature for this area. Two types of ocean waves generated by the wind were selected: swell and local sea conditions, corresponding to different wind directions.

In order to establish the best way of prescribing the wave parameters at the ocean boundaries, several simulations were carried out with the parameters and periods presented in Table 4.1. Table 4.1 presents the selected wave conditions at the waverider point relative to 1998 (Figure 4.2) and the wind velocity and direction on February 1998. This information was prescribed by either a uniform distribution along the open boundaries in some experiments, or only at selected points, edges of the various linear segments in the open boundaries (Figure 4.9).

Table 4.1 – Observed wave conditions at the waverider point and measured wind velocity and direction on February, 1998. (H_s = wave significant height, T_p = wave peak period, DIR = wave nautical direction, V = wind velocity and DIR = wind direction)

Data	Measured Wind			Observed Wave Conditions			
	Time	V (m s^{-1})	DIR(degree)	Time	H_s (m)	T_p (s)	DIR(degree)
11/2/1998	09:15	8.08	225.0	09:15	2.1	12.5	167
4/2/1998	01:10	11.20	67.5	01:10	2.1	6.3	113

Results from these numerical experiments are presented in terms of the spectral energy density calculated by the model, and compared with wave measurements (Strauch, 1998) for the same period. For swell conditions, the comparison between the computed and observed energy density with respect to the form of applying the boundary conditions at the open boundaries have shown that the shape of the spectrum is well reproduced when prescribing the spectral wave file in selected points of the ocean boundaries, although the energy level is underestimated (Figure 4.9A). A better reproduction of the energy level is obtained when prescribing the wave height (H_s), peak period (T_p) and wave nautical direction (DIR) throughout the open boundary (Figure 4.9B). Results from Figure 4.9 also show that when the wave spectrum has two spectral peaks, the model manages to reproduce the spectral level

observed in the low frequency peak, but underestimates the spectral level in the high frequency peak. When the wave spectrum has only one peak (Figure 4.13), however, the model does reproduce well the observed spectrum.

Figure 4. 9A - Comparison between energy density calculated by the SWAN model and waverider data during a period of uniform wind from the SW (velocity 8.08 m s^{-1}). Wave spectral file at February 11th, 1998 at 09:15 h with H_s = 2.1 m, T_p = 12.5s and DIR = 167º prescribed in selected points of the ocean boundaries.

Figure 4.9B - Comparison between energy density calculated by the SWAN model and waverider data during a period of uniform wind from the SW (velocity 8.08 m s^{-1}). Wave data at February 11th, 1998 at 09:15 h prescribed homogeneously along the open boundaries.

Results for sea conditions show a similar behavior (Figure 4.10). When prescribing the wave parameters in the form a spectral file in selected points of the open boundaries, the energy density is underestimated (Figure 4.10A). Better results were obtained when prescribing the wave height (H_s), peak period (T_p) and wave nautical direction (DIR) throughout the open boundary (Figure 4.10B).

Figure 4. 10A - Comparison between energy density calculated by the SWAN model and waverider data during a period of uniform wind from the ENE (velocity 11.20 m s^{-1}). Wave data at February 4th, 1998 at 01:10 h with H_s = 2.0 m, T_p = 6.3s and DIR = 113° prescribed in selected points of the ocean boundaries.

Figure 4. 10B - Comparison between energy density calculated by the SWAN model and waverider data during a period of uniform wind from the ENE (velocity 11.20 m s^{-1}). Wave data at February 4th, 1998 at 01:10 h prescribed homogeneously along the open boundaries.

In order to investigate the contribution of the terms which represents processes that generate, dissipate or redistribute wave energy in the form of the calculated spectrum, tests were carried out considering variations in the default formulations of the SWAN model for the generation of waves by the wind (S_{in}) the wave energy transfer due to conservative nonlinear wave-wave interactions (S_{nl}) and the dissipation of wave energy due to whitecapping (S_{ds}). Comparisons were carried out in terms of the spectral energy density obtained from the SWAN model computations and from the waverider data relative to February of 1998. The simulations carried out with the whitecapping process activated, and de-activated are showed here. A directional resolution of 36° was adopted over the full circle in all the simulations. The spreading frequency was schematized using 63 discrete frequencies between 0.03 Hz and 0.58 Hz and a logarithmic scale, the same resolution of the waverider. For the remaining parameters the default settings of the SWAN model were used.

Results from the numerical experiments considering the whitecaping de-activated for swell conditions indicate that the absence of the whitecapping effect over the bimodal spectra is significant, resulting in a stronger wind effect and an increase in the energy density in the higher frequencies (Figure 4.11A). Results for sea conditions (Figure 4.11B) show that the absence of the whitecapping process also increases the contribution of the wind effect. Thus, the whitecapping mechanism works as a control mechanism regulating the wave energy in the higher frequencies.

The comparison between modeling results and measurements of wave parameters indicates that the best modeling results were obtained when the wave parameters used as boundary conditions are constant along the open boundaries. With the whitecapping de-activated, the reproduction of the energy spectrum gets worse. Thus, the whitecapping process works as a control mechanism for the wind action.
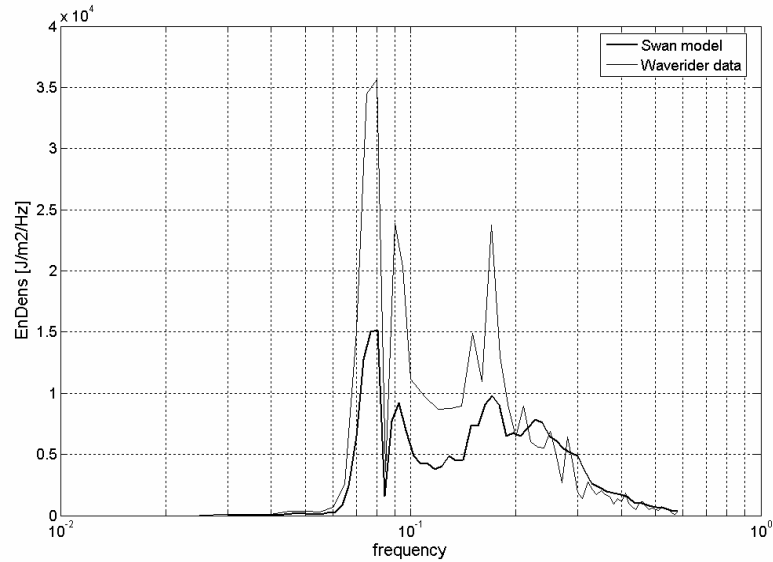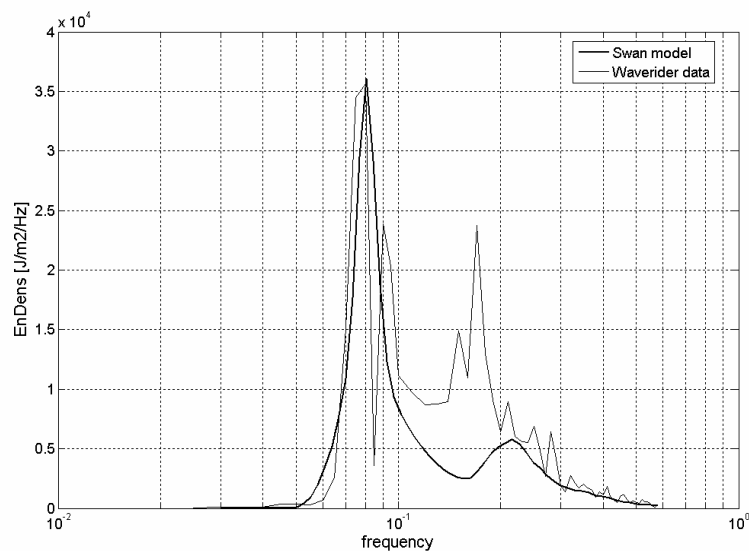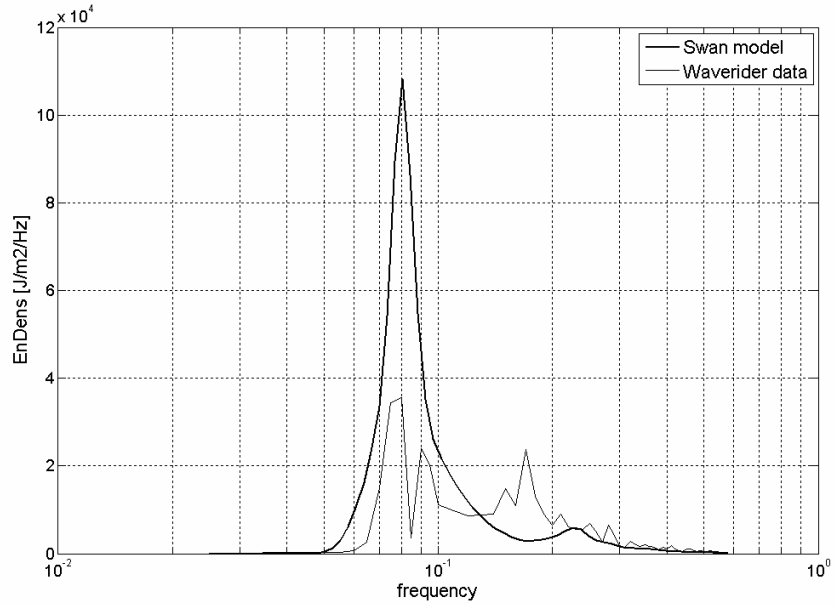
Figure 4. 11A - Comparison between energy density calculated by the SWAN model and waverider data during a period of uniform wind from the SW (velocity 8.08 m s^{-1}) in February 11th, 1998 at 09:15 h. Boundary conditions were prescribed homogenously along the open boundaries and the whitecapping process de-activated .
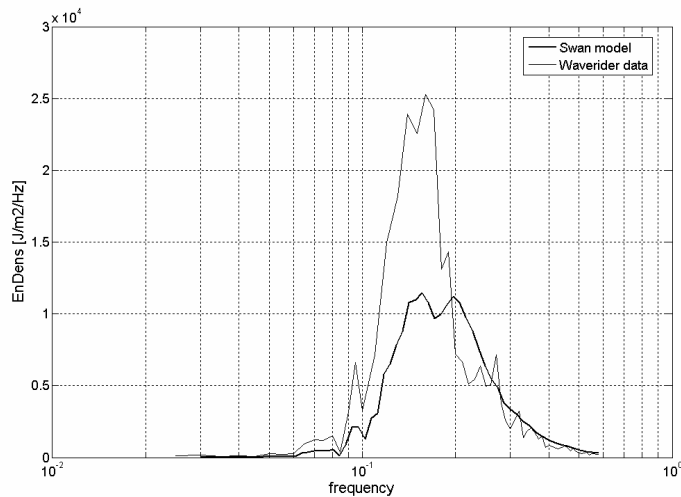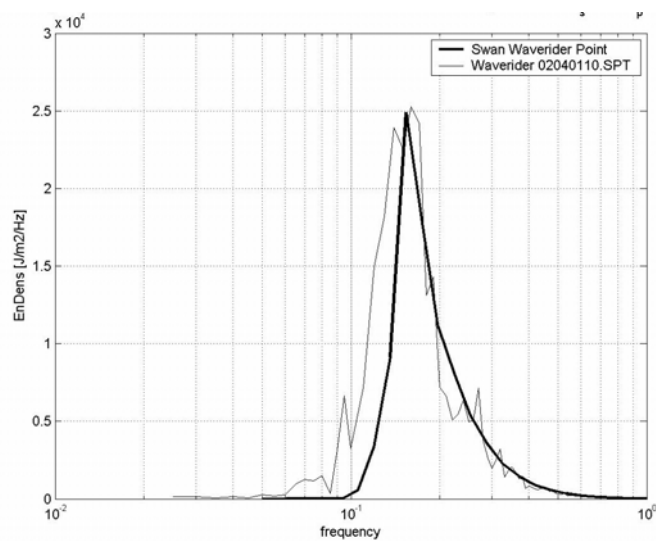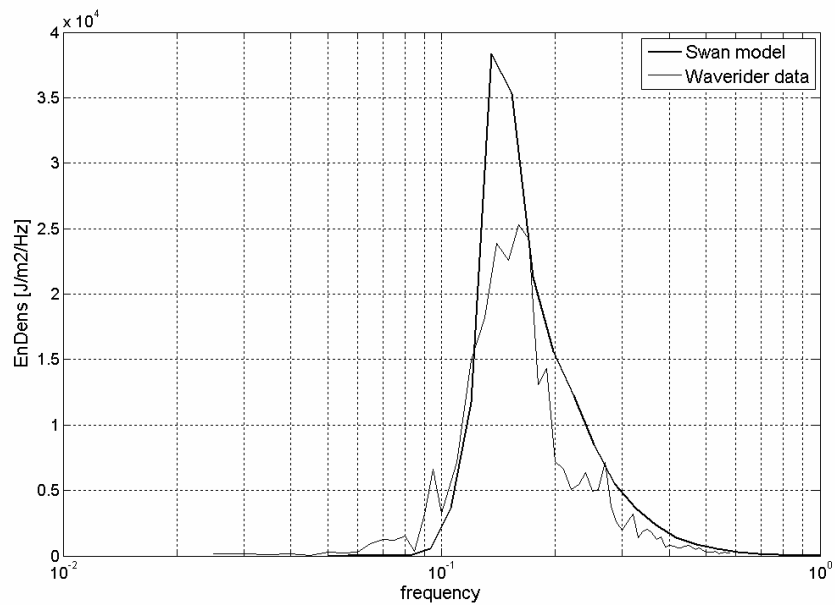

Figure 4.11B- Comparison between energy density calculated by the SWAN model and waverider data during a period of uniform wind from the ENE (velocity 11.20 m s^{-1}) at February 4th, 1998 at 01:10 h. Boundary conditions were prescribed homogenously along the open boundaries and the whitecapping process de-activated .

4.4.2. The SWAN model considering mud

In the second phase of this study, numerical simulations were carried out to analyze the response of the SWAN mud wave damping module (Winterwerp et al., 2007) with respect to the wave attenuation in terms of decreasing the significant wave height and energy density. Selected simulations without mud (Figures 4.9B and 4.11B), were reproduced including the wave-mud interaction for the predominant wind conditions.

The input parameters used for the SWAN mud-wave damping model were obtained from the mud deposits observed at Cassino Beach in 1998 (Torronteguy, 2000): thickness (σ_m = 1.00 m) and density (δ_m = 1300 kg m^{-3}). In this computation the fluid mud layer was considered constant in the entire computational domain. As no detailed information was available on the mud viscosity, this parameter was assessed from literature. Winterwerp et al., (2007) tested the mud viscosity ν_m = 0.01, 0.001 and 0.0001 m^{2}s^{-1}, and determined that better results were obtained when considering the mud viscosity of 0.001 m^2 s^{-1} , a typical value for muddy beds. This value of mud viscosity was used in the simulations. The output parameters were extracted for the five points between the location of the waverider relative to February of 1998 and the point located in the eastern open boundary (Figure 4.3).Three points were chosen between these limits and used for comparison between modeling results with and without mud with the observed data presented in Table 4.2

The results in Figure 4.9 also indicate that during periods of SW wind the presence of mud on the bottom attenuates the energy density primarily in the lower frequencies. This results in an apparent shift of the peak frequency, as shown in Figure 4.15 and also Figure 4.16 for ENE wind conditions.
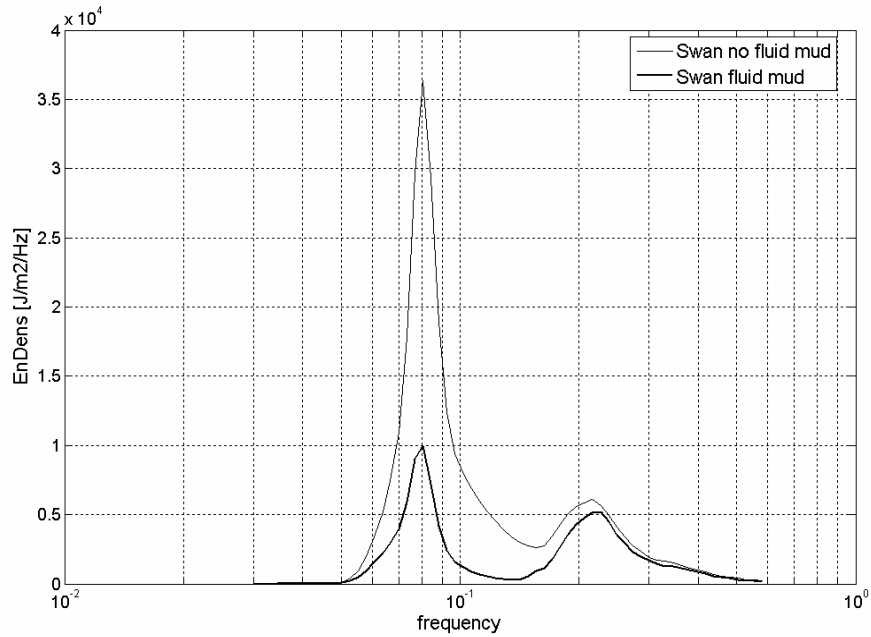
Figure 4. 12 - Comparison between energy density per frequency calculated by the SWAN model and SWAN mud wave damping model during a period of uniform wind from the SW (velocity 8.08 m s^{-1}). The mud parameters were δ_m = 1.00 m, ρ_m = 1300 kg m^{-3} and ν_m = 0.001 m^2 s^{-1}, set constant in all computational domain.

Figure 4. 13 - Comparison between energy density per frequency calculated by the SWAN wave model and SWAN mud wave damping model during a period of uniform wind from the ENE (velocity 12.20 m s^{-1}). The mud parameters   were δ_m = 1.00 m, ρ_m = 1300 kg m^{-3} and ν_m = 0.001 m^2 s^{-1}, set constant in all computational domain.

A summary of the model results with and without considering the mud-wave interaction in comparison with the observed data is presented in Table 4.2. Results during SW wind conditions indicate that the calculated significant wave height (with and without the presence of mud), was underestimated in 9.5% and 33.3% in relation to the measurements at the waverider point, respectively. During ENE wind conditions, the calculated significant wave height (with and without the presence of mud), was underestimated in 10.0% and 25.0%, respectively.

Table 4.2 - Comparison between observed significant wave height and the model results with and without the mud-wave damping. Mud parameters $\delta_m = 1.00$ m, $\rho_m = 1300$ kg m^{-3} and $\nu_m = 0.001$ m^2 s^{-1}

Location	Observed H_s (m)	Computed H_s (m) without fluid mud	Computed H_s (m) with fluid mud
SW wind conditions			
P1(Waverider point,1998)	2.1	1.9	1.4
P2		2.1	1.7
P3		2.2	1.9
P4		2.3	2.1
P5(East boundary point)		2.3	2.2
ENE wind conditions			
P1(Waverider point,1998)	2.0	1.8	1.5
P2		1.9	1.7
P3		2.0	1.8
P4		2.1	2.0
P5(East boundary point)		2.1	2.1

4.5. Model application for the 2005 survey – Cassino Experiment

4.5.1 Description of the prevailing hydro-meteo conditions

The latest field data for the study area was obtained during the Cassino Experiment, carried out in 2005, aiming to map the mud deposits off Cassino Beach, and to collect new information on the hydrodynamics and geological aspects, and their effects on the sediment dynamics in the area. Geological, geophysical, video imaging, radar, and climatological data

(including waves, currents, sediment movement and associated beach profile changes) were collected on the inner shelf and shoreface of Cassino Beach, analyzed and interpreted for the period between May 13th and June 25th. Calliari et al. (2005) present the Cassino Experiment in detail (see also Holland et al. this volume). These data, however, is still limited to fixed points during a short period of measurements.

In order to characterize in detail the wave climate of the RS State, with special emphasis to the surroundings of Cassino Beach (Figure 4.2), the SWAN model was applied in the stationary mode to reproduce the predominant wave conditions during the Cassino Experiment (2005). The stationary assumption implies instantaneous wave propagation across the domain, as well as instantaneous wave response to changes in the wind field (Rogers et al., 2005). The model domain was studied based on a curvilinear grid (Figure 4.3). The boundary conditions for the model were based on data measured during the Cassino Experiment.

A time series of hourly wind speed and direction measured at Cassino Beach (Figure 4.2) from May 13th to June 25th 2005 was used to establish selected periods for the simulations (Figure 4.14A).
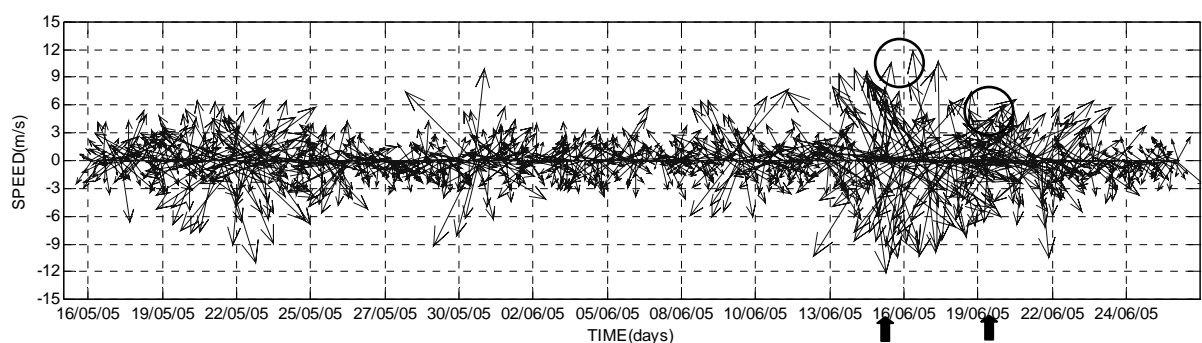
Figure 4. 14 – A) A time series of hourly wind mean speed and direction measured at Cassino Beach between 15/05 and 25/06 2005. Positive values indicate winds from the north, while negative values indicate winds from the south. The highlighted periods were selected for the numerical simulations.

The wind data was collected at 10 m height above the ground and represented 10 min averages. A statistical analysis of the data indicates that predominant winds are from the northeast (NE) and from the south (S) (Figure 4.14B). The wind was prescribed as the surface boundary condition and considered constant in time and space over the entire domain.
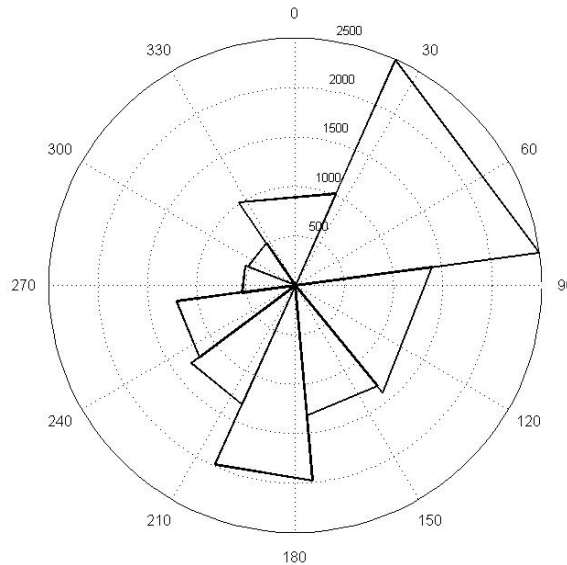
Figure 4.14 – B) Frequency of occurrence of the wind velocity and direction measured at Cassino Beach between 15/05 and 25/06 2005.

Information about the significant wave height (H_s), peak period (T_p) and mean wave direction (DIR) for the same periods were selected from measurements carried out between May 13th and June 25th with a directional waverider relative to the 2005 survey with digital acquisition installed off Cassino Beach (32° 26' 37" S and 51° 55' 53" W, Figure 2), fixed at 25 m depth (Figure 4.15B) and applied at the ocean boundaries of the domain. A preliminary statistical analysis of the data indicates significant heights between 1.0 and 3.0 m, mean period smaller than 6 s and predominant directions between northeast (NE) and south (S) (Figure 4.15B).

The wave parameters used as boundary conditions are prescribed constant along the open boundaries.
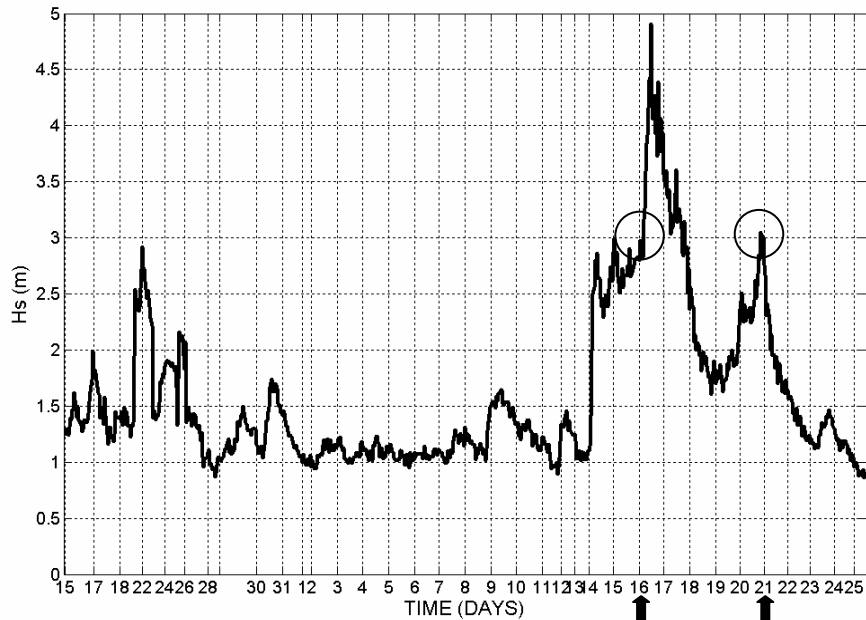
Figure 4.15 A) Significant wave height measured between May 13th to June 25th, 2005 by a directional waverider located at 32º10'002"S and 51º58'913" W.
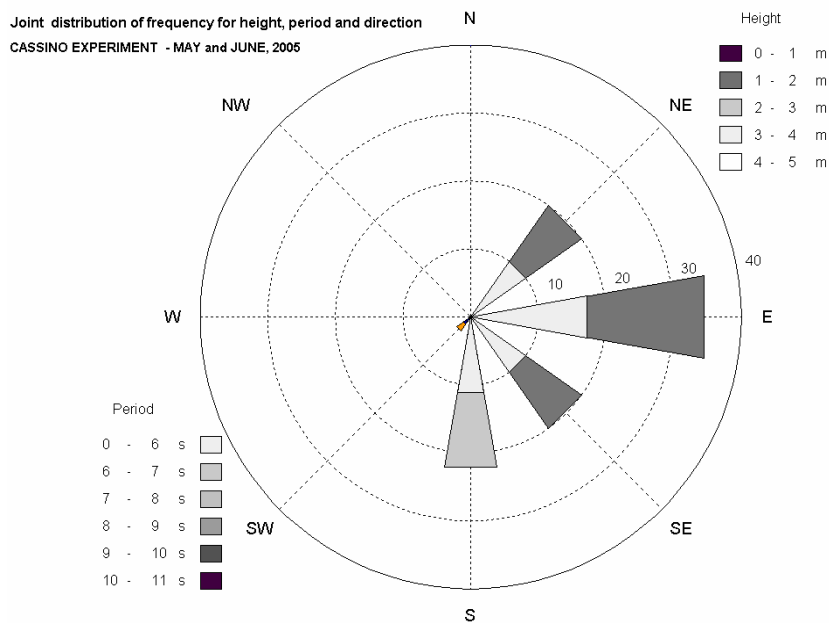
Figure 4.15 B) Joint distribution of frequency for significant height, peak period and mean direction between May 13th and June 25th, 2005.

The selection of cases for the numerical simulations with the standard SWAN model was based on the most frequent winds registered in the studied area, associated with the availability of wave data recorded for the same period. Two wind situations were selected: winds from the northeast (NE) and winds from the south (S), where the wave data represented the characteristic states of the sea. Table 4.3 presents the different wind velocity and directions and the observed wave conditions at the waverider point during the Cassino Experiment for the selected cases.

Table 4. 3 - Measured wind velocity and direction, and observed wave conditions at the waverider point during the Cassino Experiment for the selected cases.

Data	Measured Wind			Observed Wave Conditions			
	Time	V (m s^{-1})	DIR(degree)	Time	H_s (m)	T_p (s)	DIR(degree)
15/6/2005	07:45	12.08	61.94	08:37	2.56	7.70	109.20
20/6/2005	17:35	8.17	200.20	17:39	2.68	10.53	209.66

In all simulations, a directional resolution of 36° was adopted for the wave spectrum over the full circle. The spreading frequency was schematized using 63 discrete frequencies between 0.03 Hz and 0.58 Hz using a logarithmic scale. For the remaining parameters the default settings of the SWAN model were used. When considering the presence of mud at the bottom, the parameters presented in Section 4.4.2 were prescribed in all the computational domain.

The output parameters were selected for all computational domain, and also at two points in a perpendicular line to Cassino Beach, crossing through the mud deposit. The first point was located in the NDP location (32°13'14'' and 52°10'01'') at 9 m depth, and the second in the ADV location at 12 m of depth (32° 15' 47" and 52° 08' 23.7") (Figure 4.2)

4.5.2. Modeling results without mud:

Figure 4.16 presents the energy density calculated by the SWAN model at 9 and 12 m depth when prescribing a uniform wind. Results for winds from the NE (Figure 4.16A) present a unimodal spectra and the expected attenuation of the wave energy as it progresses towards the shore. Results for winds from the S (Figure 4.16B), present a bimodal spectra with sea and swell peaks and the expected attenuation onshore. Measurements from the Cassino Experiment indicate the occurrence of bimodal spectra when winds are from the south quadrant in according with information from the literature (Araújo et al., 2003)

(A)

(B)
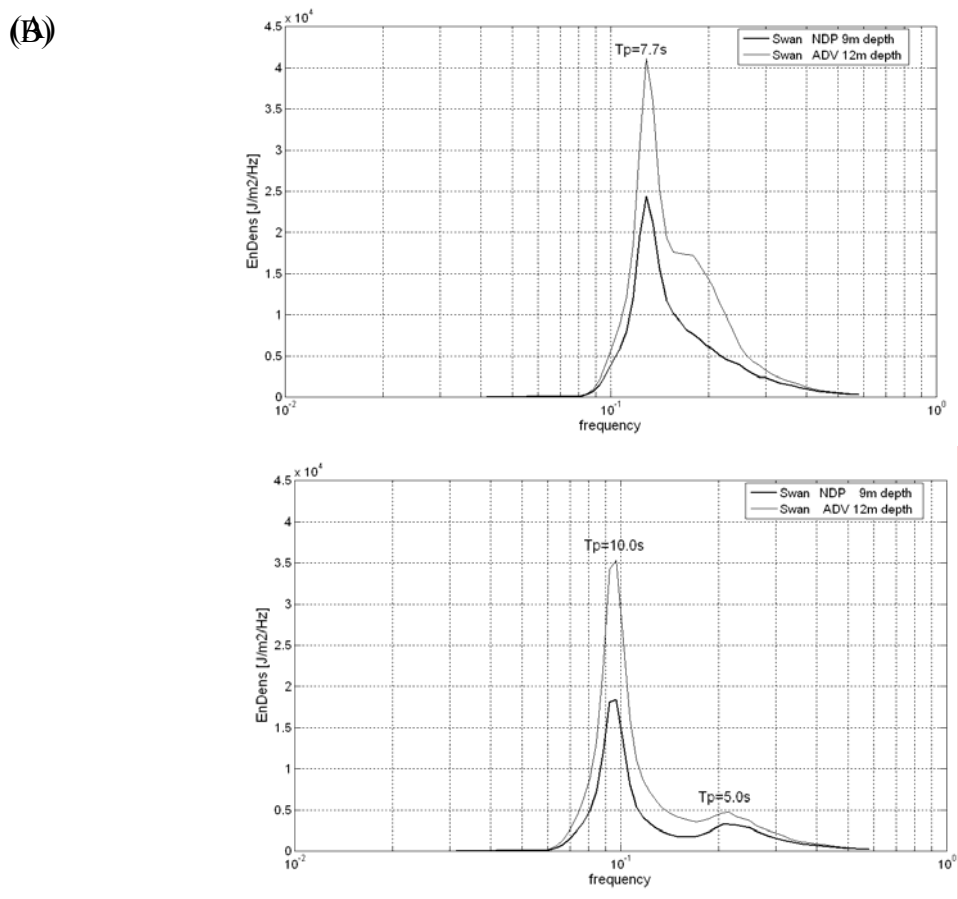
Figure 4. 16 – Energy density calculated by the SWAN model at NDP localization point and ADV localization point . A) Uniform wind velocity of 12.08 m s^{-1} from the NE. B) Uniform wind velocity of 8.17 m s^{-1} from the S.

Figure 4.17 presents the spatial distribution of significant wave height and mean wave direction calculated by the SWAN model for the selected cases. Results for winds from the NE (Figure 4.17A) indicate that the calculated significant wave height decreases towards the shore, varying from 2.5 m in the deeper area to a minimum of 0.5 m in shallow water, and the mean wave direction from the NE. Results for winds from the S (Figure 4.1B) indicate that the calculated significant wave height decreases towards the shore, varying from 2.5 m in the deeper area to a minimum of 0.5 m in shallow water, and the mean wave direction is from the S.

(A)
(B)
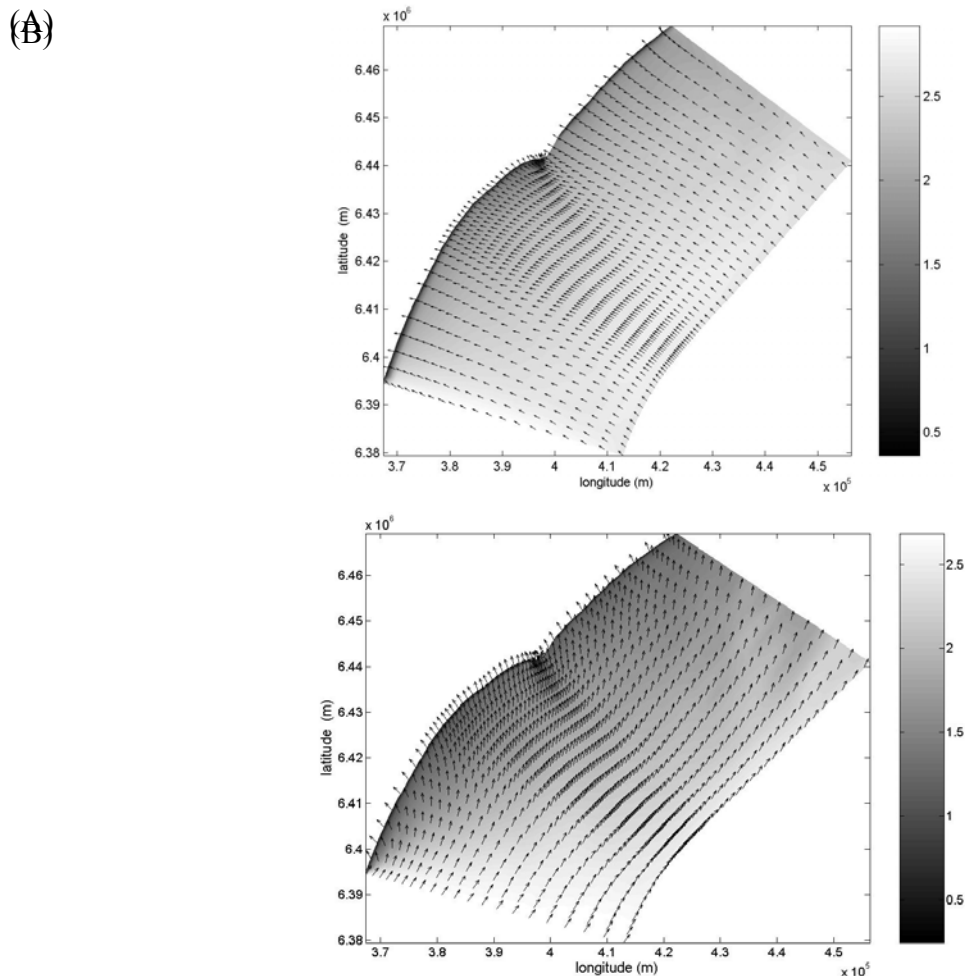
Figure 4. 17 - Spatial distribution of significant wave height and mean direction (represented by the black arrows) calculated by the SWAN model for the computational domain. A) Uniform wind velocity of from the NE and resulting mean wave direction (B) Uniform wind velocity from the S and resulting mean wave direction.

4.5.3. Modeling results with mud

In order to evaluate the contribution of mud deposits at the bottom over the wave energy observed in the area, the previously selected simulations without mud were reproduced including the wave-mud interaction (Figure 4.18).

When considering the presence of mud at the bottom, the parameters presented in Section 4.2, thickness (σ_m = 0.40 m), density (ρ_m = 1310 kg m^{-3}) and viscosity (ν_m = 0.001 m^2 s^{-1}) were prescribed in all the computational domain.

Results for winds from the NE (Figure 4.18A) indicate that the presence of mud attenuates approximately 90% of the wave energy at the peak frequency, resulting again in an apparent shift in peak period. The result shown in Figure 4.18B for winds from the S indicates that although the presence of mud attenuates around 90% of the wave energy in the low peak frequency, it has a smaller effect in attenuating the energy on the high peak frequency.
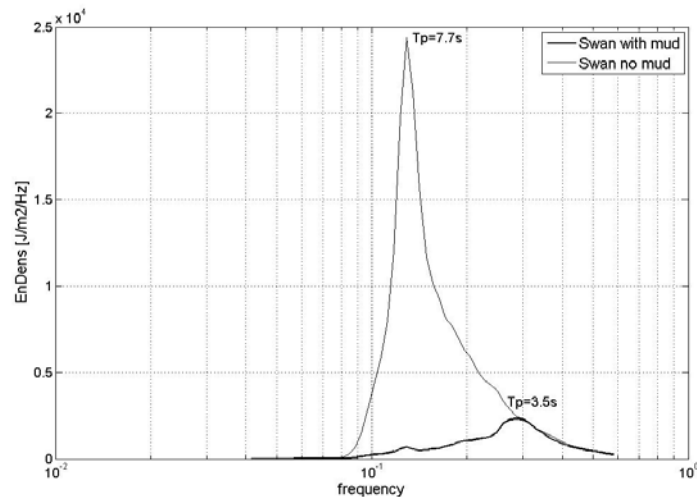
Figure 4.18 A) - Energy density calculated by the SWAN model with and without the presence of mud at NDP localization point. Uniform wind velocity from the NE.
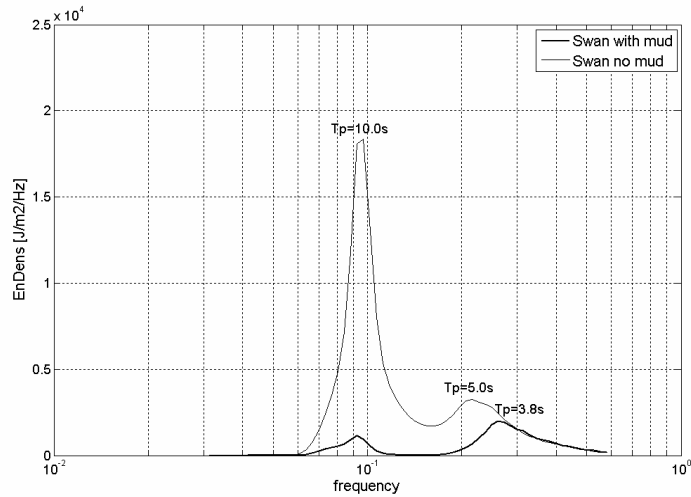
Figure 4.19 B) - Energy density calculated by the SWAN model with and without the presence of mud at NDP localization point. Uniform wind velocity from the S.

Figure 4.19 shows a comparison between significant wave heights calculated by the SWAN model (with and without mud) and measured with a NDP (Acoustic Doppler Profiler) for the NDP localization point at 9m of depth, and with data from a waverider relative to the 2005 survey at 25 m (Figure 2) for the studied period.
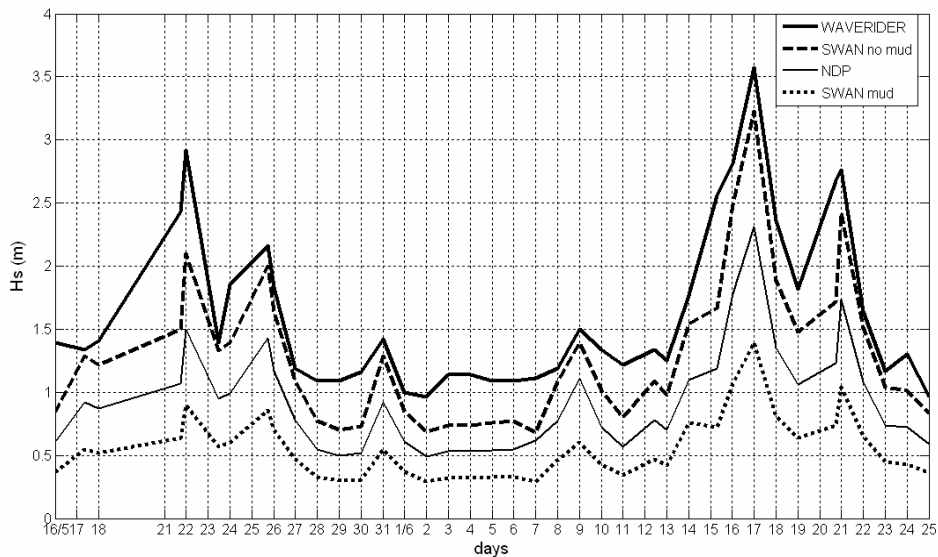
Figure 4.20 -The significant wave height measured with a waverider at 25 m, with a NDP (Acoustic Doppler Profiler), and calculated by the SWAN model without and with mud at NDP point.

In general, all the time series presented a similar pattern. Observed (large black line) and calculated results without mud (dashed black line) for the NDP point (Figure 4.2) are in agreement, following the expected behavior. The model without mud overestimates the significant wave height in 40 to 100% of the measured values with the NDP (fine black line), indicating the limitation of considering a rigid bottom in the domain. By considering the presence of mud in the whole domain (dotted black line), the model with mud shows a clear decrease of the significant wave height (30 – 40% in relation to the NDP localization point). However, the significant wave height is underestimated due to the consideration of a constant mud thickness, extension, density and viscosity in the whole domain.

6. Conclusions

The compilation of the existent data on the wave climate throughout the SBS provided a limited characterization of the typical behavior of the local wave environment indicating that the predominant wave directions are 100° and 160° (SE), with wave heights varying between 1 and 1,50 m. The predominant wave period is between 6 and 14 s. This characterization, however, was based on limited and sparse field data, highlighting the necessity of extrapolating this information for the whole domain by using numerical models.

The standard SWAN model was verified with measured wave data available in literature, indicating a satisfactory model performance in the representation of the studied cases, although some limitations were identified. When the wave spectrum has two energy peaks, results indicated that the shape of the spectrum is well reproduced, and the SWAN model agrees with the energy level observed in the low frequency peak, although underestimating the energy level in the higher frequency peak. In the wave spectrum with only one peak, the model does reproduce well the observed spectrum. The verification of the SWAN model

considering mud was carried out in the form of a sensitivity analysis. These model results indicated that although the presence of mud attenuates most of the wave energy on the low peak frequency, it has a smaller effect in attenuating the energy on the high peak frequency.

The SWAN model was then applied to characterize the wave climate in the SBS, especially in the surroundings of Cassino Beach, during the Cassino Experiment. The determination of the wave climate for the area based on results from the SWAN model indicated that when the wind comes from the south (S) bi-modal spectra is observed due to the presence of combined sea and swell waves. When the wind comes from the northeast (NE) the shape of the spectrum indicates only one peak. The spatial distribution of significant wave height and mean direction obtained from the SWAN model computations using a uniform wind velocity for the entire computational domain suggests the expected decay when moving from deep to shallow waters.

The effect of the mud-wave interaction on the significant wave height and mean wave period calculated by the model indicates that the calculated significant wave height with the presence of mud was attenuated in relation to the measurements. However, this attenuation is likely to be overestimated because the mud density, tickness, position and viscosity was considered constant over the whole domain.

Acknowledgements

Han Winterwerp and Gerben de Boer for the valuable training and special attention received during her stay at WL|Delft Hydraulics.

References

Araujo, C. E. S., Franco, D., Melo, E.,Pimenta, F. M., 2003. Wave Regime Characteristics of the Southern Brazilian Coast, Procedures COPEDEC VI, Colombo, Sri Lanka; CD press.

Benoit, M., Marcos, F.,Becq, F., 1996. Development of a third-generation shallow-water wave model with unstructured spatial meshing. Proceedings of 25th International Conference on Coastal Engineering, Am. Soc. Of Civ. Eng., New York, 465-478.

Berkhoff, J. C. W., 1972. Computation of combined refraction-diffraction, Proceedings of 13th International Conference on Coastal Engineering, Am. Soc. Of Civ. Eng., New York, 471-490.

Blomgren, S., Larson, M., Hanson, H.,2001. Numerical modeling of the wave climate in the southern Baltic Sea. *Journal of Coastal Research* 17(2), 342-352.

Booij, N., L.H. Holthuijsen and R.C. Ris, 1996, The "SWAN" wave model for shallow water, Proceedings 25th International Conference of Coastal Engineering, Orlando, pp. 668-676

Booij, N., Ris, R.C., Holthuijsen, L.H., 1999. A third-generation wave model for coastal regions, 1, Model description and validation.*Journal Geophysical Research*, Vol, 104, pp. 7649-7666.

Booij, N., Haagsma, IJ.G., Holthuijsen, L.H., Kieftenburg, A.T.M.M., Ris, R.C., Westhuysen, A.J. van der and Zijlema,.M., 2004: SWAN Cycle III Version 40.41 Users Manual, Delft University of Technology, Delft, The Netherlands, 118 p, http://fluidmechanics.tudelft.nl/swan/index.htm.

Calliari, L.J. Speranski, N. S.,Torronteguy, M. E., Oliveira, M.B., 2000. The mud banks of Cassino Beach, Southern Brazil: Characteristics, Processes and Effects. *Journal of Coastal Research*, ICS 2000, Proceedings, 1-9, New Zealand.

Calliari, L.J., Holland, T., Dias, M.S.,Vinzon, S., Thorton, E., Stanton, T. Experimento Cassino 2005: Uma síntese dos levantamentos efetuados na ante-praia e zona de arrebentação. Proceedings ABEQUA 2005 CD-ROM Published by META Marketing & Eventos Ltda.Av. Nilo Peçanha, 50/1610 -20044-900, Rio de Janeiro, RJ, Brazil.

Camargo, O. A., Silva, F. J. L., Custodio, R.S., Gravino, N., 2002. Atlas Eólico do Rio Grande do Sul. Department of energy, mine and communications, Porto Alegre,Rio Grande do Sul, Brazil. 70p. http://www.semc.rs.gov.br/

Castro, B., Miranda, L. B., 1998. Physical Oceanography of the western Atlantic continental shelf between 4°N and 34°S. In: Brink, K. and Robinson, A. (Eds.), The Sea – The Global Coastal Oceans, John Wiley & Sons, Inc. Vol. 10, chapter 8, pp. 209-251.

Coli, A. B.,1994. Análise das alturas de onda ao longo do Rio Grande do Sul: dados históricos e altimétricos. Graduation work in oceanology course. Federal University of Rio Grande – FURG, Rio Grande, Rio Grande do Sul, Brazil, 58p, unpublished.

Coli, A.B., 2000. Estudo do Clima Ondulatório em Rio Grande. Master's thesis, Engineer Oceanic course Federal University of Rio Grande – FURG, Rio Grande, Rio Grande do Sul, Brazil, 76p, unpublished.

Cuchiara D. C., Fernandes, E. H., Strauch, J. C., Calliari, L. J.(2005). Caracterização do clima de ondas na costa do Rio Grande do Sul. Final Proc.VI OMAR-SAT, Workshop on waves, tides, oceanic engineering and satellite oceanography.Arraial do Cabo, Rio de Janeiro, Brazil. CD press

Delaney, P. J. V. 1965. Fisiografia e geologia da superfície da planície costeira do Rio Grande do Sul. Special publication of Geology School, Federal University of Rio Grande do Sul, Porto Alegre, Brazil, 6, 1-195. unpublished

Ewing, J. A, 1971. A numerical wave prediction method for the North Atlantic Ocean, Deutsche Hydrographische Zeitschrift, 24(6), 241-261,

Fryberger, S. G.,1979. Dune forms and wind regime. McKee, E.D. A Study of Global Sand Seas. Geological Survey Professional, paper 1052, 137-169.

Gade, H.G., 1958. Effects of a non-rigid, impermeable bottom on plane surface waves in shallow water. *Journal of Marine Research,* **16** (2), 61–82.

Gelci, R. H. C. vassal, J., 1956. Utilization des diagrammes de propagation à la prèvision ènergetique de la houle. Bulletin d'Information du Comitê Central d'Oceanographie et d'estudes des Cotes 8 (4), 160-197

Golding, B.W., 1983: A wave prediction system for real-time sea state forecasting.*Journal Research Meteorology Society* 109, 393-416

Goldstein, R.M.; Li, F., and Smith, J., 1994. Remote sensing of ocean waves: the surface wave process program experiment. *Journal of Geophysical Research* 99(4), 7945-7950.

Hasselmann,S. and Hasselmann, K.,1981: A symmetrical method of computing the non-linear transfer in a gravity-wave spectrum, Hamburger Geophys.Einzelschr.,Serie A.,52 8

Holthuijsen, L.H., Booij, N., Ris, R. C., 1994. A spectral wave model for the coastal zone. Proceedings of the Second International Symposium honoring Professor Robert L. Wiegel sponsored by the Waterways, Port, Coastal and Ocean Division of ASCE held in New Orleans, Louisiana, July 25-28, 1993, 630-641.

Holthuijsen, L. H., and S. De Boer, 1988. Wave forecasting for moving and stationary targets, in Computer Modeling in Ocean Engineering, edited by B. Y. Schrefler and O. C. Zienkiewicz. A. A. Balkema, Rotterdam, Netherlands, 231-234

Holthuijsen, L.H., Herman, A. and Booij, N., 2003: Phase-decoupled refraction-diffraction for spectral wave models. *Coastal Engineering*, 49, 291-305

Kinsman, B., 1965. Wind waves. Englewood Cliffs, New Jersey: Prentice Hall, 676p.

Komen, G.J.; Cavalieri, L.; Donelan, M.; Hasselmann. K.; Hasselmann, S., and Janssen, P.A.E.M., 1994. Dynamics and modeling of ocean waves. Cambridge University Press, Cambridge..

Li, C. W., and M. Mao, 1992. Spectral modeling of typhoon-generated waves in shallow waters. *Journal of Hydraulics Research*, (30) 611-622.

Martins, L.R.S., Martins, I.R., Villwock, J.A. and Calllari, L.J., 1979. Ocorrência de Lama na praia do Cassino. Hydrographic Proceedings. Rio de Janeiro, RJ., Brazil pp. 3-20.

Melo Fº E., Alves, J.H.G.M.,1993. Nota sobre achegada de ondulações longíquas à costa brasileira. Final Proc. 10º Brazilian Symposium of Hydraulic Resource, Gramado, Rio Grande do Sul, Brazil, 5, 362-369.

Madsen, P. A, and Sorensen, O. R., 1992. A new form of the Boussinesq equations with improved linear dispersion characteristics, 2, A slowly-varying bathymetry. *Coastal Engineerig*, 8, 183-205.

Miles, J. W.,1981. Hamiltonian formulations for surface waves. Applied Science Research, 37, 103-110.

Motta, V. F., 1963. Análise e Previsão das Alturas de Ondas em Tramandaí, Porto Alegre. Technical Report, Institute of Hydraulics Research, Federal University of Rio Grande do Sul, Porto Alegre, Brazil 30 p, unpublished.

NCC – National Climate Center, 1980. TDF-11. Manual of surface Marine Observations. U.S. National Climate Center, NOAA, 18p.

Nimer, E., 1977. Clima. In: IBGE – Geografia do Brasil, Região Sul. SERGRAF-IBGE, Rio de Janeiro, RJ, Brazil p.35-79.

Nwogu, O., 1994: Nonlinear evolution of directional wave spectra in shallow water, Proceedings 24th International Conference of Coastal Engineering, ASCE, 467-481

Peregrine, D. H., 1966. Long waves on a beach. *Journal of Fluid Mechanics,* 27, 815-827.

Pierson, W. J., and L. Moskowitz, 1964. A proposed spectral form for fully developed wind seas based on the similarity theory of S. A Kitaigorodskii. *Journal of Geophysical Research* ,69(24), 5181-5190.

Populus, J.; Aristaghes, C.; Jonsson. L.; Augustin, J.M., and Pouliquen, E., 1991. The use of spot data for wave analysis. *Remote Sensing in the Environment* 36, 55-65.

Radder, A. C., 1979. On the parabolic equation method for water-wave propagation. *Journal of Fluid Mechanics,* 95, 159-176.

Radder, A. C., 1992. An explicit Hamiltonian formulation of surface waves in water of finite depth. *Journal of Fluid Mechanics,* 237, 435-455.

Ris, R.C., L.H. Holthuijsen and N. Booij, 1994: A spectral model for waves in the near shore zone, Proceedings 24th International Conference of Coastal Engineering, Kobe, October. 1994, Japan, pp. 68-78

Ris, R.C., 1997: Spectral modeling of wind waves in coastal areas, (Ph.D. Dissertation Delft University of Technology, Department of Civil Engineering), Communications on Hydraulic and Geotechnical Engineering, Report No. 97-4, Delft, The Netherlands.

Rogers, W. E., Kaihatu, J. M., Hsu, L., Jensen, R. E., Dykes, J. D., HoIland, K. T. ,2006. Forecasting and hindcasting waves with the SWAN model in the Southem Califomia Bight. Coastal Engineering article in press

Strauch, J.C.,1998. Um Ano de Monitoramento de Ondas em Rio Grande. Final Proc. XI National Week of Oceanography, Oceanography and their interfaces. Federal University of Rio Grande – FURG, Rio Grande, Rio Grande do Sul, Brazil.

SWAMP Group, 1985. Ocean Wave Modelling, 256 pp., Plenum, New York.

Tolman, H.L., 1991: A third-generation model for wind waves on slowly varying, unsteady and inhomogeneous depths and currents,.*Journal of Physical Oceanography*, (21), 6, 782-797.

Tomazelli, L. J.,1990. O regime dos ventos e a taxa de migração das dunas eólicas costeiras do Rio Grande do Sul, Brasil.Technical report, Institute of Hydraulics Research, Federal University of Rio Grande do Sul, Porto Alegre, Brazil ,20(1), 18-26, unpublished.

Tomazelli, L.J.,Villwock, J.A.,1992.Considerações sobre o ambiente praial e a deriva litorânea de sedimentos ao longo do litoral norte do Rio Grande do Sul, Brasil. Technical report, Institute of Hydraulics Research, Federal University of Rio Grande do Sul, Porto Alegre, Brazil 19(1), 3- 12, unpublished.

Torronteguy, M. C. (2000). Sedimentologia dos depósitos lamíticos na ante-praia do Cassino –RS – junho de 1998 - abril de 1999. Graduation work in oceanology course. Federal University of Rio Grande – FURG, Rio Grande, Rio Grande do Sul, Brazil, 58p, unpublished.

Uji, T. and Mitsuyasu, H. (1975). A comparison of observed and calculated directional wave spectra in the East China Sea. *Journal of oceanography* 45(5), 338-349.

Villwock, J. A. & Martins, L. R. S. 1972. Depósitos lamíticos de pós-praias, Cassino, RS. Technical research, Institute of Hydraulics Research, Federal University of Rio Grande do Sul, Porto Alegre, Brazil 9, 69- 85, unpublished.

WAMDI Group, 1988.The WAM model-A third generation ocean wave prediction model. *Journal of Physical Oceanography*, (18) 1775-1810.

Winterwerp, J.C., Graaff, R.F., Groeneweg, J.,Luyendijk, 2007. Modelling of wave damping at Guyana mud coast. *Coastal Engineering*, 54 (3) 249-261

Young, I. R., 1988. A shallow water spectral wave model. *Journal of Geophysical Research*,93(C5), 5113-5129

Capítulo 5

Modeling Wave Damping over Fluid Mud at Cassino
Beach Coastal Area, Brazil

Cuchiara, D.C., Fernandes E.H., Marques, W.C., Monteiro, I.O.,Calliari, L.J., Winterwerp, J.C.
Continental Shelf Research, submetido.

Modeling Wave Damping over Fluid Mud at Cassino Beach Coastal Area, Brazil

Cuchiara, D.C.[1], Fernandes E. H. [1], Marques, W.C.[1], Monteiro, I.O.[1]; Calliari, L. J. [1], Winterwerp, J.C. [2],

[1] Fundação Universidade Federal do Rio Grande, CP 474, CEP: 96201-900, Rio Grande, Brazil
dmtdc@furg.br, dfsehf@furg.br, wiliam_marques@yahoo.com.br, oceigor@furg.br, tsclauro@furg.br
[2]Delft Hydraulics, PO Box 177, 2600 MH Delft, The Netherlands, han.winterwerp@wldelft.nl

Abstract

The shoreface of Cassino Beach is characterized by extensive offshore mud deposits. Observations indicate that these mud deposits dissipate wave energy, decreasing the wave height along some stretches of the coast. Occasionally, during storms these deposits migrate and attach to the coast, exerting important effects on the surf zone and the beach. Little is known, however, about the relation between the mud properties and the attenuation of the wave's energy in the area. The main objective of this study is to evaluate the effects of the characteristic parameters of the mud deposit (thickness, spatial extension and density) in the attenuation of the wave energy at Cassino Beach. The study is based on numerical modeling experiments which take into account the real properties and position of the mud deposit and field measurements obtained in the Cassino Project. The formulation proposed by Gade (1958) and implemented by Winterwerp (2007) in the wave forecasting model SWAN, is applied to evaluate mud-induced viscous wave energy dissipation. The effect of the mud properties over the wave energy attenuation was evaluated based on the comparison of modeling results obtained with the SWAN model in the standard and modified version (considering mud), and field data obtained during the Cassino Experiment. Several simulations were carried out varying the incoming wave conditions and fluid mud characteristics to analyze their effects in the attenuation of wave height and wave energy. Results indicate that the presence of the mud deposit has an important effect on decreasing the

significant wave height and energy density as progressing from the 10 m depth line towards the coast. This behavior is due to the effects of viscous dissipation in the mud layer. A quantitative analysis indicate that thicker mud layers (T=0.60 m) produce the smallest attenuation in these three parameters. Furthermore, the density of the mud deposit presents an inverse relation with the attenuation of these parameters. Thus, the real representation of the mud deposit figures out as one of the most important input information for the numerical model in order to properly represent the wave dumping observed at Cassino Beach.

Introduction

Fluid mud deposits have been found in many coasts, rivers, and estuaries around the world. When ocean waves approach intermediate and shallow waters, seabed fluid-mud interacts with the waves propagating over it, exerting influence on each other. The seabed fluid-mud produces a gradual dissipation of the wave energy, which promotes the attenuation of the wave heights. The pressure exerted on seabed by waves, on the other hand, is the cause of mud suspension and transportation. Both effects are of practical importance, and the interaction between them has long been drawing attention due to the great importance of accurately estimating the sea state conditions for coastal engineering purposes (Holland et al. 2003).

Several studies related to the attenuation of waves over a muddy bottom were carried out based on measurements and experimental work. Tubman and Suhayda (1976) carried out measurements in the East Bay, near the Mississippi mouth, and concluded that the wave energy was dissipated within the soft mud by about 50% over a 3.5 km trajectory. Wells and Kemp (1986) measured wave heights at three stations in the coastal area of Surinam. This coastal area is characterized by thick layers of mud from the Amazon River (thickness exceeding a few 100 m). They observed that 88% to 96% of the wave energy was dissipated

traveling from the most seaward monitoring station towards the shore. Moreover, they observed wave damping throughout the entire energy spectrum, including the shorter waves. Mathew et al. (1995) analyzed wave data from Kerala coast, in India, and found a reduction of 85% in the wave height and a reduction of 95% of the incident energy as a result of wave propagation over fluid mud banks. Sheremet and Stone (2003) analyzed wave measurements offshore Atchafalaya Bay, where one of their stations was located on a sandy seabed, and the other on a muddy seabed. They observed a reduction of more than 70% in the wave heights at the muddy site in comparison with the sandy site. More recently, Winterwerp et al. (2007) studied the wave damping at the Guyana coastal system.

Conceptually, wave damping over muddy beds is characterized by a sequence of events. First, small elastic deformations are generated within the seabed by the cyclical stresses induced by the incoming waves. When these stresses exceed the strength of the bed, internal failure occurs, resulting in the liquefaction of the seabed (or part of it) (Winterwerp et al., 2007). This is a fairly rapid process, in the order of tens of seconds, up to a few minutes at most (Foda and Tzang; 1994, Lindenberg et al., 1989; De Wit, 1995; De Wit and Kranenburg, 1997) .The formed bed can then be characterized as fluid mud. The incoming waves over this bed generate internal waves at the mud-water interface, which are dissipated by internal friction within the fluid mud layer. Hence, the thickness of the liquefiable bed is a characteristic feature of each coastal system, and is determined by the mud properties and the wave climate.

Theoretical formulations of bed-induced wave dissipation are based on the assumption that wave motion reaches the bottom and interacts directly with bed sediments. The approaches typically focus on a dominant physical mechanism, defined by the bed state and composition. A number of physical mechanisms for wave dissipation over muddy seabed have been proposed over time, based on different models of sediment rheology.

One of the first analytical models to predict surface wave damping over soft mud was developed by Gade (1958). The author treated the water–bed system as a two-layer fluid system, in which the upper layer consists of non-viscous water and the lower layer of a highly viscous fluid mud. Gade's two-layer model ignores the effects of viscosity in the upper layer, and the effects of elasticity, porosity and plasticity in the lower layer. As a result of these limitations, several other models have been proposed considering the diversity of mud states and corresponding beds.

Dalrymple and Liu (1978) extended Gade's theory. They developed a two-layer fluid model to examine the attenuation of waves over a mud bottom, which was characterized as a laminar viscous Newtonian fluid. They proposed a complete model, which was solved numerically, for all mud depths, and an analytical boundary layer approximation for the case of a thick mud layer. Jiang and Zhao (1989) went further by including viscosity in the upper layer. Ng (2000) developed a model considering a mud bed characterized as a viscous fluid. Some authors also extended the problem to non-Newtonian mud (Chou et al., 1993; Foda et al., 1993). Other authors have proposed viscous, elastic and plastic models to describe the behavior of fluid mud and the subsequent wave damping. The viscous and elastic components of such models can be coupled as a series of Kelvin–Voigt models (MacPherson, 1980; Hsiao and Shemdin, 1980; Chou et al., 1993) or in parallel using the Maxwell model (Maa, 1986; Maa and Mehta, 1990; Jiang and Mehta, 1995; 1996; Rodriguez, 2000; Rodriguez and Mehta, 2001). Mehta (1996) proposed the combination of the serial and parallel coupling through a three-element approach.

Another series of models was proposed by Mei and Liu (1987) and Liu and Mei (1989), in which the effects of plastic deformations of the muddy seabed are accounted for in a so called viscous-plastic approach. The well known Bingham model (Bingham, 1922) is one of the viscous-plastic models used, but a number of other models have also been elaborated,

such as the plastic Herschel–Bulkley model (Hemphill et al., 1993). Liu (1973), Yamamoto et al. (1978), Yamamoto and Takahashi (1985) and Spierenburg (1987) included the effects of porosity of the seabed through a poro-elastic description. Verbeek and Cornelisse (1997) applied a poro-elastic-viscous model. However, with the exception of fluidization processes, these models focus on a single, well-defined mud phase. Although these models predict different damping effects (Lee, 1995), each of them may be applicable to some situations (Mei and Liu, 1987), and none of them cover the entire range of mud conditions encountered under natural conditions.

Based on the studies discussed above, Winterwerp et al. (2007) proposed a model to account for viscous damping of incoming waves ignoring the elasticity, plasticity and porosity effects. They have derived the physical and mathematical formulations of Gade's model and implemented their two-layer model in the standard SWAN model. The new formulation was compared with laboratory experiments and field observations on wave damping at the Guyana coastal system (Winterwerp et al., 2007). Their results showed fair agreement between data and predictions.
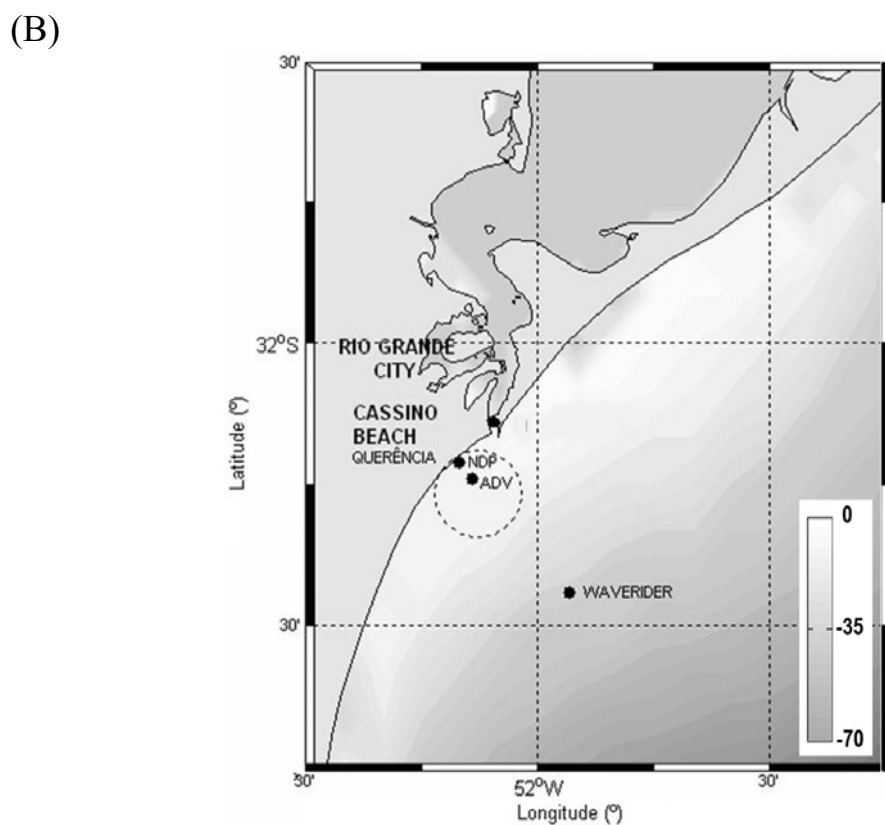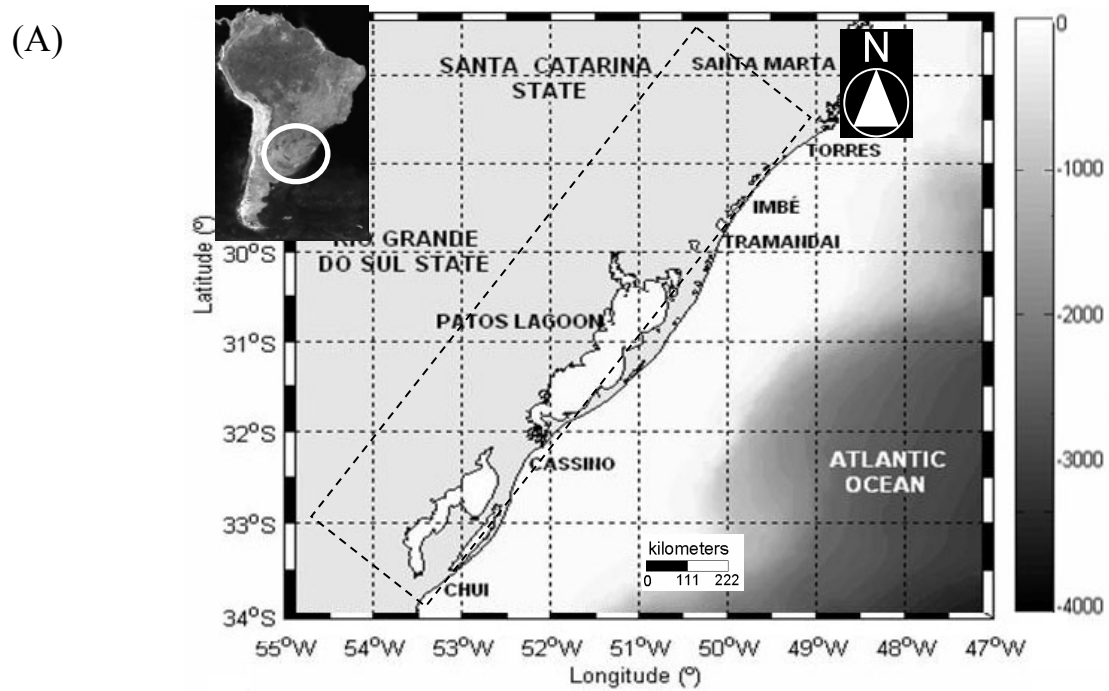
Figure 5. 1 - A) Location of the study area, highlighting the Southern Brazilian Shelf. B) Location of the stations where wind, wave and current data were obtained. The NDP, ADV and the waverider were moored at 9 m, 12 m and 25 m depth, respectively. The dotted circle indicates the position of the mud deposit during the Cassino Experiment.

(A)
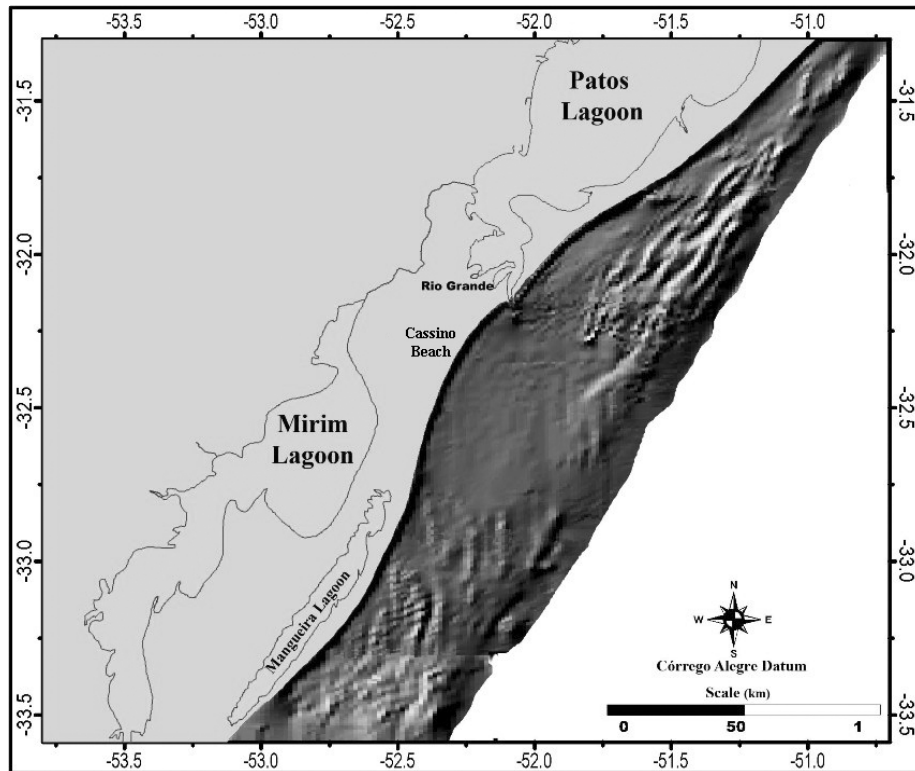
(B)

Figure 5. 2 - A) Morphology of the inner continental shelf adjacent to the Patos Lagoon inlet where mud is deposit (Calliari et al. 2007). B) Lateral variability in wave breaking and clear wave damping, associated with the presence of mud.

The occurrence of mud deposition at Cassino Beach (Figure 1A), located in the southern most part of Brazil, in the past has been described by Villwock and Martins (1972) and Calliari et al. (2000). Historical records show that, since 1972, more than 30 episodes of mud deposition were observed along Cassino Beach (Delaney, 1965; Willwock and Martins, 1972; Martins et al., 1979). The fine sediments observed in the foreshore of this area are periodically suspended, transported and deposited on shore and on the surf zone, exerting important effects on the short and long features observed at the bottom (Figure 5.2A), and bringing negative ecological and economical consequences for the area.

Studies show that the deposition of mud blocks the respiratory mechanism of the benthic fauna, and causes major mortality of mollusks, crustaceans and other invertebrates (Calliari et al, 2001). They report a significant number of dead shells of the gastropod *Heliobia* spp on the surface of the mud banks plastered on the beach. Other short-term effects induced by mud deposition at the shoreface and surf-zone are: 1) the absence of waves along vast stretches of the beach in between areas with no shallow water mud deposits (Figure 5.2B); 2) a potential hazard for surfers, which can be trapped in the surf-zone (Calliari et al., 2007); 3) risks for the traffic of vehicles along the beach, as they can be trapped in mud layers covered by a fine layer of sand. (Calliari et al, 2001); 4) negative impact on tourism activities.

Long-term effects of the mud deposition at Cassino beach are related to the geomorphology of the inner shelf and shoreface. In the relief map of the upper 33 m (Figure 2A), three distinct morphological regions can be observed. The north and the south are irregular areas characterized by the presence of linear sand ridges with heights up to 7 m between the crest and the trough. In the central area, however, the shoreface and inner shelf are extremely smooth and significant topographic features are absent (Calliari et al., 2007). Another long term effect related with the mud shoreface in front of Cassino Beach is the high

rate of shoreline accretion, reaching the order of 4.10 m year^{-1} 10 Km south of the inlet (Figure 5.2A) (Calliari et al., 2007).

Previous studies show that the source of the mud deposited offshore and on the shoreface of Cassino Beach is the Patos Lagoon (Figure 5.1A) (Martins, 1972; Martins et al., 1979), which drains a watershed of 200,000 km^2. The fine sediments are carried out from the rivers located at the north of the lagoon and transported towards the ocean by the wave action and wind driven circulation (Calliari et al., 2007). The material reaches the coastal area in the form of a coastal plume (Marques et. al, submitted), which is mainly advected southwards due to the predominant northeast wind observed over the area. Calliari and Fachin (1993) present the inner shelf sea floor mapping of the area (Figure 5.2A), which indicates a mud depocentre of 560 km^2 (40 km long and 14 km wide) southwards of the Patos Lagoon inlet. This area is known as the Patos Facies (Martins, 1972; Martins et al., 1979).

Although the dynamics of the fluid mud deposit is still not fully understood, it seems that during stormy conditions, which are associated with the periodic passage of cold fronts over the area, the deposit can be reworked and mud is transported to the surf-zone and foreshore of Cassino Beach (Calliari et al., 2007). The most obvious impact of these deposits over the depositional zone is the attenuation of the wave's energy (Figure 5.2B).

Cuchiara et al (*in press*) described the wave climate of the area and carried out preliminary numerical simulation studies to evaluate the attenuation of the wave energy over a theoretical muddy bottom. At that time, however, information about the real conditions and position of the mud deposit was not available. Furthermore, until now, little is known about the real effect of the mud properties on the attenuation of the wave's energy in the area. Thus, the main objective of this study is to evaluate the effects of the characteristic parameters of the mud layer (thickness, spatial extension, and density) in the attenuation of the wave energy at Cassino Beach through numerical modeling experiments, taking into account the real

properties and position of the mud deposit observed during the Cassino Experiment (May 2005).

5.2. Background of the study area

The Southern Brazilian Shelf (SBS), is located between Cabo de Santa Marta and Chui (28.5 ^{o}S to 34 ^{o}S) (Castro and Miranda, 1998) (Figure 5.1A). The coast presents a Northeast-Southwest orientation, and is characterized by open sandy beaches exposed to wave action. The coastal topography is complex and influences the physical processes, determining the waves and the sediment transport at the coast. Over the whole 640 Km that separates Torres headland in the north (29.5^{o}S) and the Chuí estuary in the south (33.8^{o}S), the only significant interruption occurs at the entrance of the Patos Lagoon (32°S).

The regional winds over the area are mainly related to the alternation between two high pressure systems: the South Atlantic Anticyclone and the Polar Migratory Anticyclone (Nimer, 1977). Analyses of wind data presented by Tomazzelli (1990), based on the classification proposed by Fryberger (1979), indicate the area as of high energy, presenting variability in two predominant directions. The most frequent winds come from northeast (NE) and, although it blows throughout the year, it is stronger during spring and summer months. Winds from the south (S), southwest (SW) and west (W) are also important, although more effective during the winter. Camargo et. al., (2002) corroborated this, and concluded that the stations towards the northern limit of this area present winds from the northeast (NE) and east (E) with higher frequency and intensity, while in the ones from the middle to the south, the frequency and intensity of the northeast winds (NE) is reduced, and an increase of the southeast (SE) and south (S) wind influence is observed.

The description of the wave climate of the area presented by Cuchiara et al. (*in press*) was based in the compilation of the existent wave measurements in shallow/intermediary waters in

the southern Brazil, accomplished in the surroundings of Tramandaí Beach (Figure 1A) (Motta, 1963), and Rio Grande city (Figure 5.1A) (Strauch, 1998). The data indicates that in the SBS the predominant wave directions are 100° and 160° (E-SE), with wave heights varying between 1 and 1.50 m. The wave period varies between 6 and 14 s, with predominance of mean wave period of 8 s (sea conditions) and 12 s (swell conditions).

5.3. Model description

This study was carried out based on the standard SWAN model (Simulating WAves Nearshore) version 40.41 (Booij et al. 2004), and on a modified version of the SWAN model, which considers the mud effects in the formulation (Winterwerp et al., 2007).

5.3.1. Standard SWAN model (without mud)

SWAN is a 3rd generation numerical model of high resolution, developed for obtaining realistic estimates of wave parameters in coastal areas, lakes and estuaries based on given wind field, bottom topography, water level and current field conditions, in waters of deep, intermediate and shallow depth. The SWAN model used in this study is a two-dimensional fully spectral state-of-the-art wave propagation model. The evolution of waves in the SWAN model is based on an Eulerian formulation of the spectral discrete wave action balance equation (or energy balance in the absence of currents), including sources and sinks. The model is discrete and spectral in frequencies and directions, and the kinematic behavior of the waves (including the effect of currents) is described with the linear theory of surface gravity waves. The governing equation of the model in Cartesian coordinates is described by the spectral action balance as:

$$\frac{\partial}{\partial t}N + \frac{\partial}{\partial x}c_{g,x}N + \frac{\partial}{\partial y}c_{g,y}N + \frac{\partial}{\partial \sigma}c_{g,\sigma}N + \frac{\partial}{\partial \theta}c_{g,\theta}N = \frac{S}{\sigma} \qquad (5.1)$$

Where σ is the relative frequency (the wave frequency measured from a frame of reference moving with the propagation velocity), θ the wave direction (the direction normal to the wave crest of each spectral component), N is the wave action density, equal to the energy density divided by the relative frequency $(N = E / \sigma)$, Cg is the wave action propagation speed in (x, y, σ, θ) space and S is the total of source/sink, which is generally written as the sum of a number of separate source terms, each representing a different type of process.

$$S = S_{in} + S_{ds} + S_{nl} \tag{5.2}$$

where S_{in} represents the wave generation by winds, S_{ds} the dissipation of the wave energy due to whitecapping, wave-bottom interactions and in very swallow water depth-induced wave breaking, and S_{nl} is the wave energy transfer due to conservative nonlinear wave-wave interactions (both quadruplet interactions S_{nl4} and triad interactions S_{nl3}).

$$\frac{DN}{Dt} = \frac{S_{in}}{\sigma} - \frac{S_{ds}}{\sigma} + \frac{S_{nl}}{\sigma} \tag{5.3}$$

The total wave energy is obtained by integration over frequency and direction:

$$E = \int_0^{2\pi} \int_0^{\infty} E \, d\sigma \, d\theta \tag{5.4}$$

The root-mean-square of the orbital velocity at the seabed u_{orb} and the standard deviation of the water elevation $\hat{\eta}$ read:

$$u_{orb}^2 = \int_0^{2\pi} \int_0^{\infty} \frac{\sigma^2}{\sinh^2(kh)} \frac{E}{g\rho} \, d\sigma \, d\theta \tag{5.5}$$

and

$$\frac{1}{2} \hat{\eta}^2 = \frac{E}{g\rho} \tag{5.6}$$

By definition the significant wave height is

$$H_{m0} = 4\hat{\eta} \tag{5.7}$$

The initial conditions for the model were wind speed and direction at user-specified time intervals, together with the bathymetry of the area. The boundary conditions were specified in terms of integral wave parameters: significant wave height, the characteristic wave period of the energy spectrum, which may be the value of the peak period or the value of the mean period, and the mean wave direction. From the input parameters, the model calculates the wave energy spectra, represented at discrete frequency-direction bands, in every grid cell. From these spectra, characteristic wave heights, periods, and directions of propagation are determined.

5.3.2. The SWAN model considering mud

The SWAN model considering mud consists of a fluid mud induced wave-damping formulation obtained from the modified two-layer model proposed by Gade (1958) and implemented by Winterwerp et al. (2007). The approach is applicable per wave direction, and the individual solutions may be added linearly. In the new formulation, a sink term accounting for viscous dissipation in the mud layer $S_{ds,m}$ has been implemented in equation (5.2), resulting in:
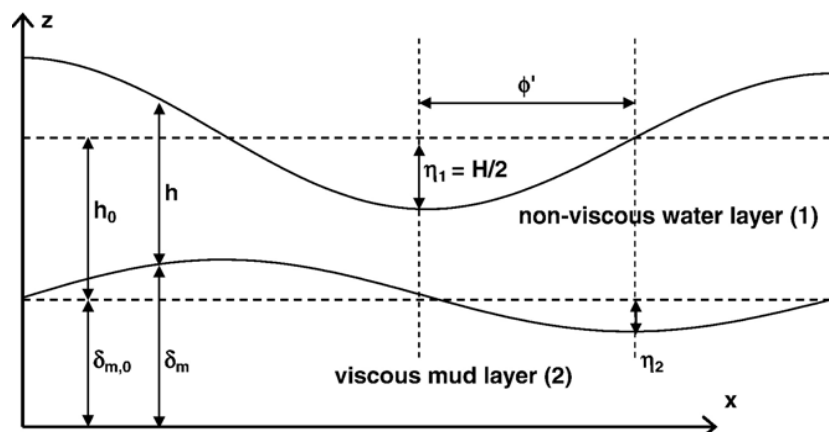

Figure 5. 3 - Sketch of the two-layer fluid mud system and definitions after Gade, 1958. (Winterwerp et al., 2007).

$$S = S_{in} + S_{ds} + S_{ds,m} + S_{nl} \qquad (5.8)$$

The formulation proposed by Gade (1958) assumes that the upper layer is non-viscous and the lower layer is viscous. Figure 5.3 presents the layout of the two-layer system and the definition of the main parameters, where the fluid mud layer depicts a bounded internal wave. The parameter h_o, is the thickness of the non-viscous water layer and $\delta_{m,o}$ of the viscous mud layer under equilibrium conditions. h and δ_m are the distance from the interface to the surface and from rigid bottom to the interface, respectively. h_1 and h_2 are the amplitudes of surface and internal wave, respectively, and H is the depth of the water. In the current situation, free internal waves in the fluid mud layer are not considered because the distances traveled by the wave are very long in relation to the extension of the fluid mud deposits.

His formulation is limited to shallow water waves, considering that the waves are sinusoidal and small compared to the water depth, being possible to neglect the vertical accelerations. The two-layer system is described with the following set of equations for continuity (Eqs. 5.9 and 5.10) and conservation of momentum (Eqs. 5.11 and 5.12) for the upper and lower layers, respectively:

$$\frac{\partial u_1}{\partial x} + \frac{\partial w_1}{\partial z} = 0 \qquad (5.9)$$

$$\frac{\partial u_2}{\partial x} + \frac{\partial w_2}{\partial z} = 0 \qquad (5.10)$$

$$\frac{\partial u_1}{\partial t} + \frac{1}{\rho_1} \frac{\partial p_1}{\partial x} = 0 \qquad \frac{\partial w_1}{\partial t} + \frac{1}{\rho_1} \frac{\partial p_1}{\partial x} = -g \qquad (5.11)$$

$$\frac{\partial u_2}{\partial t} + \frac{1}{\rho_m} \frac{\partial p_2}{\partial x} = v_m \frac{\partial^2 u_2}{\partial z^2} \qquad \frac{\partial w_2}{\partial t} + \frac{1}{\rho_2} \frac{\partial p_2}{\partial x} = -g \qquad (5.12)$$

Where p represents the pressure, u the horizontal flow velocity, w the vertical flow velocity, the number 1 indicate the upper layer and 2 the lower layer. The thickness h and δ_m, in the upper and lower layers respectively, and v_m is the constant fluid mud viscosity. The horizontal and vertical coordinate are given by x and z (x is in the direction θ of the waves), and t is time.

The equations above are solved with the following boundary conditions, where k is the complex wave number:

- at the free surface ($z=h+\delta_m$): $p=0$, $\eta_1=\hat{\eta}_1 \exp\{i(kx-\sigma t)\}$ and $w_1=\partial\eta_1/\partial t$,

- at the interface ($z=\delta_m$): $\partial p/\partial z=0$, $\partial u_2/\partial z=0$ and $w_1=w_2=\partial\eta_2/\partial t$, and

- at the consolidated bed ($z=0$): $u_2=w_2=0$.

Gade solved these equations with the harmonic method, yielding a complex wave number and amplitudes of layer thickness and velocity (see also De Wit, 1995). Gade presented results for a uni-directional, mono-chromatic wave field. However, in SWAN a formulation for the energy dissipation $S_{ds,m}$ (σ, θ) is required. The energy dissipation was obtained by integrating the work done by the surface waves over the wave period. The wave height was obtained from the harmonic solution of equations (5.9) to (5.12). Extending Gade's analysis and assuming that superposition of the solutions is allowed, the energy dissipation per wave frequency σ and direction θ results:

$$S_{ds,m} = \alpha g h_0 \sigma R \frac{\hat{\eta}_2}{\hat{\eta}_1} \sin\left(\phi' - \phi\right) E \tag{5.13}$$

$k = k_r + ik_i$, is the complex wave number (De Wit, 1995) $\qquad$ (5.14)

$$\left[\frac{\rho_m - \rho_0}{\rho_m}\frac{gk}{\sigma^2}\left(k\delta_{m,0} - \frac{k}{\lambda_g}\tanh\{\lambda_g\delta_{m,0}\}\right) - 1\right]\left[\frac{gk}{\sigma^2}\tanh\{kh_0\} - 1\right]$$
$$-\frac{\rho_0}{\rho_m}\left[k\delta_{m,0} - \frac{k}{\lambda_g}\tanh\{\lambda_g\delta_{m,0}\}\right]\left[\frac{gk}{\sigma^2} - \tanh\{kh_0\}\right] = 0 \tag{5.15}$$

Where

$$\lambda_g = (1-i)\sqrt{\sigma/2\nu_m} \qquad (5.16)$$

From equation (15) can be computed:

$$k_r, k_i, R = \left[\left(k_r{}^2 + k_i{}^2\right)/v^2\right] \qquad (5.17)$$

The phase angle between water elevation and flow velocity is

$$\phi = \left[2a\tan\left(k_i/kr\right)\right] \qquad (5.18)$$

and the phase angle between surface and internal waves is:

$$\tan\phi^{'} = \frac{h_0 gR\sin\phi}{h_0 gR\cos\phi - 1} \qquad (5.19)$$

The ratio of the amplitudes of surface and internal wave are:

$$\frac{\hat{\eta}_2}{\hat{\eta}_1} = \sqrt{\left[1 - gh_0 R\cos(\phi)\right]^2 + \left[1 - gh_0 R\sin(\phi)\right]^2} \qquad (5.20)$$

Winterwerp et al. (2007) added an extra calibration coefficient (equation 5.21) in equation (5.13) to account for possible non-linear effects, allowing a better tuning of the SWAN model with Gade's laboratory observations.

$$\Delta_m = \sqrt{\sigma/2\nu_m} \qquad (5.21)$$

The fluid mud parameters have to be provided to the model, including the thickness and extension of the mud layer (δm (x,y,t)), and its viscosity (νm) and density (ρm). The elasticity, plasticity and porosity effects were ignored.

In the work carried out by Winterwerp et al. (2007), the new SWAN model was initially validated against small-scale wave attenuation measurements carried out in a laboratory wave flume. The model predictions agreed favorably with the experimental data. After that, the model was applied to predict the wave height and wave attenuation in the Guyana coastal

system. Extension and thickness of the liquefiable mud layer could be assessed from dual-frequency echo soundings. In the absence of field data, the density of the liquefied mud layer was obtained from literature, whereas the value of the mud's viscosity had to be established by trial and error, keeping the range of values found in the literature. The computed changes in the wave energy spectrum in the area agreed qualitatively with measurements in Surinam, whereas the decrease in significant wave height reasonably agrees with historic observations along the Guyana coast.

Cuchiara et al., 2007 (*in press*) carried out the calibration of this new version of the SWAN model considering mud in the form of a sensitivity analysis, using data from Cassino Beach. In this study, preliminary numerical simulations were carried out to analyze the response of the SWAN mud wave damping module (Winterwerp et al., 2007) with respect to the wave attenuation in terms of decreasing the significant wave height and energy density. The model results indicated that the presence of mud deposits in the area attenuates most of the wave energy on the swell frequency peak, though it has a smaller effect in attenuating the wave energy on the sea frequency peak.

5.4. Application to the Cassino Beach coastal area

5.4.1. Description of the prevailing hydro-meteo conditions and mud properties

The SWAN model was applied to the studied area (Figure 5.4A), which covers 100 km along the coastal area and extends about 50 km offshore, and includes the Cassino Beach area (Figure 1A) The depth at the cross-shore boundaries of the domain vary from 1 to 29 m. The bottom topography of the area was established based on data from the Brazilian Navy Nautical Charts. The curvilinear grid comprises 41 by 104 cells, with approximately 4264 active points (Figure 5.4A). The dimensions of the grid cells vary from 1.5 km near the boundaries to approximately 1.0 km, near the jetties and around Cassino Beach.
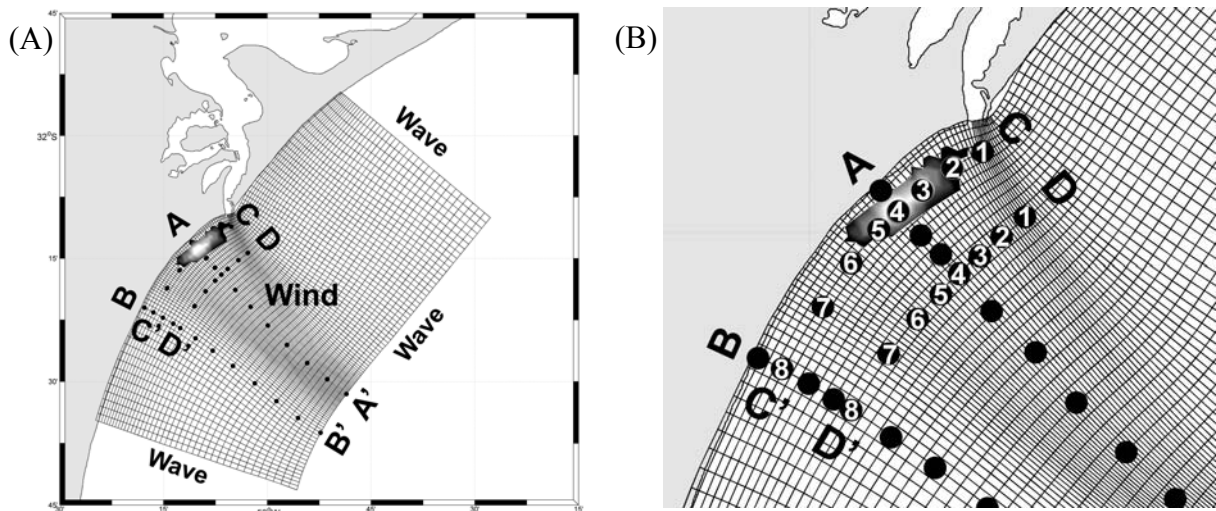
Figure 5. 4 – A) The computational domain with a curvilinear grid for the numerical experiments, highlighting the location of the initial and prescribed boundary conditions, and the position of the mud deposit, obtained by coring and echobathymetric surveys during the Cassino Experiment. The dots indicate the location of profiles AA', BB', CC' and DD'. B) Detail of the transversal profiles CC' and DD'.

The boundary conditions for the model were based on data measured during the Cassino Experiment, carried out at Cassino Beach, in collaboration with the US Naval Research during October 2004 and April - May 2005. The field experiment aimed to map the mud deposits off Cassino Beach, and to collect new information on the hydrodynamics and geological aspects of the area. Geological, geophysical, video imaging, radar, and climatological data (including waves, currents, sediment movement and associated beach profile changes) were collected on the inner shelf and shoreface of Cassino Beach (Figure 1B). Calliari et al. (2005) present the Cassino Experiment in detail. These data, however, is still limited to fixed points during a short period of measurements.

Figure 5.5 presents a time series of hourly wind speed and direction measured at Cassino Beach from May 13th to June 25th, 2005, which was used to select periods for the simulations with the SWAN model. The wind data was obtained 10 m above the ground and represent 10 min averages. A statistical analysis of the data indicates that predominant winds are from the

northeast (NE) and from the south (S) (Cuchiara et al., *in press*). The wind was prescribed as the surface boundary condition of the model and considered constant in time and space over the entire domain.
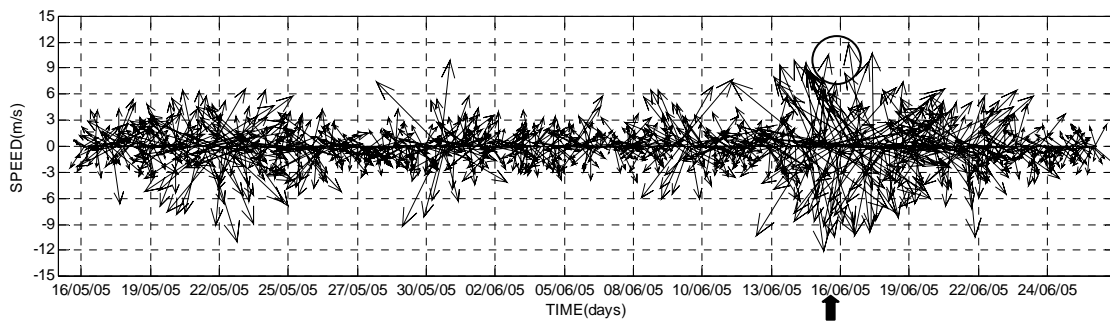

Figure 5. 5 - Time series of hourly wind speed and direction measured at Cassino Beach between May 13th and June 25th, 2005. Positive (negative) values indicate winds from the north (south). The highlighted period was selected for the wave's numerical simulations.

Information about the significant wave height (Hs), peak period (Tp) and mean wave direction (DIR) for the chosen period was selected from measurements carried out between May 13th and June 25th, 2005 with a directional waverider installed off Cassino Beach (32° 26' 37" S and 51° 55' 53" W) at 25 m depth (Figures 5.1B), and applied at the ocean boundaries of the domain (Figure 5.4A).

A preliminary statistical analysis of the data indicates significant heights between 1.0 and 3.0 m, mean period smaller than 6 s, and predominant directions between northeast (NE) and south (S) (Cuchiara et al., *in press*).
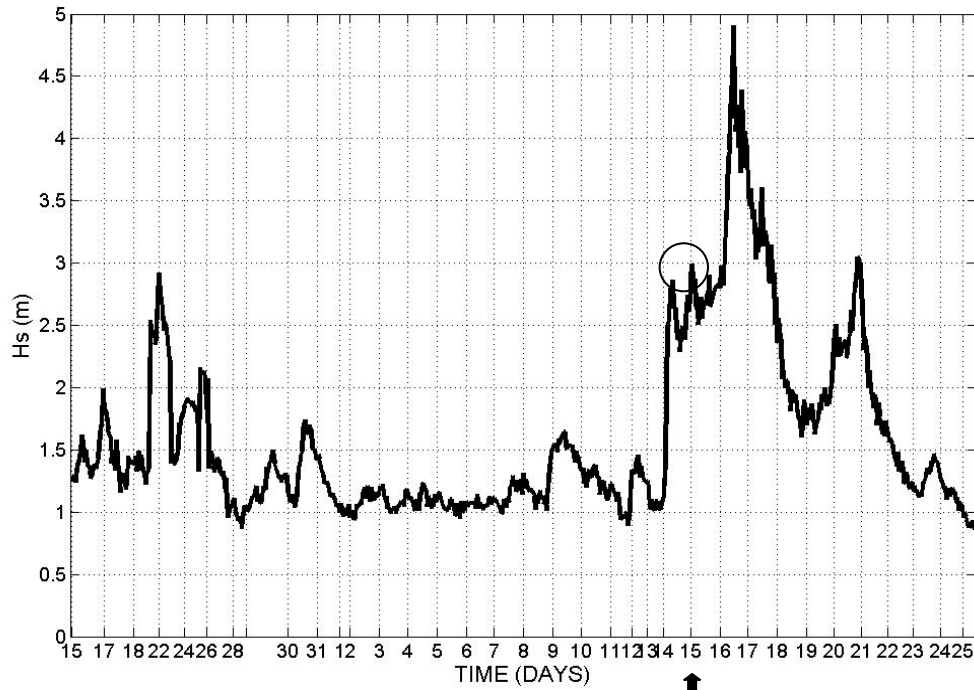
Figure 5. 6– Time series of significant wave height measured between May 13th and June 25th, 2005 by a directional waverider located at 32º10'002"S and 51º58'913" W. The highlighted period was selected for the wave's numerical simulations.

The spatially varying mud layer thickness was measured during the Cassino Experiment, between the 8 m and 14 m isobaths, reaching maximum thickness of 0.6 m in the center of the deposit (around the depth of 9.5 m) and reducing towards the deeper areas (Figure 5A). The largest width of the fluid mud deposit was coincident with the vortex associated with the jet flow leaving the mouth of the lagoon (Calliari et al. 2005). The *in-situ* density measured during the same period varied between 980 kg.m^{-3} and 1450 kg.m^{-3}. Average densities of 1310 kg.m^{-3} and 1140 kg.m^{-3} (Calliari et al. 2005) were used in this study.

As no detailed information was available for the viscosity of the fluid mud, this parameter was assessed from literature (Winterwerp et al., 2007). However, establishing δm forms a fundamental problem, as it is governed by the initial wave effects and mud properties, thus determined by nonlinear feedback processes. A proper modeling of δm would require an advanced rheological model, including the effects of plasticity, which is not available. A viscosity parameter obtained from laboratory experiments by De Wit (1995), who investigated

126

the liquefaction of cohesive sediments in a flume under varying conditions of waves and currents, was used in this study. This experiment was also used to validate the comprehensive mud dissipation model proposed by Winterwerp et al. (2007), and was also used in tests performed in comparison with laboratory data and a model for the propagation of nonlinear surface waves over viscous mud (Kaihatu et al., 2007).

5.4.2. Model Setup

In order to characterize in detail the effects of the mud layer properties in the attenuation of wave heights, mean period variation and wave energy dissipation in Cassino Beach (Figure 1A), the Swan model was applied in the stationary mode. In all simulations, a directional resolution of 36° was adopted for the wave spectrum over the full circle. The spreading frequency was schematized using 63 discrete frequencies between 0.03 Hz and 0.58 Hz using a logarithmic scale. For the remaining parameters the default settings of the SWAN model were used.

The selected period for the numerical simulations with the new SWAN model considering mud was based on the predominant wind direction registered in the studied area, associated with the availability of wave data recorded for the same period. A moment of wind from the northeast was selected (Figures 5.5 and 5.6). Table 5.1 presents the wind velocity and direction and the observed wave conditions at the waverider point during the Cassino Experiment for the selected moment.

Table 5. 1- Measured wind velocity and direction, and observed wave conditions at the waverider station during the Cassino Experiment for the selected moment.

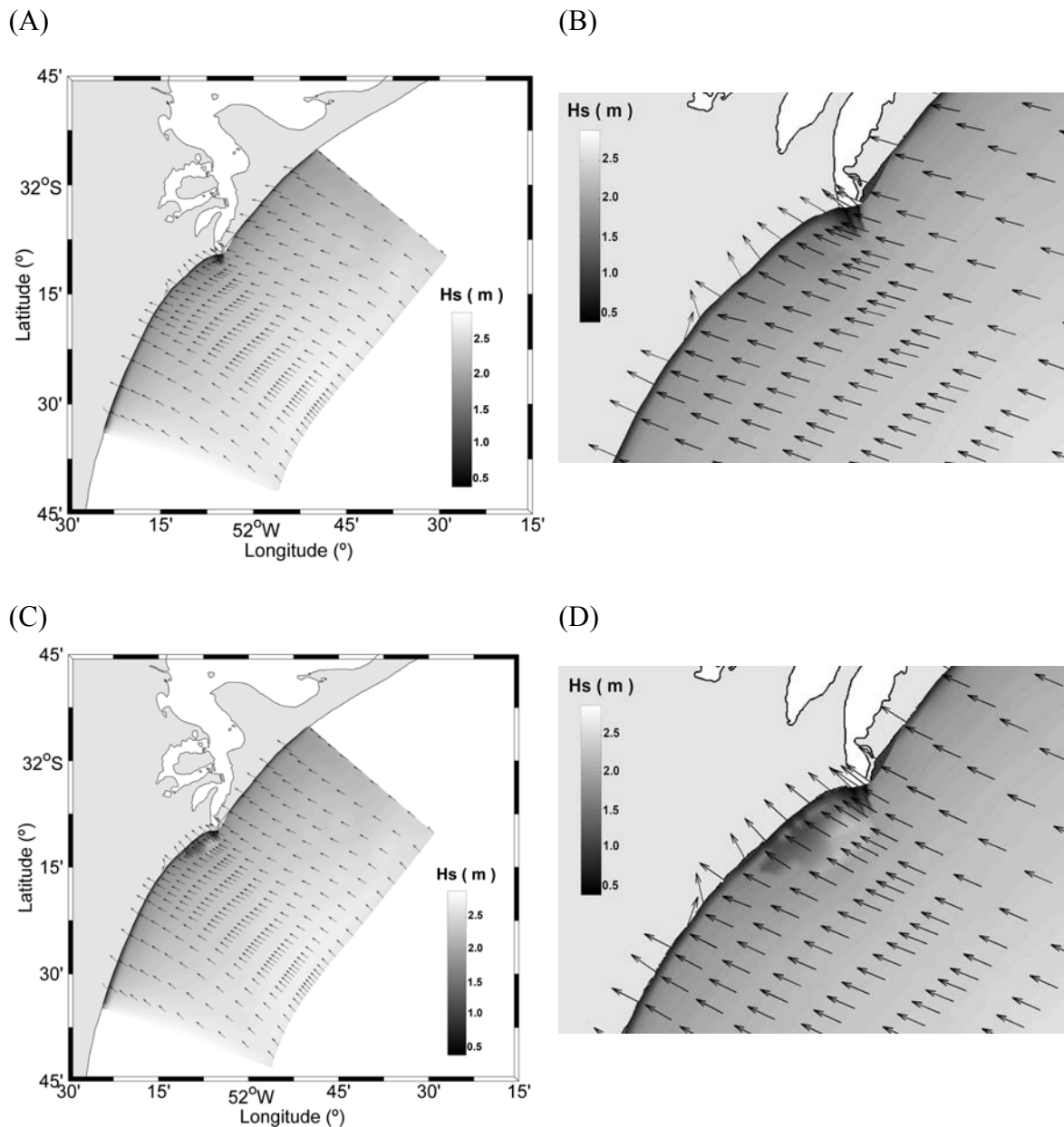| Data	Measured Wind			Observed Wave Conditions			
	Time	V (m/s)	DIR(degree)	Time	Hs (m)	Tp (s)	DIR(degree)
15/6/2005	07:45	12.08	61.94	08:37	2.56	7.70	109.20

5.5. Results

Figure 5. 7– Calculated spatial distribution of significant wave height (gray scale) and mean wave direction (arrows) for the selected NE wind period. A) Computed by the standard SWAN model and (B) in detail the Cassino Beach coastal area (no mud at the bottom), (C) Computed by the new version of the SWAN model and (D) in detail the Cassino Beach coastal area, considering the real location of the mud deposit and the mud effects

Figure 5.7 presents the spatial distribution of significant wave height and mean wave direction calculated by the SWAN model for the selected period (wind from the NE). Results computed by the standard SWAN model without mud (Figures 5.7A and 5.7B) indicate that the calculated significant wave height decreases towards the shore, varying from 2.5 m in the deeper area to a minimum of 0.5 m in shallow water. The mean wave direction is from the SE. Results computed by the SWAN model considering the real location of the mud deposit and the mud effects (Figures 5.7C and 5.7D) indicate stronger attenuation of the significant wave height in the mud deposit area, representing the observed wave damping (Figure 5.2B).

Figure 5.8 presents the response of the significant wave height when varying the mud density (ρm) (Figure 5.8A) and thickness (Figure 5.8B), considering a constant viscosity (0.0027 $m^2.s^{-1}$) and the real conditions of the mud deposit at the bottom, during the selected period of simulation. Results calculated by the model without and with mud and considering variable density (rm = 1310 kg.m^{-3} and 1140 kg.m^{-3}) (Figure 5.8A) for profile AA' (Figure 5.4A) reassure that the presence of the mud deposit at the bottom has an important effect on decreasing the significant wave height as moving from 10 m depth towards the coast. A comparison between results without mud and with mud (density of 1310 kg.m^{-3}) indicates a minimum difference (< 1%) between the calculated significant wave height at 10 m depth and maximum difference (26%) at 7 m depth. This difference increases to 30% at 7 m depth when a density of 1140 kg.m^{-3} is considered, indicating stronger attenuation.

Results calculated by the model without and with mud and considering variable thickness (measured thickness, T=0.20 m, T=0.40 m, T=0.60 m) (Figure 5.8B) for profile AA' (Figure 5.4A) also indicate the importance of correctly representing the mud deposit as moving from the 10 m depth towards the coast. Although the scale of the figure indicates no difference in the significant wave height as varying the mud thickness, a quantitative analysis (Table 5.2)

indicate that the thicker mud layer (T=0.60 m) produces the smaller attenuation in the significant wave height.
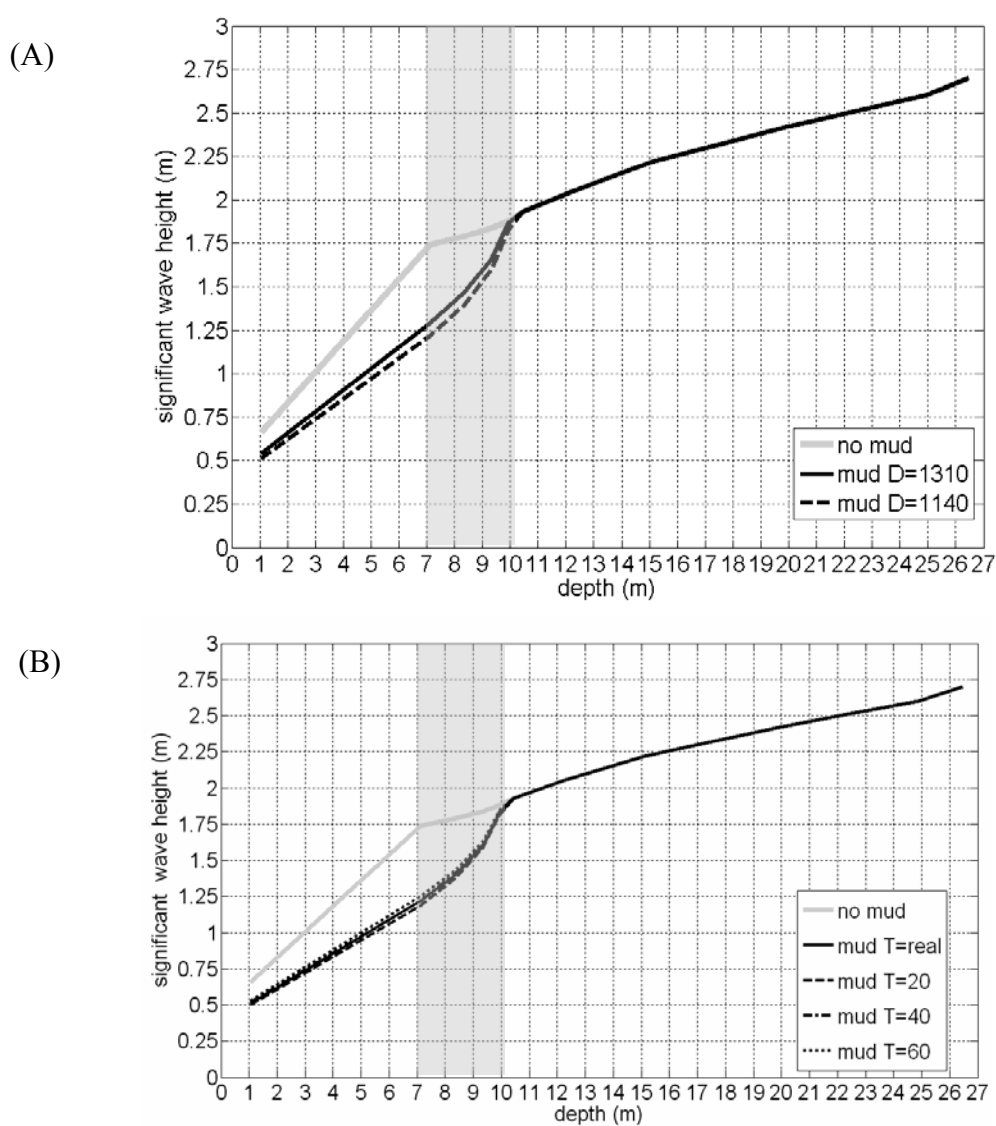

Figure 5. 8 – Comparison between the calculated significant wave height for profile AA'. A) Without mud and with mud considering the real location, constant viscosity, measured thickness and real density of 1310 kg.m^{-3} and 1140 kg.m^{-3}. B) Without mud and with mud considering the real location, constant viscosity and density of 1140 kg.m^{-3}, and with thickness varying between 0.20 m, 0.40 m and 0.60 m. The shadowed area indicates the position of the mud bank.

Table 5. 2– Significant wave height calculated by the model without and with mud considering variable thickness (measured thickness, T=0.20 m, T=0.40 m, T=0.60 m) for the selected moment.

Depth (m)	Hs (m) no mud	Hs (m) mud T=real	Difference (%)	Hs (m) mud T=0.20	Difference (%)	Hs (m) mud T=0.40	Difference (%)	Hs (m) mud T=0.60	Difference (%)
1	0.66	0.51	22	0.50	23	0.52	21	0.53	20
7	1.74	1.22	30	1.19	31	1.22	30	1.25	28
8	1.79	1.40	21	1.38	23	1.41	21	1.43	20
9	1.84	1.60	13	1.59	14	1.61	12	1.63	11
10	1.88	1.83	3	1.82	3	1.84	2	1.85	1.5

Figure 5.9 shows the response of the wave energy when varying the mud density (ρm) (Figure 5.9A) and thickness (Figure 5.9B), considering a constant viscosity (0.0027 $m^2.s^{-1}$) and the real conditions of the mud deposit at the bottom during the selected period of simulation. A spectral analysis of these results (not shown) indicates that the effect of the mud deposit on the energy density concentrated on the attenuation of high frequency energy, occurring at 7.7 s.

Results calculated by the model without and with mud and considering variable density (ρm = 1310 kg.m^{-3} and 1140 kg.m^{-3}) (Figure 5.9A) for the higher energy density point in profile AA' (Figure 5.4A) reassure that the presence of the mud deposit has an important effect in the dissipation of energy density as moving from the 10 m depth towards the coast. A comparison between results without mud and with mud (density of 1310 kg.m^{-3}) indicates a minimum difference (>1%) between the calculated energy density at 10 m depth and maximum difference (42%) at 7 m depth. The difference increases to 51% at 7 m depth when a density of 1140 kg.m^{-3} is considered, indicating stronger dissipation.

Results calculated by the model without and with mud and considering variable thickness (measured thickness, T=0.20 m, T=0.40 m, T=0.60 m) (Figure 5.9B) for the higher energy density point in profile AA' (Figure 5.4A) reassures the importance of correctly representing the mud deposit. Although the scale of the figure indicates no difference in energy density as

varying the mud thickness, a quantitative analysis (Table 5.4) indicate that the thicker mud layer (T=0.60 m) produces the smaller attenuation in energy density.
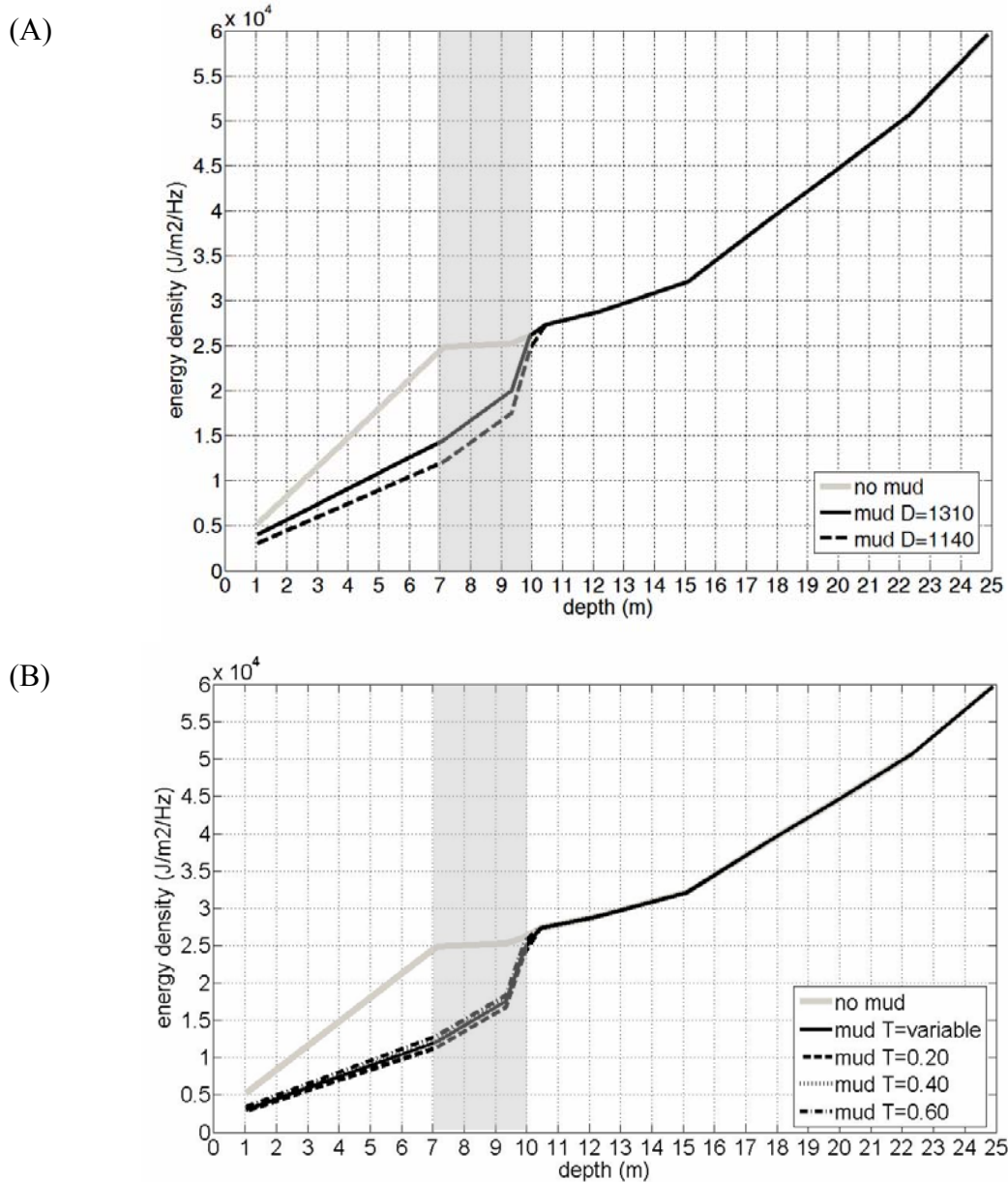
(A)

(B)

Figure 5. 9 – Comparison between the calculated energy density for the higher energy density point in profile AA'. A) Without mud and with mud considering the real location, constant viscosity, measured thickness and real density of 1310 kg.m^{-3} and 1140 kg.m^{-3}. B) Without mud and with mud considering the real location, constant viscosity and density of 1140 kg.m^{-3}, and with thickness varying between 0.20 m, 0.40 m and 0.60 m. The highlighted depths indicate the position of the mud bank.

Table 5. 3– Energy density calculated by the model without and with mud considering variable thickness (measured thickness, T=0.20 m, T=0.40 m, T=0.60 m) for the selected period.

Depth (m)	ED no mud ($J.m^{-2}.Hz^{-1}$) no mud	ED mud ($J.m^{-2}.Hz^{-1}$) T=real	Dif (%)	ED mud ($J.m^{-2}.Hz^{-1}$) T=0.20	Dif (%)	ED mud ($J.m^{-2}.Hz^{-1}$) T=0.40	Dif (%)	ED mud ($J.m^{-2}.Hz^{-1}$) T=0.60	Dif (%)
1	5237	3044	42	2838	46	3172	39	3461	34
7	24820	12060	51	11310	54	12200	50	12870	48
8	25270	17540	31	16770	34	17680	30	18340	27
9	26120	24650	6	24080	8	24920	5	25530	2
10	27340	27330	0.04	27335	0.02	27334	0.02	27333	0.03

Figure 5.10 presents the comparison between the significant wave height computed by the model for profile AA' (crossing over the center of the mud deposit) and BB' (outside the mud deposit) (Figure 5.4A), and NDP measurements carried out during the Cassino Experiment. Results calculated by the model for profile BB' indicate the expected progressive decrease of the significant wave height as progressing landwards (approximately 0.1 m for each 2.0 m of water depth). Results for profile AA' present a similar behavior until it reaches the location of the mud deposit. After that point, results indicate an attenuation of the significant wave height as the waves cross over the mud deposit (approximately 0.2 m for each 2.0 m of water depth). These modeling results are in agreement with observations in the area (Figure 5.2B) and with measurements from the Cassino Experiment, represented by the significant wave height measured with a NDP at 9.0 m of depth.

Figure 5.11 presents the significant wave height computed by the model for profile CC' (crossing over the center of the mud deposit, at 9 m depth), profile DD' (outside the mud deposit, at 15 m depth) (Figure 5.4A and 5.4B), and the NDP measurement. Results calculated by the model for profile DD' present the significant wave height varying between 2.0 m and 2.25 m, since all the points are located in the same depth .Results for profile CC' indicate that the significant wave height of points located outside the mud deposit decrease approximately 6% in relation to profile DD' (Figure 5.4A and 5.4B). The points located over

the mud deposit present a decrease of the significant wave height varying between 20% and 40% for points 3, 4 and 5 (Figure 5.4B).
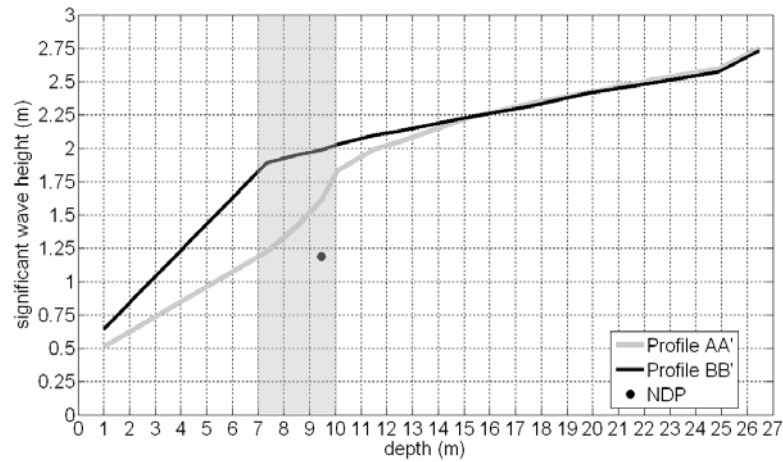

Figure 5. 9 - Comparison between the significant wave height computed for transversal profiles AA' and BB' and data from a NDP moored during the Cassino Experiment. The highlighted depths indicate the position of the mud bank.
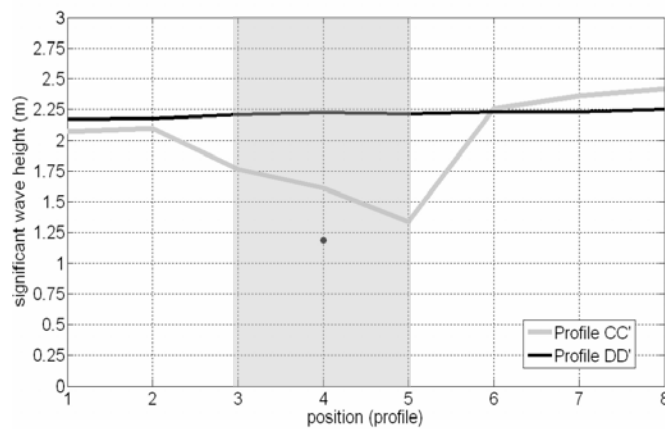

Figure 5. 10 - Comparison between the significant wave height computed for longitudinal profiles CC' and DD' and data from a NDP moored during the Cassino Experiment. In profile CC' the measured thickness of mud layer varied from 0.4 m, 0.6 m and 0.2 m in positions 3, 4 and 5, respectively. The highlighted depths indicate the position of the mud bank.

Figure 5.12 presents the relation between the significant wave height computed for profile CC' and the thickness of the mud deposit measured during the Cassino Experiment

and prescribed in the model. Results show that the decrease of significant wave height is not directly dependent of the mud layer thickness.
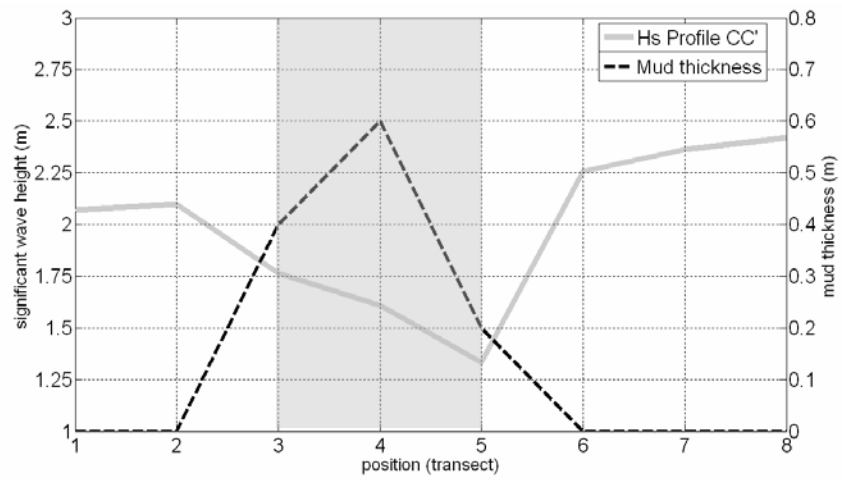

Figure 5. 11- Comparison between the significant wave height computed for profile CC' and the thickness of the mud deposit during the Cassino Experiment
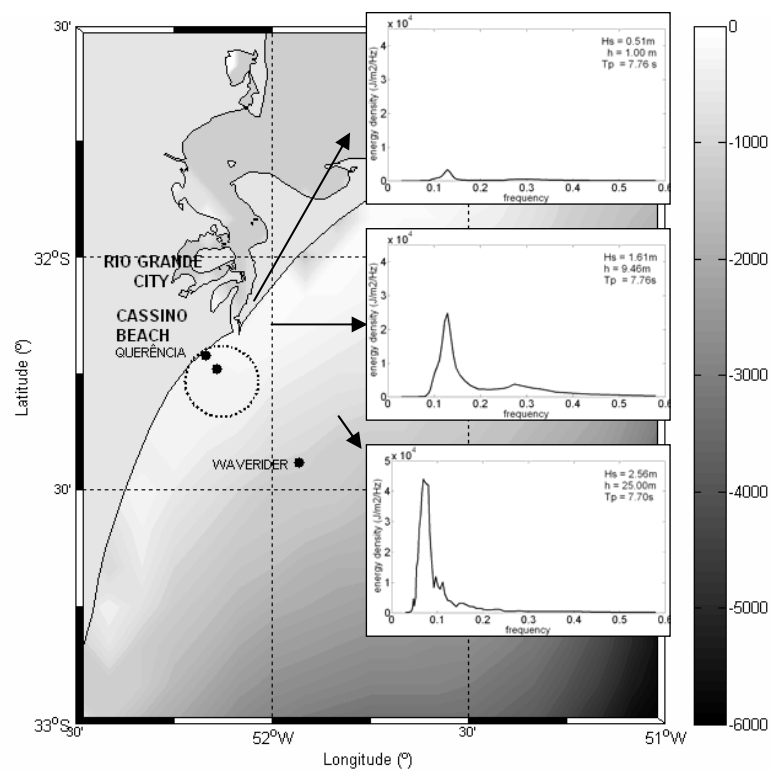

Figure 5. 12 - The progressive effect of wave damping by fluid mud at two locations of profile AA'. The seaward point is the Cassino Experiment waverider point.

The progressive effect of wave damping by fluid mud on the wave climate of the area is illustrated in Figure 5.12 by a one-dimensional wave spectra for two locations in profile AA' (the middle point over the mud deposit and the nearshore point out the mud deposit) and at the waverider point. The waverider spectra consists of a strong peak period of Tp=7.7 s, representing the energy in the sea wave frequency. Moving from the seaward station towards the coast, the total wave energy was attenuated by about 43% in the middle point, and 92% at the nearshore station. The decreasing of significant wave height started in the seaward station with a relative decrease of 37% in the middle point, and 80% in the nearshore station.

Figure 5.13 shows a comparison between significant wave heights calculated by the SWAN model (with and without mud) and measured with a NDP (Acoustic Doppler Profiler) for the NDP point (9 m of depth), and with data from a waverider relative to the 2005 survey (25 m of depth) (Figure 5.1A).
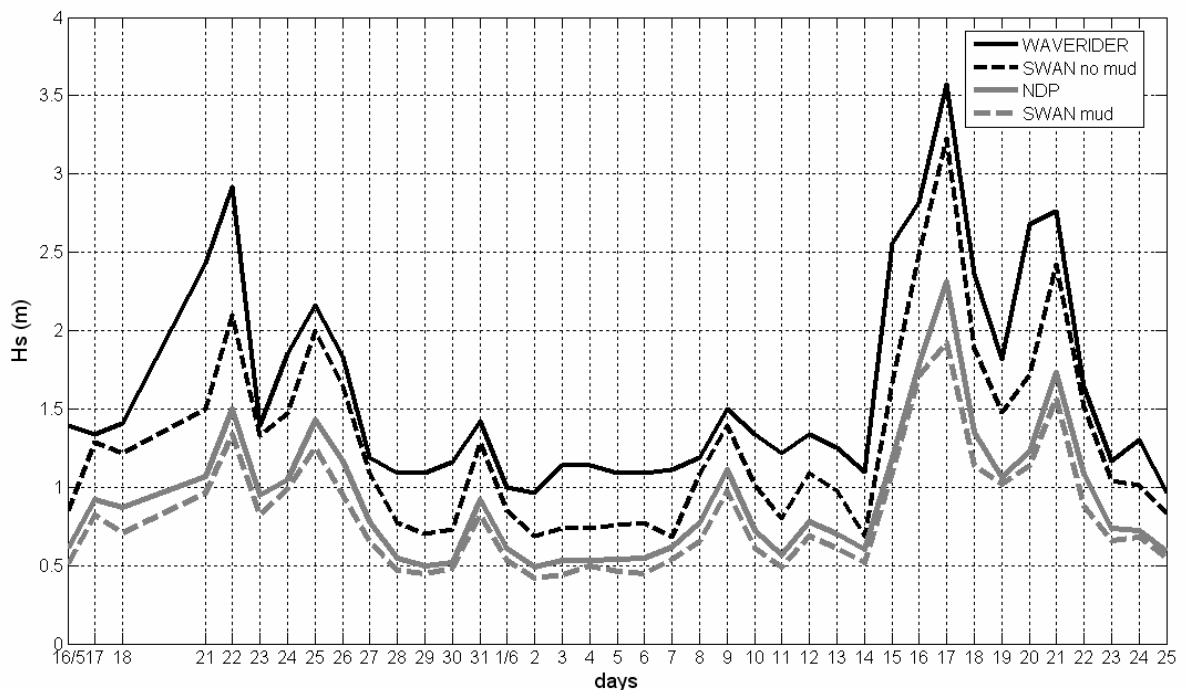

Figure 5. 13 - The significant wave height measured with a waverider at 25 m, a NDP (Acoustic Doppler Profiler), and calculated by the SWAN model without and with mud at NDP point.

Cuchiara et al. (in press) carries out numerical simulations to analyze the response of the SWAN mud wave damping module (Winterwerp et al., 2007) in terms of decreasing the significant wave height. The authors considered the thickness and density of the fluid mud layer constant in the entire computational domain and their results indicate that the attenuation is likely to be overestimated in the presence of mud in relation to the measurements (Figure 4.13). In the present simulations, the mud density (1140 $kg.m^{-3}$) and viscosity (0.0027 $m^2 s^{-1}$) were also considered constant but the real distribution of thickness of the mud deposit at the bottom were applied.

Results indicate that the model without mud overestimates the significant wave height in 40 to 100% of the measured values with a NDP (large gray line), indicating the limitation of considering a rigid bottom in the domain. By considering the real location, constant viscosity, measured thickness and real density of 1140 $kg.m^{-3}$ of the mud in the domain (dotted gray line), the model reproduction in relation to the significant wave height measured by the NDP (10 – 20% in the NDP localization point) presented a significant improvement.

The overall results from this study are in agreement with the limited published work about the interaction between waves and muddy bottoms. The significant wave height and energy density calculated with the SWAN model for the Cassino Beach coastal area, qualitatively agreed with the measured data from Wells and Kemp (1986) in the coastal area of Surinam, and with the data presented by Mathew et al. (1995) for Kerala coast, in India. Furthermore, the calculated response of significant wave height and energy density obtained with the SWAN model considering mud are in agreement with Winterwerp et al. (2007), who modeled the wave damping at the Guyana coastal system.

5.6. Conclusions

In order to evaluate the effects of the characteristic parameters of the mud layer, namely the thickness, density, and viscosity, in the attenuation of wave heights, mean period and energy dissipation at Cassino Beach, results obtained with the SWAN model considering mud were compared with the SWAN model in the standard version, and with measured field data obtained during the Cassino Experiment.

The main conclusions of this study were:

- The mud deposit at the bottom promotes significant attenuation of the significant wave height, mean period and energy due to the viscous dissipation in the liquefied seabed;

- Among the analyzed parameters, the thickness of the mud layer caused the smallest effect in the attenuation of the significant wave height, decrease of the mean period and dissipation of energy density.

- The density of the mud deposit presents an inverse relation with the attenuation of these parameters.

- The real representation of the mud deposit figures out as one of the most important input information for the numerical model to properly represent the wave dumping observed at Cassino Beach.

- The results showed that to correctly predict the nearshore wave parameters in the presence of a mud deposit at the bottom it is essential to apply a numerical model which considers the mud effects.

providing data obtained during the Cassino Experiment (2005). The first author is also grateful to WL|Delft Hydraulics Institute, Holland, for making available the SWAN model considering mud, and to Han Winterwerp and Gerben de Boer for the valuable training and special attention received during her stay in the WL|Delft Hydraulics Institute.

References

Bingham, E. C. Fluidity and Plasticity. New York: McGraw-Hill, 1922.

Calliari, L. J. and Fachin, S., 1993. Lagoa dos Patos: Influência nos depósitos lamíticos costeiros. *Pesquisas*, 20(1),57-69.

Calliari, L.J.; Speranski, N. S.; Torronteguy, M. and Oliveira, M.B., 2001. The Mud Banks of Cassino Beach, Southern Brazil: Characteristics, Processes and Effects. *Journal of Coastal Research Special Issue 34*, (lCS 2000 New Zealand). ISSN 0749-0208 .

Calliari, L.J., Holland, T., Dias, M.S.,Vinzon, S., Thorton, E., Stanton, T. Experimento Cassino, 2005. Uma síntese dos levantamentos efetuados na ante-praia e zona de arrebentação. *Proceedings ABEQUA 2005* CD-ROM Published by META Marketing & Eventos Ltda. Av. Nilo Peçanha, 50/1610 -20044-900, Rio de Janeiro.

Calliari, L. J., Holland, K. T., Pereira, P. S., Guedes, R. M. C., Santo, R. E., 2007. The influence of mud on the inner shelf, shoreface, beach and surf zone morphodynamics – Cassino, southern Brazil. *Proceedings, Coastal Sediments '07*

Camargo, O. A., Silva, F. J. L., Custodio, R.S., Gravino, N., 2002. *Atlas Eólico do Rio Grande do Sul*.

Department of energy, mine and communications, Porto Alegre,Rio Grande do Sul, Brazil. 70p. http://www.semc.rs.gov.br/

Chou, H.-T., 1989. Rheological response of cohesive sediments to water waves. *PhD-dissertation*. University of California, Berkeley, USA.

Chou, H.T., Foda, M.A., Hunt, J.R., 1993. Rheological response of cohesive sediments to oscillatory forcing. In: Mehta, A.J. (Ed.), *Nearshore and Estuarine Cohesive Sediment Transport, Coastal and Estuarine Sciences*, vol. 42. AGU, pp. 126–148.

Cuchiara, D.C., Fernandes, E. H., Strauch, J.C., Winterwerp, J.C., Calliari, L.J.,2007. Detemination of the Wave Climate for the Southern Brazilian Shelf .Special Issue Continental Shelf Research – Proceedings mud deposit in coastal areas, 13-17 November 2006 , Porto Alegre,Brazil (in press)

Dalrymple, R.A., Liu, P.L.F., 1978. Waves over soft muds: a two-layer fluid model. *Journal of Physical Oceanography* 8, 1121–1131.

De Wit, P.J., 1995. Liquefaction of cohesive sediment by waves. *PhD dissertation,* Delft University of Technology, The Netherlands.

De Wit, P.J., Kranenburg, C., 1997. On the liquefaction and erosion of mud due to waves and current. *In: Burt, N., Parker, R., Watts, J. (Eds.), Cohesive Sediments*. John Wiley & Sons, pp. 331–340.

Delaney, P.J.V. 1965. Fisiografia e Geologia de Superfície da Planície Costeira do Rio Grande do Sul. *Publicação Especial da Escola de Geologia*, UFRGS, Porto Alegre, 6, 105p.

Foda, M.A., Hunt, J.R., Chou, H.T., 1993. A nonlinear model for the fluidization of marine mud by waves. *Journal of Geophysical Research* 98, 7039–7047.

Foda, M.A., Tzang, S.Y., 1994. Resonant waves of silty soil by water waves. *Journal of Geophysical Research* 99 (C10), 20,463–20,475.

Fryberger, S. G. 1979. Dune forms and wind regime. In: McKEE, E. D. (Ed.), A Study of Global Sand Seas. Washington, D. C., *U. S. Geological Suvey Professional Paper*, 1052, 137-169.

Gade, H.G., 1958. Effects of a non-rigid, impermeable bottom on plane surface waves in

shallow water. *Journal of Marine Research* 16 (2), 61–82.

Golden, S.P., Godwin, J.W., Olal, A.D., 1982. The dependence of the elastic properties of clay dispersions on the mode of interaction between the particles. *Transactions and Journal of the British Ceramic Society* 81 (3), 84–87.

Godolphim, M. F. 1976. Geologia do Holoceno costeiro do município de Rio Grande, RS. *PhD-dissertation*. Curso de Pós-graduação em Geociências, UFRGS, Porto Alegre, 146p.

Hemphill T, Campos W and Pilehvari A: "Yield-Power Law Model More Accurately Predicts Mud Rheology," Oil & Gas Journal 91, no. 34 (August 23, 1993): 45-50.

Holland, K.T., Keen, T., and Kaihatu, J.M. 2003. Understanding coastal dynamics in heterogeneous sedimentary environments, *Coastal Sediments '03*, Clearwater Beach, FL.

Hsiao, S.V., Shemdin, O.H., 1980. Interaction of ocean waves with a soft bottom. *Journal of Physical Oceanography* 10, 605–610.

Jiang, F., 1993. Bottom mud mass transport due to water waves. *PhD-thesis*. University of Florida, Gainesville, Florida, USA.

Jiang, F., Mehta, A.J., 1995. Mudbanks of the southwest coast of India IV: mud viscoelastic properties. *Journal of Coastal Research* 11, 918–926.

Jiang, F., Mehta, A.J., 1996. Mudbanks of the southwest coast of India V: wave attenuation. *Journal of Coastal Research* 12, 890–897.

Jiang, L., Zhao, Z., 1989. Viscous damping of solitary waves over fluid mud sea beds. *Journal of Waterway, Port, Coastal and Ocean Engineering* (ASCE) 115, 345–362.

Kaihatu, J. M., Sheremet, A., Holland, T.K., (2007) A model for the propagation of nonlinear surface waves over viscous muds, *Coastal Engineering* 54, 752–764

Kurup, 1972. Littoral currents in relation to the mud bank formation along the coast of Kerala. *Mahasagar, Bulletin of the National Institute of Oceanography and Fisheries*, 5 (3).

Lee, S.C. 1995.Response of mud profiles to waves. *PhD dissertation*. Department of Civil

and Coastal Engineering, University of Florida, Gainesville, FL.

Lindenberg, J., Van Rijn, L.C., Winterwerp, J.C., 1989. Some experiments on wave-induced liquefaction of soft cohesive soils. *Journal of Coastal Research* 5, 127–138.

Liu, P.L.F., 1973. Damping of water waves over porous bed. ASCE *Journal of the Hydraulic Division* 92 (12), 2263–2271.

Liu, K., Mei, C.C., 1989. Effects of wave-induced friction on a muddy seabed modeled as a Bingham-plastic fluid. *Journal of Coastal Research* 5 (4), 777–789.

Maa, P.-Y., 1986. Erosion of soft mud beds by waves. *PhD-dissertation*. University of Florida, Coastal and Oceanographic Engineering Department, Gainesville, Florida, USA, rep. UFL/COEL-TR-059.

Maa, P.-Y., Mehta, A.J., 1990. Soft mud response to water waves. *ASCE Journal of Waterway, Port, Coastal, and Ocean Engineering* 116 (5), 634–650.

Macpherson, H., 1980. The attenuation of water waves over a non-rigid bed. *Journal of Fluid Mechanics* 97, 721–742.

Malaval, M. B. 1922. Travaux du port et de la barre de Rio Grande do Sul (Brésil). Paris, Librairie de l'Enseignement Technique, Leon Eyralles, Éditeur.

Mallik, T.K.; Mukherji, K.K. and Ramachandran, K.K., 1988. Sedimentology of the Kerala Mudbanks (Fluid muds?). *Marine Geology*, 80, 99-118.

Marques, W. C., Monteiro, I. O., Fernandes, E. H. ,2007 (submetido): Numerical modeling of the Patos Lagoon coastal plume, Brazil. Continental Shelf Research

Martins, L. R., 1972. Distribuição faciológica dos sedimentos da margem continental Sul-Riograndense, trecho Rio Grande Torres. *Resumos dos Anais do XXVII Congresso Brasileiro de Geologia* (CBG),pp. 210-211

Martins, L.R.; Martins,I.R.; Villwock, J.A. and Calliari, L.J., 1979. Ocorrência de Lama na praia do Cassino. *Anais Hidrográficos*. Rio de Janeiro. pp. 3-20.

Mathew, J.; Baba, M. and Kurian, N.P., 1995. Mud banks of the Southwest Coast of India. Wave characteristics. *Journal of Coastal Research*, 1(1), 168-178.

Mehta, A.J., 1996. Interaction between fluid mud and water waves. In: Singh, V.P., Hager, W.H. (Eds.), *Environmental Hydraulics. Kluwer Academic Publishers*, The Netherlands, pp. 153–187.

Mei, C.C., Liu, K.F., 1987. A Bingham-plastic model for a muddy seabed under long waves. *Journal of Geophysical Research* 92, 14581–14594.

Motta, V. F., 1963. Análise e Previsão das Alturas de Ondas em Tramandaí, Porto Alegre. Technical Report, Institute of Hydraulics Research, Federal University of Rio Grande do Sul, Porto Alegre,Brazil 30 p,

Nair, R.R., 1976. Unique mud banks, Kerala, Southwest India. *Bulletin Association of Petroleum Geologists*, 60, 616-621.

Ng, C.O., 2000. Water waves over a muddy bed: a two-layer Stokes' boundary layer model. *Coastal Engineering* 40, 221–242.

Rodriguez, H.N., 2000. Mud bottom evolution at open coasts. *PhD-dissertation*.University of Florida, Coastal and Oceanographic Engineering Department, Florida, USA.

Rodriguez, H.N., Mehta, A.J., 2001. Modelling of muddy coast response to waves. *Journal of Coastal Research* SI21, 132–148.

Sheremet, A., Stone, G.W., 2003. Observations of nearshore wave dissipation over muddy sea beds. *Journal of Geophysical Research* 108 (C11) 21–1/21–11

Sperle, M., Vinzon, S., Calliari, L.J. , Rech, M., Fabri, J.B., Bispo, L., 2005. Aplicação de métodos geofísicos na avaliação da ocorrência de lamas fluidas na praia do Cassino, Rio Grande. *II Proceedings Congresso Brasileiro de Oceanografia* 09 a 12 de Outubro de 2005 - Vitória - ES – Brasil.

Spierenburg, S.E.J., 1987. Seabed response to water waves. *PhD dissertation*. Delft

University of Technology, The Netherlands.

Strauch, J.C.,1998. Um Ano de Monitoramento de Ondas em Rio Grande. *Final Proc. XI National Week of Oceanography, Oceanography and their interfaces*. Federal University of Rio Grande – FURG, Rio Grande, Rio Grande do Sul, Brazil.

Tomazelli, L. J.,1990. O regime dos ventos e a taxa de migração das dunas eólicas costeiras do Rio Grande do Sul, Brasil.*Technical report*, Institute of Hydraulics Research, Federal University of Rio Grande do Sul, Porto Alegre, Brazil ,20(1), 18-26, unpublished.

Tubman, M.W., Suhayda, J.N., 1976. Wave action and bottom movements in fine sediments. *Proceedings, 15th International Conference on Coastal Engineering*, Honolulu, HI, pp. 1168–1183.

Verbeek, H., Cornelisse, J.M., 1997. Erosion and liquefaction of natural mud under surface waves. In: Burt, N., Parker, R., Watts, J. (Eds.), *Cohesive Sediments*. John Wiley & Sons, pp. 353–364.

Villwock, J. A. and Martins, LR., 1972. Depósitos lamíticos de pós-praia. Cassino, RS. *Pesquisas*, I, 69-85.

Wells, J.T., 1983. Dynamics of Coastal Fluid Muds in Low Moderate, and High-Tide Range Environments. *Canadian Journal Fisheries and Aquatic Sciences*, 40, 130-142.

Wells, J.T. and Coleman L.M., 1977. Nearshore suspended sediment variations, Central Surinam Coast .*Marine Geology*, 24, M47-M54.

Wells, J.T.; Coleman, J.M. and Wiseman, W.J., 1979. Suspension and transportation of fluid mud by solitary-like waves. *Procdings of the 16th International Coastal Engineering Conference*, ASCE/Hamburg, Germany, pp. 1932-1951.

Wells, J.T. and Coleman, I.M., 1981. Physical processes and fine-grained sediment dynamics coast of Surinam, South America. *Journal of Sedimentary Petrology*, 51(4), 1053-1068.

Wells, J. T. and Roberts, H.H., 1980. Fluid Mud Dynamics and shoreline stabilization:

Lousiana Chenier Plain. *Proceedings of the 17th International Coastal Engineering Conference*, ASCEI Sidney, Australia, pp. 1382-1401.

Wells, J.T., Kemp, G.P., 1986. Interaction of surface waves and cohesive sediments: field observations and geologic significance. In: Mehta, A.J. (Ed.), *Lecture Notes on Coastal and Estuarine Studies. Estuarine Cohesive Sediment Dynamics*, vol. 14, pp. 43–65.

Winterwerp, J.C., Van Kesteren, W.G.M., 2004. An introduction to the physical processes of cohesive sediment in the marine environment. Elsevier, *Developments in Sedimentology* vol. 56.

Winterwerp, J.C., de Graff, R.F., Groeneweg, J., Luijendijk, A.P., 2007. Modeling of wave damping at Guyana mud coast. *Coastal Engineering*, 54, 249–261.

Yamamoto, T., Koning, H.L., Sellmeiher, H., van Hijum, E.V., 1978. On the response of a poro-elastic bed to water waves. *Journal of Fluid Mechanics* 87, 193–206.

Yamamoto, T., Takahashi, S., 1985. Wave damping by soil motion. *Journal of Waterway, Port, Coastal and Ocean Engineering* (ASCE) 111, 62–77.

Capítulo 6

Discussões

Capítulo 6

Discussões

As regiões costeiras são locais de grande importância para a população mundial. Elas representam uma importante zona de produção de alimentos para a população mundial através da agropecuária, pesca e aqüicultura, e oferecem facilidades para o desenvolvimento industrial, portuário e de modais de transporte, representando uma fonte significativa de recursos minerais, como petróleo e gás natural. Além disso, de representar o principal destino turístico em todos os continentes, as regiões costeiras funcionam como um abundante reservatório de biodiversidade e ecossistemas, dos quais depende o funcionamento do planeta.

As pressões exercidas por estas atividades têm causado o aparecimento de conflitos de uso das regiões costeiras, e gerado a necessidade de ações de gerenciamento costeiro integrado, como os adotados para as áreas continentais interiores. Esta utilização cada vez mais intensa da zona costeira resulta na necessidade de um entendimento maior dos

fenômenos relacionados com a interação entre o mar e a costa, visando a ocupação racional da região litorânea, bem como um melhor aproveitamento dos recursos ali existentes

Especificamente em relação à dinâmica sedimentar, a contribuição dos estuários e da plataforma interna é determinante. Os estuários desempenham um importante papel, pois funcionam como bacias receptoras naturais capazes de transportar e acumular os sedimentos fluviais. Entretanto, a dinâmica dos estuários pode fazer com que as águas e sedimentos fluviais passem diretamente para o oceano, com um curto tempo de residência e diluição. Neste caso, os estuários alteram seu papel geológico de ser predominantemente um sumidouro e passam a ser uma fonte de sedimentos fluviais, implicando na exportação deste material para a zona costeira adjacente e contribuindo para a formação de depósitos de lama na plataforma. A plataforma interna recebe estes sedimentos finos de origem continental, e estes ficam sujeitos aos processos dinâmicos de transporte e deposição resultantes da interação entre as correntes costeiras geradas por ventos, ondas associadas à passagem de sistemas frontais, e a baixa amplitude das marés. A presença de depósitos lamíticos em plataformas internas tem sido estudada por vários autores: Avoine et al. (1981) no estuário do Seine, França, Castaing & Allen (1981) no estuário de Gironde, França, Nair & Hashimi (1986) em estuários no Oeste da Índia, entre outros.

A contribuição das ondas neste processo é essencial, pois estas quando estão se propagando de águas profundas para águas intermédiárias e rasas interagem com o fundo. O processo da fricção com o fundo não é a única causa da dissipação de energia da onda na interface da água com o fundo; dois outros mecanismos principais são observados (Shemdin et al. ,1978). As pressões exercidas no fundo pelas ondas causam dissipação de energia devido à percolação, induzindo um fluxo que ressuspende os sedimentos neles existentes contribuindo desta forma para a formação e o transporte dos bancos de lama. (Dean and Dalrymple, 1984; Suhayda, 1984; Wolanski et al., 1988; Odd et. al., 1993). Por outro lado, as

camadas de lama fluida absorvem a energia das ondas (Dean e Dalrymple, 1984; Gade, 1958; Hsiao e Shemdin, 1980; Dalrymple e Liu, 1978; Jiang e Mehta, 1996; e Ng, 2000).

Esses efeitos são de grande importância prática, e o entendimento e a quantificação desta interação entre as ondas e os fundos lamosos tem despertado o interesse da comunidade científica (Holland et al. 2003). Embora estes processos sejam bem entendidos teoricamente através de modelos conceituais e experimentos de laboratório, ainda existem limitações em relação à sua quantificação em situações reais. A quantificação da dissipação da energia da onda torna-se difícil porque a camada de lama fluida é dinâmica, mas ao mesmo tempo não se comporta como um processo local violento (Cavaleri et al.,2007). A variação na composição dos sedimentos de fundo devido às mudanças nas condições hidrodinâmicas é outro fator limitante. A medição da dissipação de energia da onda em termos de seu decaimento espectral constitui outra forma de quantificação (Nielsen, 1992). Além disso, a determinação dos parâmetros necessários a serem medidos para o entendimento destes processos, bem como a escolha, colocação e manutenção de equipamentos oceanográficos para realizar estas medições não são uma tarefa simples (Young e Gorman, 1995, Wolf, 1999). Por outro lado, experimentos de laboratório não cobrem a totalidade de fenômenos envolvidos (Cavaleri et al.,2007).

Uma forma possível de contornar estes obstáculos consiste na combinação de dados de campos com experimentos de modelagem numérica, através da utilização de modelos de ondas espectrais, desde que os mesmos contenham em sua formulação termos de dissipação de energia em fundos lamosos. Este termo fonte específico não está disponível na versão padrão dos modelos de ondas espectrais, com exceção do modelo de ondas SWAN. No modelo SWAN, Winterwerp et al (2007) implementaram o termo fonte de dissipação formulado a partir da teoria do fluído de duas camadas proposta por Gade (1958).

Logo, a quantificação da energia das ondas em regiões costeiras, e da sua atenuação em função da existência de depósitos lamíticos de fundo, é um estudo dinâmico e particular para cada região. O entendimento desta interação é fundamental para qualquer obra costeira de engenharia, podendo afetar também atividades esportivas náuticas, navais e portuárias realizadas nas proximidades da costa. Além disso, a quantificação do efeito deste processo de interação com os depósitos lamíticos encontrados em regiões costeiras é essencial para a exploração da energia das ondas, uma fonte limpa e inesgotável de energia renovável, ainda pouco explorada na atualidade, que pode contribuir para a melhoria da qualidade da matriz energética brasileira. As atividades e perspectivas acima apresentadas, e suas respectivas conseqüências e necessidades, destacam a importância deste trabalho.

A costa do Estado do Rio Grande do Sul se caracteriza por praias arenosas abertas predominantemente dominadas por ondas, que devido a sua topografia complexa, influencia os processos físicos que determinam as características das ondas e o transporte de sedimentos na costa. A Praia do Cassino, área de interesse deste estudo, está localizada na região adjacente à Lagoa dos Patos, e a lama depositada na ante-praia da Praia do Cassino se origina no interior deste sistema. Os sedimentos finos presentes na ante-praia do Cassino, que são esporadicamente remobilizados e lançados sobre a praia e zona de arrebentação, ocasionam importantes efeitos de curta e longa duração sobre as características praiais e sobre as atividades turísticas na região. Pelas conseqüências ambientais e econômicas observadas na região, é fundamental o entendimento dos fatores que controlam a dinâmica dos depósitos lamíticos observados na Praia do Cassino, cujos relatos mencionados estão baseados em observações e mapeamentos superficiais. (Calliari et al, 1999, Calliari et al, 2000, entre outros) Entretanto, nunca foram feitos estudos científicos buscando caracterizar o clima de ondas do nesta região, considerando a influência dos fundos lamosos existentes nesta região da costa.

Vários pesquisadores, tais como Tubman and Suhayda (1976), Wells e Kemp (1986), Sheremet e Stone (2003), que através de medições, observações e utilizando modelos analíticos estudaram e quantificaram a dinâmica destes depósitos de lama, concluíram que a sua ocorrência e os efeitos causados estão diretamente relacionados ao clima de ondas da região. Conseqüentemente, é essencial o entendimento da contribuição da dinâmica das ondas na formação dos depósitos lamíticos e no estudo da atenuação da energia das ondas em função da existência destes depósitos de fundo. Os primeiros trabalhos que investigam em detalhe estas interações através de modelos numéricos são muito recentes, e foram realizados por Winterwerp et al. (2007) e por Ledden et al. (2008) para a região da Guiana Francesa.

Dentro deste contexto, o objetivo geral deste estudo foi de caracterizar o clima de ondas ao longo da costa do Rio Grande do Sul, com especial enfoque na investigação da atenuação da energia das ondas sobre os depósitos lamíticos existentes na região costeira adjacente à Praia do Cassino. Estas metas foram atingidas através da caracterização do clima de ondas na costa do Rio Grande do Sul com base em dados pretéritos e dados de campo combinados com experimentos de modelagem numérica, em um estudo de caso realizado na região costeira adjacente a Praia do Cassino, que investigou o amortecimento da energia das ondas nesta região de fundo lamoso. Além disso, foi avaliada a influência dos parâmetros característicos da lama fluida na atenuação das ondas na região de estudo. Nestes estudos foram utilizados os modelos SWAN padrão e com lama fluída em sua formulação. Apesar de limitação de dados de ondas medidos nesta área foi possível a realização das simulações utilizando os dados disponíveis na literatura.

Embora exista uma evidente limitação de informações sobre o clima e a dinâmica das ondas na região de estudo, e ao mesmo tempo uma crescente demanda em relação a este entendimento, não existe um estudo sistemático do clima de ondas na costa do Rio Grande do Sul como um todo. Alguns trabalhos foram realizados buscando caracterizar certas regiões da

costa, mas estes trabalhos estão baseados em diferentes fontes de dados que abrangem desde a utilização esparsa de ondógrafos, algumas observações limitadas de campo, dados históricos em navios de oportunidade e sensores remotos.

Logo, é evidente que os dados disponíveis na atualidade não apresentam regularidade, e nem um padrão espacial e temporal característico. Os dados medidos foram realizados com ondógrafos fundeados em águas rasas, utilizando aparelhos direcionais e não direcionais. Os dados provenientes das observações de campo, de navios de oportunidade e sensores remotos, apresentam escalas espaciais e temporais variadas e limitações características. Conseqüentemente, a determinação do clima de ondas na plataforma sul do Brasil com base nestes dados resulta em uma caracterização limitada do padrão típico do comportamento destas ondas locais. Dentro deste contexto, este trabalho representa uma significativa contribuição a nível regional e nacional, pois possibilitou a implementação de uma série de modelos numéricos em diferentes escalas espaciais, que permitirão a realização de estudos pretéritos e futuros sobre diversos aspectos relacionados à dinâmica das ondas na região. Além de atender a demanda pelo conhecimento regional, os resultados deste trabalho fornecem os subsídios necessários para a realização de estudos semelhantes em outras regiões do País.

Além disso, a utilização de um modelo numérico de ondas que considere a presença de fundos lamosos em sua formulação possibilitou obter resultados precisos e realísticos para a região onde este fenômeno é observado, apesar da carência de registro de dados característicos do depósito de lama existente. A implementação desta ferramenta para a região possibilitará a recomposição de eventos passados, contribuindo para o entendimento dos processos relacionados à dinâmica sedimentar do banco de lama existente na costa gaúcha. De forma complementar, esta ferramenta contribuirá sobremaneira para a determinação do potencial energético das ondas na costa do Rio Grande do Sul, pois conforme este estudo

comprovou, a presença dos depósitos lamíticos afeta de forma significativa a energia das ondas na região.

Embora este trabalho apresente um caráter local, seus resultados representam uma contribuição inédita a nível nacional, e corroboram a limitada bibliografia internacional sobre a atenuação da energia das ondas sobre fundos lamosos. Além disso, este trabalho deu origem a um inédito sistema de previsão do comportamento das ondas, abrangendo as escalas espaciais oceânica, regional e local, que terá aplicação direta nas demandas comerciais e científicas da região.

Capítulo 7

Conclusões

Capítulo 7

Conclusões

Os principais resultados obtidos para a caracterização do clima de ondas na plataforma sul do Brasil baseada na revisão de dados disponíveis na literatura e experimentos de modelagem numérica, onde um estudo de caso foi realizado na praia do Casssino foram:

- A compilação dos dados existentes sobre o clima de ondas ao longo da plataforma sul do Brasil caracterizou um comportamento típico de agitação local, indicando que a direção predominante das ondas é entre 100º e 160º(E-SE), com altura das ondas variando entre 1 e 1,50 m. O período das ondas variou entre 6 e 14 s. Essa caracterização, entretanto, foi baseada em limitados e escassos dados de campo, salientando a necessidade de extrapolação dessas informações para todo o domínio através de modelos numéricos.

- A verificação do modelo SWAN realizada através da comparação dos resultados do modelo com dados medidos de ondas disponíveis na literatura, indicaram uma performance satisfatória do modelo na representação dos casos estudados. Entretanto, algumas limitações foram identificadas. Quando o espectro da onda possuiu dois picos de energia, os resultados indicaram que a forma do espectro é bem reproduzida, e o SWAN concorda com o nível de energia nas baixas freqüências, mas subestima o nível de energia nos picos de alta freqüência. O espectro de onda com um único pico é bem reproduzido pelo modelo.

- Na verificação do modelo SWAN considerando lama, realizada através de análise de sensitividade, os resultados do modelo indicaram que para os espectros bimodais, a presença da lama causa maior atenuação na energia da onda no pico de baixa freqüência, e menor atenuação no pico de alta freqüência.

- A caracterização do clima de ondas da plataforma sul do Brasil com base nos resultados obtidos pelo modelo SWAN, indicaram que em situações de vento Sul (S) ocorrem ondas com espectros bimodais devido a ocorrência de vagas e ondulações combinadas. Em situações de vento de nordeste (NE), a forma do espectro unimodal. A distribuição espacial da altura significativa e da direção média computadas pelo SWAN, utilizando como condição inicial vento com velocidade constante em todo o domínio computacional, mostra o decaimento esperado da onda se propagando de águas profundas para rasas.

- O efeito da lama sobre a altura significativa e o período médio da onda calculados pelo modelo indicaram que a altura significativa foi atenuada em relação ao valor medido. Entretanto essa atenuação foi superestimada, provavelmente devido aos parâmetros

característicos da lama (densidade, espessura, localização e viscosidade) terem sido considerados constantes no domínio inteiro.

Com a finalidade de avaliar os efeitos dos parâmetros característicos de lama fluida (espessura, densidade e viscosidade), na atenuação da altura da onda, período médio e dissipação de energia na Praia do Cassino, os resultados obtidos com o modelo SWAN considerando lama foram comparados com o modelo SWAN na versão padrão, e com dados de campos medidos durante o Experimento Cassino. As principais conclusões deste estudo foram:

- Os depósitos de lama no fundo causam significativa atenuação da altura significativa da onda, período médio e energia devido à dissipação viscosa em fundo do mar liquefeito;

- Entre os parâmetros analisados, a espessura da camada de lama causa menor efeito na atenuação da altura significativa, diminui o período médio e dissipa a densidade de energia.

- A densidade do depósito de lama apresenta uma relação inversa com a atenuação dos parâmetros característicos da lama

- A representação real do deposito de lama é uma das mais importantes informações de inicialização para o modelo numérico representar corretamente o amortecimento da energia da onda observado na praia do Cassino.

- Os resultados mostram que para avaliar corretamente o comportamento dos parâmetros da onda na presença de fundos com depósitos lamosos é essencial aplicar modelos de ondas que consideram os efeitos da lama em sua formulação.

Capítulo 8

Referências Bibliográficas

Capítulo 8

Referências Bibliográficas

BANNER, M.L., YOUNG, I.R., 1994. Modeling Spectral Dissipation in the Evolution of Wind Waves. Part I : Assessment on Existing Model Perfomance. *Journal of Physical Oceanography*, 24:1550-1571.

BATTJES J.A., JANSSEN J.P.F.M. 1978. Energy loss and set-up due to breaking of random waves. Proc. 16th Int. Conf. on Coastal Eng., 569-587 p.

BERTOTTI, L & CAVALERI, L. 1994. Accuracy of wind and wave evaluation in coastal regions. Proc. 24th Int. Conf. Coastal Engineering, ASCE, 57-67p.

BINGHAM, E.C. 1922. Fluidity and Plasticity. New York, McGraw-Hill, 404p.

BOOIJ, N., RIS, R.C., HOLTHUIJSEN, L.H. 1999. A third-generation wave model for coastal regions, 1, Model description and validation. *Journal Geophysical Research*, 104:7649-7666.

BRETSCHNEIDER, C.L. 1970. Forecasting Relations for Wave Generation. *Look Lab Hawaii*, 1:31-34.

BRETSCHNEIDER, C.L. 1973. Prediction of waves and currents. *Look Lab Hawaii*, 3:1-17.

CALLIARI, L.J., KLEIN, A.H.F. 1992. Características morfodinâmicas e sedimentológicas das praias oceânicas entre Rio Grande e Chuí, RS. 37º Congresso Brasileiro de Geologia, São Paulo.

CALLIARI, L.J. & FACHIN, S. 1993. Lagoa dos Patos: Influência nos depósitos lamíticos costeiros. *Pesquisas*, 20(1):57-69.

CALLIARI, L.J. & GRIEP, M.F. 1999. Uma análise histórica dos efeitos produzidos por modificações antrópicas no estuário da Lagoa dos Patos-Natural versus provocado. In: FLORES, FF (ed.). Por uma história multidisciplinar do Rio Grande. Edigraf FURG, Brasil, 97-105.

CALLIARI, L.J., SPERANSKI, N.S., TORRONTEGUY, M.E., OLIVEIRA, M.B. 2000. The mud banks of Cassino Beach, Southern Brazil: Characteristics, Processes and Effects. *Journal of Coastal Research*, ICS 2000 Proceedings:1-9.

CALLIARI, L.J., PEREIRA, P.S., DE OLIVEIRA, A.O., FIGUEIREDO, S.A. 2005. Variabilidade das Dunas Frontais no Litoral Norte e médio do Rio Grande do Sul, Brasil. *Gravel*, 3:15-30.

CAMARGO, O.A., SILVA, F.J.L., CUSTODIO, R.S. & GRAVINO, N. 2002. Atlas Eólico do Rio Grande do Sul. Secretaria de Energia, Minas e Comunicações, Porto Alegre/RS. 70p.

CAVALERI, L. & MALANOTTE-RIZZOLI, P. 1981. Wind wave prediction in shallow water: Theory and applications. *Journal of Geophysical Research*, 86(C11):10,961-10,973

CAVALERI, L., ALVES, J.-H.G.M., ARDHUIN, F., BABANIN, A., BANNER M., BELIBASSAKIS, K., BENOIT, M., DONELAN, M., GROENEWEG, J., HERBERS, T.H.C., HWANG, P., JANSSEN, P.A.E.M., JANSSEN, T., LAVRENOV, L.V., MAGNE, R., MONBALIU, J., ONORATO, M., POLNIKOV, V., RESIO, D., ROGERS, W.E., SHEREMET, A., MCKEE SMITH, J., TOLMAN, H.L., VAN VLEDDER, G., WOLF, J., YOUNG, L. 2007. Wave modelling – The state of the art. *Progress in Oceanography,* 75 (4):603-674.

CHOU, H.T., FODA, M.A., HUNT, J.R. 1993. Rheological response of cohesive sediments to oscillatory forcing. In: MEHTA, A.J. (ed.). Nearshore and Estuarine Cohesive Sediment Transport. Coastal and Estuarine Sciences, AGU, 42:126–148.

COLI, A. B. 1994. Análise das alturas de onda ao longo do Rio Grande do Sul: dados históricos e altimétricos. Trabalho de graduação, Curso de Oceanologia, Fundação Universidade Federal do Rio Grande – FURG, 58p.

COLI, A. B. 2000. Estudo do Clima Ondulatório em Rio Grande. Dissertação de Mestrado, Curso de Engenharia Oceânica, Fundação Universidade Federal do Rio Grande – FURG, 76p.

CUCHIARA D. C., FERNANDES, E. H., STRAUCH, J. C., CALLIARI, L. J. 2005. Caracterização do clima de ondas na costa do Rio Grande do Sul. Anais do VI Seminário sobre ondas, mares, engenharia oceânica e oceanografia por satélite. VI OMAR-SAT, Arraial do Cabo, Rio de Janeiro, Brasil.

DALRYMPLE, R.A., LIU, P.L.F., 1978. Waves over soft muds: a two-layer fluid model. *Journal of Physical Oceanography*, 8:1121–1131.

DE WIT, P.J. 1995. Liquefaction of cohesive sediment by waves. PhDdissertation. Delft University of Technology, The Netherlands.

DEAN, R. G. & DARLYMPLE, R. A., 1991. Water Wave Mechanics for Engineers and Scientists. World Scientific Publishing Co. Pte. Ltd, 343 p.

DELANEY, P. J. V., 1965. Fisiografia e geologia de superfície da planície costeira do Rio Grande do Sul. Universidade Federal do Rio Grande do Sul, escola de Geologia, Porto Alegre, publicação especial 9, 104 p.

DRAKE, D. E. 1976. Suspended Matter on Continental Shelves. In: STANLEY, D. J. & SWIFT, D. J. P. (ed.). Marine Sediment Transport and Environmental management, New York, 127-158 p.

DYER, K.R. 1986. Coastal and Estuarine Sediment Dynamics. New York, John Wiley and Sons Ltd. 342 p.

FODA, M.A., HUNT, J.R., CHOU, H.T. 1993. A nonlinear model for the fluidization of marine mud by waves. *Journal of Geophysical Research,* 98:7039–7047.

FRYBERGER, S. G. 1979. Dune forms and wind regime. In: Mckee, E.D. (ed). A Study of Global Sand Seas. Geological Survey Professional, Paper, 1052: 137-169.

GADE, H.G., 1958. Effects of a non-rigid, impermeable bottom on plane surface waves in shallow water. *Journal of Marine Research,* 16 (2):61–82.

GELCI, R. H. C. VASSAL, J. 1956. Utilization des diagrammes de propagation à la prèvision ènergetique de la houle. *Bulletin d'Information du Comitê Central d'Oceanographie et d'estudes des Cotes,* 8 (4):160-197.

GOLDING, B. W. 1983. A wave prediction system for real-time sea state forecasting. *Q. J. Roy. Meteor. Soc.*, 109:393-416.

HASSELMANN, K. 1962. On the non-linear energy transfer in a gravity-wave spectrum. Part 1. General theory. *Journal of Fluid Mechanics* 12:481- 500.

HASSELMANN, K. 1974. On the spectral dissipation of ocean waves due to whitecapping. *Bound.-layer Meteor.*, 6(1-2):107-127.

HASSELMANN, S., HASSELMANN, K. 1981. A symmetrical method of computing the non-linear transfer in a gravity-wave spectrum. *Hamburger Geophys. Einzelschr.,* Serie A, 52:138.

HEMPHILL, T., CAMPOS, W., PILEHVARI, A. 1993 Yield-Power Law Model More Accurately Predicts Mud Rheology. *Oil & Gas Journal*, 91(34):45-50.

HOLLAND, K.T., KEEN, T. & KAIHATU, J.M. 2003. Understanding coastal dynamics in heterogeneous sedimentary environments. Coastal Sediments 2003, Clearwater Beach, Florida, Estados Unidos.

HOLTHUIJSEN L.H., BOOIJ N., HERBERS T.H.C. 1989. A prediction model for stationary, short crested waves in shallow water with ambient currents. *Coastal Eng.,* 13:23-54).

HSIAO, S.V., SHEMDIN, O.H. 1980. Interaction of ocean waves with a soft bottom. *Journal of Physical Oceanography,* 10:605–610.

JANSSEN, P. A., KOMEN, G. J., VOOGT, W. J. P. 1984, An operational coupled hybrid wave prediction model. *Journal of Geophysical Research*, 89:3635 - 3654.

JANSSEN, P.A.E.M. 1991. Quasi-linear theory of wind-wave generation applied to wave forecasting. *Journal of Geophysical Research*, 21:1631-1642.

JIANG, F., MEHTA, A.J. 1995. Mudbanks of the southwest coast of India IV: mud viscoelastic properties. *Journal of Coastal Research,* 11:918–926.

JIANG, F., MEHTA, A.J. 1996. Mudbanks of the southwest coast of India V: wave attenuation. *Journal of Coastal Research*, 12:890–897.

JIANG, L., ZHAO Z. 1989. Viscous damping of solitary waves over fluid-mud seabeds. *Journal of Waterway, Port, Coastal, and Ocean Engineering*, 115(3):345-362.

KHANDEKAR, M. L. 1989. Operational Analysis and Prediction of Ocean Wind Waves, New York, Springer-Verlag. 214p.

KJERFVE, B. G., PERILLO, M. E., GARDNER, L. R., RINE, J. M., DIAS, G. T. M., MOCHEL, F. R. 2003. Morphodynamics of muddy environments along the Atlantic coasts of North and South America. In: HEALY, T., WANG, Y. & HEALYMUDDY, J.-A. (eds.). Muddy Coasts of the World: Processes, Deposits and Functions. Elsevier Science, Amsterdam. p.479-532.

KOMAR, P. D. 1998. Beach Processes and Sedimentation. Englewood Cliffs, New Jersey, Prentice Hall, 544 p. Second Edition.

KOMEN, G.J., CAVALIERI, L., DONELAN, M., HASSELMANN, K., HASSELMANN, S., AND JANSSEN, P.A.E.M., 1994. Dynamics and modeling of ocean waves. Cambridge, Cambridge University Press, 530p.

KRUSCHE, N., SARAIVA, J.M.B., REBOITA, M.S. 2003. Normais climatológicas provisórias de 1991 a 2000 para Rio Grande, RS. 104p.

LEE, S.C. 1995. Response of mud profiles to waves. PhD dissertation. Department of Civil and Coastal Engineering, University of Florida, Gainesville, Florida.

LIU, P.L.F. 1973. Damping of water waves over porous bed. *Journal of the Hydraulic Division,* 92(12):2263–2271.

LIU, K., MEI, C.C. 1989. Effects of wave-induced friction on a muddy seabed modeled as a Bingham-plastic fluid. *Journal of Coastal Research* 5(4):777–789.

MAA, P.-Y. 1986. Erosion of soft mud beds by waves. PhD-dissertation, University of Florida, Coastal and Oceanographic Engineering Department, Gainesville, Florida, USA, rep. UFL/COEL-TR-059.

MAA, P.-Y., MEHTA, A.J. 1990. Soft mud response to water waves. *ASCE Journal of Waterway, Port, Coastal, and Ocean Engineering,* 116 (5):634–650.

MACPHERSON, H. 1980. The attenuation of water waves over a non-rigid bed. *Journal of Fluid Mechanics,* 97:721–742.

MARTINS, L.R. 1972. Distribuição faciológica dos sedimentos da Margem Continental Sul-Riograndense, trecho Rio Grande-Torres. Resumos dos Anais do XXVII Congresso Brasileiro de Geologia (CBG), p. 210 -211.

MARTINS, L.R.S., MARTINS, I.R.,VILLWOCK, J.A., CALLIARI, L.J. 1979. Ocorrência de Lama na praia do Cassino. Anais Hidrográficos. Rio de Janeiro. p. 3-20.

MASTENBROEK, C., BURGERS, G. & JANSSEN, P.A.E.M. 1993. The dynamical coupling of a wave model in a storm surge model through the atmospheric boundary layer. *Journal of Physical Oceanography*, 23:1856- 1866.

MATHEW, J.; BABA, M. & KURIAN, N.P. 1995. Mud banks of the Southwest Coast of India. Wave characteristics. *Journal of Coastal Research*, 1(1):168-178.

McCAVE, I.N. 1970. Wave effectiveness at the sea bed and its relationship to bed-forms and deposition of mud. *Journal of Sedimentary Research*, 41(1):89-96.

McCAVE, I.N. 1972. Transport and escape of fine-grained sediment from shelf areas. In Swift, D.J.P., Duane, D.B., and Pilkey, O.H. (eds.). Shelf Sediment Transport: Process and Pattern, Stroudsburg, PA (Dowden, Hutchinson and Ross), 225–248 p.

MEI, C.C., LIU, K.F. 1987. A Bingham-plastic model for a muddy seabed under long waves. *Journal of Geophysical Research,* 92:14581–14594.

MELO FILHO, E., ALVES, J. H. G. de M. 1993. Nota sobre a chegada de ondulações longínquas á costa brasileira. Anais do X Simpósio Brasileiro de Recursos Hídricos (X ABRH), Gramado, RS, Brasil, 5:362-369.

MEHTA, A.J. 1996. Interaction between fluid mud and water waves. In: SINGH, V.P., HAGER, W.H. (eds.), Environmental Hydraulics. Kluwer Academic Publishers, The Netherlands, 153–187 p.

MEI, C.C., LIU, K.F. 1987. A Bingham-plastic model for a muddy seabed under long waves. *Journal of Geophysical Research*, 92:14581–14594.

MILES, J. W. 1957. On the generation of surface waves by shear flows. *Journal of Fluid Mechanics,* 3:185- 204.

MILES, J. W. 1981. Hamiltonian formulations for surface waves. *Applied Science Research*, 37:103-110.

MOTTA, V. F., WAINER, I. J. 1963. Análise e Previsão das Alturas de Ondas em Tramandaí, Porto Alegre. Instituto de Pesquisas Hidráulicas, Universidade Federal do Rio Grande do Sul, 30 p.

NG, C.O. 2000. Water waves over a muddy bed: a two-layer Stokes' boundary layer model. *Coastal Engineering,* 40:221–242.

NICHOLS, M.M. 1986. Effects of fine ressuspension in estuaries. In: MEHTA, A.J. (ed.). Estuarine Cohesive Sediment Dynamics. Springer-Verlag, New York Inc, N.Y. 473 pp.

NICHOLS, M.M. & BIGGS, R.B. 1985. In: DAVIES, R.A. (ed.). Coastal Sedimentary Environments. Springer-Verlag, New York Inc, N.Y., 420p.

PHILIPS, O.M., 1957. On the generation of waves by turbulent wind. *Journal of Fluid Mechanics,* 2:417- 445.

PIERSON, W. J., & MOSKOWITZ, L.1964. A proposed spectral form for fully developed wind seas based on the similarity theory of S. A Kitaigorodskii. *Journal of Geophysical Research ,*69(24), 5181-5190.

PIERSON W. J., NEUMANN, G.& JAMES, R. 1955. Practical methods for observing and forecasting ocean waves by means of wave spectra and statistics. H.O. Publ. 603, U. S. Navy Hydrographic Office, 284 p.

RODRIGUEZ, H.N. 2000. Mud bottom evolution at open coasts. PhD-dissertation, University of Florida, Coastal and Oceanographic Engineering Department, Florida, USA.

RODRIGUEZ, H.N., MEHTA, A.J. 2001. Modelling of muddy coast response to waves. *Journal of Coastal Research,* SI21:132–148.

SHEMDIN, P., HASSELMANN, K., HSIAO, S.V. & HERTERICH, K. 1978. Non-linear and linear bottom interaction effects in shallow water. In: Turbulent Fluxes through the Sea Surface, Wave Dynamics and Prediction, NATO Conf. Ser., 1:347-372.

SHEREMET, A., STONE, G.W. 2003. Observations of nearshore wave dissipation over muddy sea beds. *Journal of Geophysical Research,* 108 (C11):21–1/21–11.

SNYDER, R.L., DOBSON, F.W., ELLIOTT, J.A. & LONG, R.B. 1981. Array measurement of atmospheric pressure fluctuations above surface gravity waves. *Journal of Fluid Mechanics*,102:1-59.

SPIERENBURG, S.E.J. 1987. Seabed response to water waves. PhD dissertation, Delft University of Technology, The Netherlands.

STRAUCH, J.C. 1997. Monitoramento de Ondas em Rio Grande. Anais do XII Simpósio Brasileiro de Recursos Hídricos, Vitória, ES, Brasil, 4:385-391.

STRAUCH, J.C. 1998. Um Ano de Monitoramento de Ondas em Rio Grande. XI Semana Nacional de Oceanografia, Oceanografia e suas interfaces, Fundação Universidade Federal do Rio Grande – FURG, Rio Grande, RS, Brasil.

SVERDRUP, H.U., MUNK, W. H. 1947. Wind, sea and swell: Theory of relations for forecasting. Publication 601, Hydrographic Office, U.S. Navy, 50 pp.

SWAMP GROUP. 1985. Ocean Wave Modeling, New York, Plenum Press, New York, 266 p.

TOMAZELLI, L. J. 1992. O regime dos ventos e a taxa de migração das dunas eólicas costeiras do Rio Grande do Sul, Brasil. *Pesquisas*, 20(1): 18-26.

TOMAZELLI, L.J., VILLWOCK, J.A. 1992. Considerações sobre o ambiente praial e a deriva litorânea de sedimentos ao longo do litoral norte do Rio Grande do Sul, Brasil. *Pesquisas* 19(1):3-12.

TUBMAN, M.W., SUHAYDA, J.N. 1976. Wave action and bottom movements in fine sediments. Proceedings, 15th International Conference on Coastal Engineering, Honolulu, HI, p. 1168–1183.

VAN LEDDEN, M.,. VAUGHN, G, LANSEN, J., WIERSMA, F., AMSTERDAM, M. (2008) Extreme wave event along the Guyana coastline in October 2005. *Continental Shelf Research*, doi:10.1016/j.csr.2008.03.010

VERBEEK, H., CORNELISSE, J.M. 1997. Erosion and liquefaction of natural mud under surface waves. In: BURT, N., PARKER, R., WATTS, J. (eds.). Cohesive Sediments. John Wiley & Sons, 353–364.

VILLWOCK, J. A. & MARTINS, LR. 1972. Depósitos lamíticos de pós-praia. Cassino, RS. *Pesquisas*, I:69-85.

ZIJLEMA, M. & VAN DER WESTHUIJSEN, A.J. 2005. On convergence behaviour and numerical accuracy in stationary in stationary SWAN simulations of nearshore wind wave spectra. *Coastal Engineering*, 52:237-265.

WAMDI GROUP. 1988. The WAM model - a third generation ocean wave prediction model. *Journal Physical Oceanography*, 18(12):1775-1810.

WELLS, J.T., COLEMAN, I.M. 1981. Physical processes and fine-grained sediment dynamics coast of Surinam, South America. *Journal of Sedimentary Petrology*, 51(4):1053-1068.

WELLS, J.T., KEMP, G.P. 1986. Interaction of surface waves and cohesive sediments: field observations and geologic significance. In: MEHTA, A.J. (Ed.). Lecture Notes on Coastal and Estuarine Studies. Estuarine Cohesive Sediment Dynamics, 14:43–65.

WILSON, B.W. 1965. Numerical prediction of ocean waves in the North Atlantic for December 1959. *Dtsch. Hydrogr. Z.*, 18(3):114-130.

WINTERWERP, J.C., DE GRAFF, R.F., GROENEWEG, J., LUIJENDIJK, A.P. 2007. Modeling of wave damping at Guyana mud coast. *Coastal Engineering*, 54:249–261.

WMO, WORLD METEOROLOGICAL ORGANIZATION. 1998. Guide to Wave Analysis and Forecasting. Publicação WMO - nº 702, Editora A. K. Laing, Geneva, Switzerland.159 p.

WU, J. 1982. Wind-stress coefficients over sea surface from breeze to hurricane. *Journal of Geophysical Research*, 87(C12):9704-9706.

YAMAMOTO, T., KONING, H.L., SELLMEIHER, H., VAN HIJUM, E.V. 1978. On the response of a poro-elastic bed to water waves. *Journal of Fluid Mechanics,* 87:193–206.

YAMAMOTO, T., TAKAHASHI, S. 1985. Wave damping by soil motion. *Journal of Waterway, Port, Coastal and Ocean Engineering*, 111:62–77.

Anexo I

Modeling of wave damping induced by fluid mud in Cassino Beach coastal area

Modeling of wave damping induced by fluid mud in Cassino Beach coastal area

Debora Copstein Cuchiara

Modeling of wave damping induced by fluid mud in Cassino Beach coastal area

Abstract

This report presents results of the work carried out by D. C. Cuchiara from February to May of 2006 at WL|Delft Hydraulics Institute, as part of collaboration between institutions (WL|Delft Hydraulics, FURG, UFRJ) within the Phase 2 of the Cassino Project (Z-3672). The activities planned for this period included to participate with interpretation of hydrodynamic and wave data, in order to carry out wave modeling experiments and to work on the interpretation of the results. The main purposes of this collaboration were to optimize the transference of data and knowledge of the local conditions, as well as to develop wave modeling experiments for the Cassino Beach Coastal area.

The work carried out at WL|Delft Hydraulics was divided in two parts. The first part involves the calibration of the SWAN model without the mud module, based on the comparison between modeling experiments and data available from wave measurements carried out by Cassino Project, and modeling the deep water wave climate in the region. The second part of this work involves the calibration of the new SWAN model, which includes the presence of fluid mud, against the same data. The model calibration was carried out in the form of a sensitivity analysis.

The proposed work was successfully accomplished and this report presents results of the calibration of the SWAN model with and without considering the presence of mud at the bottom, as well as results of the application of the SWAN model to study the wave attenuation over mud deposits in terms of significant wave height and energy density.

SUMMARY

Modeling of wave damping induced by fluid mud in Cassino Beach coastal area

1. Introduction

The importance of coastal zones has long being recognized, not only by the scientific community, but also by the coastal population, for presenting privileged natural, economic and human resources. These areas represent an interface between the ocean and the continents, and play a fundamental role in several activities, such as tourism, recreation, fishing and harboring. Thus, understanding the past and future effects of variations in the oceanographic and meteorological energy conditions of the coastal zone is essential for most of the engineering projects, representing a basic requirement for coastal planning. Studies carried out on the Brazilian Coast show that the origin, development and disappearance of coastal morphologic features were studied based on the understanding of the physical processes controlling the dynamics of the system, which involves the interaction between waves, currents, tides and the continental shelf topography (CERC, 1986; Morton, 1991).

The coast of Rio Grande do Sul state (approximately 610 km long), presents a Northeast-Southwest orientation, and is characterized by open sandy beaches exposed to the action of the waves. The coastal topography is complex and influences the physical processes determining the waves and sediment transport at the coast.

The fine sediments observed in the foreshore of Cassino beach (Figure 1), are periodically suspended, transported and deposited on shore and on the surf zone (Villwock and Martins, 1972; Calliari et al. 2000), exerting important effects on the short and long features observed on the beach. Furthermore, tourist activities in the area are strongly affected by the occurrence of mud deposits on Cassino Beach, which receives more than 100 thousand tourists in the summer.

Since 1972, more than 18 episodes of mud deposition along Cassino beach were recorded (Calliari, et at. 2000), associated with storm waves that are able to suspend mud deposits bringing negative consequences for the ecosystem and the economy of the area. Although registrations of fatal accidents associated to the swimmers imprisonment in the mud banks do not exist, the occurrence of several incidents involving surfers stands out the eminent risk of casualties. Under this aspect, it is fundamental to develop and to improve tools through which it is possible to increase the current knowledge about the conditions and in which circumstances the deposits of mud are suspended and thrown in the shore of Cassino Beach .

The waves are perturbations of the state of equilibrium of the oceans and represent an essential factor on the dynamics of mud banks. The association between the wind acting on the water surface and the atmospheric regime produce these disturbances in the ocean, which present great spatial and temporal variability. Among the several types of waves that happen in the ocean, gravity waves stand out. Gravity waves are the main and more constant source of energy in the sea.

There are several physical processes on a wave field in the sea, where waves spread from deep waters to the coastal zone. The main existent waves near the coast or seawards can be classified in sea (wind-sea) and swell. Sea waves are observed in the generation zone and receive energy from the wind, while swell waves are composed by waves that spread outside of the generation zone, and do not receive energy from the wind.

Several mechanisms conserve, add or remove the wave energy. The dissipation of energy at the bottom due to friction is a way of dissipating the energy transported by the waves. This dissipation becomes important when the continental shelf on which the wave field spreads is large and formed by coarse sediments, or is composed by muddy bottoms.

The effect of no linear interactions among waves can be observed in the wave spectrum in the area of energy pick, when the gain of energy is larger than the dissipation, and is transferred to high and low frequencies. The whitecapping process is represented by the increase in the relation between the wave length and period. That happens in the high frequencies, because those waves have short period and small length. The energy transferred for the low frequencies induce the growth of new wave components in the spectrum, resulting in the migration of the energy pick in that direction.

Thus, waves play a fundamental role in the formation of coastal features, and affect several recreational and economical activities (e.g. sailing, harbor operations, oil extraction), highlighting the importance of developing mechanisms to predict the wave climate in coastal areas, and to evaluate the interaction between waves and the type of bottom.

2. Objectives

2.1 General Objective

The aim of this work is to carry out the calibration of the SWAN model with data from the Cassino Project. This calibration was carried out in the form of a sensitivity analysis, using the deepwater wave climate.

2.2 Specific Objectives

- To calibrate the standard SWAN model based on a comparison between modeling results and wave data obtained during surveys of the Cassino Beach Project.

- To calibrate the new SWAN model (including the fluid mud module) based on the same method.

- To study the wave damping induced by the mud deposits observed at Cassino Beach.

3. Study area

The study area is located in the southern Brazilian coast between 30-32°15' S and 50°30'-52°15' W (Figure 1)
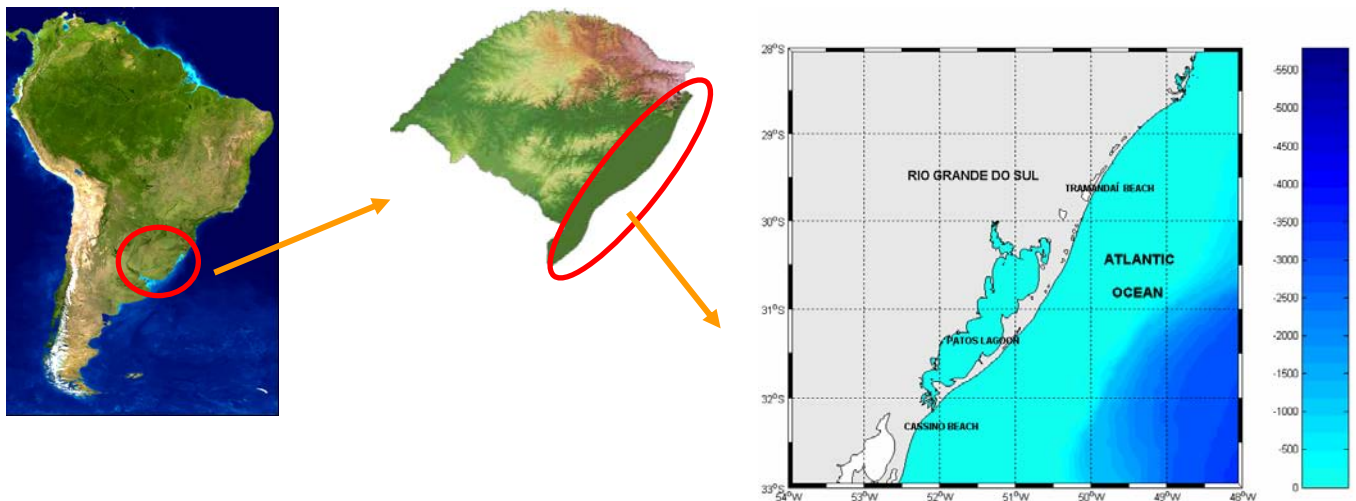
Figure 1 - Study area

3.1. Characterization of the wave climate:

Observational data on the wave climate in the Southern Brazilian Shelf (SBS) are sparse, and a systematic study of the wave climate does not exist, although some local efforts have been done in order to characterize certain areas. These previous studies were based on several sources of data, which include field measurements and observations, historical data from opportunity ships, and remote sensing.

The data obtained through field measurements for this area result from two studies accomplished in the surroundings of Tramandaí Beach (Motta, 1963), and Rio Grande city (Strauch, 1998), which define the northern and southern limits of the Rio Grande do Sul State coastal area. Motta (1963) determined the maximum wave height in Tramandaí based on data obtained between October 1962 and September 1963 (12 months of data), using a non-directional wave meter, fixed at 17,5 m depth. The observed maximum height was 7,0 m in April 1963, the maximum value of the significant height was 4,8 m, both for a 30 years return period. For a 100 years return period, the maximum height reached 7,6 m and the maximum significant height 5,5 m. The direction of wave incidence was visually obtained, indicating that crests are almost parallel to the coast.

Strauch (1998) carried out field measurements with a directional Waverider with digital acquisition, fixed at 15 m, with the objective of supplying preliminary information about the characteristics of the local agitation and the determination of the project wave for the area. This information is important to give support to the recovery project of the jetties located at the mouth of the Patos Lagoon estuary. The obtained data showed mean significant height of 1,0 m in the 100º direction (SE), corresponding to swell conditions, and mean significant height of 1,5 m in the 160ºdirection, corresponding to a state of the sea of the type "sea". (Figure 2). The largest picks of wave energy were observed in this direction. They were still observed in April 1998, where the maximum values of significant wave height reached 4,2 m, with direction of propagation of 140º (Figure 3).
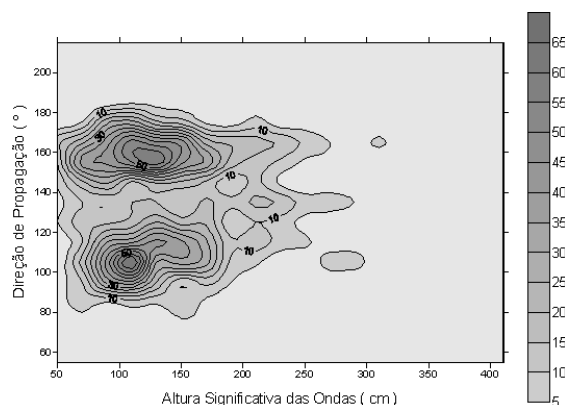
Figure 2– Frequency of occurrence - Significant Wave Height and Direction of Propagation
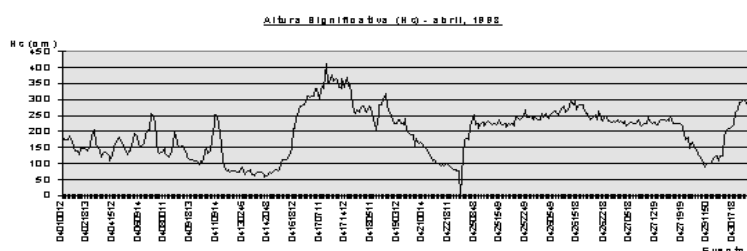
Figure 3– Maximum Significant Height (April 1998)

Colli (1994) combined the analysis of data of wave height and direction obtained through opportunity ships (between 1946 and 1979), with data of the satellite Topex/Poseidon (1993), and determined the spatial and temporal variation in wave height and direction in the coastal and oceanic area of Rio Grande do Sul. His results showed that the winter waves are larger than summer waves. The northeast, east and southeast waves are more frequent in spring time, while the north, west and southwest waves are amplified during autumn and winter time. The most expressive values of medium height correspond to the Southwest direction and, secondarily to the south, west and north directions. Regarding the annual mean for each of the wave propagation direction quadrants, the data demonstrated great variability, with waves coming mainly from the northeast and from the south. Through the analysis of the Topex/Poseidon data, it was possible to determine that in the southern

oceanic limit of the study area the largest waves prevail in relation to the north. Under the latitude of 33ºS, historical maps demonstrate the occurrence of centers of larger wave heights, which are intensified during autumn, and reach its maximum during the winter.

Coli (2000) described the climate of surface waves for the area near the jetties of the bar of Rio Grande Port, based on a historical file (1949 and 1979) composed by waves calculated visually from informations from opportunity ships, and wave data acquired by directional measurements between October 1996 and August 1997. These data provided the base for a short and long period statistics analysis. The author concluded that the short period characteristic wave had significant height between 1,0 and 1,5 m, mean period between 5 and 6 s and southeast predominant direction. There were not waves with significant heights larger than 4 m and mean period larger than 12 s. Although the height and period parameters have not presented significant seasonal variations, there were differences in the form of the wave spectrum. In the summer months the spectral pick was more frequent in the "swell" conditions (8 to 10 s), while in the winter the spectral pick was characteristic of "sea" conditions (10 to 14 s).

Furthermore, Machado (2000) calculated the wave height for specific return times, with data collected in the south of Rio Grande do Sul State (at Cassino Beach). The author determined the maximum wave project for return periods of 1, 10, 20, 30, 50 and 100 years, with the objective of providing information for future coastal engineering projects. The author concluded that waves in the area present two different types. The first corresponds to local or sea waves, with predominant SE direction (around 100°), and the second also with predominant direction SE, but around 140°, corresponding to storm or swell waves . The largest wave significant heigh during the period was 5,5 m and the registered maximum wave was 7,6 m. The significant mean height was 1,2 m and maximum height was 2,0 m.

3.2. Characterization of the wind climate:

The regional winds that affect the coast of Rio Grande do Sul are mainly related to two high pressure systems observed in this area: the South Atlantic Anticyclone and the Polar Migratory Anticyclone (Nimer,1977). From January to December of 1982, Tomazelli (1990), analyzed data registered in three meteorological stations located in the cities of Torres, Imbé and Rio Grande, and established the wind regime for the coast of Rio Grande do Sul.

Based on the classification proposed by Fryberger (1979), the area was characterized as being of high energy, presenting variability in two predominant directions. The most frequent winds come from northeast (NE) and, although it blows throughout the year, it is stronger in the spring and summer months. Winds from the west (W)-southwest (SW) are also important, although more effective during the winter. Krusche et. al. (2003) in studies acomplished for Rio Grande city from 1991 and 2000, also found the northeast wind (NE) as predominant, and the southeast wind (SE) as secondary.

Calculations of the wind potential to transport sand carried out by Tomazelli (1992), based on Fryberger (1979), indicated that the wind velocity capable of transporting sand decreases from Imbé to Torres and Rio Grande. With this result, the author found the northeast wind (NE) predominant for the largest occurrence frequency of this velocity wind varying between 5 and 7m/s.

According to the wind rose diagram presented by the Eolic Atlas of Rio Grande do Sul (Camargo et. al., 2002), the stations more to the north present winds northeast (NE) and east (E) with larger frequency and intensity. From Mostardas to the south the frequency and intensity of the northeast winds (NE) are reduced observing a increase of the southeast components (SE) and south (S). (Figure 4)
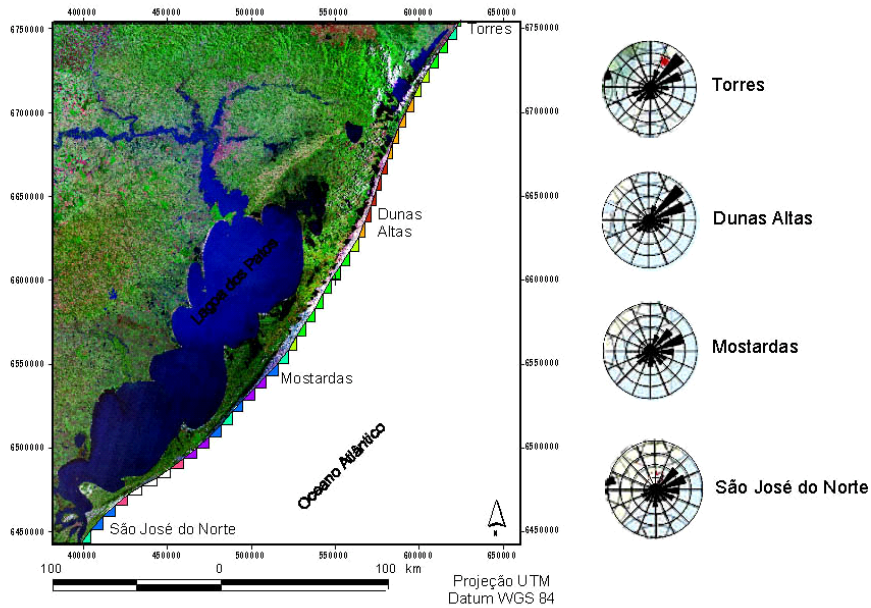
Figure 4 - Frequency and intensity of winds in the north and medium coast (Camargo et. al.,2002).

3.3. Characterization of the mud layer

In 1998, three storms happened in Cassino Beach, where mud deposits from the coastal area were suspended, transported and deposited on the shoreface and surf zone. Torronteguy (2000) made maps and characterized these deposits. During at year, the Laboratory of Geological Oceanography at FURG (LOG/DEGEO), together with the Hydrographical and Navigational Department of the Brazilian Navy (DHN), carried out an operation in the Cassino beach shoreface, where the mud deposits located between 12 to 4 m (an area approximately of 48 km^2 - 6 km x 8 km) were sampled (Figure5). The author concluded that the data obtained in the sediment analysis, were in agreement with the general pattern of muddy sediments, and presented a high percentile of fine, organic matter and content of water. The volume of fluid mud found deposited close the beach was relatively low, covering approximately 12 km of extension and around 3 to 4 km of width, from the beach line towards the sea.

The fluid mud map revealed that the thickness of the fluid mud increased gradually from the south, and towards the coast, achieving 1,24 meters. The density varied between 0,98 and 1,45 g/cm3.
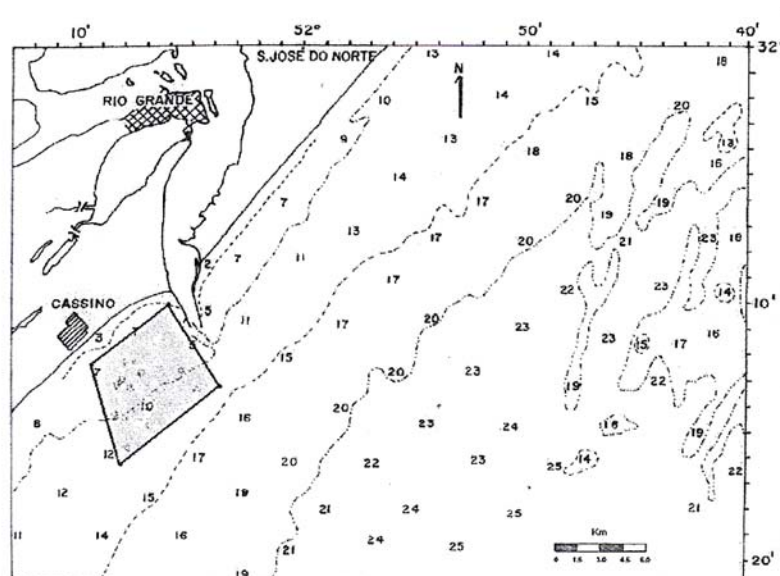
Figure 5– Bathymetric map. The darkest zone represents the studied region.

12

4. Methodology

4.1. Data

The bottom topography for the studied area was established based on data from the Brazilian Nautical Charts (Hydrographical and Navigational Department of the Brazilian Navy - DHN). The charts were digitalized using Golden Software Surfer 8 and each bathymetric point was correlated with its UTM coordinates, supplied by the Federal University of Rio de Janeiro (UFRJ), Brazil.

The nautical charts used were:

- DH 2100: *Costa Sul: de Mostardas a Rio Grande*, scale 1:269516, published in 31/10/1964 and reviewed in 15/10/1999; bathymetry related to the mean low-water spring tide;
- DH2112: *Costa Sul: de Rio Grande a Feitoria*, scale 1:80000, published in 21/03/1965 and reviewed in 30/09/2000; bathymetry related to the mean of the low-water levels;
- DH2140: *Costa Sul: Lagoa dos Patos*, scale 1:271653, published in 28/09/1965 and reviewed in 30/09/2000; bathymetry related to the mean low-water spring tide.

The available data is presented in Table 1.
. The stations are located in the Figure 8.

Table 1 - Table of available data

Parameter	Station	Sampling Time	Begin	End
Data 1996				
Waves	East jetty	3 hours	11-10-1996	31-12-1996
Data 1997				
Wind (1)	Pilot Station	3 hours	01-08-1997	31-12-1997
Waves	East jetty	3 hours	01-01-1997	31-08-1997
Data 1998				
Wind (1)	Pilot Station	hour	28-01-1998	31-12-1998
Wind (2)	Pilot Station	hour	01-01-1998	30-04-1998
Waves	East jetty	3 hours	01-01-1998	30-04-1998
Data 1999				
Wind (1)	Pilot Station	hour	01-01-1999	31-12-1999
Data 2000				
Wind (1)	Pilot Station	hour	01-01-2000	31-12-2000
Data 2001				
Wind (1)	Pilot Station	hour	01-01-2001	22-09-2000

A time series of hourly wind speed and direction measured at the Pilot station (Figure 8), relative to February of 1998 was prescribed as a superficial boundary condition over the entire domain. In this work phase, the wind was considered constant in space and time. (Figure 6)

The wave data used for model calibration were relative to February of 1998 (Figure 7) and were obtained from the directional waverider with digital acquisition, located at 32º10'002"S and 51º58'913" W (close to the mouth of the Patos Lagoon estuary) and fixed at 15 m of depth. (Figure 8)

Information about the mud parameters were based on Torronteguy (2000), which presented results from mud deposits observed at Cassino Beach in 1998. He concluded that the thickness of the fluid mud increased gradually towards the south, and towards the coast, achieving 1,24 m, and density varied between 0,98 and 1,45 g/cm^3
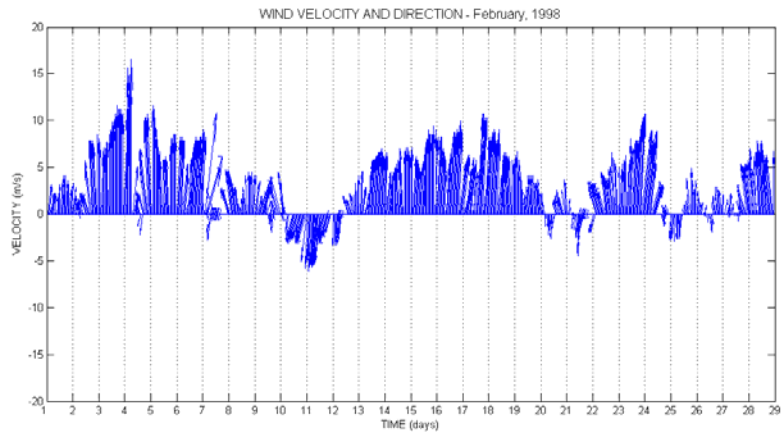
Figure 6 - A time series of hourly wind velocity and direction measured at Pilot station relative to February of 1998.

.
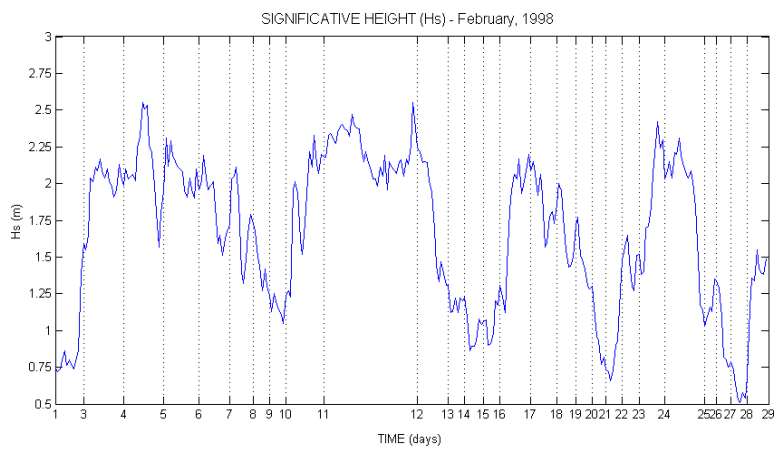
Figure 7- Significant height measured from the directional waverider located at 32º10'002''S and 51º58'913'' W (close to the mouth of the Patos Lagoon estuary) relative to February of 1998.
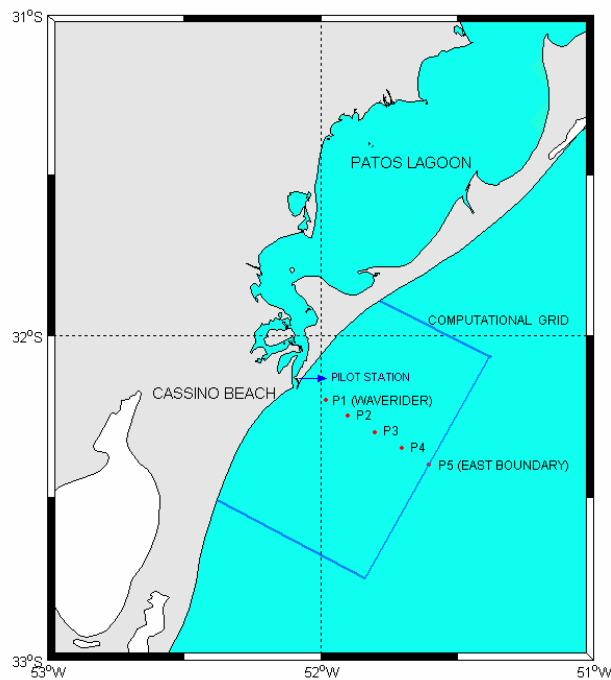
Figure 8- Localization of the stations where the measured wind and wave data were obtained and the output parameters.

4.2. The numerical grid

The SWAN model was applied to the studied area presented in Figure 9, which covers a 100 km wide coastal area and extends about 50 km offshore throughout the Rio Grande do Sul State, and includes the Cassino Beach area. The depth at the offshore boundary of the model varies between 1 to 29 m.
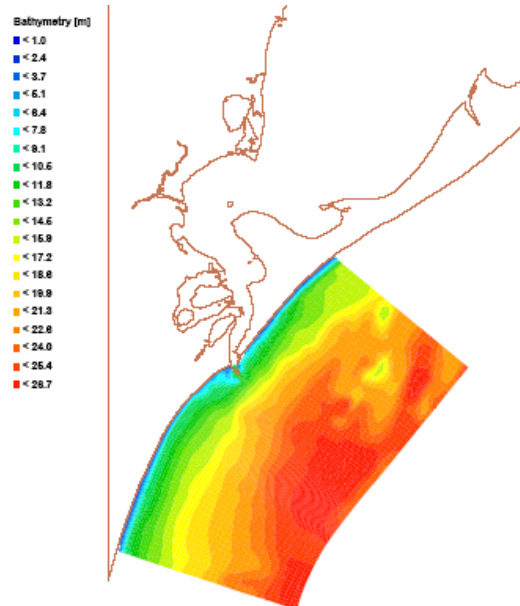
Figure 9- Studied area and depth distribution

The wave model uses a curvilinear grid that comprises 41 by 104 points, with approximately 4264 active points. This computational grid is presented in Figure 10. The dimensions of the grid cells vary from 1.5 km near the boundaries to approximately 1.0 km, near the jetties and around Cassino Beach.
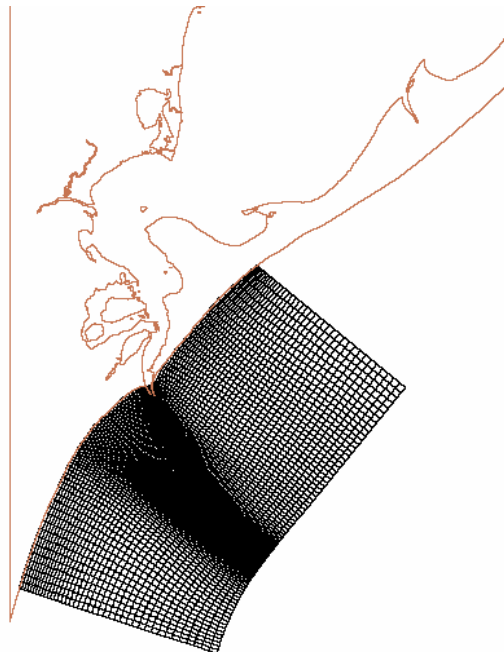
Figure 10 - Computational curvilinear grid for the numerical experiments.

4.3. Standard SWAN model (without mud)

The SWAN model is a two-dimensional fully spectral state-of-the-art wave propagation model developed by Delft University of Technology (Booij et al., 1999; Zijlema and Van der Westhuijsen, 2005), which simulates the wave propagation, wave generation by wind, non-linear wave-wave interactions and dissipation. This model is the wave module of Delft3D, but can be run independently.

The model is used for obtaining realistic estimates of wave parameters in coastal areas, lakes and estuaries based on given wind field, bottom topography, water level and current field conditions in waters of deep, intermediate and finite depth.

The evolution of the waves in the SWAN model is based on an Eulerian formulation of the spectral discrete wave action balance equation (or energy balance in the absence of currents) with sources and sinks. The model is discrete spectral in frequencies and directions, and the kinematics behavior of the waves (including the effect of currents) is described with the linear theory of surface gravity waves. The model includes refractive propagation with shoaling and shifting of the relative frequency due to space variations in depth and current.

The wave propagation processes represented in SWAN are: propagation through geographic space, refraction and shoaling due to spatial variations in bottom and current, blocking and reflections by opposing currents, and transmission through, blockage by or reflection against obstacles. The wave generation processes are represented by a wind generation. Moreover, the dissipation processes are represented by whitecapping, depth-induced wave breaking, bottom friction and wave-wave interactions (quadruplets and triads). In addition, the wave-induced set-up of the mean sea surface can be computed.

The SWAN model can be applied in the stationary or non-stationary mode, and can be formulated in cartesian or curvilinear coordinates (recommended for small scales), or spherical coordinates (for small scales and large scales). The stationary mode should be used for waves with a relatively short residence time in the computational area under consideration, i.e. the travel time of the waves through the region should be small compared to the time scale of the geophysical conditions (wave boundary conditions, wind, tides and storm surge). A quasi-stationary approach can be employed with stationary SWAN computations in a time-varying sequence of stationary conditions.

In the SWAN model, the waves are described with the two-dimensional wave action density spectrum, even when non-linear phenomena dominate. The spectrum that is considered in SWAN is the action density spectrum N (σ, θ) rather than the energy density spectrum E (σ, θ) since in the presence of currents, action density is conserved whereas energy density is not (Whitham, 1974). The independent variables are the relative frequency σ (as observed in a frame of reference moving with the action propagation velocity) and the wave direction θ (the direction normal to the wave crest of each spectral component). The action density is equal to the energy density divided by the relative frequency: N (σ, θ) = E (σ, θ) / σ.

The evolution of the wave spectrum in SWAN is described by the spectral action balance equation which for Cartesian co-ordinates is (Hasselmann et al., 1973):

$$\frac{\partial}{\partial t} N(\sigma,\theta) + \frac{\partial}{\partial x} c_x N(\sigma,\theta) + \frac{\partial}{\partial y} c_y N(\sigma,\theta) + \frac{\partial}{\partial \sigma} c_\sigma N(\sigma,\theta) + \frac{\partial}{\partial \theta} c_\theta N(\sigma,\theta) = \frac{S(\sigma,\theta)}{\sigma}$$

The first term in the left-hand side of this equation represents the local rate of change of action density in time, the second and third term represent propagation of action in geographical space (with propagation velocities cx and cy in x - and y -space, respectively). The fourth term represents shifting of the relative frequency due to variations in depths and currents (with propagation velocity cσ in σ - space). The fifth term represents depth-induced and current-induced refraction (with propagation velocity cθ in θ -space). The term S (σ, θ) at the right-hand side is the energy source, which is generally written as the sum of a number of separate source terms, each representing a different type of process.

$$S(\sigma,\theta) = S_{in}(\sigma,\theta) + S_{ds}(\sigma,\theta) + S_{nl}(\sigma,\theta)$$

S_{in} represents the generation of wave by wind, S_{ds} the dissipation of the wave energy due to whitecapping, wave-bottom interactions and in very swallow water depth-induced wave breaking, and S_{nl} is the wave energy transfer due to conservative nonlinear wave-wave interactions (both quadruplet interactions S_{nl4} and triad interactions S_{nl4})

The formulation was used for the source terms in SWAN is the following in according to User Manual **of SWAN Cycle III version 40.41**:

- Input by wind: The corresponding source term for the resonance and a feed-back mechanism that transfer the wind energy to the waves described in SWAN as the sum of linear and exponential growth:
$$S_{in}(\sigma,\theta) = A + BE(\sigma,\theta)$$
in which A and B depend on wave frequency and direction, and wind speed and direction. The effects of currents are accounted for in SWAN by using the apparent local wind speed and direction.

-The dissipation term of wave energy is represented by the summation of three different contributions: whitecapping S $_{ds,w}$ (σ , θ), bottom friction S $_{ds,b}$ (σ , θ) and depth-induced breaking S $_{ds,br}$ (σ , θ).

Whitecapping is primarily controlled by the steepness of the waves and these formulations are based on a pulse-based model (Hasselmann, 1974), as adapted by the WAMDI group (1988):
$$S_{ds,w}(\sigma,\theta) = -\Gamma \tilde{\sigma} \frac{k}{\tilde{k}} E(\sigma,\theta)$$

where Γ is a steepness dependent coefficient, k is wave number and $\tilde{\sigma}$ and $\tilde{k}$ denote a mean frequency and a mean wave number, respectively (cf. the WAMDI group, 1988).
Komen et al. (1984) estimated the value of Γ by closing the energy balance of the waves in fully developed conditions. This implies that this value depends on the wind input formulation that is used.

Depth-induced dissipation may be caused by bottom friction, by bottom motion, by percolation or by back-scattering on bottom irregularities (Shemdin et al., 1978). For continental shelf seas with sandy bottoms, the dominant mechanism appears to be bottom friction (e.g., Bertotti and Cavaleri, 1994) which can generally be represented as:
$$S_{ds,b}(\sigma,\theta) = -C_{bottom} \frac{\sigma^2}{g^2 \sinh^2(kd)} E(\sigma,\theta)$$

in which C$_{bottom}$ is a bottom friction coefficient. Considering the large variations in bottom conditions in coastal areas (bottom material, bottom roughness length, ripple height etc.), there is no field data evidence to give preference to a particular friction model (Luo and Monbaliu, 1994). For this reason, the simplest of each of these types of friction models has been implemented in SWAN: the empirical JONSWAP model of Hasselmann et al. (1973), the drag law model of Collins (1972) and the eddy-viscosity model of Madsen et al. (1988).

The process of depth-induced wave-breaking is still poorly understood and little is known about its spectral modeling. In contrast to this, the total dissipation (i.e., integrated over the spectrum) due to this type of wave breaking can be well modeled with the dissipation of a bore applied to the breaking waves in a random field (Battjes and Janssen, 1978; Thornton and Guza, 1983). Eldeberky and Battjes (1995) to formulate a spectral version of the bore model of Battjes and Janssen (1978) which conserves the spectral shape. Expanding their expression to include directions, the expression used in SWAN is:

$$S_{ds,br}(\sigma,\theta) = -\frac{D_{tot}}{E_{tot}}E(\sigma,\theta)$$

in which E_{tot} is the total wave energy and D_{tot} is the rate of dissipation of the total energy due to wave breaking according to Battjes and Janssen (1978). The value of D_{tot} depends critically on the breaking parameter $\gamma = H_{max} / d$ (in which H_{max} is the maximum possible individual wave height in the local water depth d). In Delft3DWAVE a constant value is considered ($\gamma = 0.73$ the mean value of the data set of Battjes and Stive, 1985).

The quadruplet wave-wave interactions, in deep water, dominate the evolution of the spectrum. They transfer wave energy from the spectral peak to lower frequencies (thus moving the peak frequency to lower values) and to higher frequencies (where the energy is dissipated by whitecapping). In very shallow water, triad wave-wave interactions transfer energy from lower frequencies to higher frequencies often resulting in higher harmonics (Beji and Battjes, 1993; low-frequency energy generation by triad wave-wave interactions is not considered here).

In a (geographic) 1D case, the computation of the wave induced set-up is based on the vertically integrated momentum balance equation which is a balance between the wave force (gradient of the wave radiation stress) and the hydrodynamic pressure gradient (no wave-induced currents exist).

$$F_x + gd\frac{\partial \overline{\eta}}{\partial x} = 0$$

where d is the total water depth (including the wave-induced set-up) and $\overline{\eta}$ is the mean surface elevation (including the wave-induced set-up).

In a 2D case, computations are also based on the vertically integrated momentum balance equation (in two geographic dimensions), supplemented with the observation of Dingemans et al., (1987) that the wave-induced currents are mainly driven by the divergence-free part of the wave forces, whereas the set-up is mainly due to the rotation-free part of these forces. To compute the set-up, it would then be sufficient to compute the set-up as if the currents are zero, which implies that the divergence of all forces considered would be zero:

$$\frac{\partial F_x}{\partial x} + \frac{\partial F_y}{\partial y} + \frac{\partial}{\partial x}\left(gd\frac{\partial \eta}{\partial x}\right) + \frac{\partial}{\partial y}\left(gd\frac{\partial \eta}{\partial y}\right) = 0$$

Note that divergence=0 is only an approximation of the true divergence. These two equations were implemented in SWAN.

The integration of the action balance equation has been implemented in SWAN with finite difference schemes in all five dimensions (time, geographic space and spectral space). Time is discretized with a simple constant time step Δt for the simultaneous integration of the propagation and the source terms. Geographic space is discretized with a rectangular grid with constant resolutions Δx and Δy in x and y –direction, respectively (this rectangular grid is a special case of the curvilinear grid that has been programmed in SWAN). The spectrum in the model is discretized with a constant directional resolution $\Delta\theta$ and a constant relative frequency resolution $\Delta\sigma / \sigma$ (logarithmic frequency distribution).

The boundary conditions in SWAN, both in geographic space and spectral space, are fully absorbing the wave energy that is leaving the computational domain or crossing a coastline. The incoming wave energy along open geographic boundaries needs to be prescribed by the user. The boundaries of the computational spatial grid in SWAN are either land or water. In the case of land, there is no problem: the land does not generate waves in SWAN, and it absorbs all incoming wave energy. However, in the case of a water boundary there may be a problem. For coastal regions such

incoming energy is usually provided only along the deep-water boundary and not along the lateral geographic boundaries (i.e., the spectral densities are assumed to be zero). This implies that such erroneous lateral boundary conditions may be propagated into the computational area. The affected areas are typically triangular regions with the apex at the corners between the deep-water boundary and the lateral boundaries spreading towards shore at an angle between 30° and 45° for wind sea conditions. On either side of the deep-water mean wave direction, less for swell conditions, this angle is essentially equal to the one-sided width of the directional distribution of the incoming wave spectrum. For this reason, the lateral boundaries should be sufficiently far away from the area of interest to avoid the propagation of this error into the area. This is effect can be investigated by varying the location of these boundaries and check the effect of this on the results.

The input data provided by the user is organized into a file which stores all the parameters used for the wave computation. The parameters can be divided in three categories: parameters defining the physical processes being modeled, parameters defining the numerical techniques used to solve the equations that describe the physical processes, and parameters controlling the wave computation and storing the results. Among the parameters that define the physical processes, the following options are possible to specify:

- Constants: based on this information is possible to assign values to parameters such as gravitational acceleration, water density, direction of north with respect to the x-axis, minimum depth, Cartesian convention or the Nautical convention, wave setup activated or deactivated, and to compute the wave forces on the basis of the energy wave dissipation rate or on the gradient of the radiation stress tensor
- Wind: based on these data is possible to specify the wind conditions, i.e. uniform wind or space-varying wind.
- Processes: based on these parameters the user can establish some of the physical processes in SWAN that add or withdraw wave energy to or from the wave field. The processes included are wave growth by wind action, whitecapping, bottom friction, depth induced wave breaking, non-linear wave-wave interactions (quadruplets and triads), and the model can run in several modes, indicating the level of parameterization. When the SWAN model runs in the third-generation mode, wind input, quadruplet interactions and whitecapping are activated, whereas triads, bottom friction and depth-induced breaking are not activated by this option. With the bottom friction option activated the formulations proposed by Hasselmann et al. (1973, JONSWAP), Collins (1972), and Madsen et al. (1988) are available. The JONSWAP formulation indicates that the semi-empirical expression derived from the results for bottom friction dissipation (Hasselmann et al., 1973, JONSWAP are also activated. The coefficient of the JONSWAP formulation is equal to 0.067 m^2s^{-3} for wind sea conditions and equal to 0.038 m^2s^{-3} for swell conditions.
- Various: With these parameters you can influence the wave propagation in the spectral space and some of the physical processes in SWAN may be modified by the user.

The incident wave boundary conditions may be specified at one or more boundary sides. The general procedure to specify the incident wave boundary condition for each of the boundaries is the following:
- Specify if the boundary should be defined by orientation, grid (MN) coordinates or XY coordinates;
- Select the orientation of the boundary considered (i.e. at which direction it is located);
- Specify if the values of the incident wave conditions are constant or variable along the boundary
- Select if the incident wave conditions are specified in terms of integral wave parameters or are read from a file (with 1D or 2D wave spectra).

If the conditions along the boundary are uniform and the boundary specification is done in terms of integral wave parameters, then the following parameters have to be specified: significant wave height, the characteristic wave period of the energy spectrum, which may be the value of the peak period or the value of the mean period, the mean wave direction and the directional spreading.

The output of the model is available for many different wave and wave related parameters. However, the general rule is that SWAN produces outputs only at the user's request. The instructions of the user to control outputs can be divided in three categories:

- Definition of the geographic location(s) of the output, which may be either on a regular geographic grid, or along user specified lines (e.g., a given depth contour line) or at individual output locations. For the output locations the model has three types of output file: Table, 1D spectrum and 2D spectra. The parameters written in the Table file are: XP,YP co-ordinates of output location, DEPT water depth (in m), HSIG significant wave height (in m), DIR mean wave direction (degree), Tpeak peak wave period (in s), TM01 mean wave period (Tm01) in s, DSPR directional spreading of the waves (in degrees), UBOT root-mean-square value of the maximum of the orbital motion near the bottom, XWindv, YWindv wind components (in m/s) and XVEL, YVEL current velocity components (in m/s). In the 1D spectra file the parameters written are: absolute frequencies (in Hz), energy densities (in J/m2/Hz), average nautical direction (in degrees) and directional spreading (in degrees).The parameters written in the 2D spectra file are: absolute frequencies (in Hz), spectral nautical directions (in degrees) and energy densities (in J/m2/Hz/degrees).

- Definition of times in which the output is requested, only in non-stationary runs.

- Type of output quantities: wave parameters, currents or related quantities.

In the first phase of this work, the standard SWAN model (without considering mud) was applied within Delft3D. The model was calibrated based on the comparison between modeling results and measurements of wave parameters from the Cassino Project. The model was forced with a time series of wind velocity and direction measured at Pilot station (Figure 8). In order to evaluate the model results, they were compared against data from a directional waverider with digital acquisition located close to the mouth of the Patos Lagoon estuary (at 15 m of depth). Comparisons were carried out in terms of significant wave height, peak period, mean wave direction and energy density.

The selection of significant cases for the experiments with the standard SWAN model was based on the characterization of the state of the sea found in literature for the studied area. Two types of ocean waves generated by wind were selected: swell and local sea conditions. Wave data based on Strauch (1998) showed the predominance of swell from the south, with period peak at 12 seconds and sea conditions with period peak of 8 seconds. The work presented by Tomazelli (1990) showed that the predominant winds in the studied area come from the northeast (NE) and from the southwest (SW).

Two periods corresponding to different wind directions were selected, where the wave waverider data represented the two characteristic states of the sea. Table 2 presents the observed swell wave conditions at the waverider point and the wind velocity and direction at three different times on February 11th 1998 . Table 3, presents the observed sea wave conditions at the waverider point and the wind velocity and direction at three different times on February 4th, 1998.

Table 2 – Observed wave conditions at the waverider point and measured wind velocity, wind direction at three different times on February 11th, 1998.

11/2/1998	Observed Conditions					Measured Wind		
	Hs (m)	Tm01 (s)	Tp (s)	NDIR(degree)	DSPR(degree)	V (m/s)	DIR(degree)	
09:15 UTC	2.1	4.8	12.5	167	18.2	8.08	225.0	SW
17:00 UTC	2.0	5.2	12.5	159	17.9	7.15	202.5	SSW
22:00 UTC	2.0	5.9	12.5	159	12.9	4.48	180.0	S

Table 3 – Observed wave conditions at the waverider point and measured wind velocity, wind direction at three different times on February 4th, 1998.

4/2/1998	Observed Conditions					Measured Wind		
	Hs (m)	Tm01 (s)	Tp (s)	NDIR(degree)	DSPR(degree)	V (m/s)	DIR(degree)	
01:10 UTC	2.0	4.7	6.3	113	27.6	11.20	67.5	ENE
04:00 UTC	2.7	5.0	6.7	105	22.0	14.80	90.0	E
07:00 UTC	1.8	5.0	7.1	125	21.5	7.20	45.0	NE

Based on this information, several simulations were carried out varying the input parameters and location of the output parameters. In all simulations, the SWAN model was used in the stationary mode, currents were not considered, and the computational grid was the same output grid. The description of the accomplished simulations and the considerations for the input and output files is presented in Tables 4 -11.

The first and second simulations were carried out with purpose of getting a feeling about the model, focusing on learning about the input and output files, and about running and visualizing results. In these simulations, the boundary conditions (wind, wave and other physical parameters) were either represented by theoretical values or by data from literature.

In the first simulation, the model was forced with a constant wind velocity and direction along the open boundaries. The prescribed wave boundary conditions were the significant wave height (Hs), the mean wave period (Tm) and direction, uniformly applied along the open boundaries . The output parameters were significant wave height (Hs) and direction for all computational grid. The description of the parameters considered as input and output in these preliminary simulations is presented in Table 4.

Table 4 - Parameters considered as input and output in the first simulation.

SIMULATION 1						
INPUT	Physical Parameters	Wind velocity and direction uniform along open boundaries				
	Boundary Conditions	Hs,Tm e Dir uniform along open boundaries				
OUTPUT	Types	Hs, Dir				
	Locations	Computational grid				

	INPUT				OUTPUT	
	Physical Parameters		Boundary Conditions			
	Wind	Source	Wave	Source	Parameters	Specific Locations
RG001	V=20.00m/s NE	theoretical value	Hs = 1.8 m Tm = 5.0 s D = 125°	data from literature	Hs, Dir	computational grid
RG002	V =20.00m/s NE	theoretical value	Hs = 7.0 m Tm = 12.0 s D = 140°	theoretical value	Hs, Dir	computational grid
RG003	V =7.20m/s NE	data from literature	Hs = 1.8 m Tm = 5.0 s D = 125°	data from literature	Hs, Dir	computational grid
RG004	V=20.00m/s NE	theoretical value	Hs = 1.0 m Tm = 8.0 s D = 100°	data from literature	Hs, Dir	computational grid
RG005	V =7.15m/s SSW	data from literature	Hs = 2. 0 m Tp = 12.5 s D = 159°	data from literature	Hs, Dir	computational grid
RG006	V =20.00m/s NE	theoretical value	Hs = 1.5 m Tm = 12.0 s D = 160°	data from literature	Hs, Dir	computational grid
RG007	V =7.00m/s NE	data from literature	Hs = 2.0 m Tm = 12.0 s	data from literature	Hs, Dir	computational grid

RG008	V =20.00m/s NE	theoretical value	Hs = 2.0 m Tm = 12.0 s D = 150º	data from literature	Hs, Dir	computational grid

In the second simulation, the same considerations were applied for the input parameters, but the output parameters were requested in the form of table, 1D spectra and 2D spectra for all the computational grid, and also for the waverider point. The description of the considerations for the input and output files is presented in Table 5.

Table 5 - Parameters considered as input and output in the second simulation.

SIMULATION 2		
INPUT	Physical Parameters	Wind velocity and direction uniform along open boundaries
	Boundary Conditions	Hs,Tm e Dir uniform along open boundaries
OUTPUT	Types	Table, 1D spectra and 2D spectra
	Locations	Computational grid
		waverider point Xw = 407285 Yw = 6440656

	INPUT				OUTPUT	
	Physical Parameters		**Boundary Conditions**			
	Wind	**Source**	**Wave**	**Source**	**Types**	**Locations**
RG009	V =20.00m/s NE	theoretical value	Hs = 7.0 m Tm = 12.0 s D = 140º	data from literature	table 1D spectra 2D spectra	computational grid waverider point
RG010	V =7.20m/s NE	data from literature	Hs = 1.8 m Tm = 5.0 s D = 125º	data from literature	table 1D spectra 2D spectra	computational grid waverider point
RG011	V =7.15m/s SSW	data from literature	Hs = 2. 0 m Tp = 12.5 s D = 159º	data from literature	table 1D spectra 2D spectra	computational grid waverider point
RG012	V =20.00m/s NE	theoretical value	Hs = 2.0 m Tm = 12.0 s D = 150º	data from literature	table 1D spectra 2D spectra	computational grid waverider point

In the third simulation the SWAN model was setup using the realistic data representing the two characteristic states of the sea for the study area, as presented in Table 2 and Table 3. The wind velocity and direction was considered uniform along the open boundaries. The significant wave height (Hs), mean period (Tm) and direction from the observed data (waverider) were prescribed uniform along open boundaries as the wave boundary condition. Default values were considered for the physical parameters. The output parameters were requested for all computational grid, in the waverider point and in the east boundary point. The description of the considerations for the input and output files is presented in the Table 6.

In the fourth simulation, the mean period (Tm) prescribed as an input parameter was replaced by the peak period (Tp). In the SWAN wave model if the conditions along the boundary are uniform and the boundary specification is in terms of integral wave parameters, the characteristic wave period of the energy spectrum may be specified as the peak period or the value of the mean period. The description of parameters considered as input and output is presented in Table 7.

Table 6 - Parameters considered as input and output in the third simulation

SIMULATION 3			
INPUT	**Physical Parameters**		Wind velocity and direction uniform along open boundaries
	Boundary Conditions		Hs,Tm e Dir uniform along open boundaries
OUTPUT	**Types**		Table, 1D spectra and 2D spectra
	Locations		Computational grid
			waverider point Xw = 407285 Yw = 6440656
			east boundary Xb = 435000 Yb = 6415000

	INPUT				OUTPUT	
	Physical Parameters		**Boundary Conditions**			
	Wind	**Source**	**Wave**	**Source**	**Types**	**Locations**
RG013	V =7.15 m/s SSW	Pilot Station 02/98 - 11/02/98 at 17:00	Hs =2.0m Tm = 5.2s Dir =159	Waverider 02/98 02111716.SPT	table 1D spectra 2D spectra	computational grid waverider point
RG014	V =7.15 m/s SSW	Pilot Station 02/98 - 11/02/98 at 17:00	Hs =2.0m Tm = 5.2s Dir =159	Waverider 02/98 02111716.SPT	table 1D spectra 2D spectra	computational grid east boundary
RG015	V =4.48 m/s S	Pilot Station 02/98 - 11/02/98 at 22:00	Hs =2.0m Tm = 5.9s Dir =159	Waverider 02/98 02112246.SPT	table 1D spectra 2D spectra	computational grid waverider point
RG016	V =4.48 m/s S	Pilot Station 02/98 - 11/02/98 at 22:00	Hs =2.0m Tm = 5.9s Dir =159	Waverider 02/98 02112246.SPT	table 1D spectra 2D spectra	computational grid east boundary
RG017	V =8.08m/s SSW	Pilot Station 02/98 - 11/02/98 at 09:00	Hs =2.1m Tm = 4.8s Dir =167	Waverider 02/98 02110915.SPT	table 1D spectra 2D spectra	computational grid waverider point
RG018	V =8.08m/s SSW	Pilot Station 02/98 - 11/02/98 at 09:00	Hs =2.1m Tm = 4.8s Dir =167	Waverider 02/98 02110915.SPT	table 1D spectra 2D spectra	computational grid east boundary
RG019	V =11.2m/s ENE	Pilot Station 02/98 - 04/02/98 at 01:10	Hs = 2.0m Tm = 4.7s Dir = 113	Waverider 02/98 02040110.SPT	table 1D spectra 2D spectra	computational grid waverider point
RG020	V =11.2m/s ENE	Pilot Station 02/98 - 04/02/98 at 01:10	Hs = 2.0m Tm = 4.7s Dir = 113	Waverider 02/98 02040110.SPT	table 1D spectra 2D spectra	computational grid east boundary
RG021	V =7.2m/s ENE	Pilot Station 02/98 - 04/02/98 at 07:00	Hs = 1.8m Tm = 5.0s Dir = 125	Waverider 02/98 02040640.SPT	table 1D spectra 2D spectra	computational grid waverider point
RG022	V =7.2m/s ENE	Pilot Station 02/98 - 04/02/98 at 07:00	Hs = 1.8m Tm = 5.0s Dir = 125	Waverider 02/98 02040640.SPT	table 1D spectra 2D spectra	computational grid east boundary
RG023	V=14.8m/s E	Pilot Station 02/98 - 04/02/98 at 04:00	Hs = 2.7m Tm =5.0s Dir = 105	Waverider 02/98 02040410.SPT	table 1D spectra 2D spectra	computational grid waverider point
RG024	V=14.8m/s E	Pilot Station 02/98 - 04/02/98 at 04:00	Hs = 2.7m Tm =5.0s Dir = 105	Waverider 02/98 02040410.SPT	table 1D spectra 2D spectra	computational grid east boundary

Table 7 - Parameters considered as input and output in the fourth simulation

SIMULATION 4		
INPUT	**Physical Parameters**	Wind velocity and direction uniform along open boundaries
	Boundary Conditions	Hs,Tp e Dir uniform along open boundaries
OUTPUT	**Types**	Table, 1D spectra and 2D spectra
		Computational grid
		waverider point Xw = 407285 Yw = 6440656
	Locations	east boundary Xb = 435000 Yb = 6415000

	INPUT				OUTPUT	
	Physical Parameters		**Boundary Conditions**			
	Wind	**Source**	**Wave**	**Source**	**Types**	**Locations**
RG031	V =7.15 m/s SSW	Pilot Station 02/98 - 11/02/98 at 17:00	Hs =2.0m Tp = 12.5 s Dir =159	Waverider 02/98 02111716.SPT	table 1D spectra 2D spectra	computational grid east boundary
RG032	V =7.15 m/s SSW	Pilot Station 02/98 - 11/02/98 at 17:00	Hs =2.0m Tp = 12,5 s Dir =159	Waverider 02/98 02111716.SPT	table 1D spectra 2D spectra	computational grid waverider point
RG033	V =4.48 m/s S	Pilot Station 02/98 - 11/02/98 at 22:00	Hs =2.0m Tp = 12.5 s Dir =159	Waverider 02/98 02112246.SPT	table 1D spectra 2D spectra	computational grid east boundary
RG034	V =4.48 m/s S	Pilot Station 02/98 - 11/02/98 at 22:00	Hs =2.0m Tp = 12.5 s Dir =159	Waverider 02/98 02112246.SPT	table 1D spectra 2D spectra	computational grid waverider point
RG035	V =8.08m/s SSW	Pilot Station 02/98 - 11/02/98 at 09:00	Hs =2.1m Tp = 12.5 s Dir =167	Waverider 02/98 02110915.SPT	table 1D spectra 2D spectra	computational grid east boundary
RG036	V =8.08m/s SSW	Pilot Station 02/98 - 11/02/98 at 09:00	Hs =2.1m Tp = 12.5 s Dir =167	Waverider 02/98 02110915.SPT	table 1D spectra 2D spectra	computational grid waverider point
RG059	V =11.2m/s ENE	Pilot Station 02/98 - 04/02/98 at 01:10	Hs = 2.0m Tp =6.3s Dir = 113	Waverider 02/98 02040110.SPT	table 1D spectra 2D spectra	computational grid east boundary
RG060	V =11.2m/s ENE	Pilot Station 02/98 - 04/02/98 at 01:10	Hs = 2.0m Tp =6.3s Dir = 113	Waverider 02/98 02040110.SPT	table 1D spectra 2D spectra	computational grid waverider point
RG067	V =7.2m/s ENE	Pilot Station 02/98 - 04/02/98 at 07:00	Hs = 1.8m Tp = 7.1s Dir = 125	Waverider 02/98 02040640.SPT	table 1D spectra 2D spectra	computational grid east boundary
RG068	V =7.2m/s ENE	Pilot Station 02/98 - 04/02/98 at 07:00	Hs = 1.8m Tp = 7.1s Dir = 125	Waverider 02/98 02040640.SPT	table 1D spectra 2D spectra	computational grid waverider point
RG065	V=14.8m/s E	Pilot Station 02/98 - 04/02/98 at 04:00	Hs = 2.7m Tm =6.7s Dir = 105	Waverider 02/98 02040410.SPT	table 1D spectra 2D spectra	computational grid waverider point
RG066	V=14.8m/s E	Pilot Station 02/98 - 04/02/98 at 04:00	Hs = 2.7m Tm =6.7s Dir = 105	Waverider 02/98 02040410.SPT	table 1D spectra 2D spectra	computational grid east boundary

In the fifth simulation, the wave boundary condition was replaced by a wave spectrum file along the open boundaries. The description of the parameters and considerations for the input and output of the simulation is presented in Table 8.

Table 8 - Parameters considered as input and output in the fifth simulation.

SIMULATION 5		
INPUT	**Physical Parameters**	Wind velocity and direction uniform along open boundaries
	Boundary Conditions	Wave spectrum file along open boundary
OUTPUT	**Types**	Table, 1D spectra and 2D spectra
	Locations	Computational grid
		waverider point Xw = 407285 Yw = 6440656
		east boundary Xb = 435000 Yb = 6415000

	INPUT				OUTPUT	
	Physical Parameters		**Boundary Conditions**			
	Wind	**Source**	**Wave**	**Source**	**Types**	**Locations**
RG039	V =7.15 m/s SSW	Pilot Station 02/98 - 11/02/98 at 17:00	02111716.bnd	Waverider 02/98 w02111716.bnd	table 1D spectra 2D spectra	computational grid east boundary
RG040	V =7.15 m/s SSW	Pilot Station 02/98 - 11/02/98 at 17:00	02111716.bnd	Waverider 02/98 w02111716.bnd	table 1D spectra 2D spectra	computational grid waverider point
RG041	V =4.48 m/s S	Pilot Station 02/98 - 11/02/98 at 22:00	02112246.bnd	Waverider 02/98 w02112246.bnd	table 1D spectra 2D spectra	computational grid east boundary
RG042	V =4.48 m/s S	Pilot Station 02/98 - 11/02/98 at 22:00	02112246.bnd	Waverider 02/98 w02112246.bnd	table 1D spectra 2D spectra	computational grid waverider point
RG043	V =8.08m/s SSW	Pilot Station 02/98 - 11/02/98 at 09:00	02110915.bnd	Waverider 02/98 w02110915.bnd	table 1D spectra 2D spectra	computational grid east boundary
RG044	V =8.08m/s SSW	Pilot Station 02/98 - 11/02/98 at 09:00	02110915.bnd	Waverider 02/98 w02110915.bnd	table 1D spectra 2D spectra	computational grid waverider point
RG061	V =11.2m/s ENE	Pilot Station 02/98 - 04/02/98 at 01:10	02040110.bnd	Waverider 02/98 w02040110.bnd	table 1D spectra 2D spectra	computational grid east boundary
RG062	V =11.2m/s ENE	Pilot Station 02/98 - 04/02/98 at 01:10	02040110.bnd	Waverider 02/98 w02040110.bnd	table 1D spectra 2D spectra	computational grid waverider point
RG069	V =7.2m/s ENE	Pilot Station 02/98 - 04/02/98 at 07:00	02040640.bnd	Waverider 02/98 w02040640.bnd	table 1D spectra 2D spectra	computational grid east boundary
RG070	V =7.2m/s ENE	Pilot Station 02/98 - 04/02/98 at 07:00	02040640.bnd	Waverider 02/98 w02040640.bnd	table 1D spectra 2D spectra	computational grid waverider point
RG037	V=14.8m/s E	Pilot Station 02/98 - 04/02/98 at 04:00	02040410.bnd	Waverider 02/98 w02040410.bnd	table 1D spectra 2D spectra	computational grid waverider point
RG038	V=14.8m/s E	Pilot Station 02/98 - 04/02/98 at 04:00	02040410.bnd	Waverider 02/98 w02040410.bnd	table 1D spectra 2D spectra	computational grid east boundary

In the sixth simulation, values of significant wave height (Hs), peak period (Tp) and direction were prescribed in several points along the open boundaries. The output parameters were requested in

the form of table, 1D spectra and 2D spectra, for the points presented in Figure 8. The description of the parameters and considerations for the input and output of the simulation is presented in Table 9.

Table 9 - Parameters considered as input and output in the sixth simulation.

SIMULATION 6		
INPUT	**Physical Parameters**	Wind velocity and direction uniform along open boundaries
	Boundary Conditions	Hs,Tp, Dir in various points in open boundaries
OUTPUT	**Types**	Table, 1D spectra and 2D spectra
		Computational grid
	Locations	Various points in waverider direction (P1, P2, P3, P4, P5)

	INPUT				OUTPUT	
	Physical Parameters		**Boundary Conditions**			
	Wind	**Source**	**Wave**	**Source**	**Types**	**Locations**
RG083	V =7.15 m/s SSW	Pilot Station 02/98 - 11/02/98 at 17:00	Hs =2.0m Tp = 12.5 s Dir =159	Waverider 02/98 02111716.SPT	table 1D spectra 2D spectra	computational grid various points in waverider direction
RG085	V =4.48 m/s S	Pilot Station 02/98 - 11/02/98 at 22:00	Hs =2.0m Tp = 12.5 s Dir =159	Waverider 02/98 02112246.SPT	table 1D spectra 2D spectra	computational grid various points in waverider direction
RG081	V =8.08m/s SSW	Pilot Station 02/98 - 11/02/98 at 09:00	Hs =2.1m Tp = 12.5 s Dir =167	Waverider 02/98 02110915.SPT	table 1D spectra 2D spectra	computational grid various points in waverider direction
RG087	V =11.2m/s ENE	Pilot Station 02/98 - 04/02/98 at 01:10	Hs = 2.0m Tp =6.3s Dir = 113	Waverider 02/98 02040110.SPT	table 1D spectra 2D spectra	computational grid various points in waverider direction
RG091	V =7.2m/s ENE	Pilot Station 02/98 - 04/02/98 at 07:00	Hs = 1.8m Tp = 7.1s Dir = 125	Waverider 02/98 02040640.SPT	table 1D spectra 2D spectra	computational grid various points in waverider direction
RG089	V=14.8m/s E	Pilot Station 02/98 - 04/02/98 at 04:00	Hs = 2.7m Tp =6.7s Dir = 105	Waverider 02/98 02040410.SPT	table 1D spectra 2D spectra	computational grid various points in waverider direction

In the seventh simulation, the wave spectrum file in various points throughout the open boundaries was prescribed as an input parameter. The output parameters were requested in the form of table, 1D spectra and 2D spectra, for the points presented in Figure 8. The description of the parameters and considerations for the input and output of the simulation is presented in Table 10.

Table 10 - Parameters considered as input and output in the seventh simulation.

SIMULATION 7		
INPUT	**Physical Parameters**	Wind velocity and direction uniform along open boundaries
	Boundary Conditions	Wave spectrum file in various points in open boundaries
OUTPUT	**Types**	Table, 1D spectra and 2D spectra
		Computational grid
	Locations	Various points in waverider direction (P1, P2, P3, P4, P5)

	INPUT				OUTPUT	
	Physical Parameters		**Boundary Conditions**			
	Wind	**Source**	**Wave**	**Source**	**Types**	**Locations**
RG084	V =7.15 m/s SSW	Pilot Station 02/98 - 11/02/98 at 17:00	02111716.bnd	Waverider 02/98 w02111716.bnd	table 1D spectra 2D spectra	computational grid various points in waverider direction

					table	computational grid
RG086	V =4.48 m/s S	Pilot Station 02/98 - 11/02/98 at 22:00	02112246.bnd	Waverider 02/98 w02112246.bnd	1D spectra	various points in waverider
					2D spectra	direction
RG082	V =8.08m/s SSW	Pilot Station 02/98 - 11/02/98 at 09:00	02110915.bnd	Waverider 02/98 w02110915.bnd	table 1D spectra 2D spectra	computational grid various points in waverider direction
RG088	V =11.2m/s ENE	Pilot Station 02/98 - 04/02/98 at 01:10	02040110.bnd	Waverider 02/98 w02040110.bnd	table 1D spectra 2D spectra	computational grid various points in waverider direction
RG092	V =7.2m/s ENE	Pilot Station 02/98 - 04/02/98 at 07:00	02040640.bnd	Waverider 02/98 w02040640.bnd	table 1D spectra 2D spectra	computational grid various points in waverider direction
RG090	V=14.8m/s E	Pilot Station 02/98 - 04/02/98 at 04:00	02040410.bnd	Waverider 02/98 w02040410.bnd	table 1D spectra 2D spectra	computational grid various points in waverider direction

The objective of the eighth simulation was to analyze the response of the SWAN wave model with respect two physical processes that dissipate wave energy from the wave field: the dissipation of wave energy caused by bottom friction and whitecapping. For that study, two of the previous cases (highlighted tests in Tables 2 and 3) were selected. One case is representative of swell conditions (February 11th 1998 at 09:15 h), and another case is representative of sea conditions (February 4th 1998 at 01:10 h). The computation considered whitecapping activated and de-activated with a coefficient for bottom friction dissipation equal to 0.067 m^2s^{-3} for sea conditions; equal to 0.038 m^2s^{-3} for swell conditions and equal to 0.001 without bottom friction dissipation. The description of the considerations for the input and output files is presented in the Table 11.

Table 11 - Parameters considered as input and output in the eighth simulation.

SIMULATION 8			
INPUT	**Physical Parameters**	Wind velocity and direction uniform along open boundaries	
		Change coefficient bottom friction (0.067; 0.038;0.001)	
		Activated and de-activated whitecapping	
	Boundary Conditions	Hs,Tp, Dir in various points in open boundaries	
		Wave spectrum file in various points in open boundaries	
OUTPUT	**Types**	Table, 1D spectra and 2D spectra	
		Computational grid	
	Locations	Various points in waverider direction (P1, P2, P3, P4, P5)	

	INPUT				OUTPUT	
	Physical Parameters			**Boundary Conditions**		
	Wind	**Process**	**Process Activated**	**Wave**		
		Bottom Friction	**Whitecapping**		**Types**	**Locations**
RG113	V =8.08m/s SSW	0.067	activated	Hs =2.1m Tp = 12.5 s Dir =167	table 1D spectra 2D spectra	computational grid various points in waverider direction
RG117	V =8.08m/s SSW	0.067	de-activated	Hs =2.1m Tp = 12.5 s Dir =167	table 1D spectra 2D spectra	computational grid various points in waverider direction
RG112	V =8.08m/s SSW	0.038	activated	Hs =2.1m Tp = 12.5 s Dir =167	table 1D spectra 2D spectra	computational grid various points in waverider direction
RG118	V =8.08m/s SSW	0.038	de-activated	Hs =2.1m Tp = 12.5 s Dir =167	table 1D spectra 2D spectra	computational grid various points in waverider direction

RG114	V =8.08m/s SSW	0.001	activated	Hs =2.1m Tp = 12.5 s Dir =167	table 1D spectra 2D spectra	computational grid various points in waverider direction
RG119	V =8.08m/s SSW	0.001	de-activated	Hs =2.1m Tp = 12.5 s Dir =167	table 1D spectra 2D spectra	computational grid various points in waverider direction
RG100a	V =8.08m/s SSW	0.067	activated	02110915.bnd	table 1D spectra 2D spectra	computational grid various points in waverider direction
RG101a	V =8.08m/s SSW	0.067	de-activated	02110915.bnd	table 1D spectra 2D spectra	computational grid various points in waverider direction
RG102a	V =8.08m/s SSW	0.038	activated	02110915.bnd	table 1D spectra 2D spectra	computational grid various points in waverider direction
RG103a	V =8.08m/s SSW	0.038	de-activated	02110915.bnd	table 1D spectra 2D spectra	computational grid various points in waverider direction
RG102a1	V =8.08m/s SSW	0.001	activated	02110915.bnd	table 1D spectra 2D spectra	computational grid various points in waverider direction
RG103a1	V =8.08m/s SSW	0.001	de-activated	02110915.bnd	table 1D spectra 2D spectra	computational grid various points in waverider direction
RG120	V =11.2m/s ENE	0.067	activated	Hs = 2.0m Tp =6.3s Dir = 113	table 1D spectra 2D spectra	computational grid various points in waverider direction
RG121	V =11.2m/s ENE	0.067	de-activated	Hs = 2.0m Tp =6.3s Dir = 113	table 1D spectra 2D spectra	computational grid various points in waverider direction
RG122	V =11.2m/s ENE	0.038	activated	Hs = 2.0m Tp =6.3s Dir = 113	table 1D spectra 2D spectra	computational grid various points in waverider direction
RG123	V =11.2m/s ENE	0.038	de-activated	Hs = 2.0m Tp =6.3s Dir = 113	table 1D spectra 2D spectra	computational grid various points in waverider direction
RG124	V =11.2m/s ENE	0.001	activated	Hs = 2.0m Tp =6.3s Dir = 113	table 1D spectra 2D spectra	computational grid various points in waverider direction
RG125	V =11.2m/s ENE	0.001	de-activated	Hs = 2.0m Tp =6.3s Dir = 113	table 1D spectra 2D spectra	computational grid various points in waverider direction
RG108	V =11.2m/s ENE	0.067	activated	02040110.bnd	table 1D spectra 2D spectra	computational grid various points in waverider direction
RG109	V =11.2m/s ENE	0.067	de-activated	02040110.bnd	table 1D spectra 2D spectra	computational grid various points in waverider direction
RG110	V =11.2m/s ENE	0.038	activated	02040110.bnd	table 1D spectra 2D spectra	computational grid various points in waverider direction
RG116	V =11.2m/s ENE	0.038	de-activated	02040110.bnd	table 1D spectra 2D spectra	computational grid various points in waverider direction

					table	computational grid
RG111	V =11.2m/s ENE	0.001	activated	02040110.bnd	1D spectra	various points in waverider
					2D spectra	direction
RG115	V =11.2m/s ENE	0.001	de-activated	02040110.bnd	table	computational grid
					1D spectra	various points in waverider
					2D spectra	direction

4.4. The SWAN model considering mud

The SWAN model considering mud consists of a fluid mud induced wave-damping formulation obtained from the modified two-layer model proposed by Gade (1958), which was implemented in the standard version of the SWAN model by Winterwerp et al. (2005). The new SWAN model is a standalone program, and the fluid mud parameters have to be provided to the model, including the thickness and extension of the mud layer (dm (x,y,t)), and its viscosity (nm) and density (rm). The density of the mud is not expected to vary significantly, and the viscosity of the mud can be established from laboratory experiments. When no detailed information is available on the characteristics of the fluid mud itself, the mud parameters have to be assessed from literature or sensitivity analyses. The elasticity, plasticity and porosity effects were ignored. In the work carried out by Winterwerp et al. (2005), the new SWAN model was applied to simulate laboratory experiments and field observations on wave damping in the Guyana coastal system. The model results were compared favorably with the observations, though detailed field data were not available for an in depth calibration.

In the second phase of the proposed work for Cassino Beach, the SWAN model considering the presence of mud in the whole domain was applied to predict significant wave height and energy wave attenuation in the studied area (Figure 1). The objective of the numerical simulations were to analyze the response of the SWAN mud wave damping model with respect to wave attenuation in terms of decreasing the significant wave heights and loss of energy density. Two of the previous cases (highlighted tests in Tables 2 and 3) were selected to apply the SWAN mud-wave damping model. One case is representative of swell conditions (February 11th 1998 at 09:15 h), where the computation considered whitecapping and a friction coefficient of 0.038. Another case is representative of sea conditions (February 4th 1998 at 01:10 h), where the computation considered whitecapping and a friction coefficient of 0.067.

The SWAN mud-wave damping model requires the thickness of the fluid mud layer in the model area as an input. In this computation, the thickness was considered constant in the studied area. The density of the fluid mud was also considered constant, since it will not vary significantly. The mud viscosity was determined by trial and error and is therefore a calibration factor. Computations were carried out with nm = 0.01 m^2/s, nm = 0.001 m^2/s and nm = 0.0001 m^2/s. The input parameters, settings and description for the SWAN mud-wave damping model are presented in Table 12.

Table 12 -Input parameters, settings and description for the SWAN mud wave damping model.

parameter	settings	description
thickness of the fluid mud layer	dm = 1.00m	spatially varying on computational grid [m] untill to 1.24 m
density of fluid mud	rm = 1300 kg/m^3	varying between 98 and 1450 kg/m^3
viscosity of fluid mud	nm = 0.001 m^2/s	calibration parameter [m^2/s], ranging between 0.01, 0.001 and 0.0001 m^2/s
calibration parameter	α = 1	1.0 [-]

The output parameters were selected for the five points between the location of the waverider and the point located in the eastern open boundary (Figure 8). The waverider is located near the coast at 15 m of depth, and the east open boundary point is located at 22 m of depth.

5. <u>Results and Conclusions</u>

5.1. Modeling results without mud:

     Figure 11 shows the significant wave height and mean direction obtained from the SWAN model computations in all computational grid. The model was forced with uniform wind (velocity = 7.2 m/s) from the NE, applied along the open boundaries Wave parameters were obtained from waverider data in February 4th 1998 at 07:00 h, with significant wave height (Hs) of 1.8 m, mean period (Tm) of 5.0 s and wave nautical direction (NDIR) of 125°. These values were considered constant along the open boundaries. The computed significant wave height is consistent with the theory about wave propagation, where the significant wave height reduces gradually from the deep water towards shallow water. The mean wave direction (represented by the white arrows) follows the pattern of the observations.

     Figure 12 shows the significant wave height and mean direction obtained from SWAN model computations in all computational grid. The model was forced with uniform wind (velocity = 7.15 m/s) from the SSW, applied along the open boundaries. Wave parameters were obtained from waverider data in February 11th 1998 at 17:00 h, with significant wave height (Hs) of 2.0 m, peak period (Tp) of 12.5 s and wave nautical direction (NDIR) of 159°. These values were considered constant along the open boundaries. The computed significant wave height is consistent with the theory about wave propagation where the significant wave height reduces gradually from the deep water to shallow water. The mean wave direction follows the pattern of the observations. In both results it is possible to see regions of disturbance in the computational grid, mostly near the lateral open boundaries, which are probably related to the wave information prescribed as boundary condition. The values used as input at the open boundaries were the significant wave height, peak and mean period and direction taken from the observed wave parameters in the waverider point.

     Figures 13 and 14 illustrate results of computed energy density for the computational grid and the waverider point location written in 2D spectra output file for the selected cases presented in Tables 2 and 3. One case is representative of swell conditions (February 11th 1998 at 09:15 h), and another case is representative of sea conditions (February 4th 1998 at 01:10 h).

     Figure 13 shows the energy density obtained from SWAN model computations at the waverider point. The model was forced with uniform wind (velocity = 11.20 m/s) from the ENE, applied along the open boundaries. Wave parameters were obtained from waverider data in February 4th, 1998 at 01:10 h. The waverider spectral file was considered in various points throughout the open boundaries. The parameters in the output file were written in 2D spectra form, where the energy density is represented as a function of frequency and direction. This representation showed the energy density spectrum with one principal direction around 150° and pick period of 8 s.

     Figure 14 shows energy density obtained for SWAN model computations in waverider point. The model was forced with uniform wind (velocity = 8.08 m/s) from the SW, applied along the open boundaries. Wave parameters were obtained from waverider data in February 11th, 1998 at 09:15 h. The waverider spectral file was considered in various points throughout the open boundaries. The parameters in the output file were written in 2D spectra form. This representation highlights the occurrence of two main directions in the energy density spectrum, where the principal is around 120° and has pick period of 12 s.

     In order to make it easier to compare the results, the spectral energy density was analyzed for the selected sea conditions indicated in Tables 2 and 3, one representative of swell conditions (February 11th 1998 at 09:15 h), and another of sea conditions (February 4th 1998 at 01:10 h).

     Figure 15 shows the comparison between spectral energy density obtained from the SWAN model computations and from the waverider data at the waverider point. The model was forced with uniform wind (velocity = 11.20 m/s) from the ENE, applied along the open boundaries. Wave parameters were obtained from waverider data in February 4th, 1998 at 01:10 h with significant wave height (Hs) of 2.0 m, mean period (Tm) of 4.7s and wave nautical direction (NDIR) of 113°. These values were considered constant along the open boundaries. Results indicate that the shape of the

spectrum is fairly reproduced. However, the SWAN model tends to underestimate the energy level and the peak frequency of the spectrum. Figure 16 shows a similar comparison, but now with the simulation considering the wave peak period as 6.3 s. Results indicates that, in this case, the shape of the spectrum is well reproduced. The SWAN model agrees with the energy level and the peak frequency observed in the data.

Figure 17 shows the comparison between spectral energy density obtained from the SWAN model computations and from the waverider data at the waverider point. The model was forced with uniform wind (velocity = 11.20 m/s) from the ENE, applied along the open boundaries. Wave parameters were obtained from waverider data in February 4th, 1998 at 01:10 h, and prescribed as a spectral file throughout the open boundaries. Results indicate that the shape of the spectrum is reasonably reproduced. Although the model tends to underestimate the energy level, the peak frequency is in agreement with the observed spectrum. Figure 18 shows that by prescribing the spectral file in selected points in the open boundary the shape of the spectrum is improved, although the energy is still underestimated. Figure 19 indicates that this limitation is overcome when forcing the model with wave parameters obtained from the waverider in February 4th, 1998 at 01:10 h, considering significant wave height (Hs) of 2.0 m, peak period (Tp) of 6.3s and wave nautical direction (NDIR) of 113⁰ in several points at the open boundaries. In this case, the shape of the spectrum indicates only one peak, but the energy density is better reproduced.

Figure 20 shows the comparison between spectral energy density obtained from the SWAN model computations and from the waverider data at the waverider point. The model was forced with uniform wind (velocity = 8.08 m/s) from the SW, applied along the open boundaries. Wave parameters were obtained from waverider data in February 11th, 1998 at 09:15 h with significant wave height (Hs) of 2.1 m, mean period (Tm) of 4.8s and wave nautical direction (NDIR) of 167⁰. These values were considered constant along the open boundaries. Results indicate that the SWAN model tends to overestimate the energy level and the peak frequency of the spectrum. These results are improved when forced with the wave parameters obtained from the waverider data in February 11th, 1998 at 09:15 h, considering significant wave height (Hs) of 2.1 m, peak period (Tp) of 12.5 s and wave nautical direction (NDIR) of 167⁰ constant along the open boundaries (Figure 21). Results indicate that the shape of the spectrum is well reproduced, and the SWAN model now agrees with the energy level observed in the high frequency peak, although underestimating the energy level in the low frequency peak.

Figure 22 shows that by considering the waverider spectral file throughout the open boundaries the model tends to underestimate the energy level in the high frequency peak, although it does improve a little the reproduction of the low frequency peak in comparison with the observed spectrum. When prescribing the wave spectral file at several boundary points (Figure 23), the model tends to underestimate energy level in the high frequency peak and in the low frequency peak in comparison with the observed spectrum. Figure 24 shows that when prescribing the wave parameters obtained from the waverider data in February 11th, 1998 at 09:15 h, consisting in significant wave height (Hs) of 2.1 m, peak period (Tp) of 12.5 s and wave nautical direction (NDIR) of 167⁰ in several points at the open boundaries, results changed. The model results agree with the energy level in the high frequency peak but still tend to underestimate the energy level in the low frequency peak in comparison with the observed spectrum.

The comparison between the computed and observed energy density with respect to the form of applying the boundary conditions at the open boundaries have shown that the shape of the spectrum is better reproduced when using the spectral wave file, although the energy level is underestimated. A better reproduction of the energy level is obtained when prescribing the wave height (Hs), peak period (Tp) and wave nautical direction (NDIR) throughout the open boundary.

In order to overcome this limitations, a sensitivity analysis based on the variation of physical parameters related to wave energy was carried out. The SWAN model was applied considering swell and sea wave conditions jointly, and the selected cases presented in Tables 2 and 3 were analyzed. Results from these experiments were compared in terms of the spectral energy density with the waverider data for swell and sea wave condition at the waverider point and at east boundary point. In

the first study, the model was forced with uniform wind (velocity = 8.08 m/s) from the SW, applied along the open boundaries. Wave parameters were obtained from the waverider data in February 11th, 1998 at 09:15 h, with significant wave height (Hs) of 2.1 m, peak period (Tp) of 12.5 s and wave nautical direction (NDIR) of 167º. The waverider spectral file was considered in several points along open boundaries using 0.038 for friction coefficient and witheapping was activated (Figures 25 and 27) and deactivated (Figure 26 and 28). Results were analyzed at the waverider point and east boundary point, respectively, and indicate that the whitecapping process works as a mechanism for controlling the energy calculated by the model for the sea condition spectral peak.

In order to investigate the contribution of the friction coefficient with the bottom in the form of the calculated spectrum, several tests were carried out to compare the spectral energy density obtained from the SWAN model computations and from the waverider data at the waverider point and at the east boundary point.

Initially, the model was forced with uniform wind (velocity = 8.08 m/s) from the SW, applied along the open boundaries. Wave parameters were obtained from the waverider data in February 11th, 1998 at 09:15 h, considering significant wave height (Hs) of 2.1 m, peak period (Tp) of 12.5 s and wave nautical direction (NDIR) of 167º. The waverider spectral file was considered in several points throughout the open boundaries and the friction coefficient was reduced to 0.001, indicating a situation with almost no friction (non-realistic situation). Results are presented with the whitecapping activated (Figure 29) and deactivated (Figure 30) for the waverider point. The contribution of the whitecapping over the sea peak is significant and still works as controlling mechanism. However, by lowering the friction with the bottom, the reproduction of the swell peak is greatly improved.

When looking at results from the east boundary point with (Figure 31) and without (Figure 32) the whitecapping contribution, we can see that the control exerted by the whitecapping is still observed, but friction does not play a significant hole in the swell peak.

A similar study was carried out with a constant wind (velocity = 11.20 m/s) from the ENE applied along the open boundaries. Wave parameters were obtained from the waverider data in February 04th, 1998 at 01:10 h, considering significant wave height (Hs) of 2.0 m, peak period (Tp) of 6.3 s and wave nautical direction (NDIR) of 113º. The waverider spectral file was considered in several points throughout the open boundaries and the friction coefficient was reduced to 0.001, indicating a situation with almost no friction (non-realistic situation). Results are presented with the whitecapping activated (Figure 33) and deactivated (Figure 34) for the east boundary point, where the sea wave condition is generated, and indicate that there is no whitecapping contribution for the sea peak under such conditions. However, if we move towards the coast and look at results from the waverider point, we can see that the whitecapping mechanism is again influencing the sea wave peak (Figures 35 and 36).

When similar tests were carried out considering a realistic friction coefficient of 0,067, results at east boundary point confirm that at this point there is no whitecapping contribution for the sea peak (Figures 37 and 38). However, if we move towards the coast and look at results from the waverider point, the behavior observed in the simulation with almost no friction changed. Although the whitecapping mechanism is still influencing the sea wave peak (Figures 39 and 40), friction does affect the sea wave peak by making it out of phase in relation to the observations.

The comparison between modeling results and measurements of wave parameters indicates that The best modeling results were obtained when the wave parameters used as boundary conditions were considered constant along the open boundaries, when whitecapping was considered activated, and applying a bottom friction coefficient of 0.067 m^2s^{-3} for sea wave conditions and of 0.038 m^2s^{-3} for swell wave conditions. The fact that the friction coefficient has to be constant throughout the simulation represents one of the limitations of this version of the SWAN model in reproducing conditions where two wave peaks (swell and sea) are observed.

5.2. Modeling results with mud

In order to evaluate the contribution of mud deposits at the bottom over the wave energy observed in the area, the simulations without mud which provided the best results were reproduced including the wave-mud interaction for the predominant wind conditions (tests highlighted in Table11).

Figure 41 shows the comparison between the spectral energy density calculated by the SWAN model with and without the mud-wave interaction during SW wind conditions. The model was forced with uniform wind (velocity = 8.08 m/s), applied along the open boundaries. Wave parameters were obtained from waverider data in February 11th, 1998 at 09:15 h. with significant wave height (Hs) of 2.1 m, peak period (Tp) of 12.5s and wave nautical direction (NDIR) of 167⁰. The waverider spectral file was considered in various points along the open boundaries using a friction coefficient of 0.038 and withecapping was activated. Mud parameters were obtained from mud deposits observed at Cassino Beach in 1998: thickness (dm = 1.00m), density (rm = 1300 kg/m3) and mud viscosity (nm = 0.01 m^2/s) of the fluid mud layer were considered constant in all computational grid. Results indicate that although the presence of mud attenuates all the wave energy on the swell peak frequency, it has a smaller effect in attenuating the energy on the sea peak frequency. However, it seems that the presence of mud makes the sea peak out of phase. During ENE wind conditions (Figure 42), results indicate that the presence of mud is not promoting the attenuation of the sea wave energy, but it seems that the presence of mud is also making the sea peak out of phase.

As the mud viscosity is considered as a calibration parameter, the two tests mentioned above were reproduced varying its value. Figures 43 and 44 present results when considering the mud viscosity = 0.001 m^2/s, for the two wind conditions studied above. Results indicate that by considering mud with lower viscosity the attenuation of the wave energy is smaller, although still more efficient in attenuating the swell peak under SW wind conditions (Figure 43). During ENE wind conditions (Figure 44), results indicate that the presence of mud is neither promoting the attenuation of the sea wave energy nor making the sea peak out of phase. Thus, the presence of mud with lower viscosity seems to have no effect in this situation. These tests indicate that the best results were obtained for a mud viscosity of 0.001 m^2/s (typical value for muddy beds) under both wind conditions.

The effect of the mud-wave interaction over the significant wave height and mean wave period calculated by the model was also evaluated. Figure 45 shows the comparison between significant wave height (Hs) caculated with and without mud during SW wind conditions. Results were obtained for five selected points between the waverider point and the east boundary point (Table 13), and indicate that at the east boundary point 3% of the significant wave height is attenuated. When progressing towards the coast, the mud-wave interaction attenuates 26% of the significant wave height. During ENE wind conditions (Figure 46), the attenuation was 0.2 % and 16%, respectively. The calculated mean wave period for the same situations is presented in Figures 47 and 48.

A summary of the model results with and without considering the mud-wave interaction in comparison with the observed data is presented in Table 13, and will be discussed considering a mud thickness of 1.00m, density 1300 kg/m^3, and viscosity of 0.001 m^2/s, constant in all computational grid.

Results during SW wind conditions indicate that the calculated significant wave height (with and without the presence of mud), was underestimated in 9.5 % and 33.3% in relation to the measurements at the waverider point, respectively. During ENE wind conditions, the calculated significant wave height (with and without the presence of mud), the attenuation was 10.0 % and 25.0%, respectively.

Table 13 - The comparison between observed significant wave height and the model results with and without the mud- wave damping with $dm = 1.00m$, $rm = 1300$ kg/m^3 and $nm = 0.001$ m^2/s.

Location	Observed Hs (m)	Computed Hs (m) without fluid mud	Computed Hs (m) with fluid mud
SW wind conditions			
P1(Waverider point)	2.1	1.9	1.4
P2		2.1	1.7
P3		2.2	1.9
P4		2.3	2.1
P2(East boundary point)		2.3	2.2
ENE wind conditions			
P1(Waverider point)	2.0	1.8	1.5
P2		1.9	1.7
P3		2.0	1.8
P4		2.1	2.0
P5(East boundary point)		2.1	2.1

6. **Preliminary conclusions**

Results show that the model performance is satisfactory in the representation for the studied cases, although some limitations were identified.

- When the wave spectrum has two energy peaks, results indicated that the shape of the spectrum is well reproduced, and the SWAN model agrees with the energy level observed in the high frequency peak, although underestimating the energy level in the low frequency peak.

- When the wave spectrum has only one peak, the model does reproduce well the observed spectrum.

- The whitecapping process works as a mechanism for controlling the energy peak of sea wave conditions.

7. **Suggestions**

- Make the same simulations using the SWAN Cycle III version 40.51 (August 2006). In this new version, an alternative way of dealing with the whitecapping is included. The combination of the alternative wind input and whitecapping expressions is expected to improve the results presented in this report.

- To reproduce the best simulations using different wind data sources, and considering the wind varying in time.

- To apply the new SWAN model with the mud-wave interaction module in the same study area using the Cassino project data (May 2005).

8.References

CALLIARI, L.J. SPERANSKI, N. S.,TORRONTEGUY, M E OLIVEIRA, M.B. (2000). The mud banks of Cassino Beach, Southern Brazil: Characteristics, Processes and Effects. *Journal of Coastal Research*, ICS 2000 Proceedings, 1-9, New Zealand.

CAMARGO, O. A., SILVA, F. J. L., CUSTODIO, R.S. e GRAVINO, N. (2002). *Atlas Eólico do Rio Grande do Sul*. Secretaria de Energia, Minas e Comunicações, Porto Alegre/RS. 70p.

CERC (Coastal Engineering Research Center), (1986). Measuring Shoreline Change. *U.S. Army Engineer Waterways Experiment Station, Coastal Engineering Technical Note*, II-86, 7p.

COLI, A. B., 1994. Análise das alturas de onda ao longo do Rio Grande do Sul: dados históricos e altimétricos. *Trabalho de graduação*, Curso de Oceanologia, Fundação Universidade Federal do Rio Grande – FURG, 58p.

COLI, A. B., (2000). Estudo do Clima Ondulatório em Rio Grande. *Dissertação de Mestrado*, Curso de Engenharia Oceânica, Fundação Universidade Federal do Rio Grande – FURG, 76p.

FRYBERGER, S. G. (1979). Dune forms and wind regime. In: McKee, E.D. (ed) A Study of Global Sand Seas. *Geological Survey Professional*, Paper 1052: 137-169.

HASSELMANN, K., T.P. BARNETT, E. BOUWS, H. CARLSON, D.E. CARTWRIGHT, K. ENKE, J.A. EWING, H.GIENAPP, D.E. HASSELMANN, P. KRUSEMAN, A. MEERBURG, P. MÜLLER, D.J. OLBERS, K. RICHTER, W. SELL and H. WALDEN, (1973): Measurements of wind-wave growth and swell decay

during the Joint North Sea Wave Project (JONSWAP), Dtsch. Hydrogr. Z. Suppl., 12, A8

KRUSCHE, N., SARAIVA, J.M.B. e REBOITA, M.S. (2003). Normais climatológicas provisórias de 1991 a 2000 para Rio Grande, RS. 104p.

MACHADO, D. M., (2000). Previsão de Eventos Extremos de Ondas para a Praia do Cassino, Rio Grande, RS. *Dissertação de Mestrado*, Curso de Engenharia Oceânica, Fundação Universidade Federal do Rio Grande – FURG, 76p.

MORTON, R.A., (1991). Accurate shoreline mapping: past, present, and future. *Coastal Sediments '91*, 1, 997-1010.

MOTTA, V. F., (1963). Análise e Previsão das Alturas de Ondas em Tramandaí, Porto Alegre. *Instituto de Pesquisas Hidráulicas*, Universidade Federal do Rio Grande do Sul, 30 p.

STRAUCH, J.C., (1998). Um Ano de Monitoramento de Ondas em Rio Grande. *XI Semana Nacional de Oceanografia*, Fundação Universidade Federal do Rio Grande – FURG. Oceanografia e suas interfaces, resumos expandidos.

TOMAZELLI, L. J. (1992). O regime dos ventos e a taxa de migração das dunas eólicas costeiras do Rio Grande do Sul, Brasil. Pesquisas 20(1): 18-26.

TOMAZELLI, L.J. e VILLWOCK, J.A. (1992). Considerações sobre o ambiente praial e a deriva litorânea de sedimentos ao longo do litoral norte do Rio Grande do Sul, Brasil. *Pesquisas 19(1): 3- 12.*

WINTERWERP, J.C., R.F. DE GRAAFF, J. GROENEWEG, A.P. LUYENDIJK, (2005). Modelling of wave damping at Guyana mud coast, *submitted to Coastal Engineering in11/15/2005*.

WHITHAM, G.B., (1974) *Linear and nonlinear waves*, Wiley, New York, 636 p.

ZIJLEMA, M. AND A.J. VAN DER WESTHUIJSEN, (2005), On convergence behaviour and numerical accuracy in stationary in stationary SWAN simulations of nearshore wind wave spectra, *Coastal Engineering*, 52, 237-265.

SWAN Cycle III version 40.41, User Manual, 2004. 118 p.

Atlas eólico ➔ http://www.semc.rs.gov.br/

8.Appendix
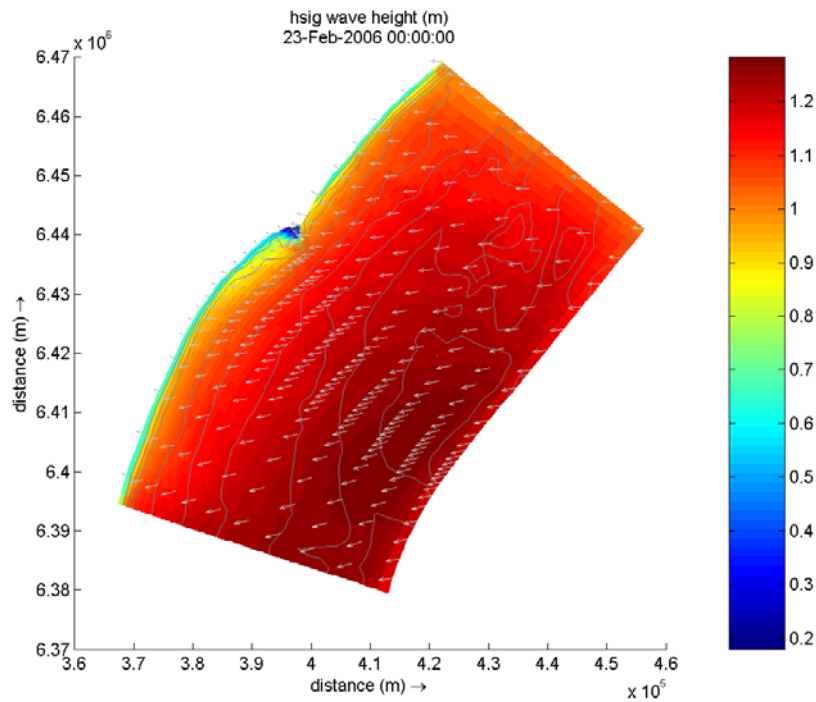
Figure 11 - Significant wave height and mean direction obtained from the SWAN model computations for the computational grid. Uniform wind velocity of 7.2m/s NE. Wave data at 4/02/1998 in 07:00 h with Hs =1.8m, Tm = 5.0s and NDIR=125° considered constant along the open boundaries.
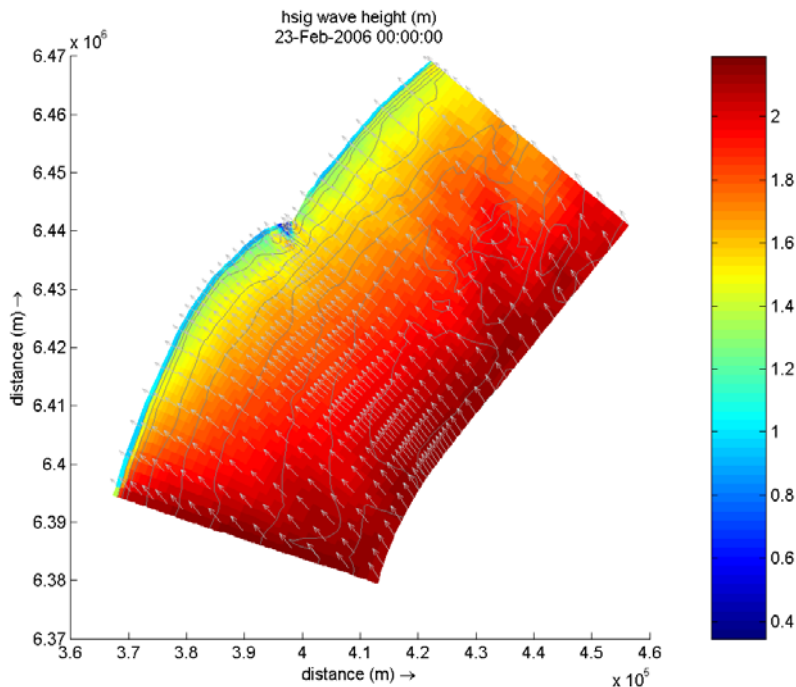
Figure 12 - Significant wave height and mean direction obtained for SWAN model computations for the computational grid. Uniform wind velocity of 7.15m/s SSW. Wave data at 11/02/1998 in 17:00 h with Hs = 2.0m, Tp = 12.5s and NDIR=159° considered constant along the open boundaries.
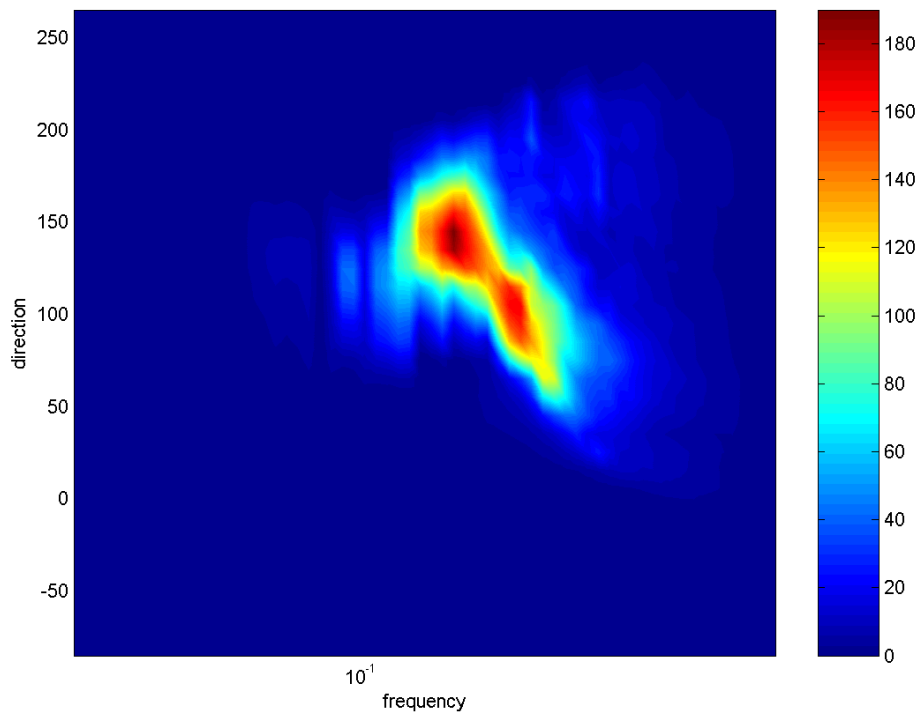
Figure 13 – Energy density obtained from the SWAN model computations for the computational grid. Uniform wind velocity of 11.20 m/s ENE. Wave data spectral file at 04/Feb/1998 in 01:10 h considered in several points along the open boundaries.
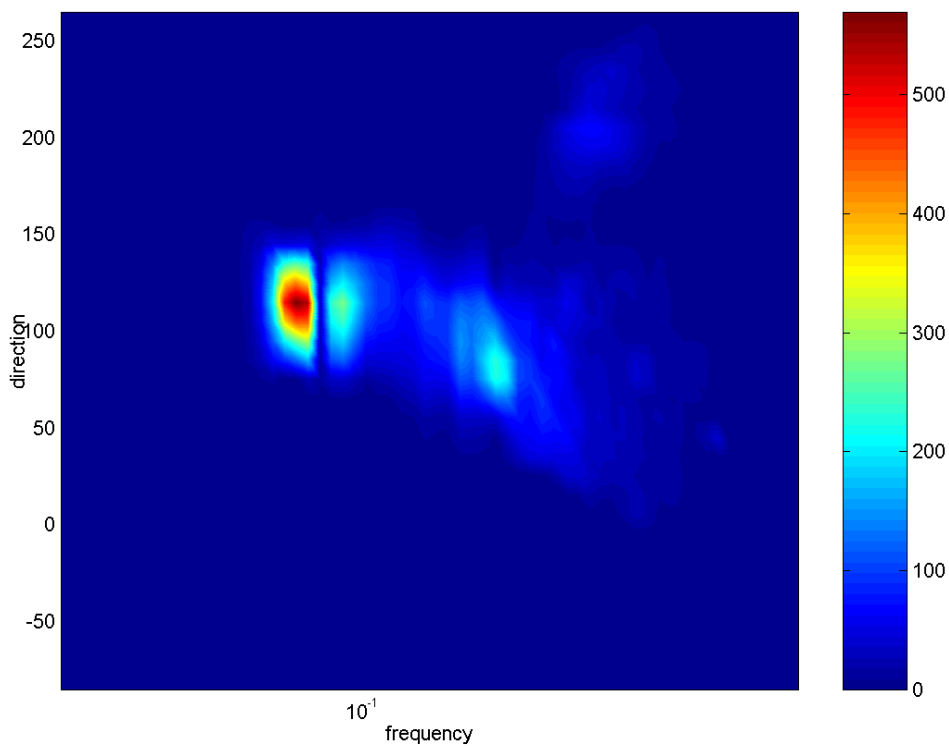
Figure 14 - Energy density obtained for SWAN model computations in computational grid. Uniform wind velocity of 8.08 m/s SW. Wave data spectral file at 11/Feb/1998 in 09:15 h considered in several points along the open boundaries .
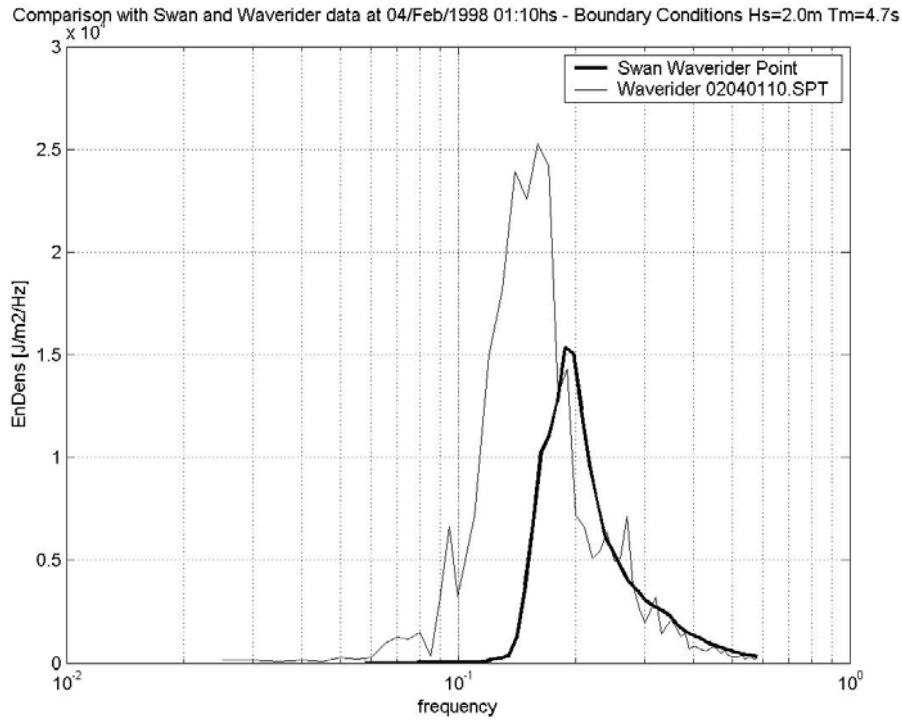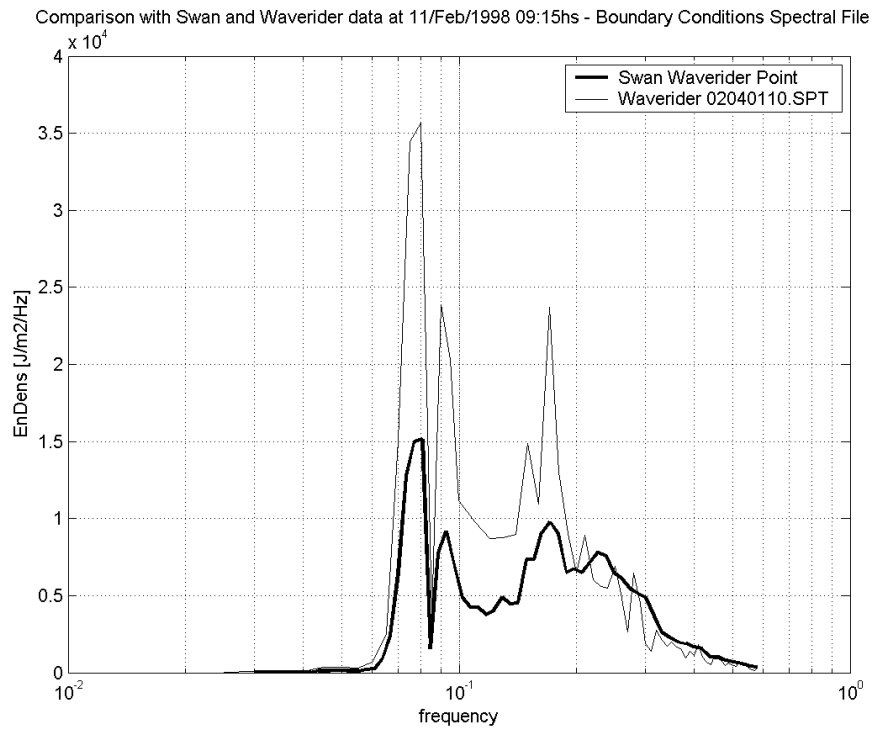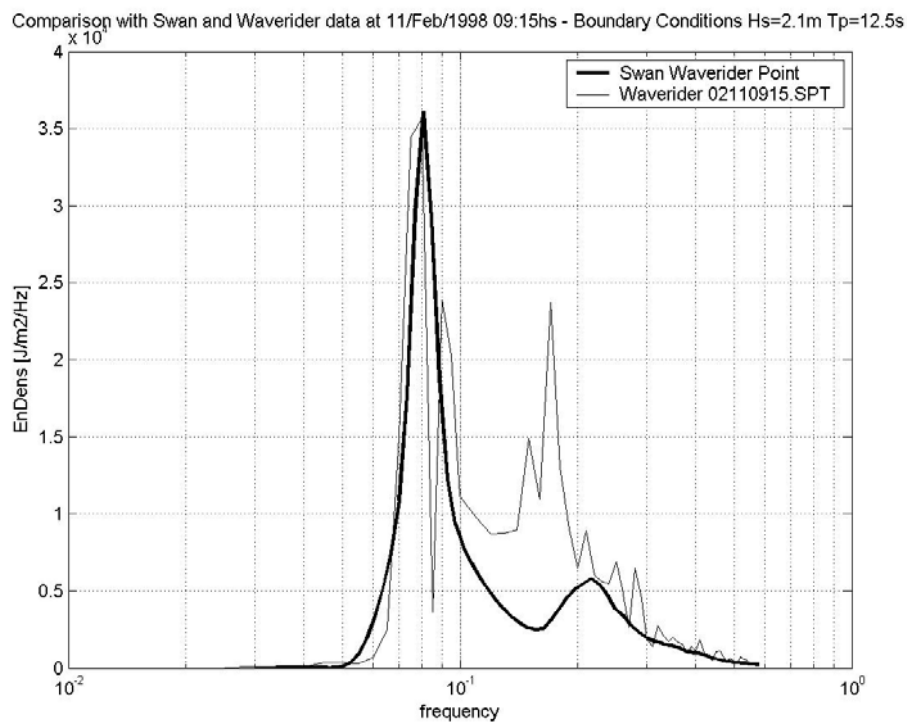
Figure 15 - Comparison between energy density obtained from SWAN model computations and Waverider data at the waverider point. Uniform wind velocity of 11.20 m/s ENE. Wave data at February 4th, 1998 in 01:10 h with Hs=2.0 m, Tm = 4.7s and NDIR=113º considered constant along the open boundaries.
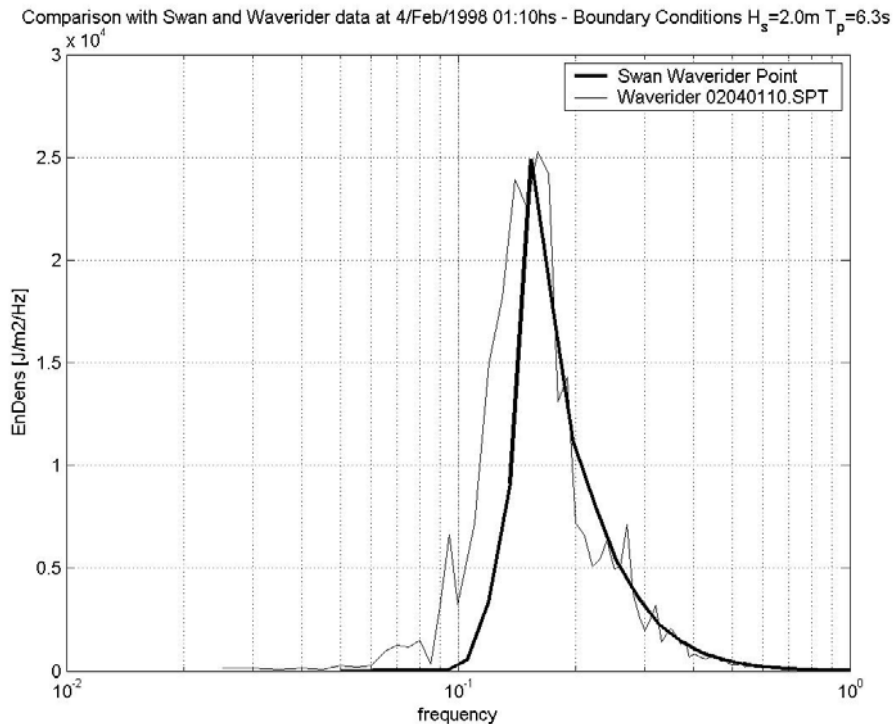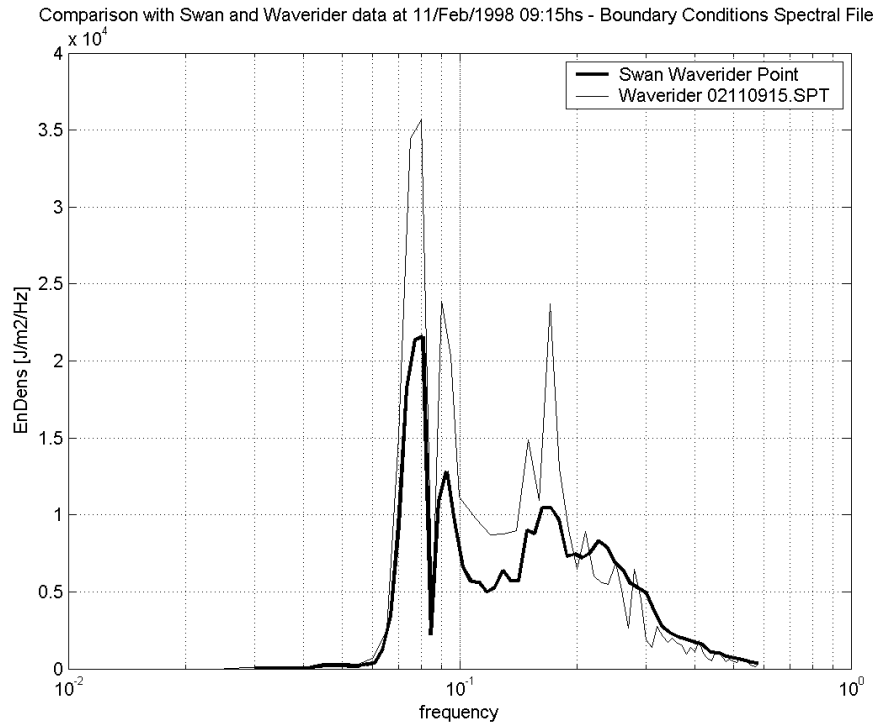

Figure 16 - Comparison between energy density obtained for SWAN model computations and Waverider data at waverider point. Uniform wind velocity of 11.20 m/s ENE. Wave data at February 4th, 1998 in 01:10 h with Hs=2.0 m, Tp = 6.3s and NDIR=113º considered constant along the open boundaries.
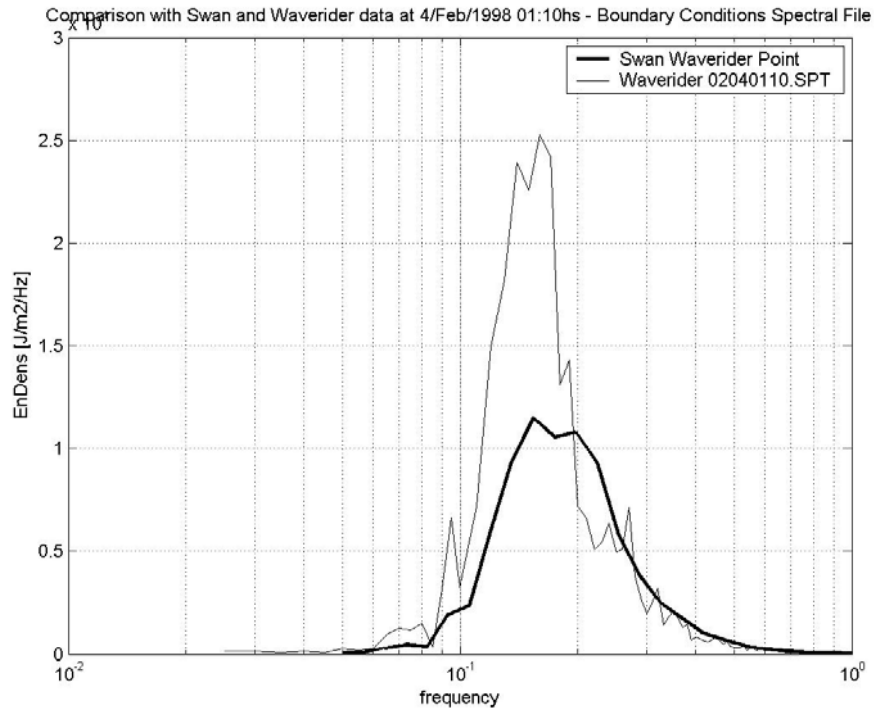
Figure 17 - Comparison between energy density per frequency obtained for SWAN model computations and Waverider data for sea wave condition at waverider point. Uniform wind of 11.20 m/s ENE. Wave spectral file at February 4th, 1998 in 01:10 h.considered along the open boundaries.
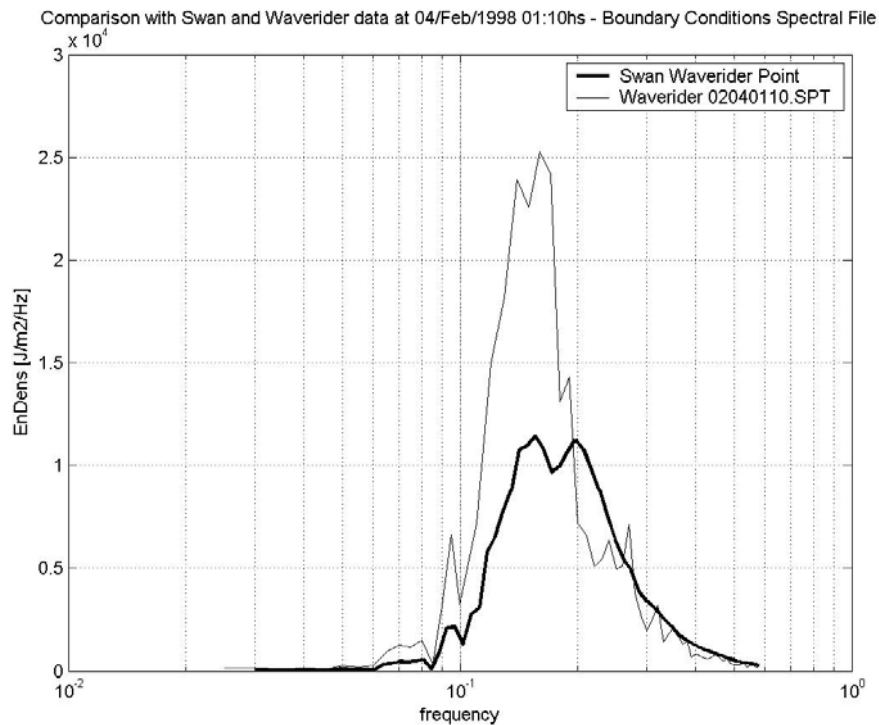
Figure 18 - Comparison between energy density per frequency obtained for SWAN model computations and Waverider data at waverider point. Uniform wind of 11.20 m/s ENE. Wave spectral file at February 4th, 1998 in 01:10 h. considered in various points in the open boundaries.
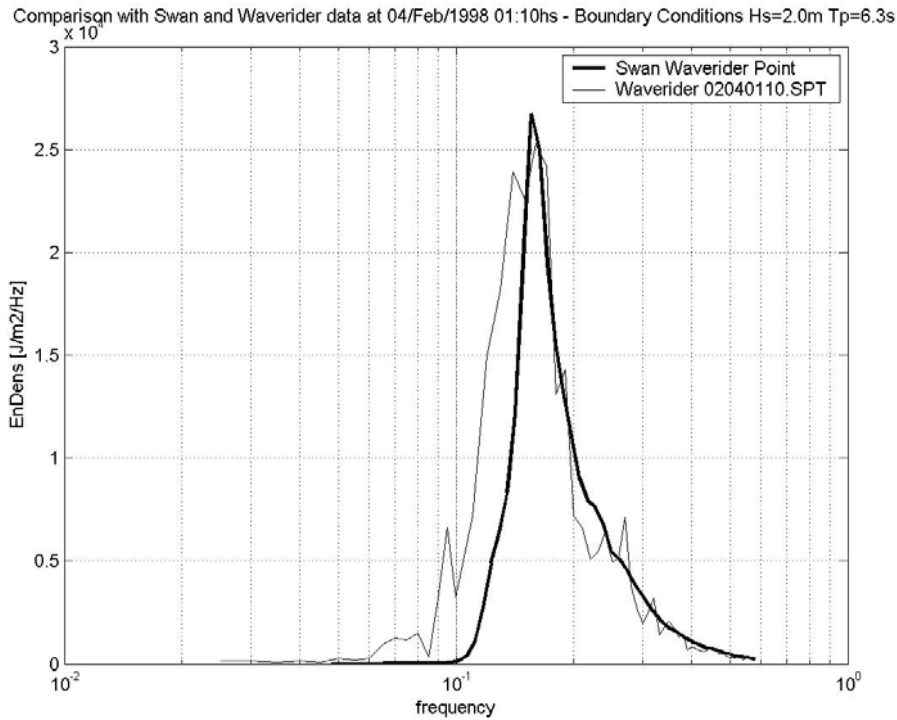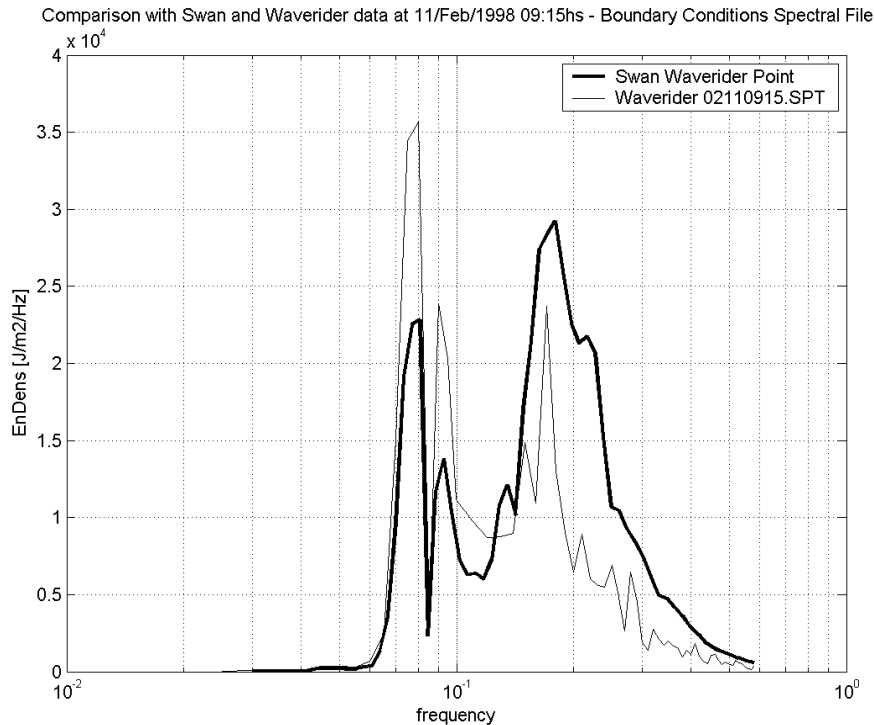
Figure 19 - Comparison between energy density obtained for SWAN model computations and Waverider data at waverider point. Uniform wind velocity of 11.20 m/s ENE. Wave data at February 4th, 1998 in 01:10 h with Hs=2.0 m, Tp = 6.3s and NDIR=113º considered in various points in the open boundaries.
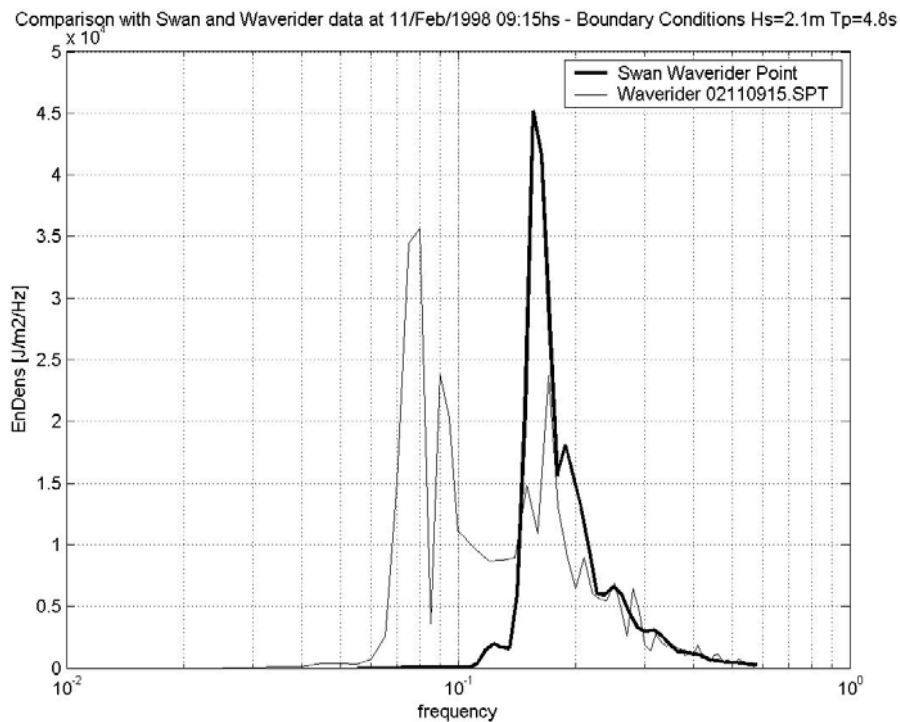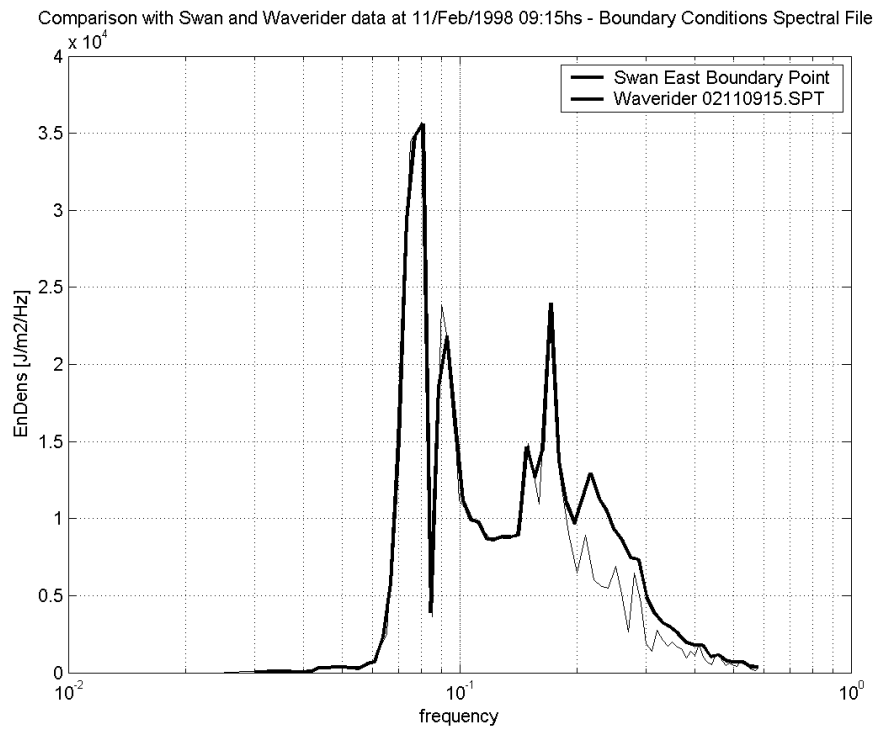

Figure 20 - Comparison between energy density obtained for SWAN model computations and Waverider data at waverider point. Uniform wind velocity of 8.08 m/s SW. Wave data at February 11th, 1998 in 09:15 h with Hs=2.1 m, Tm = 4.8s and NDIR=167º considered constant along the open boundaries.

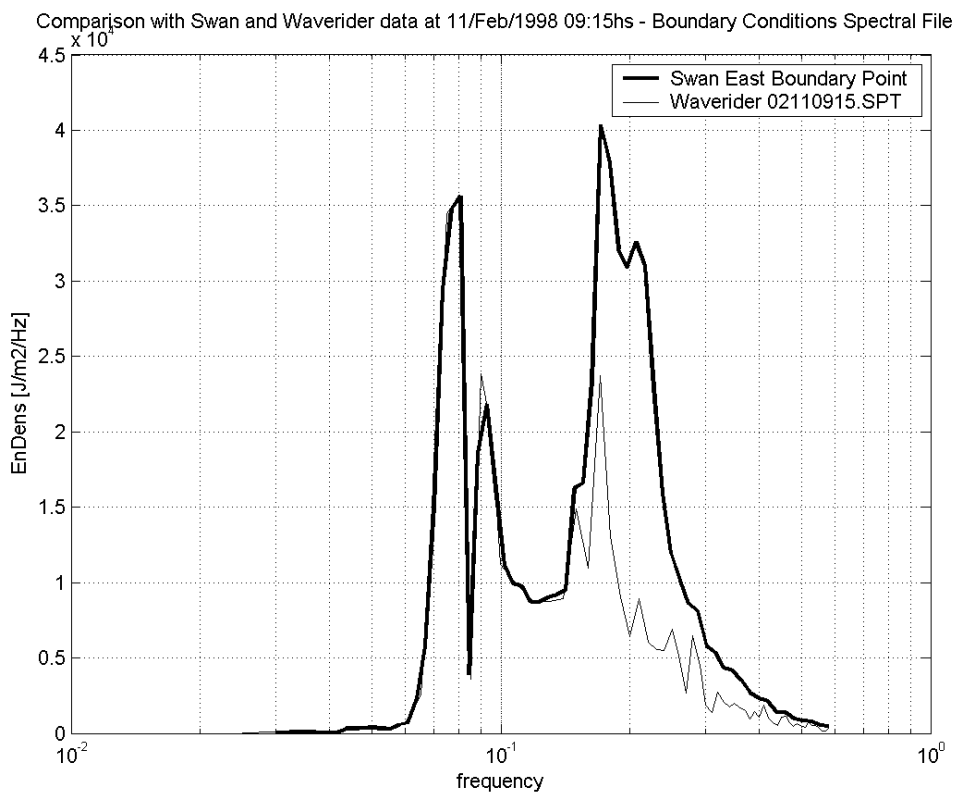Comparison with Swan and Waverider data at 11/Feb/1998 09:15hs - Boundary Conditions Hs=2.1m Tp=12.5s
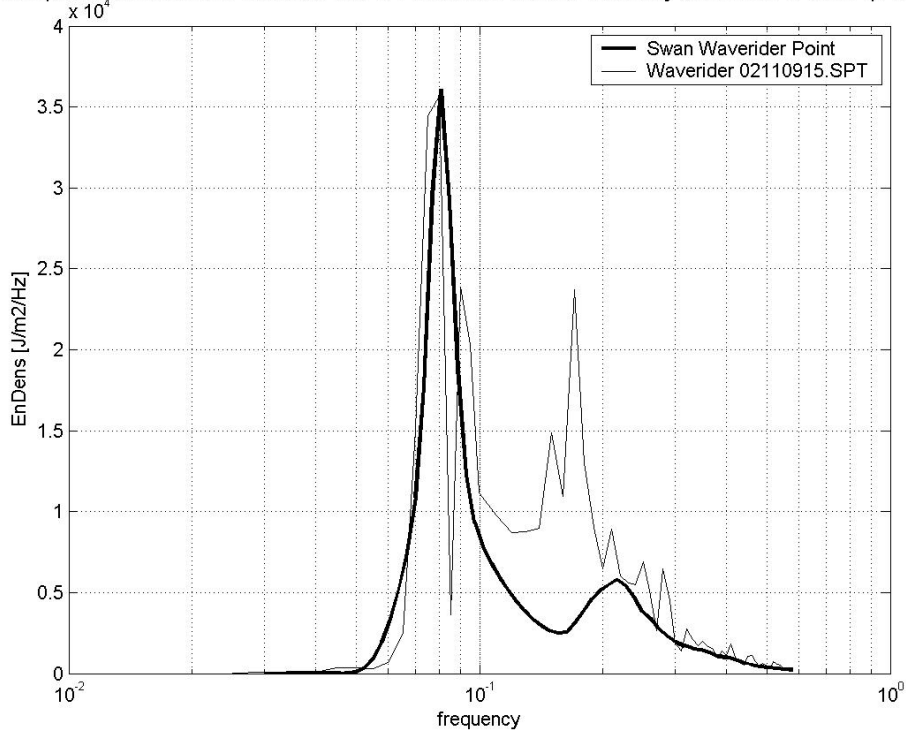
Figure 21 - Comparison between energy density obtained for SWAN model computations and Waverider data at waverider point. Uniform wind velocity of 8.08 m/s SW. Wave data at February 11th, 1998 in 09:15 h with Hs=2.1 m, Tp = 12.5s and NDIR=167° considered constant along the open boundaries

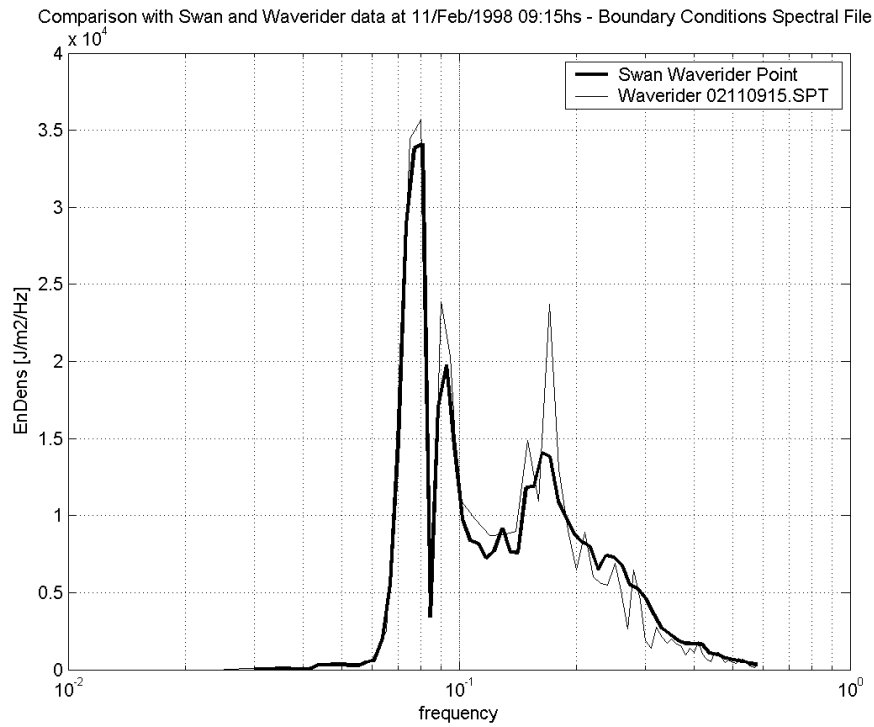Comparison with Swan and Waverider data at 11/Feb/1998 09:15hs - Boundary Conditions Spectral File
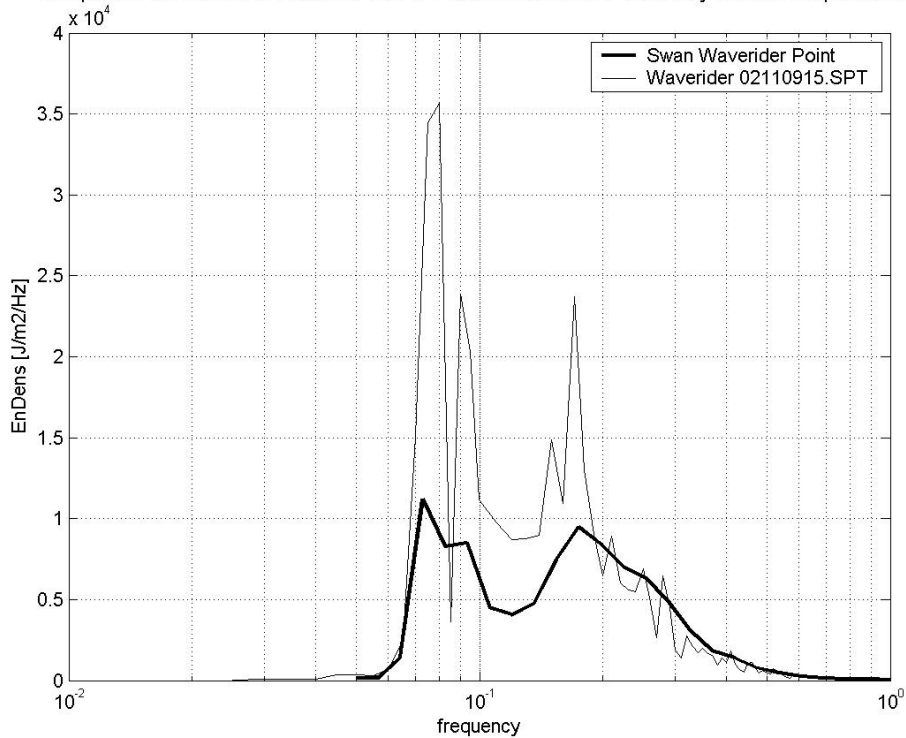
Figure 22 - Comparison between energy density obtained for SWAN model computations and Waverider data at waverider point. Uniform wind velocity of 8.08 m/s SW. Wave spectral file at February 11th, 1998 at 09:15 h. considered along the open boundaries.

Figure 23 - Comparison between energy density obtained for SWAN model computations and waverider data at waverider point. Uniform wind of 8.08 m/s SW. Wave spectral file at February 11th, 1998 at 09:15 h. considered in several points in the open boundaries.
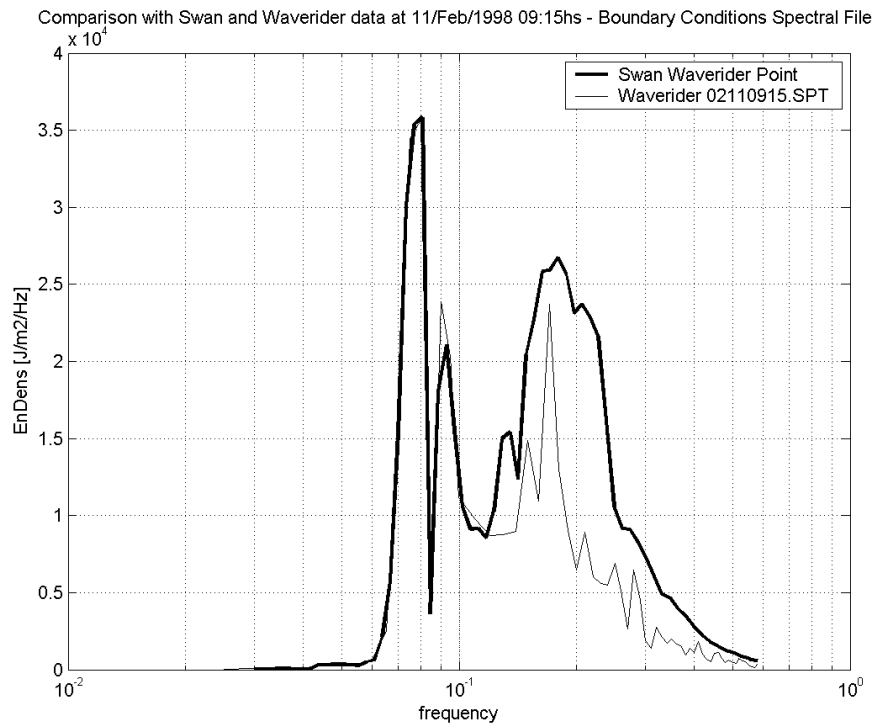

Figure 24 - Comparison between energy density obtained for SWAN model computations and waverider data at waverider point. Uniform wind velocity of 8.08 m/s SW. Wave data at February 11th, 1998 at 09:15 h with Hs=2.1 m, Tp = 12.5s and NDIR=167° considered in several points in the open boundaries.

Comparison with Swan and Waverider data at 11/Feb/1998 09:15hs - Boundary Conditions Spectral File

Figure 25 - Comparison between energy density obtained for SWAN model computations and waverider data at waverider point. Uniform wind velocity of 8.08 m/s SW. Wave spectral file at February 11th, 1998 at 09:15 h considered in various points in the open boundaries with friction coefficient = 0.038, yes whitecapping.

Comparison with Swan and Waverider data at 11/Feb/1998 09:15hs - Boundary Conditions Spectral File

Figure 26 - Comparison between energy density obtained for SWAN model computations and waverider data at waverider point. Uniform wind velocity of 8.08 m/s SW. Wave spectral file at February 11th, 1998 at 09:15 h considered in various points in the open boundaries with friction coefficient = 0.038, no whitecapping.
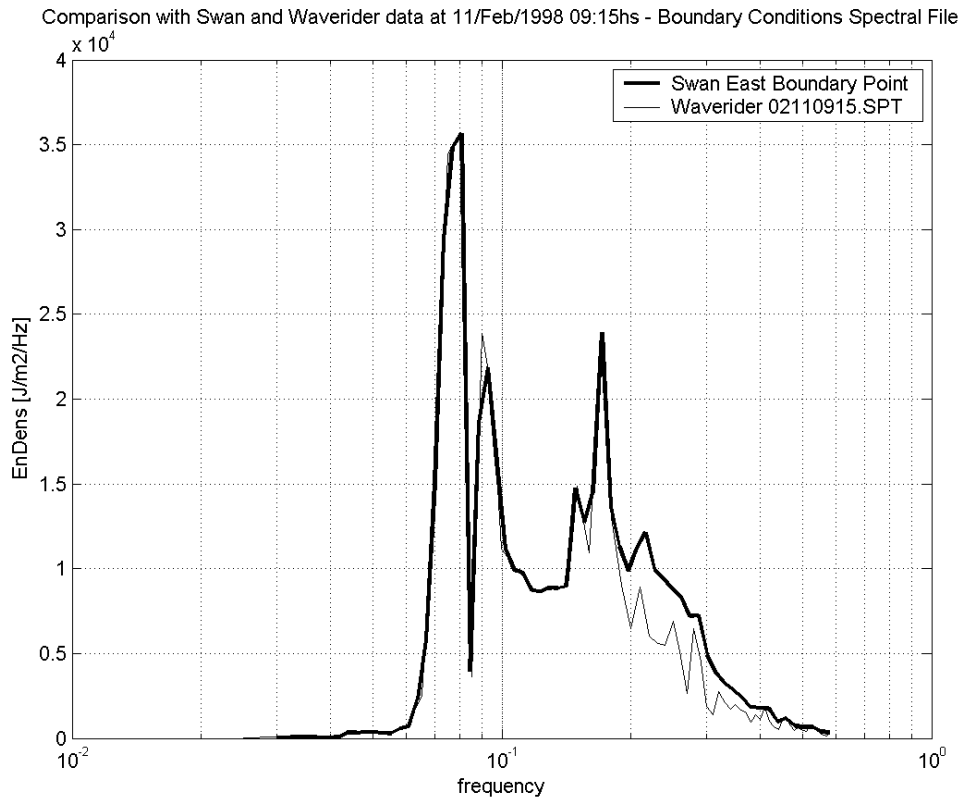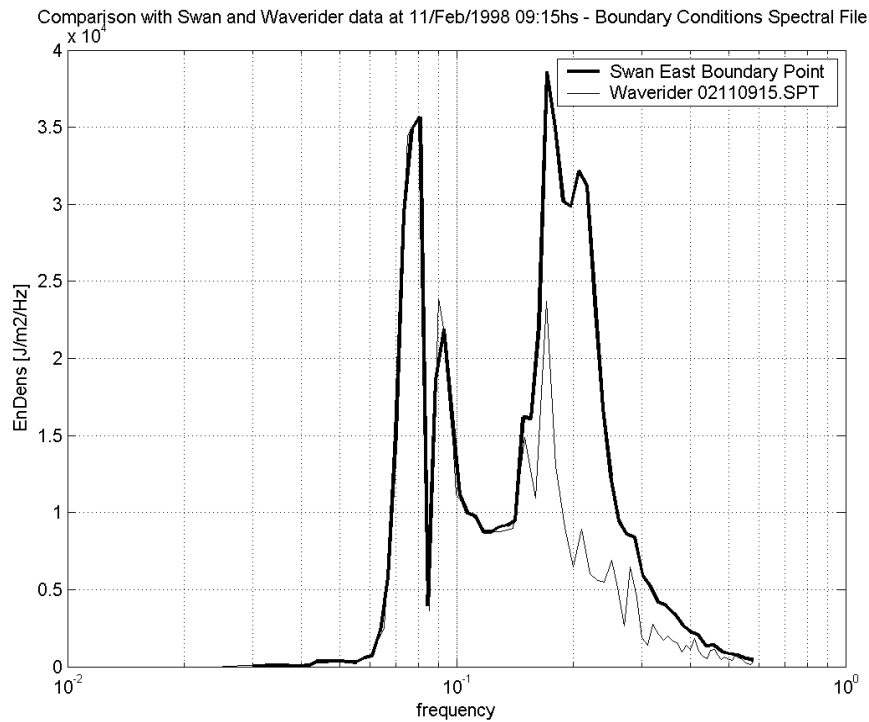
Figure 27 - Comparison between energy density obtained for SWAN model computations and waverider data at east boudary point. Uniform wind velocity of 8.08 m/s SW. Wave spectral file at February 11th, 1998 at 09:15 h considered in various points in the open boundaries with friction coefficient = 0.038, yes whitecapping
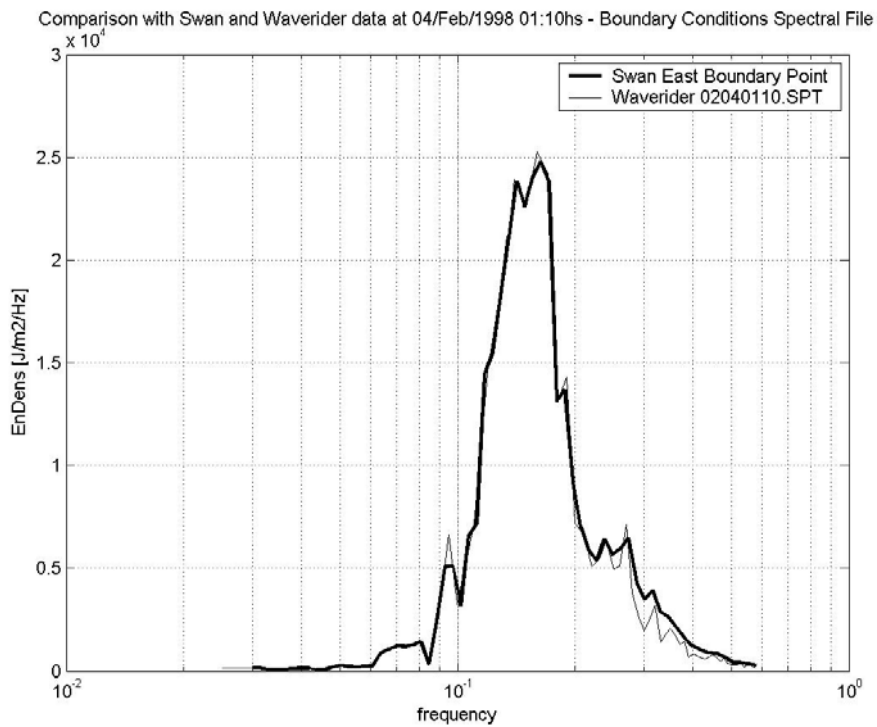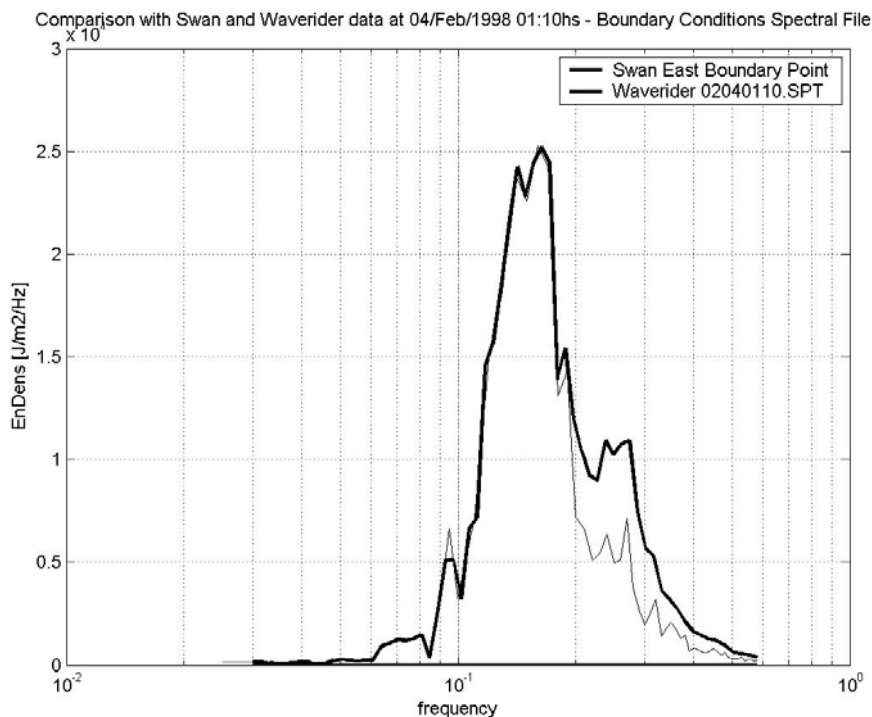

Figure 28 - Comparison between energy density obtained for SWAN model computations and waverider data at east boudary point. Uniform wind velocity of 8.08 m/s SW. Wave spectral file at February 11th, 1998 at 09:15 h considered in various points in the open boundaries with friction coefficient = 0.038, no whitecapping.

Figure 29 - Comparison between energy density obtained for SWAN model computations and waverider data at waverider point. Uniform wind velocity of 8.08 m/s SW. Wave spectral file at February 11th, 1998 at 09:15 h considered in various points in the open boundaries with friction coefficient = 0.001, yes whitecapping.

Figure 30 - Comparison between energy density obtained for SWAN model computations and waverider data at waverider point. Uniform wind velocity of 8.08 m/s SW. Wave spectral file at February 11th, 1998 at 09:15 h considered in various points in the open boundaries with friction coefficient = 0.001, no whitecapping.
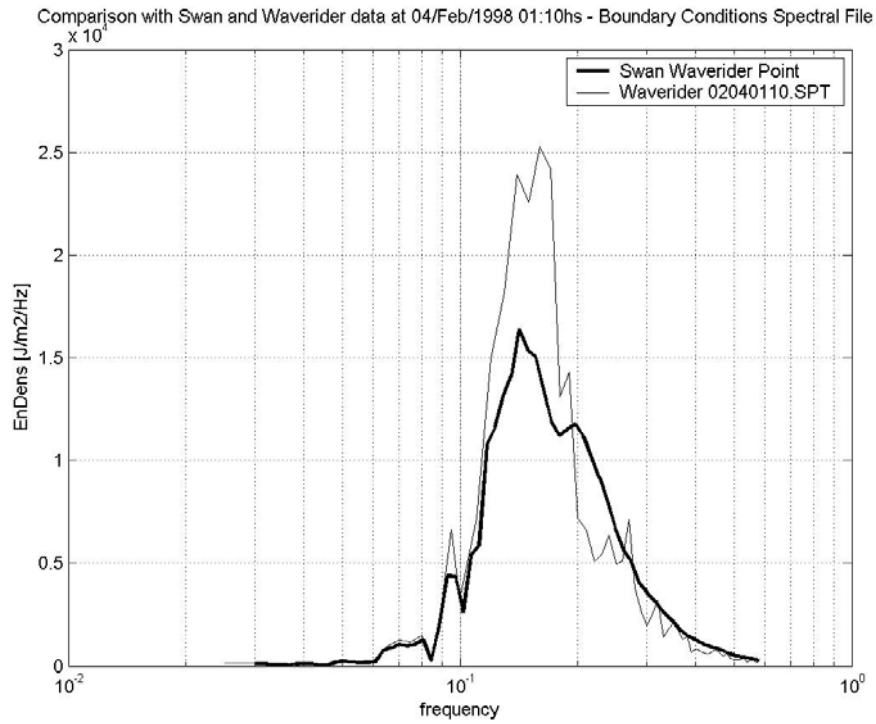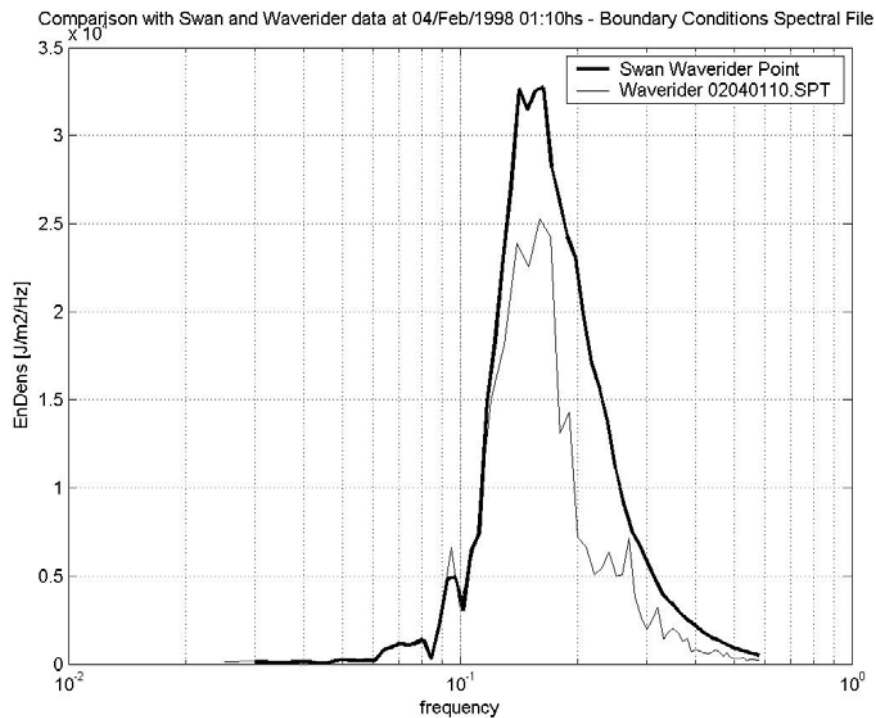
Figure 31 - Comparison between energy density obtained for SWAN model computations and waverider data at east boudary point. Uniform wind velocity of 8.08 m/s SW. Wave spectral file at February 11th, 1998 at 09:15 h considered in various points in the open boundaries with friction coefficient = 0.001, yes whitecapping.

Figure 32 - Comparison between energy density obtained for SWAN model computations and waverider data at east boudary point. Uniform wind velocity of 8.08 m/s SW. Wave spectral file at February 11th, 1998 at 09:15 h considered in various points in the open boundaries with friction coefficient = 0.001, no whitecapping.
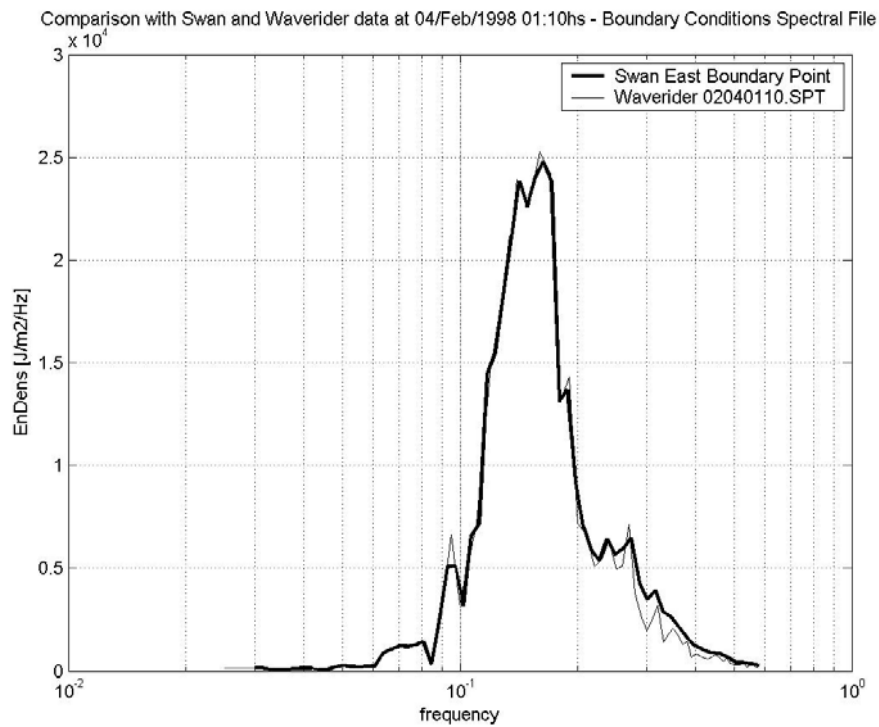
Figure 33 - Comparison between energy density obtained for SWAN model computations and waverider data at east boundary point. Uniform wind velocity of 12.20 m/s ENE. Wave spectral file at February 4th, 1998 at 01:10 h considered in various points in the open boundaries with friction coefficient = 0.001, yes whitecapping.
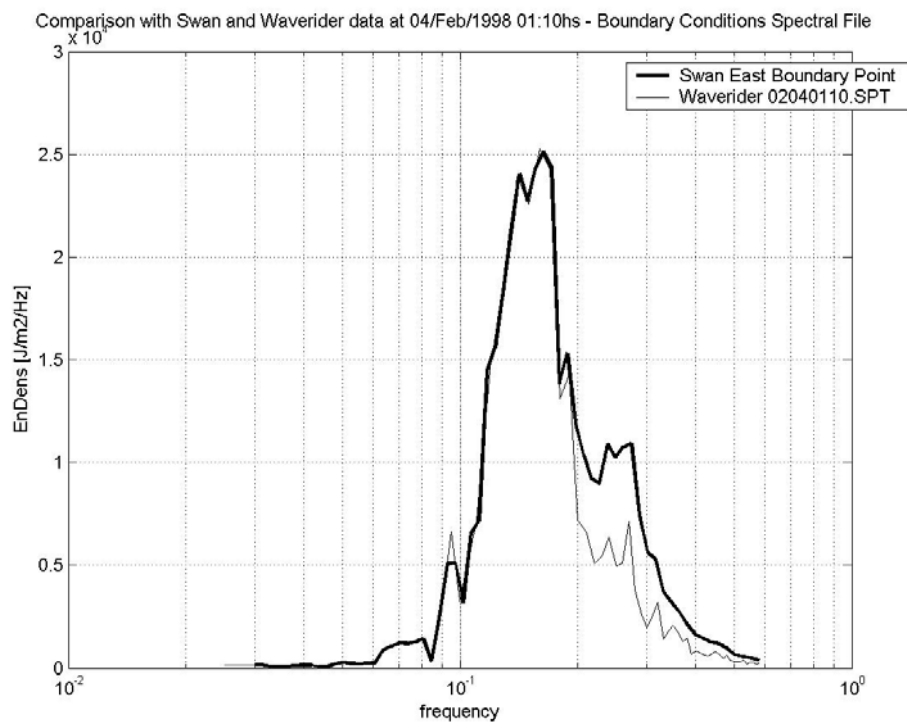

Figure 34- Comparison between energy density obtained for SWAN model computations and waverider data at east boundary point. Uniform wind velocity of 12.20 m/s ENE. Wave spectral file at February 4th, 1998 at 01:10 h considered in various points in the open boundaries with friction coefficient = 0.001, no whitecapping.

Figure 35 - Comparison between energy density obtained for SWAN model computations and waverider at waverider point. Uniform wind velocity of 12.20 m/s ENE. Wave spectral file at February 4th, 1998 at 01:10 h considered in various points in the open boundaries with friction coefficient = 0.001, yes whitecapping.
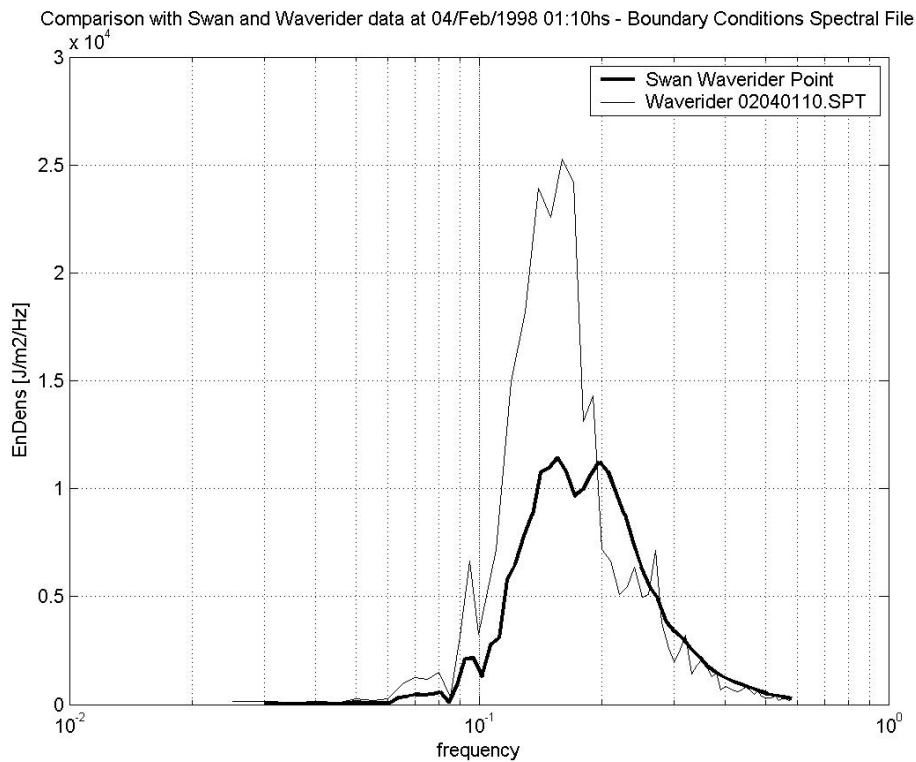

Figure 36 - Comparison between energy density obtained for SWAN model computations and waverider data at waverider point. Uniform wind velocity of 12.20 m/s ENE. Wave spectral file at February 4th, 1998 at 01:10 h considered in various points in the open boundaries with friction coefficient = 0.001, no whitecapping.

Figure 37 - Comparison between energy density obtained for SWAN model computations and waverider data at east boundary point. Uniform wind velocity of 12.20 m/s ENE. Wave spectral file at February 4th, 1998 at 01:10 h considered in various points in the open boundaries with friction coefficient = 0.067, yes whitecapping.
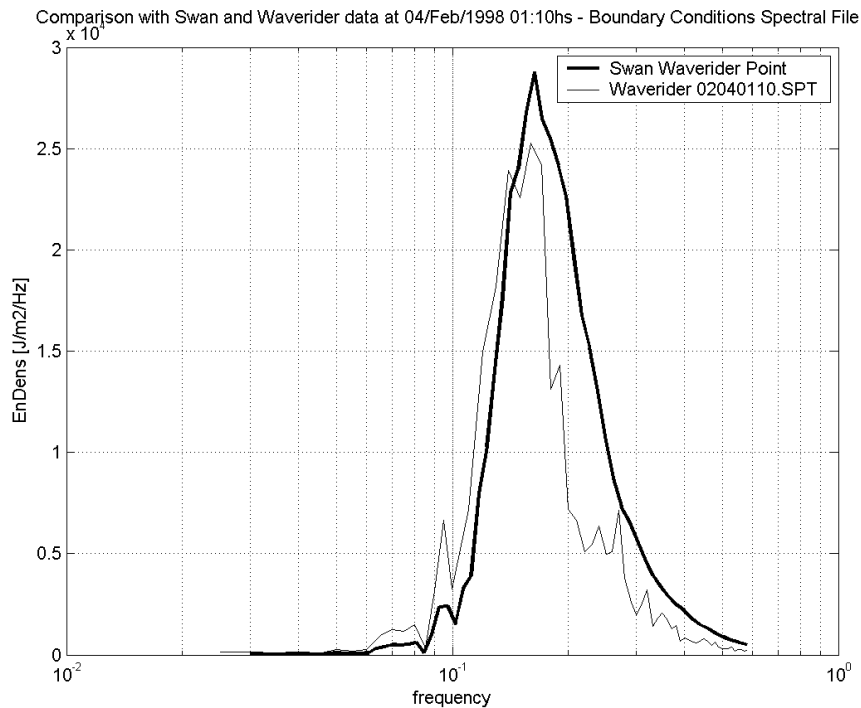

Figure 38 - Comparison between energy density obtained for SWAN model computations and waverider data at east boundary point. Uniform wind velocity of 12.20 m/s ENE. Wave spectral file at February 4th, 1998 at 01:10 h considered in various points in the open boundaries with friction coefficient = 0.067, no whitecapping.

Figure 39 - Comparison between energy density obtained for SWAN model computations and waverider data at waverider point. Uniform wind velocity of 12.20 m/s ENE. Wave spectral file at February 4th, 1998 at 01:10 h considered in various points in the open boundaries with friction coefficient = 0.067, yes whitecapping.

Figure 40 - Comparison between energy density obtained for SWAN model computations and waverider data at waverider point. Uniform wind velocity of 12.20 m/s ENE. Wave spectral file at February 4th, 1998 at 01:10 h considered in various points in the open boundaries with friction coefficient = 0.067, no whitecapping.
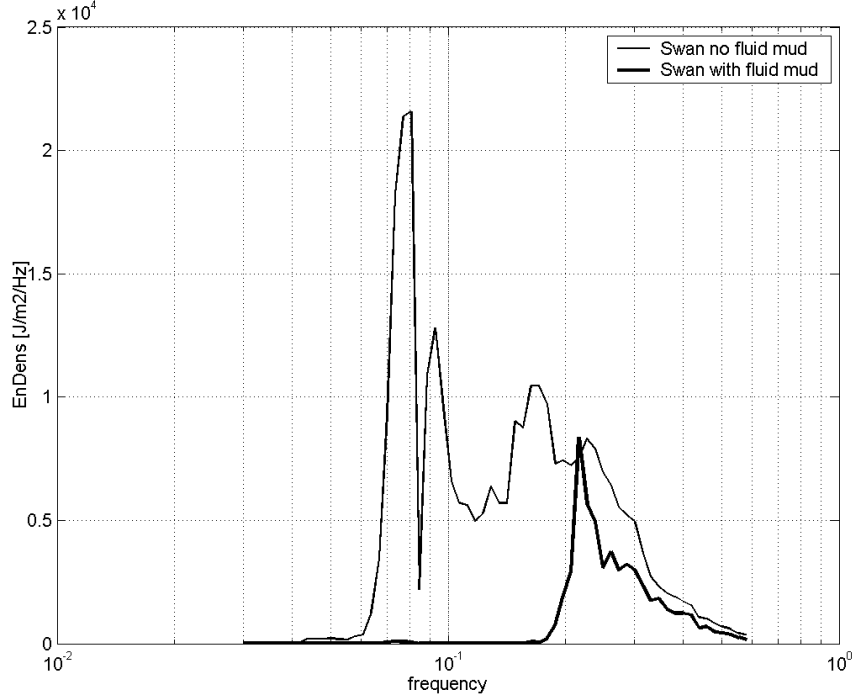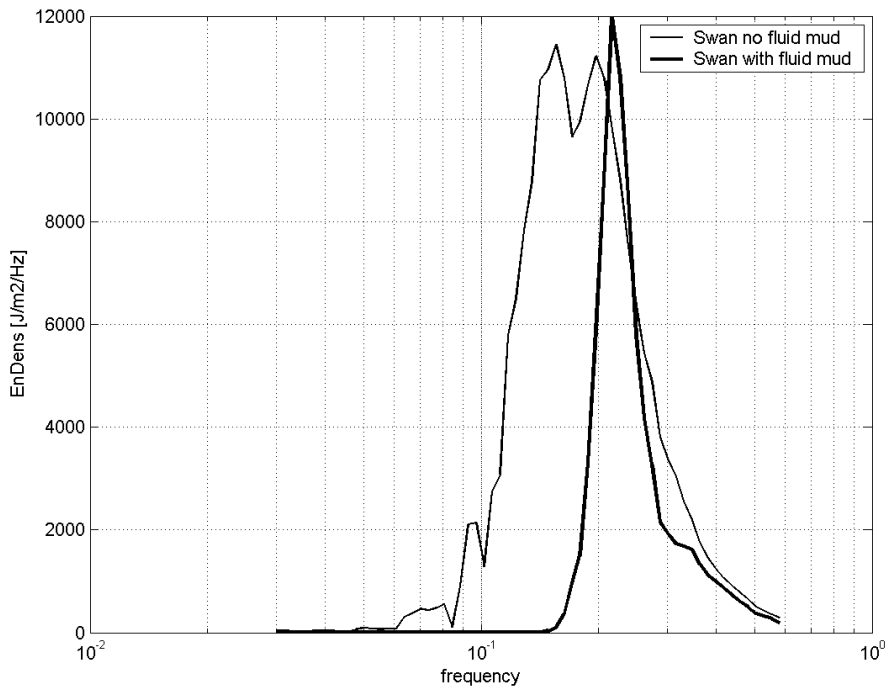
Figure 41 - Comparison between energy density per frequency obtained for SWAN wave model computations and SWAN mud wave damping model computations at waverider point. Mud parameters at Cassino Beach in 1998 with dm = 1.00m, rm = 1300 kg/m3 and nm = 0.01 m^2/s considered constant in all computational grid.
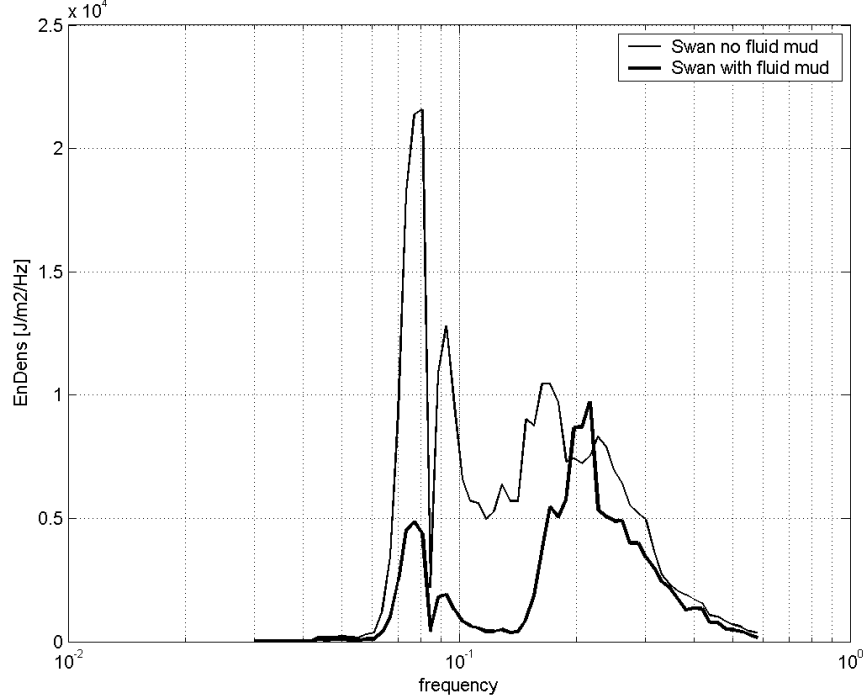

Figure 42 - Comparison between energy density per frequency obtained for SWAN wave model computations and SWAN mud wave damping model computations at waverider point. Mud parameters at Cassino Beach in 1998 with dm = 1.00m, rm = 1300 kg/m3 and nm = 0.01 m^2/s considered constant in all computational grid.

Figure 43 - Comparison between energy density per frequency obtained for SWAN wave model computations and SWAN mud wave damping model computations at waverider point. Mud parameters at Cassino Beach in 1998 with dm = 1.00m, rm = 1300 kg/m3 and nm = 0.001 m^2/s considered constant in all computational grid.
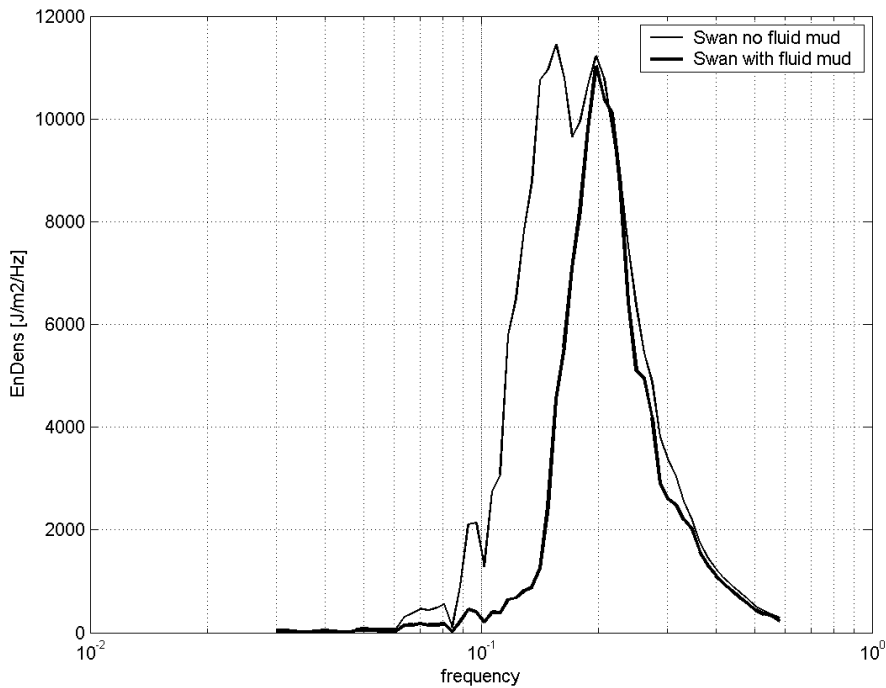
Figure 44 - Comparison between energy density per frequency obtained for SWAN wave model computations and SWAN mud wave damping model computations at waverider point. Mud parameters at Cassino Beach in 1998 with dm = 1.00m, rm = 1300 kg/m3 and nm = 0.001 m^2/s considered constant in all computational grid.
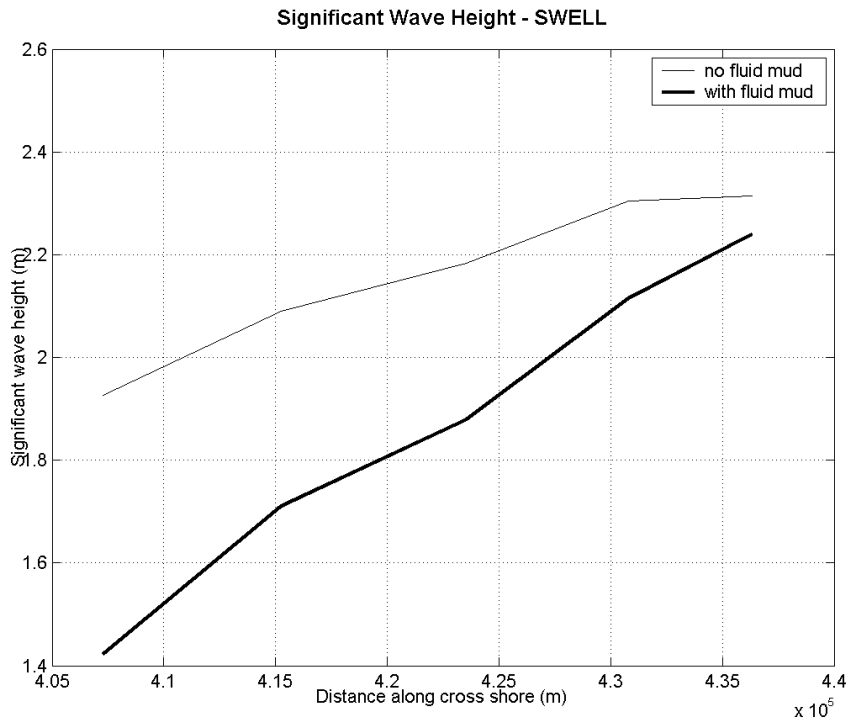
Significant Wave Height - SWELL

Figure 45 - Comparison between significant wave height obtained for SWAN wave model computations and SWAN mud wave damping model computations for swell wave condition in five points located between the waverider point and east open boundary point. Mud parameters at Cassino Beach in 1998 with dm = 1.00m, rm = 1300 kg/m3 and nm = 0.001 m^2/s considered constant in all computational grid.
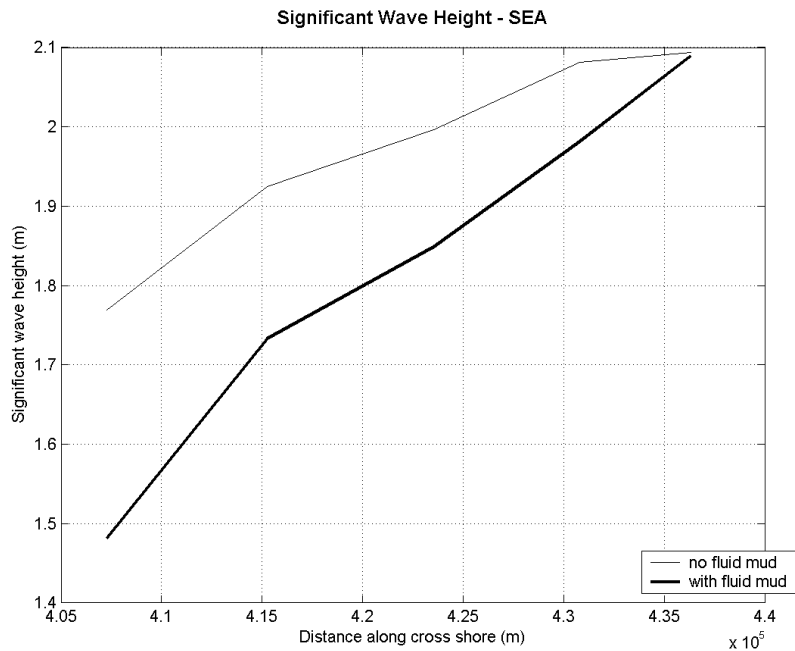

Significant Wave Height - SEA

Figure 46 - Comparison between significant wave height obtained for SWAN wave model computations and SWAN mud wave damping model computations in five points located between the waverider point and east open boundary point. Mud parameters at Cassino Beach in 1998 with dm = 1.00m, rm = 1300 kg/m3 and nm = 0.001 m^2/s considered constant in all computational grid.

Figure 47 - Comparison between mean wave period obtained for SWAN wave model computations and SWAN mud wave damping model computations in five points located between the waverider point and east open boundary point. Mud parameters at Cassino Beach in 1998 with $dm = 1.00m$, $rm = 1300$ kg/m3 and $nm = 0.001$ m^2/s considered constant in all computational grid.
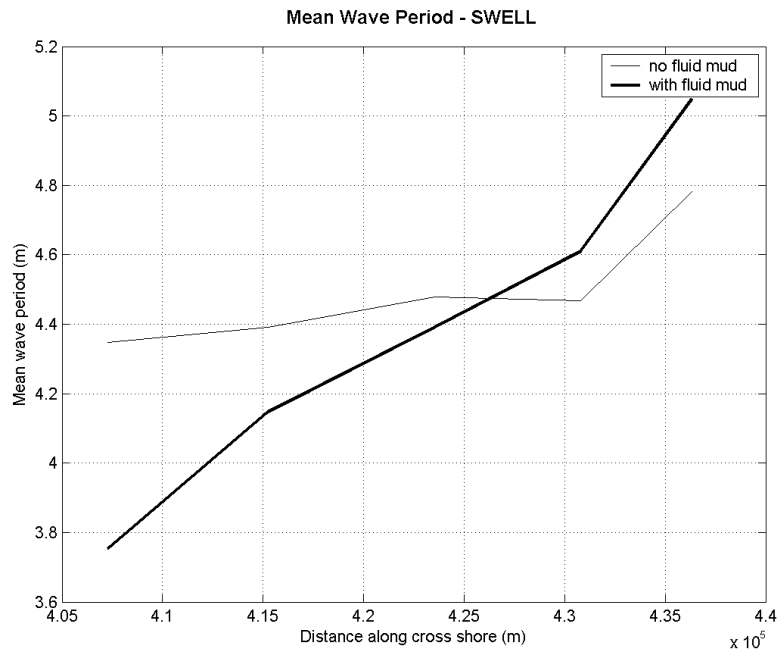

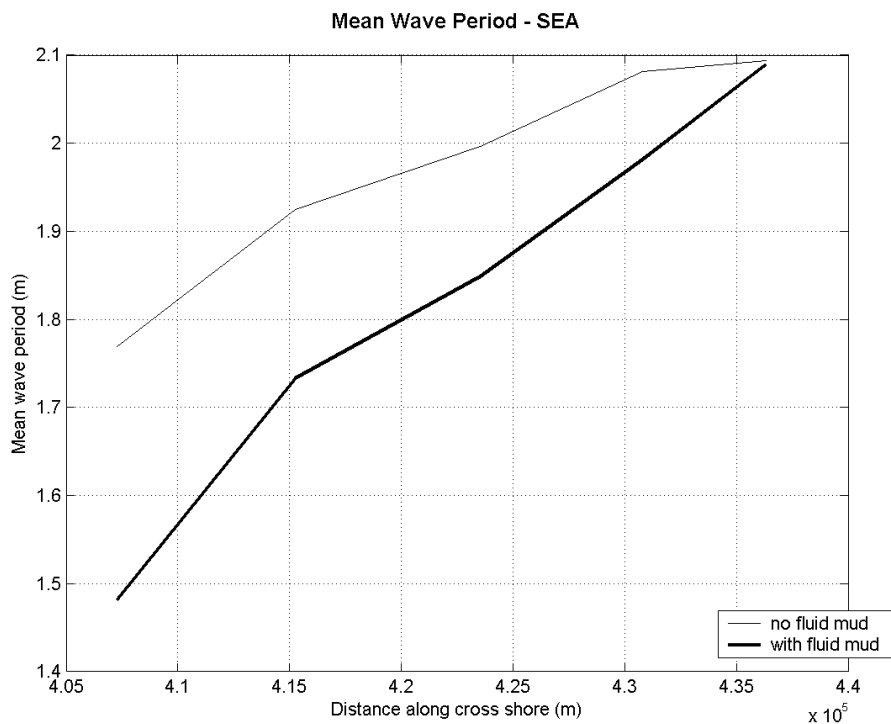Figure 48 - Comparison between mean wave period obtained for SWAN wave model computations and SWAN mud wave damping model computations in five points located between the waverider point and east open boundary point. Mud parameters at Cassino Beach in 1998 with $dm = 1.00m$, $rm = 1300$ kg/m3 and $nm = 0.001$ m^2/s considered constant in all computational grid.

Anexo II

Produção Científica

Arquivo   Editar   Exibir   Ferramentas   Mensagem   Ajuda

Responder   Responde...   Encaminhar   Imprimir   Excluir   Anterior   Avançar   Endereços

De: Todd Holland
Data: segunda-feira, 7 de abril de 2008 12:06
Para: dmtdc@furg.br; dfsehf@furg.br; dfsjcss@furg.br; Lauro Calliari; Han Winterwerp
Cc: Susana Vinzon
Assunto: Reviews of CSR submission
Anexar: comments_cuchiara.pdf (58,9 KB)

Dear authors,

First off I want to apologize for my extremely tardy review of your submission "Determination of the Wave Climate for the Southern Brazilian Shelf " for the Special Issue of CSR. The version of the paper I received was dated June 18 2007, but due to some significant miscommunications, I did not send the paper out for review until Feb 29, 2008. Please forgive me for this inefficiency.

I would like to congratulate you on your submission as both reviewers stated that the paper could be made acceptable with minor revision. Please consider their suggestions (attached and below) and return to me a detailed response of changes made or your reasons for disagreement with the reviewer's comments. I would like the revised paper and written response back by April 28.

There were no evaluation comments with a rating of low in the evaluation summaries (not attached).

Best regards,

Todd Holland

----- Reviewer #1 comments ---------

Review of
"Determination of the Wave Climate for the Southern Brazilian Shelf"
by Cuchiara et al.

Synopsis of paper:
The authors design a wave model (SWAN) implementation for a region of interest (RGDS, Brazil) and verify it using the limited available field measurements (a waverider buoy that was there in 1998). They apply this verified model to generate climatology for the time period of interest (May-June 2005). Comparisons are made to three instruments deployed during 2005. The impact of fluid mud on the wave frequency distribution is estimated using model vs. model comparisons. The impact of fluid mud on the total wave energy is estimated using model vs. model vs. observations comparisons.

Recommendation:
The paper will be acceptable if appropriate revisions are made. These revisions should not require major effort. However, some of these revisions are very important.

De: Continental Shelf Research
Data: 07/31/08 18:23:35
Para: dmtdc@furg.br
Assunto: Submission Confirmation

Dear Mrs Cuchiara,

Your submission entitled "MODELING WAVE DUMPING OVER FLUID MUD AT CASSINO BEACH COASTAL AREA, BRAZIL" has been received by Continental Shelf Research.

Please note that submission of an article is understood to imply that the article is original and is not being considered for publication elsewhere. Submission also implies that all authors have approved the paper for release and are in agreement with its content.

You will be able to check on the progress of your paper by logging on to http://ees.elsevier.com/csr/ as Author.

Your manuscript will be given a reference number in due course.

Thank you for submitting your work to this journal.

Kind regards,

Continental Shelf Research

_____ NOD32 3292 (20080723) Information _____

This message was checked by NOD32 antivirus system.
http://www.eset.com

Resumos Expandidos Publicados em Anais de Congressos

1.MONTEIRO, I.O., CUCHIARA, D. C., MARQUES, W. C., GONÇALVES, GLAUBER A., STRAUCH, J. C., FERNANDES, E. H.

Estudo comparativo da implementação de dois modelos de ondas de terceira geração na plataforma sul do Brasil

VII Simpósio Sobre Ondas, Marés, Engenharia Oceânica E Oceanografia Por Satélite, Arraial do Cabo, RJ, 2007

2. CUCHIARA, D. C., MARQUES, W. C., CALLIARI, L. J., FERNANDES, E. H.

Modelagem Numérica da atenuação das ondas na presença de lama fluida na Praia Do Cassino (RS), Brasil

VII Simpósio Sobre Ondas, Marés, Engenharia Oceânica E Oceanografia Por Satélite, Arraial do Cabo, RJ, 2007

3. CUCHIARA, D. C., FERNANDES, E. H., STRAUCH, J. C., CALLIARI, L. J.

Caracterização do Clima de Ondas na Costa do Rio Grande do Sul

XVIII Semana Nacional de Oceanografia, Pontal do Paraná, 2006.

4. CUCHIARA, D. C., FERNANDES, E. H., STRAUCH, J. C., CALLIARI, L. J.

Caracterização do Clima de Ondas na Costa do Rio Grande do Sul

II Seminário e Workshop em Engenharia Oceânica, Rio Grande - RS, 2006.

4. CUCHIARA, D. C. ; FERNANDES, E. H. ; STRAUCH, J. C. ; CALLIARI, L. J. .

Modelagem Numérica do Comportamento das Ondas na Costa do Rio Grande do Sul.

VI Jornadas Nacionales de Ciencias del Mar, Puerto Madryn, Argentina, 2006.

5. FREITAS, A. C., KERR, R., PIOVESAN, R., CUCHIARA, D. C., SZEWCZYK, S, RIBEIRO, C., AZAMBUJA, F, MATA, M. M

Análise da Variabilidade de Longo Período do Nível do Mar

VI Seminário sobre Ondas, Marés, Engenharia Oceânica e Oceanografia por Satélite, 2005, Arraial do Cabo – RJ, 2005.

6. CUCHIARA, D. C., FERNANDES, E. H., STRAUCH, J. C., CALLIARI, L. J.

Caracterização do Clima de Ondas na Costa do Rio Grande do Sul

VI Seminário sobre Ondas, Marés, Engenharia Oceânica e Oceanografia por Satélite, 2005, Arraial do Cabo - RJ, 2005

Resumos Publicados em Anais de Congressos

1.CUCHIARA, D. C., FERNANDES, E. H., STRAUCH, J. C., CALLIARI, L. J.

Determination of the wave climate for the Southern Brazilian Shelf

First International Conference on the Application of Physical Modelling of Port and Coastal Protection, Porto – Portugal, 2006

2. CUCHIARA, D. C., FERNANDES, E. H., STRAUCH, J. C., CALLIARI, L. J.

Determination of the wave climate for the Southern Brazilian Shelf

Symposium International on Mud Deposit in Coastal Areas, Porto Alegre – RS, 2006

3. CUCHIARA, D. C., FERNANDES, E. H., STRAUCH, J. C., CALLIARI, L. J.

Determination of the wave climate for the Southern Brazilian Shelf

8th International Conference on Southern Hemisphere Meteorology and Oceanography, Foz do Iguaçu - PR. 2006.

Apresentação de Trabalho

1. CUCHIARA, D. C., MARQUES, W. C., CALLIARI, L. J., FERNANDES, E. H.

   Modelagem Numérica da atenuação das ondas na presença de lama fluida na Praia Do Cassino (RS), Brasil

   VII Simpósio Sobre Ondas, Marés, Engenharia Oceânica E Oceanografia Por Satélite, Arraial do Cabo, RJ, 2007

2. CUCHIARA, D. C. ; FERNANDES, E. H. ; STRAUCH, J. C. ; CALLIARI, L. J. .

   Determination of the Wave Climate for the Southern Brazilian Shelf. 2006.

   Symposium International on Mud Deposit in Coastal Areas, Porto Alegre – RS, 2006

3. CUCHIARA, D. C., FERNANDES, E. H., STRAUCH, J. C., CALLIARI, L. J.

   Caracterização do Clima de Ondas na Costa do Rio Grande do Sul

   II Seminário e Workshop em Engenharia Oceânica, Rio Grande- RS, 2006.

4. CUCHIARA, D. C. ; FERNANDES, E. H. ; STRAUCH, J. C. ; CALLIARI, L. J. .

   Modelagem Numérica do Comportamento das Ondas na Costa do Rio Grande do Sul.

   VI Jornadas Nacionales de Ciencias del Mar, Puerto Madryn, Argentina, 2006.

Trabalhos submetidos

- Determination of the Wave Climate for the Southern Brazilian Shelf (2007)

Cuchiara, D.C., Fernandes E. H. , Strauch, J. C. , Winterwerp, J.C., Calliari, L. J.

Continental Shelf Research, aceito

- Modeling Wave Dumping over Fluid Mud at Cassino Beach Coastal Area, Brazil (2008)

Cuchiara, D.C., Fernandes E. H. , Marques, W.C., Monteiro, I.O.; Calliari,

L. J. , Winterwerp, J.C.

Continental Shelf Research, submetido

- On the fine-sediment dynamics in the Patos Lagoon – Cassino Beach system

Calliari L. J., Vinzon, S, Fernandes E. H., Winterwerp, H. , Cuchiara, D. Holland ,K. T.

Continental Shelf Research, aceito

Livros Grátis

(http://www.livrosgratis.com.br)

Milhares de Livros para Download:

Baixar livros de Administração
Baixar livros de Agronomia
Baixar livros de Arquitetura
Baixar livros de Artes
Baixar livros de Astronomia
Baixar livros de Biologia Geral
Baixar livros de Ciência da Computação
Baixar livros de Ciência da Informação
Baixar livros de Ciência Política
Baixar livros de Ciências da Saúde
Baixar livros de Comunicação
Baixar livros do Conselho Nacional de Educação - CNE
Baixar livros de Defesa civil
Baixar livros de Direito
Baixar livros de Direitos humanos
Baixar livros de Economia
Baixar livros de Economia Doméstica
Baixar livros de Educação
Baixar livros de Educação - Trânsito
Baixar livros de Educação Física
Baixar livros de Engenharia Aeroespacial
Baixar livros de Farmácia
Baixar livros de Filosofia
Baixar livros de Física
Baixar livros de Geociências
Baixar livros de Geografia
Baixar livros de História
Baixar livros de Línguas

[Baixar livros de Literatura](#)
[Baixar livros de Literatura de Cordel](#)
[Baixar livros de Literatura Infantil](#)
[Baixar livros de Matemática](#)
[Baixar livros de Medicina](#)
[Baixar livros de Medicina Veterinária](#)
[Baixar livros de Meio Ambiente](#)
[Baixar livros de Meteorologia](#)
[Baixar Monografias e TCC](#)
[Baixar livros Multidisciplinar](#)
[Baixar livros de Música](#)
[Baixar livros de Psicologia](#)
[Baixar livros de Química](#)
[Baixar livros de Saúde Coletiva](#)
[Baixar livros de Serviço Social](#)
[Baixar livros de Sociologia](#)
[Baixar livros de Teologia](#)
[Baixar livros de Trabalho](#)
[Baixar livros de Turismo](#)